POLITECNICO
MILANO 1863
ABC PhD DOCTORAL PROGRAMME
in ARCHITECTURE, BUILT ENVIRONMENT
and CONSTRUCTION ENGINEERING

Kondratenko Aleksei

Thesis final draft

Cycle 36°

Major academic discipline: *ICAR/09 – Tecnica delle Costruzioni (Structural Engineering)*

Topic:

Data-Driven Design of Steel Buildings with Metal Yielding Dampers

Supervisor:
Alper Kanyilmaz, Assistant Professor, DABC Politecnico di Milano

Co-supervisor:
Carlo Andrea Castiglioni, Full Professor, DABC Politecnico di Milano

Tutor:
Marco Valente, Associate Professor, DABC Politecnico di Milano

Contents

ABSTRACT

After many years of research and development, the dissipative components and systems such as hysteretic metallic yielding dampers (MYDs) are still rarely implemented in the common construction practice. It is mainly because there is not enough experience obtained from the buildings with dissipative components, repair and reassembly procedures have not yet been adequately addressed, and their long-term benefits have not been well quantified. Moreover, current methods for the evaluation of nonlinear seismic response in structural engineering are time-consuming: the calculation of nonlinear seismic structural response for buildings equipped with MYDs could take hours using nonlinear time history (NLTH) analysis in finite element modelling (FEM) software. Therefore, there is a need for faster solutions without a decrease in structural response prediction accuracy, which can also consider the repairability, life cycle environmental and economic assessment for such systems. Another significant issue is that the Architecture, Engineering and Construction (AEC) industry is responsible for around 40% of global CO_2 emissions: up to 11% of it comes from embodied carbon - emissions related to production, manufacturing, maintenance, and end of life disposal of building materials. Consideration of embodied carbon adds another important design criteria to structural design making the task of finding optimized solutions even harder. Since current design approach leaves a lot of sustainable and cheaper structural solutions simply undiscovered, there is an urgent need for the modernization of the design workflow.

This thesis explores the potential of data-driven methods in enhancing the sustainability of earthquake-resistant structures, particularly those equipped with a new type of MYDs. Experimental results obtained from shaking table testing have informed the correct modeling of MYDs in the finite element modeling (FEM) software. A case study has demonstrated that buildings equipped with new hysteretic MYDs offer significant advantages over conventional structures in terms of Life Cycle Cost (45% reduction) and embodied CO_2 (25% reduction for life-cycle stages A-C). The results proved the hypothesis that the introduction of these MYDs into the building can yield to more sustainable structures in seismic areas. Machine Learning (ML)-based surrogate models have been trained to approximate the results of the NLTH analysis. The surrogate models have been developed taking into account practical needs of structural engineers executing nonlinear seismic analysis: these models have been integrated into a building optimization tool developed in this PhD thesis project. The tool allows engineers to quickly iterate on different design scenarios for structures that require nonlinear seismic analysis. Thanks to the surrogate models, the generation and design of all possible structural options for a given inputs took seconds instead of days needed for FEM approach. Empirical case studies showed that the utilization of this tool facilitates the discovery of structures that are not only up to 30% more sustainable but also up to 25% more cost-effective when compared with structural configurations found using conventional design methodologies employed by industry practitioners and academic experts.

Keywords: Earthquake Engineering; Hysteretic metallic yielding dampers; Machine Learning; Surrogate Models; Design Optioneering

ACKNOWLEDGMENTS

The writing and development of this thesis was a memorable and challenging journey that could not have happened without the guidance from some people and heart-warming support from others. First of all, I am grateful to my supervisor, Alper Kanyilmaz, for the continuous support and encouragement. In particular, I thank Alper for his open-mindedness, high expectations, and the high level of freedom he provided me with. He taught me to be ambitious, confident, and tackle even the most challenging problems with a smile on the face.

I acknowledge the help of the participants of the DISSIPABLE project. In particular, Professor Harris Mousakis, and Lydia Panoutsopoulou from the National Technical University of Athens, Professor Carlos Calado from Istituto Superior Tecnico, Michalis Sofras from Sofman, Elena Rocco from RINA S.p.A, and Professor Nicola Tondini from University of Trento (UNITN). Especially, Roberto Andreotti and Giulia Giuliani from UNITN helped me tremendously with hybrid tests data and with a general understanding of how new dissipative components work. We spent a nice time together in Trento during the tests that helped me to feel a part of a team.

I am grateful to the guys from Digital Blue Foam, where I spent my period abroad. Especially, to Sayjel Patel, Camiel Wejdenberg, Rutvik Deshpande, and Maciej Nisztuk for the continuous support and constant feedback. During my internship there, I significantly improved my technical capabilities which helped me tremendously during the work on this thesis. Moreover, I learned some valuable skills on how to efficiently present my work to a non-technical audience.

I am grateful to the master's students I co-supervised with Alper: Van Hoi Dang, Mussie Birhane, and Hassan Haidar. I gained a lot of valuable insights about Machine Learning algorithms working with these guys. Moreover, I acknowledge the support of my colleagues who are also PhD candidates in the ABC department of Politecnico di Milano. I will miss our conversations (technical and not) and informal meetings after the work.

Last but not least, I am extremely grateful to my family. Without my mother and grandmother, the whole PhD journey would not be possible. They always provided me with a kind word and love. Thanks to them even in the most challenging days I was motivated to go forward and finish my dissertation. Finally, my friends were always close to me even when the physical distance with some of them reached 10 thousand kilometers. Without them I would not be able to periodically detach from my work and refresh my mind.

1 Introduction

Earthquakes cannot be prevented, but their actions on the structures can be mitigated. The main goals for seismic design engineers all over the world are to limit the damage to buildings during the earthquake and assure the safety of their occupants. Modern seismic design codes (EN 1998-1 [1] and ANSI/AISC 341-10 [2]) have been developed mainly to solve these problems. Current seismic design provisions of steel-concrete composite buildings propose to use the capacity design approach to avoid progressive building's collapse (Figure 1 [3]). Its main goal is to guarantee a ductile behaviour of the structure during the earthquake event. According to capacity design rules, earthquake energy should be dissipated by the structure in the so-called "dissipative zones", where the inelastic deformations occur. In traditional buildings, they are located in structural elements (i.e., beams, base connections). Therefore, conventional buildings suffer significant inelastic deformations in their main structural members during seismic action, which causes expensive repair procedures, interruption of the building's functionality, and discomfort for tenants. However, in past decades it was discovered that dissipative zones can also be located in dissipative systems. The focus of this thesis will be on a particular type of dissipative systems called hysteretic metallic yielding dampers (MYDs) which dissipate seismic energy through the yielding of the steel material.

Figure 1. The collapse of a steel building during Kobe, Japan earthquake in 1995 [3]

Apart from potential seismic damage, new buildings located in seismic areas have another significant issue that is common for all structures regardless of their location – environmental impact. Embodied carbon that is Carbon Dioxide equivalent (CO_2e) emissions related to building materials production, manufacturing, maintenance, and disposal is becoming a huge problem and now presents 11% of total CO_2e emissions in the world [4]. There is a potential for hysteretic MYDs to reduce not only seismic damage for the new buildings but also their embodied carbon due to their ease of repairability and replaceability. Several innovative systems based on energy dissipation via metal yielding and damping have been recently invented all over the world as summarized in detail by Castaldo [5] Saravanan [6], and EU-RFCS DISSIPABLE project [7]. Although there is a big variety of MYDs, they all have following issues in common:

- MYDs have been developed mainly considering their structural and dissipative performance without evaluating their repairability, economic feasibility and environmental performance.
- Behaviour of structures equipped with these dampers is evaluated by complicated and time-consuming nonlinear structural analysis that limits possible design iterations.

- The optimisation tool that considers both economic and environmental criteria for the buildings equipped with MYDs does not exist.

Since the design space (all the possible structural configurations of a building given geometric constraints, loading, and material inputs) is quite large in structural engineering applications, there is a need for search optimization procedure that can help the engineer to efficiently navigate through different design criteria and their trade-offs to design sustainable and cost-efficient structures. Structural analysis is an essential part of this procedure since the design space must consist of well-designed and safe buildings. Due to the expected yielding of MYDs in earthquake scenario, nonlinear analysis is required to adequately evaluate a structural behaviour of buildings equipped with them, in particular nonlinear time history (NLTH) analysis is implemented in engineering practice for this purpose. Currently, the finite element method (FEM) is used to conduct nonlinear time history (NLTH) analysis which is a physics-based process consisting of the integration of the structural equation of motion in each of the arbitrarily chosen time steps. Conventionally, the number of time steps is huge which results in computationally expensive analysis procedure that can take hours to finish. It makes the generation of the above-mentioned design space an extremely computationally expensive task. Consequently, structural engineers are discouraged to use seismic resistant buildings equipped with MYDs in their designs choosing their conventional counterparts which need to be repaired or even demolished after significant seismic events.

One of the main approaches to improve productivity and accelerate processes all over the world regardless of the industry is digitalisation. Nowadays, there is an undergoing digital transformation in Structural Engineering industry which involves development of advanced software, improvement of interoperability between existing programs, paperless projects execution, etc. One of the novel concepts of this industry's digital transformation is data-driven design where the choice of the structural system is driven by data or performance which is opposed to conventional design practice where the choice of the structure is based on a past experience of the senior engineer and always precedes its performance evaluation (Figure 2). The core technology of data-driven structural design is Artificial Intelligence (AI). It has been extensively applied in healthcare, retail, e-commerce, and other industries and now getting traction also in Structural Engineering [8], [9]. There is a tremendous potential of AI in seismic engineering applications [10] and some of the branches of AI such as Machine Learning (ML) and evolutionary algorithms can be particularly suitable for the problems related to design optimisation of buildings equipped with MYDs stated above.

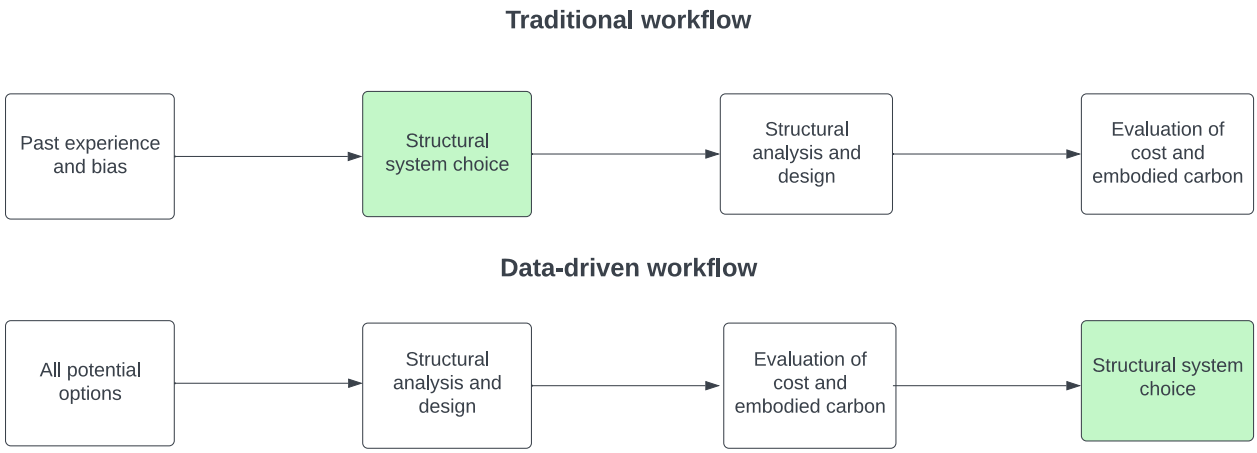

Figure 2. Traditional vs data-driven workflows for structural design

The goal of this research is to improve sustainability of earthquake resistant structures using advanced digital technologies, such as data-driven structural design. To achieve this goal, the following steps are planned:

- Investigate the environmental and economic impacts of buildings equipped with innovative MYDs and compare them with conventional structures.
- Accurately predict the nonlinear structural behaviour of buildings equipped with these MYDs and their conventional counterparts using fast ML-based surrogate models instead of conventional time-consuming FEM-based NLTH analysis.
- Create an optimisation procedure via efficient design space exploration. Full life-cycle cost and embodied carbon will be used as design criteria for optimisation.

Experimental and Life Cycle Analysis (LCA) data obtained within DISSIPABLE project [7] to support and validate the developments have been used. As a final deliverable of the thesis the web-based structural optimisation tool (SUSTEZ – Sustainable Structures in Earthquake Zones) has been developed. The tool allows engineers to find which columns' span and lateral load resisting system provides the most sustainable and cost-efficient solution from all the possible options.

2 State of the art

This section presents a literature overview on hysteretic metallic yielding dampers (MYDs) applied in composite steel-concrete buildings, life cycle and sustainability analysis for earthquake resistant structures, running time reduction for NLTH analysis, applications of ML for data-driven structural seismic analysis and design, and design space exploration for building located in seismic areas.

2.1 An overview of hysteretic MYDs in composite steel-concrete buildings

Conventional concepts for the seismic design of the buildings allow some damage in structural elements under severe earthquakes ensuring the safety of humans and an absence of sudden collapse of the structure. However, devastating Northridge (1994) and Kobe (1995) earthquakes showed the need for protective systems that can dissipate earthquake energy leaving all the structural members undamaged. Several passive energy dissipation devices have been developed, such as hysteretic MYDs, friction dampers (FDs), fluid viscous dampers (FVDs), tuned mass dampers, and base isolation systems [11]. This research will be focused on MYDs which absorb energy induced by the earthquake through the metal yielding. These dampers can be categorized as displacement-dependent i.e., their force output depends on the magnitude of their displacement. A number of hysteretic yielding dampers have been successfully developed in the civil engineering industry:

- ADAS [12] and its variation TADAS [13] consist of a series of steel plates. The bottom part of the plates is attached to the top of a chevron bracing arrangement and the top part of the plates is connected to the floor level above the bracing (Figure 3.a). During the earthquake upper end of the plates moves with respect to the lower end and it causes out-of-plane bending of the plates and their subsequent flexural yielding (Figure 3.b,c). Furthermore, a variation of this damper made of copper Cu-ADAS [14] has been investigated. Honeycomb damper [15], Slit damper [16] and Shear Panel [17] are used in a similar configuration as ADAS, but utilizing shear yielding instead of flexural one (Figure 3.d).
  Issues: even though these dampers are easily replaceable their economic and environmental cost has not been evaluated.
- Buckling Restrained Braces (BRBs) [18] consists of steel brace encased in hollow steel shape filled with concrete-like material (Figure 3.e). The confinement provided by the concrete-filled tube allows the steel brace to yield under compressive loads without buckling. Therefore, the damper behaviour is identical in tension and compression which allows significant energy dissipation. This is the most widely used hysteretic MYD in the civil engineering industry by now.
  Issues: expensive replacement of the damaged damper after the seismic event.
- Pi damper [19] applies to the column's weak axis. In this system, a wide-flange beam is joined to a wide-flange column by bolted splices at the top flange of the beam and steel hysteretic dampers at the bottom flange of the beam (Figure 3.f). The system is designed in a way that the beam's rotation centre is located at the end of its top flange. Therefore, all the damage from seismic events concentrates on the damper leaving the floor slab and other structural elements undamaged.
  Issues: all the tests have been performed on only a part of the structure without investigating the global behaviour of the entire construction with these dampers. Repairability and economic feasibility aspects have not been addressed.
- Steel Self Centering Device (SSCD) [20] consists of a hysteretic MYD and a steel pretension system for re-centering (Figure 3.g). This typology of dissipative devices is

characterized by the presence of a re-centering force that mitigates and eliminates the residual deformations of the building after the earthquake. The main dissipative elements are steel fuses that experience yielding during the seismic event and can be easily replaced when damaged.
Issues: repairment procedures are complicated and can be expensive. Economical and sustainability aspects are not addressed.

- Removable Link Device [21] can be applied exclusively to steel frames with eccentric bracing. In eccentrically braced frames links are conventionally designed to be a dissipative component (Figure 3.h). This device represents a typical link that is connected to the beam using bolts and can be easily replaced after the seismic event.
  Issues: applicable only to the one type of structures. The sustainability aspect has not been addressed.
- Tube-in-Tube Damper (TTD) [22] consists of a tube-in-tube assemblage of two commonly available hollow structural sections (Figure 3.i). The outer hollow section of the damper has a series of strips created by cutting a series of slits through the wall, and it is welded to the inner hollow section in such a way that when the brace damper is subjected to forced displacements in the direction of its axis, the strips dissipate energy through flexural/shear yielding.
  Issues: the absence of the tests on the entire structure equipped with this damper. High efforts for the repair (the whole race needs to be replaced).
- Dissipative column [23] is a new type of hysteretic dampers consisting of two or more adjacent steel vertical elements connected to each other with continuous mild/low strength steel shear links. Numerical tests showed that doubly-hinged dissipative column (DC) elements with low eccentricity can fully yield along their length while columns are subjected to axial strain and so, small bending moments can be neglected flexural deformation.
  Issues: numerical tests have not been supported by experiments.
- Yield-Link Moment Connection [24] is special patented connection for moment resisting frames. It consists of plats that are bolted to the bottom and top flanges of a beam. The plate is weakened to have a desirable yielding location, another plate is bolted on top of this weakened part to avoid its buckling. There is also a configuration with a cover plate for steel-concrete composite structures. It is a widely used in a practice connection that is also a qualified connection for the American design code [25].
  Issues: the life-cycle sustainability aspect has not been addressed.
- DuraFuse Frames connection system [26]. During severe earthquakes, deformations are accommodated by bolt slip and shear yielding of fuse plate attached to the bottom flange of the beam. These connections were extensively tested in the lab and are commonly used in practice.
  Issues: the life-cycle sustainability aspect has not been addressed.

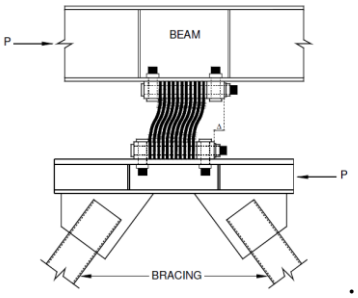

a. ADAS-type dampers in the structure [13].

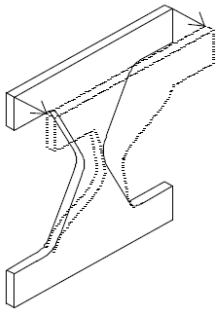

b. Deformed shape of ADAS [22].

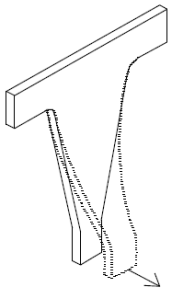

c. Deformed shape of TADAS [22].

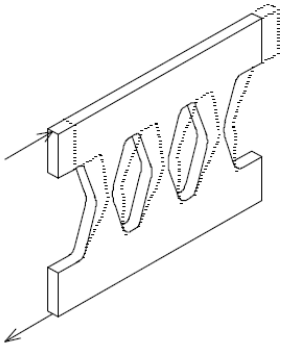

d. Deformed shape of Honeycomb damper [22].

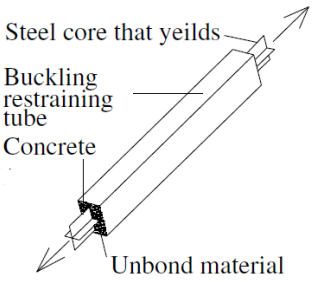

e. Buckling Restrained Brace (BRB) [22].

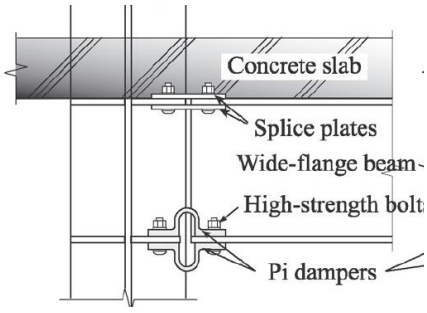

f. Pi damper [19].

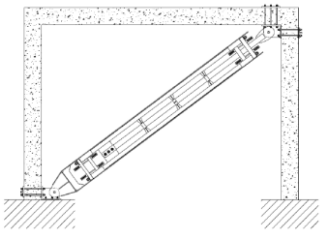

g. Steel Self Centering Device (SSCD) [21].

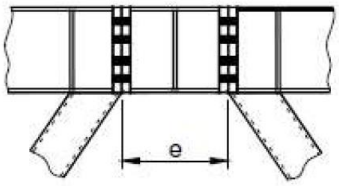

h. Removable Link Device [22].

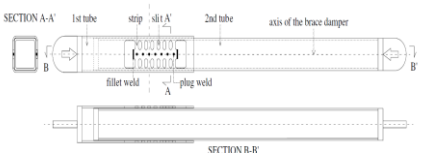

i. Tube-in-Tube Damper (TTD) [23].

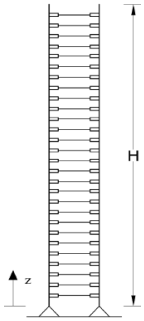

j. Dissipative column [24].

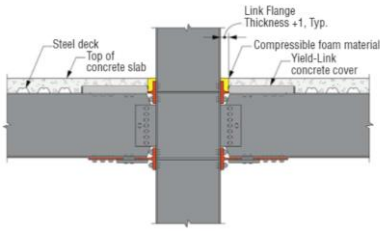

k. Yield-Link Moment Connection [25]

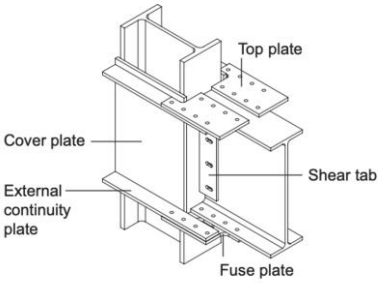

k. DuraFuse Frame connection [27]

Figure 3. Hysteretic yielding dampers

Even though a lot of hysteretic MYDs have been developed and recently implemented into the engineering practice, their environmental cost required for the manufacturing, repair and possible recycling has not been considered. Therefore, there is a need for a life-cycle assessment of buildings equipped with MYDs both on component and global structural levels.

2.2 Life-cycle cost and sustainability analysis for earthquake resistant structures

Reduction of post-earthquake damage of structural and non-structural elements becomes a fundamental aspect for improving long-term sustainability and resource conservation. The resources spent in the reconstruction after a disaster can be significantly reduced through innovative structural systems for new buildings and retrofitting measures for existing buildings, dropping economic and environmental costs from a life cycle perspective. The application of dissipative and repairable MYDs enables long-term use of structural elements, which do not require replacement or demolition after string earthquake events, improving the sustainability of building construction. Recent circular economy policies and the European Green Deal [28] confirm that energy-intensive industries, such as steel, are crucial to Europe's economy, providing several key value chains, therefore their decarbonization and modernization are vital.

Numerous LCA studies quantified environmental impact of seismic events on buildings and concluded that seismic damage can significantly increase structural carbon footprint [29], [30], [31], [32], [33]. A few researchers performed a comparative LCA to investigate the environmental impact of design decisions for structures located in seismic areas. The European research project "High Strength Steel (HSS) in Seismic Resistant Building Frames" [34] concluded that the use of high strength steel leads to the reduction of the size of structural elements and consequently to environmental savings compared to traditional steel material. In another study different concrete mixes were compared and the replacement of cement with fly ash was the most efficient environmental impact reduction strategy [35]. Moreover, environmental impact of different reinforced concrete retrofitting alternatives has been quantified [36] as well as the consequence of building new structure instead of strengthening the existing one [37]. The LCA impact of dissipative systems was calculated by Ribakov et al. [38] where non-retrofitted building was compared with use of concrete diaphragms for seismic strengthening, application of high-damping rubber bearings, and use of seismic isolation columns. The study concluded that the use of base isolation can reduce building's environmental impacts up to 50%. LCC methodologies related to buildings located in seismic areas have also been proposed in the literature [39], [40]. The approach relates to quantification of seismic damage in monetary terms. Other applications consider LCC optimization of tuned mass dampers [41], analysis of self-centering structures equipped with buckling restrained braces [42], performance of smart bridges with shape memory alloy (SMA) [43], and comparative LCC between steel frames equipped with SMA dampers and their conventional analogues [44]. In the latter study it was observed that passive dampers can decrease life cycle cost of 4-story steel frame by 53%, and 12-story steel frame by 90%, respectively.

Literature review reveals that nonlinear structural analysis is crucial for both LCA and LCC since it is the most accurate way to estimate potential structural damage due to the seismic event [45]. Most of the considered studies quantify environmental or economic impact of seismic resistant structure without comparing different solutions (e.g., dampers vs non-dampers). The few studies that make this comparison concentrate either on LCA or on LCC but do not perform both comparisons at the same time. For instance, the positive economic impact of particular energy dissipation strategy is quantified while environmental aspect is not considered and vice versa. The study that quantifies both economic and environmental benefits of buildings equipped with MYDs has not been found in the literature.

2.3 Running time reduction for NLTH analysis using physics-based procedures

Since nonlinear time history (NLTH) analysis could run for hours even for a few DOF models, several attempts have been done to obtain reliable results spending less time for this analysis. Domingues Costa et al. [46] developed a simplified procedure for NLTH analysis based on the Theory of Plasticity. The computational procedure has been developed on a single degree of freedom (SDOF) system where plastic bending moment at the column's base has been calculated based on

the Theory of Plasticity assuming rigid-plastic behaviour. Then, in each step of the integration of the equation of motion (EOM), it was checked whether the plasticity at the base was reached and then EOM was modified (and simplified when the structure was elastic assuming that its relative displacements to the ground are equal to 0). Furthermore, the proposed procedure has been applied to 4-storey RC frame. In this case, the equation of motion is established by using the virtual work equation. After comparing the results of simplified NLTH with standard NLTH in FEM software authors found that in the former approach maximum average displacement is 18% lower than in the latter one. This difference can be considered significant and it is not on the safe side. In addition, only rigid-plastic behaviour has been considered and time savings compared to conventional NLTH analysis have not been quantified. Another study proposed a simplified NLTH analysis where leading and trailing weak signals in the acceleration record are trimmed, and remaining record is downsampled [47]. The proposed method preserves significant frequency characteristics of the original record including its S-phase. To identify the proportions of acceleration record to be trimmed maximum roof displacement has been used (Figure 4). It allowed to keep the most important part of the accelerogram for the representation of structural behavior. The proposed method has been applied to 5, 10, 15 and 20 – storey 3D R/C structures. The authors concluded that the proposed procedure is able to evaluate the peak roof displacement within the 5% error to the conventional NLTH analysis. The average time savings of this method are 60%. Even though the proposed methodology reducing NLTH analysis time more than two times without losing much accuracy, the peak structural response needs to be calculated in advance by another nonlinear method (pushover analysis) in order to efficiently cut the input accelerograms.

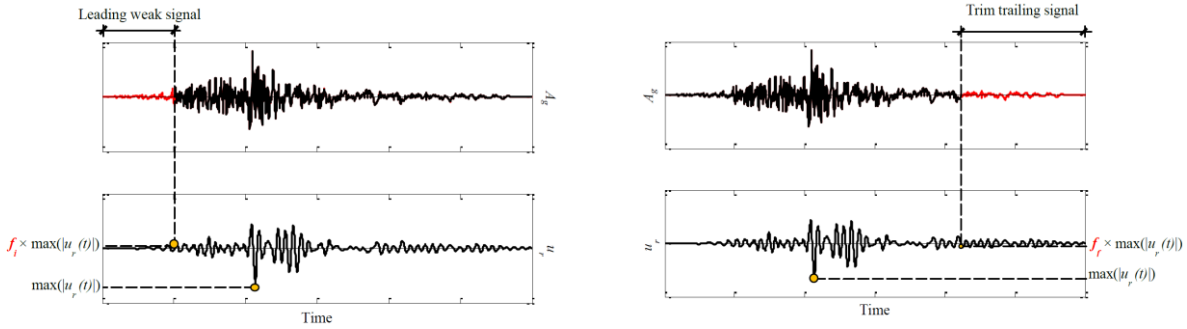

a. Trimming leading signal before peak roof displacement is reached

b. Trimming trailing signal after peak roof displacement is reached

Figure 4. Trimming leading and trailing signals [47].

Faroughi and Hosseini [48] invented a method for simplification of accelerograms based on the modification of their Fourier analyses. In the proposed method the Fourier Spectrum of the accelerogram is calculated first, and then, by using a computer program, developed by the authors, the corresponding Inverse Fourier Transform is calculated using a relatively large time step, depending on the structure's periods. By use of this technique, the time step of original accelerograms has been increased 5-10 times reducing the time required for NLTH analysis in the same proportion. Maximum displacement values have been overestimated by 5-10% using altered acceleration input comparing to the original one. However, the proposed method has been applied only to SDOF systems and only two ground motion records have been used. Therefore, there is no guarantee that this method is uniform and can be applied to a big variety of ground motions and structural systems. Mehmood et al. [49] developed the Uncoupled Modal Response History Analysis (UMRHA) procedure. It can be viewed as an extended version of the classical modal analysis procedure, where the nonlinear response of each vibration mode is first computed, and they are later on combined into the total response of the structure. The proposed method has been applied to 4 buildings with a height variation of 20-44 storeys. The results of UMRHA procedure have been compared with conventional NLTH analysis and the average difference of 18% in terms of interstorey drift has been

found. This methodology needs 6 times less time to finish the analysis in comparison with NLTH. However, it still required 5 hours and the knowledge of the modal hysteretic behavior, which can be obtained from a cyclic modal pushover analysis is needed. Zhao et al. [50] introduced fast convolution integration method based on Duhamel integration to enhance the efficiency of the frequency domain approach (FDA) for the nonstationary response analysis of nonproportionally damped structures. An impulse excitation approach has been proposed to determine the structural impulse response matrix. Then, the response statistic has been directly evaluated by the convolution with respect to the discrete-time impulse response. Finally, Fast Fourier Transformation (FFT) algorithm has been applied has been used to accelerate the computation of this convolution. To evaluate the efficiency of the proposed methodology the lateral displacements of 20-300 storey buildings was calculated and compared with outputs from FDA approach. The authors concluded that their method achieved good accuracy with a significant reduction of analysis time (up to 154 times). However, real accelerograms have not been applied and the generalization of the proposed approach to the real structures has not been investigated by authors.

There are numerous attempts to reduce the time required for NLTH using physics-based methods. However, these studies either suffer from a lack of accuracy, require complicated pre-processing procedures, or their analysis time reduction is relatively small. Therefore, alternative procedures are needed to boost the quality and speed of physics-based simulations.

2.4 Running time reduction for NLTH analysis using ML-based surrogate models

Another method to reduce the time required for NLTH analysis without a significant loss in the accuracy is Machine Learning – based surrogate models. To provide the reader with a better understanding of this technology, general introduction for Artificial Intelligence and surrogate models is presented.

2.4.1 Artificial Intelligence (AI) and Machine Learning (ML)

Four decades ago, new families of computational methods, denoted as soft computing (SC) methods, have been proposed [51]. These methods are based on heuristic approaches of artificial intelligence (AI) rather than on rigorous mathematics. They were initially received with suspicion because they do not take explicit physics-based formulations into account. However, according to numerous numerical and experimental investigations, they have turned out in many cases to be extremely powerful [52], [53], [54]. Consequently, their use in various areas of engineering science is continuously growing. As one of the most conspicuous and widely adopted digital technologies, ML can refer to a series of methodologies that can prominently mimic the learning and reasoning process of the human brain to automatically extract knowledge from the data and, subsequently, improve the decision making [55]. Nonetheless, it is easy to confuse the relationships between ML, AI, and Deep Learning (DL), which are concepts that are frequently used in the corresponding literature related to ML (Figure 5).

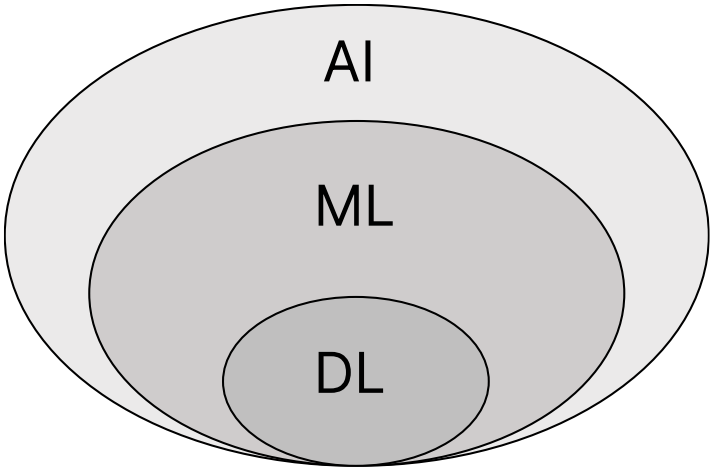

Figure 5. Relationship between AI, ML, and DL [55]

ML can be categorized into four types, namely supervised learning, semi-supervised learning, unsupervised learning, and reinforcement learning. For the first three types, Figure 6 provides an intuitive representation in terms of relationships between the training processes and the utilization of data. In the reinforcement learning an agent makes decisions in an environment, learns from its actions based on rewards and penalties, aiming to maximize cumulative reward over time.

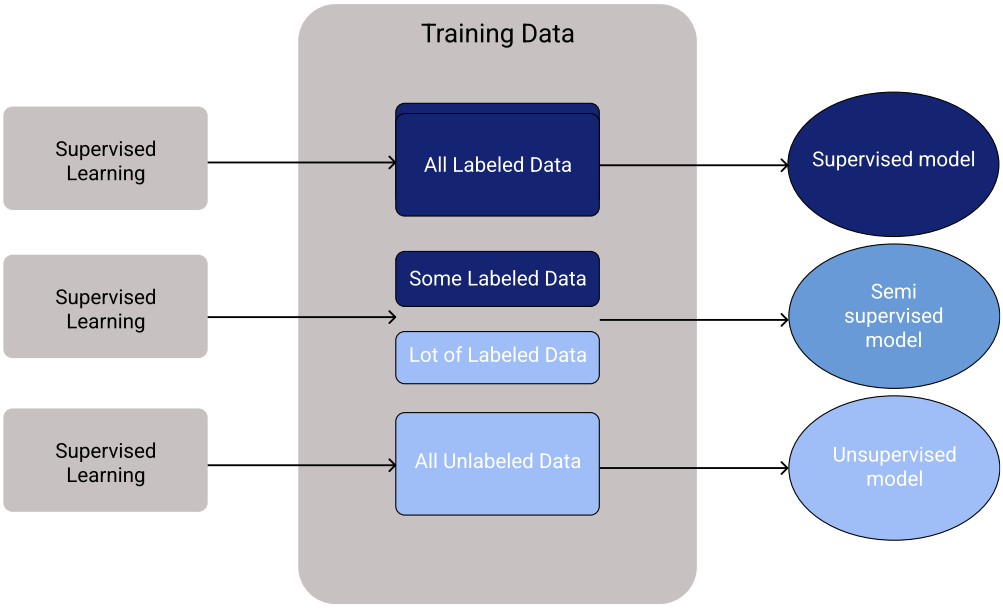

Figure 6. Typical representations of three types of ML methods [56]

In the past decades, various ML algorithms have been developed and utilized. In the work conducted by Ray [57], a brief review of several widely applied ML algorithms has been provided, including linear regression, logistic regression, decision tree and its derivations (random forests, gradient boosting, etc.), support vector machine, Bayesian learning, Naïve Bayes, K-nearest neighbours, K-means clustering, gradient descent algorithms, and backpropagation algorithms. Specifically, among them, the decision tree is a supervised ML algorithm that is widely adopted to solve regression and classification problems by splitting data and making decisions in “nodes” and “leaves”. Besides, the performance of the decision tree can be further improved by applying ensemble modelling techniques. For instance, a ML algorithm named random forest can be built by randomly ensembling various decision trees using the bagging method and obtaining the output(s) through voting [57]. As a powerful ML algorithm, random forest can overcome the overfitting

problem and improve the robustness against the outliers, without compromising the performance in handling non-linear classification and regression problems [57], [58]. In addition, algorithms such as gradient descent algorithms and backpropagation algorithms have been applied as the basis of various ML methods, such as artificial neural networks (ANN). ANN has also been categorized as a DL structure, especially when multiple hidden layers are used. Nonetheless, there is no universal threshold to classify if an ANN structure should belong to DL or simply the conventional ML structure. Therefore, to avoid confusion, in this research, all the ANN structures identified through literature will be considered as ML.

When it comes to the development process of ML models, Figure 7 provides a general workflow. Firstly, data that can reflect the input and output correlation under the problem context will be collected through various ways. Not only the quality of the data but also its quantity matters for the ML model to yield accurate predictions. Subsequently, analysis is performed on the collected data to statistically investigate, clean, transform, and structure it. This step is essential in providing better understanding and organization of the data. Traditionally used in the field of software development, features refer to the coherent and identifiable representations that can portray the system functionalities. However, under the context of ML development, features normally refer to the input variables of the models while feature engineering is the process of constructing, reshaping, and selecting these input variables using statistical or mathematical techniques or domain knowledges to improve the predictive performance of the models [59]. Eventually, the ML models are trained using the prepared dataset and tested on utilized error metrics [60] to judge the performance before final deployment.

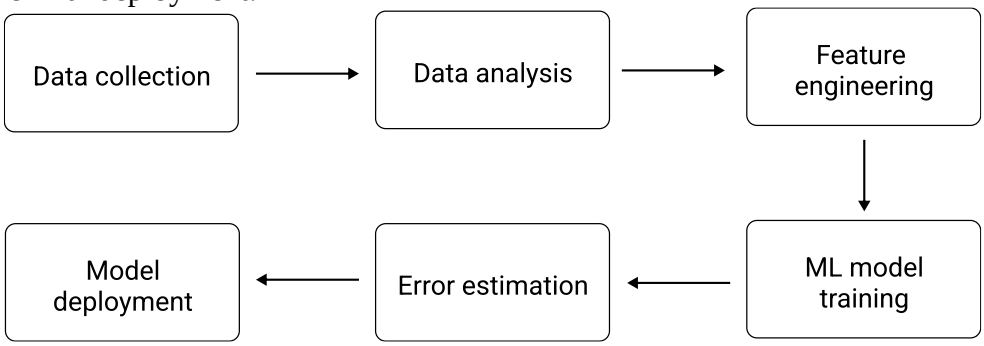

Figure 7. Typical ML/DL model development workflow

2.4.2 ML-based surrogate models

Provided the necessary amount of data, ML algorithms can learn the hidden relationship between inputs and outputs for the problem and make accurate predictions in a short amount of time. In the application of nonlinear structural analysis, ML can rapidly predict the structural response (internal forces, displacements, etc.) given the required inputs (building geometry, elements' cross-sections, acting loads, etc.), thus creating the approximations of the non-linearities. These approximations are called surrogate models and can be considered as an alternative to the typical Finite Element Model (FEM) analysis.

Widely applied in various engineering fields, surrogate models can be developed using physically based approximation techniques to create lower fidelity analysis [61]. With the gradual improvement and vigorous development of related research, as well as the fact that enormous data has been generated in the industry over the past decades, surrogate modelling has also been greatly stimulated by the utilization of data-driven techniques, such as ML, to relate the needed response surface surrogates to the original simulation models. Since the availability of data in structural engineering is poor, it is common to generate the data for ML training in FEM software [62], [63], [64]. ML models often struggle to extrapolate beyond their training data [65], meaning they may not perform well on unseen examples, making it crucial to find training data that adequately represents the

diverse scenarios and situations in the application space to ensure better generalization and performance. Figure 8 illustrates a comparison between the surrogate model and the FEM-based simulation method. Overall, ML-based surrogate model follows the ML training workflow depicted in Figure 7 where features are typical inputs required for structural analysis and the output is a structural response.

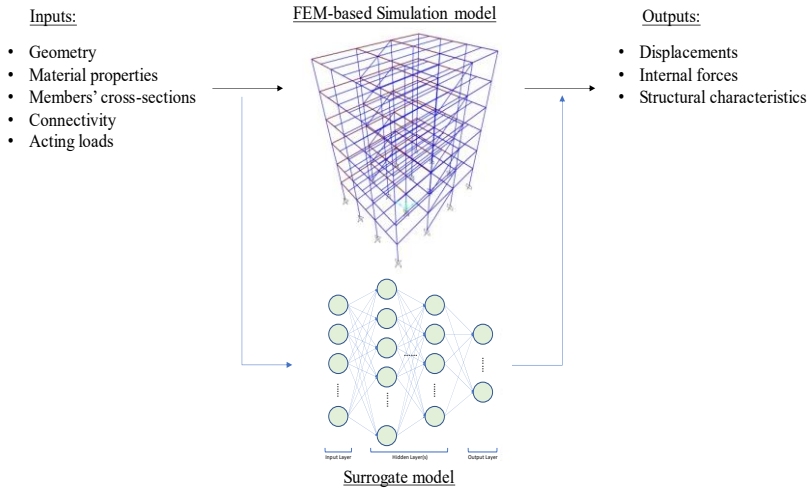

Figure 8. Surrogate model

2.4.3 Application of ML-based surrogate models for NLTH analysis prediction

The biggest issue with NLTH is that it takes a lot of computational time since the problem needs to be discretised in small time steps to accurately catch nonlinearity. Therefore, ML algorithms could be very helpful in the fast prediction of nonlinear seismic structural behaviour. This chapter presents an overview of the available ML-based surrogate models to predict the maximum nonlinear seismic structural response.

Artificial Neural Network (ANN) was the first ML technique used to predict nonlinear seismic structural response. The first attempt to use ANN for nonlinear structural seismic response prediction was conducted by Molas and Yamazaki [66].They used ground parameters such as peak ground acceleration, peak ground velocity, spectral intensity, etc., to predict the ductility factor of a single degree of freedom timber building. The root mean square error of 0.406 proved that ML-based surrogate model is capable to predict nonlinear seismic structural response with adequate accuracy and this approach worth further research. To investigate the applicability of this technology for the bigger structure, Lagaros and Fragiadakis [67] predicted the interstorey drift of 10 storey steel Moment Resisting Frame (MRF) using ANN to build its fragility curves. Apart from ground motion parameters, the variability of material characteristics (Young's modulus and yielding strength) has been considered as the input of the algorithm. This research showed that ML-based surrogate models can be successfully applied even to predict nonlinear seismic response of a real-scale buildings. However, the application was restricted only to one structure without any indication of the ability and accuracy of a model to make reliable predictions for buildings with different geometry, cross-sections, or material.

De Lautour and Omenzetter [68] performed the first study where trained ANN was applicable not only for one building but for a set of structures. They trained their neural network to be able to predict the damage index of Reinforced Concrete (RC) frames with different geometry, strength class of concrete, elements' cross-sections, and damping ratio subjected to seismic loading with different ground motion parameters. This successful attempt pushed the researchers to investigate

which features can be the most predictive for the nonlinear seismic structural response. Aiming to investigate this issue Arslan [69] predicted the results of pushover analysis using ANN for seismic damage classification of the group of the RC buildings. The author used different structural and material parameters to investigate their importance to the algorithm's prediction power. Shear wall ratio and short column formation were the most significant structural parameters that affect ANN's performance. Doran et al. [70] trained ANN to predict the nonlinear seismic response of concentrically braced frames with various geometrical, and structural characteristics subjected to a range of ground motions. They discovered that structural period and peak ground acceleration were the most critical parameters for the neural network to predict the interstorey drift. Additionally, ANN that uses only structural parameters as inputs had a higher error than the model that used also ground motion parameters as an input (13% vs 8% average error). Digging deeper into ground motion parameters' influence on the nonlinear seismic response prediction, Morfidis & Kostinakis [71] concluded that ANN can achieve a remarkably high degree of accuracy in the prediction of RC buildings' damage level (expressed in terms of maximum interstorey drift) when at least five seismic input parameters are used. These conclusions are applicable for 3-7 storey 3D buildings with fixed geometries in plan. Stefaninin et al. [72] trained ANN to predict multiple outputs for nonlinear seismic behaviour of RC buildings in Bologna, Italy (Figure 9). The size of the column turned out to be the most predictive parameter of the algorithm. Other attempts to predict the nonlinear seismic behaviour of buildings using neural networks were focused on the particular unique inputs, such as the hysteretic loop of the structure [73], and resonance area [74]. In these cases, instead of explicitly using structural properties (geometries, cross-sections, materials, etc.) the authors used the encoded nonlinear structural behaviour as an input.

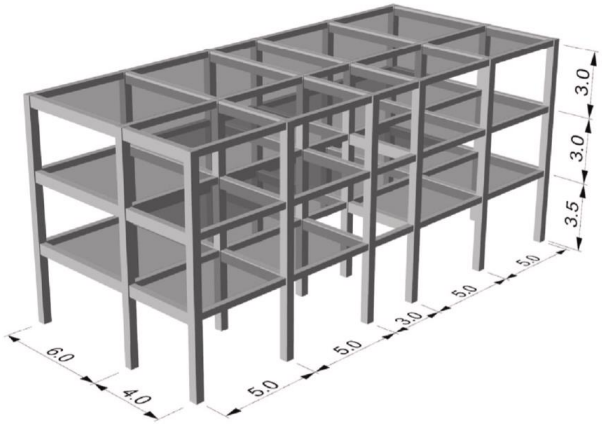

a. One of the considered RC buildings

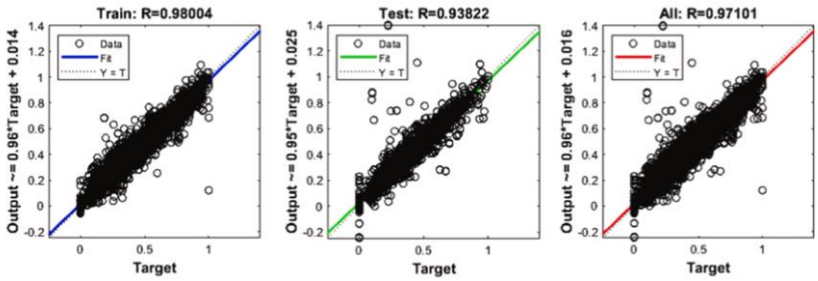

b. The accuracy of the ML algorithm predictions

Figure 9. ML-based surrogate model applied for nonlinear seismic response prediction of RC building [72]

Even though ANN showed a great performance as a main algorithm for ML-based surrogate model for nonlinear seismic structural response prediction, other ML algorithms have been applied

for the same purpose. Comparison between ANN and other ML techniques has been performed in several studies. Kia and Sensoy [75] compared Support Vector Machine (SVM) and SVM combined with ANN for seismic damage classification of various RC frames. The latter model yielded more accurate results – ANN was used for the prediction of structural displacements, which were used as an input for SVM classification model. Gudipati and Cha [76] trained ANN and SVM surrogate models and concluded that the former leads to much smaller errors in the prediction of the nonlinear seismic response of mid-rise steel MRF structures. These two studies showed than ANN outperformed SVM in nonlinear seismic structural response prediction. Therefore, comparison with other ML algorithms had to be done. Nguyen et al. [77] used ANN and eXtreme Gradient Boosting (XGBoost) algorithms for the prediction of the nonlinear seismic structural response of the wide range of steel MRFs. They observed that the accuracy of these 2 algorithms in terms of the coefficient of determination was very close, but XGBoost slightly outperformed ANN (0.975 vs 0.962). Moreover, aiming to find the most predictive features they discovered that peak ground velocity and spectral acceleration at the 1st natural period of the structure are the most important inputs for the surrogate models. It proved the outcomes of previous research in terms of significance of structural natural period as an input feature. This research also showed that tree-based models can be competitive with ANN for this task and even outperform it.

Zaker Esteghamati and Flint [78] decided not to use ANN at all and concentrated on other ML algorithms (Multiple Linear Regression, Random Forests (RF), SVM, K-nearest neighbours (KNN), and XGBoost) to predict a seismic loss in mid-rise RC buildings in South Carolina, USA. They found SVM and XGBoost surrogates to be the most accurate for this purpose with floor area and building height being the most influential parameters for the algorithms. However, all the mentioned in this chapter studies considered purely data-driven surrogate model without trying to include the underlying physics of the nonlinear seismic structural response. To tackle this issue, Guan et al. [79] compared the mechanical, purely data-driven, and hybrid approach for nonlinear seismic structural response prediction. A hybrid (mechanics-based + data-driven) model requires the user to perform some type of mechanics-based analysis (e.g., a modal or linear static structural analysis) to generate some intermediate results (e.g., elastic story drifts). Then, the gap between the intermediate results and the target response variable (with the predictors as input) is bridged using ML model. The results showed that the hybrid approach yielded the highest accuracy; however, it required greater effort compared to the purely data-driven approach since a preliminary structural analysis needed to be performed for hybrid surrogate models. For hybrid and purely data-driven models, they calculated the accuracy of linear regression, random forests, XGBoost, and ANN concluding that random forests were the most accurate algorithm of all. Moreover, they proposed a new performance metric that represents the fraction of the data set whose relative difference does not exceed a predefined percentage.

Table 1 provides a summary of above-mentioned papers, including the range of application, ML algorithms used, their inputs and outputs. The application of surrogate models' is always limited and rarely exceeded more than 10 storeys range. Moreover, the lateral load resisting system was fixed in all studies which is a big limitation for seismic engineering applications. Even though ANNs were used extensively as an ML model, recently they have been outperformed by tree-based models. Ground motion and structural (material, cross-sections, geometry) parameters were commonly used as an input while peak interstorey drift is the most common output representing structural seismic behaviour.

Study	Structure	Inputs	Outputs	Algorithm
[66]	1 DOF timber frame	Ground motion parameters	Ductility factor	ANN
[67]	10 storey steel MRF	Material characteristics, ground motion parameters	Peak interstorey drift	ANN
[68]	3-7 storey RC frame	Material characteristics, structural geometry, elements' cross-sections, damping ratio, ground motion parameters	Damage index	ANN
[69]	4-7 storey RC frame	Material characteristics, structural geometry, elements' cross-sections	Peak interstorey drift	ANN
[75]	4-8 storey RC frame	Structural geometry, elements' cross-sections, ground motion parameters	Damage index	ANN, and SVM
[70]	3, and 9 storey steel braced frame	Structural geometry, elements' cross-sections, natural period, ground motion parameters	Peak interstorey drift	ANN
[71]	3-7 storey RC frame	Structural geometry, ground motion parameters	Peak interstorey drift	ANN
[73]	SDOF system	Structural hysteretic loop, and ground excitation	Peak structural displacement	CNN
[74]	3 storey RC frame	Ground motion parameters, resonance area	Peak interstorey drift, peak structural displacement	ANN
[76]	4, and 6 storey steel MRF	Structural geometry, elements' cross-sections, structural damping, material characteristics, ground motion parameters	Peak interstorey drift	ANN, and SVM
[77]	3-20 storey steel MRF	Structural geometry, structural periods, ground motion parameters	Peak interstorey drift	ANN, and XGBoost
[79]	1-19 storey steel MRF	Structural geometry, elements' cross sections, structural periods, ground motion parameters	Peak interstorey drift	Linear regression, Random forests, XGBoost, and ANN
[78]	3-6 storey RC frame	Structural geometry, elements' cross sections, ground motion parameters	Seismic loss, global warming potential	Linear regression, SVM, KNN, Random forests, and XGBoost
[72]	2-8 storey RC building	Structural geometry, gravity loads, elements' cross sections, material properties	Base shears, structural displacements, activated mass, structural periods	ANN

Table 1. Summary of ML-based surrogate models for NLTH analysis

ML-based surrogate models showed a great performance for the prediction of NLTH analysis response of buildings. This technique can be clearly considered as faster and more accurate alternative of physics-based attempts to reduce the time of NLTH structural analysis. However, in all the considered study either one of very few structural responses were taken as outputs of ML models which limits their potential application to the practice. The considered studies were mainly aimed at the exploration of ML-based surrogate models' capabilities rather than making them really useful for the structural engineering practice. The only industrial application is The SP3 Structural Response Prediction Engine [80]. The goal of this engine is to create a better alternative to FEMA P-58 [81] which is commonly used for a probabilistic seismic performance prediction in the USA to

assess the risk of the building in terms of economic loss, repair time, and casualties. More than 4 million nonlinear seismic structural analyses were performed to train a surrogate model that can predict structural displacements and accelerations. Unfortunately, the authors did not reveal any information about ML algorithm used and further details of the model.

2.5 Buildings optimisation in seismic areas

To introduce the problem of building optimisation in seismic areas, the general scope of the structural optimisation and its types are given. Then, different algorithms to solve this issue are discussed and the applications of Genetic Algorithm for the structural optimisation of buildings located in seismic areas are highlighted.

2.5.1 Optimisation of a building's structural system

Optimisation is an essential part of the structural design of all buildings. An optimization problem can be written mathematically in the following generic form:

$$\begin{aligned} &minimize\ f_i(x)\ ,\ (i = 1,2,\dots,M),\ x \epsilon R^n \\ &subject\text{ed }to, \quad h_j(x) = 0,\ (j = 1,2,\dots,J) \\ &\qquad\qquad\ \ g_k(x) \leq 0\ (k = 1,2,\dots,K) \end{aligned}$$

Where $f_i(x)$ is the objective function, $h_j(x)$ and $g_k(x)$ the constraints and x the vector of design variables. When working with real problems usually there is not just one objective to optimize but several of them that should be considered simultaneously. This is called multi-objective optimization (MOO) problem, and the best compromise solutions must be found among the whole solution space. These problems are commonly approached with non-dominated sorting and Pareto sets concepts. Let's suppose a MOO problem with m objectives. Each solution can be represented in a m-dimensional space based on its objective values. If the vectors u1 and u2 represent two different solutions, we can say that the solution u1 is dominated by the solution u2 if all the objective values of u2 are better than the corresponding ones of u1. Mathematically it can be expressed as:

$$\forall i \in \{1,2,\dots,m\}: f(u\ ) \leq f(u\ )$$

We can say a solution is non-dominated if it is not dominated by any of the solutions. The set of non-dominated solutions conform what is called the Pareto front [82], which is the set of most interesting solutions in a MOO problem. Figure 10 illustrates the explained concepts.

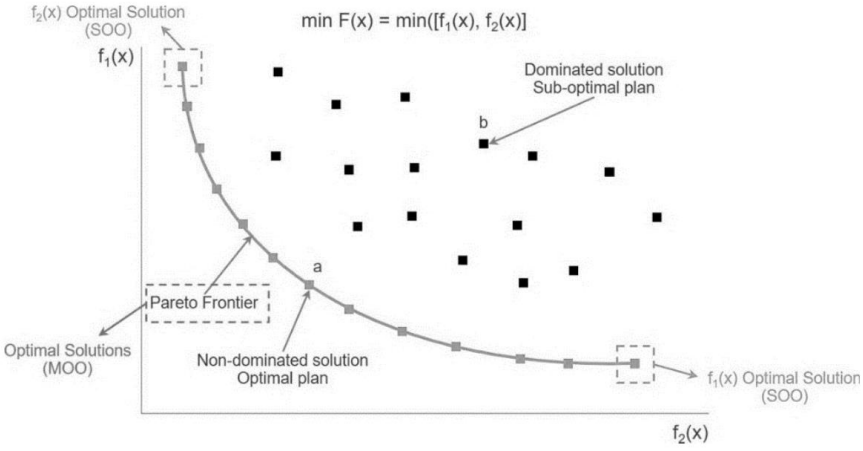

Figure 10. Pareto front [83]

There are 3 main types of structural optimization [63]:

- **Topology optimisation:** for discrete structures, such as trusses and frames, searches for the optimal numbers of elements, and how they are connected. Topology optimisation for the

entire structure will include location and number of columns, span directions of beams, structural types and materials.

- **Shape optimisation:** looks at the overall dimensions and form of a structure, including the locations of its nodes. Shape optimisation is particularly important for tension-only structures but can also improve the performance of trusses and similar frames.
- **Size optimisation:** the optimal design is found by changing aspects such as the sectional sizes of members in trusses and frames, or the thicknesses of plates in a girder.

Size optimization is the most common form of all since it is related to the optimization of member's cross-section. It is already fully integrated into structural engineering practice where from the early stages of their career young professionals are encouraged to optimize the size of cross-sections given the acting loads. Unfortunately, it is the least impactful type of structural optimizations. Shape optimization is usually applied for trusses in a current practice. It involves the form finding via reciprocal force diagrams [84]. Finally, typology optimization brings the most impact to the structural design while also being the most complex type of all. Nowadays, it is mainly used by the biggest engineering firms that develop the scripts in parametric engineering software [85]. This thesis will be focused on layout optimization which is a form of typology optimization and is concerned with the best overall form of the structure, such the choice of material, floor type, lateral load resisting system, etc. Therefore, the literature review shows the studies related mainly to the layout optimisation.

Layout optimisation have been applied in the concept stage of building design to different types of structures, such as trusses [62], [86], [87], domes [88], [89], residential [90], [91], [92], [93], and industrial buildings [94]. As an objective function usually structural stiffness [91], [93], internal stresses or cost were selected [62]. However, in some studies multiple objective functions were implemented, such as cost, free space, end embodied carbon [92]; embodied and operational energy [95]; structural and energy cost [96]; plan irregularity, energy efficiency, and construction cost [97]; structural, heating, and cooling energy [98]. Structural limit states and compatibility were mainly considered as constraints which leads to discarding of solutions where either serviceability or safety criteria were not satisfied. Geometrical, material and loading parameters have been used as design variables, combination of which constructed a design space.

2.5.2 Optimisation algorithms

Optimisation algorithms are step-by-step strategies to solve the optimisation problem stated in the previous subchapter. They can be divided in 2 classes:

- **Deterministic algorithms** (Direct Analysis, Gradient Descent, Exhaustive Enumeration, Heuristic Solutions). They require an initial configuration and a gradient of a constraint function.
- **Stochastic algorithms** (Monte Carlo, Stochastic Gradient Descent, Evolutionary Algorithms, Particle Swarm). They do not require the gradient of objective functions, but instead they use probabilistic transition rules.

Which method to choose depends on the way in which an optimization problem is described, and the kind of information we have about the objective and constraint functions [99]. When the design space (the all possible options) is extremely big or even infinite (when continuous variables are involved) evolutionary algorithms, in particular Genetic Algorithm (GA) proved to be the most efficient option for the structural optimisation [62], [99], [100], [101].

Genetic algorithm (GA) is a numerical optimization technique used to optimize undifferentiable optimization objective functions. It uses concepts from evolutionary biology to search for a

global optimum (minimum or maximum) of an optimization problem, by mimicking evolutionary biological processes [82]. GA starts with the initialization of candidates' solutions, then it evaluates their fitness based on the predefined objective function and, if stopping criteria (adequate number of optimized solutions) is not met, it creates a subsequent generation of solutions based on evolutionally inspired procedures such as selection, crossover, and mutation. The cycle repeats until an optimal number of optimized solutions is found (Figure 11 [10]).

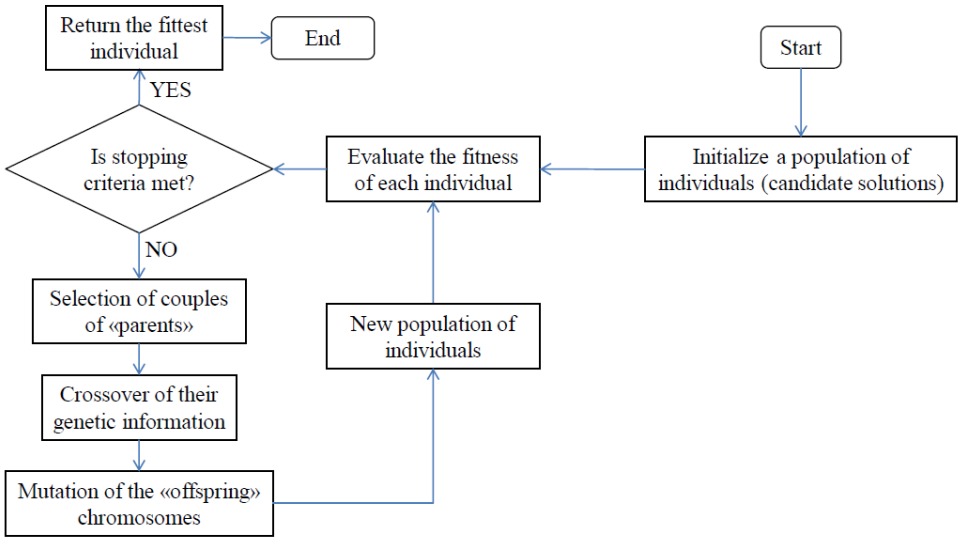

Figure 11. Flowchart of GA [10]

On the contrary, an Exhaustive Enumeration (EE), also known as a brute-force search, is a straightforward algorithmic approach to solving a problem by considering all possible solutions within a defined search space [99]. It systematically explores every combination or permutation of variables or parameters to find the optimal solution. While EE guarantees finding the best solution, it can become impractical and computationally intensive as the search space grows exponentially with the number of variables. However, if the search space is relatively small it can be considered as the most straightforward and easily explainable optimisation technique [103] also in structural engineering applications [104].

2.5.3 Optimisation of the structural system of a building in seismic areas

For structural design optimization, Genetic Algorithm (GA) combined with structural nonlinear seismic analysis in FEM software has been widely used. Wongprasert and Symans [105] investigated an optimal viscous dampers distribution within the scope of 20-storey building. The optimization has been performed by minimizing four different frequency-domain objective functions. Structural analysis has been performed outside the GA with most appropriate damper distributions according to authors. Each of the resulting optimized damper configurations provided an improvement in the seismic response of the benchmark building as compared to the uncontrolled building. An automated procedure that combines performance-based seismic design methodology and GA for steel structures has been proposed by Liu et al. [106]. Requirements of a code-compliant design are assessed by multiple objective functions, which reflect either initial expenses in terms of the steel material weight and the number of different steel section types or future seismic risks in terms of interstorey drift demands at selected seismic hazard levels. Pushover analysis has been used inside the GA to evaluate structural response. In total 400 generations were needed to reach the optimization goal and each generation took 10 minutes. A similar study has been performed by Fragiadakis et al. [107].Static pushover analysis has been used inside the design phase of the optimization algorithm to determine the level of damage for different earthquake intensities. The proposed

methodology is based on the Eurocode design standards while two objective functions have been considered: initial material weight, and lifecycle cost. This methodology has been applied for the design of a ten-storey steel moment-resisting frame. It took more than 3 hours for the algorithm to optimize the structure.

Lagaros et al. [108] used NLTH analysis within GA to optimize a seismic design of 6-storey space frame made of steel (Figure 12). Maximum interstorey drift ratio has been used as a main threshold for the design population generation and the obtained optimal designs are compared, in terms of both material weight (cost) and seismic performance. From 15 to 23 hours was needed for algorithm to propose a best set of different design outputs.

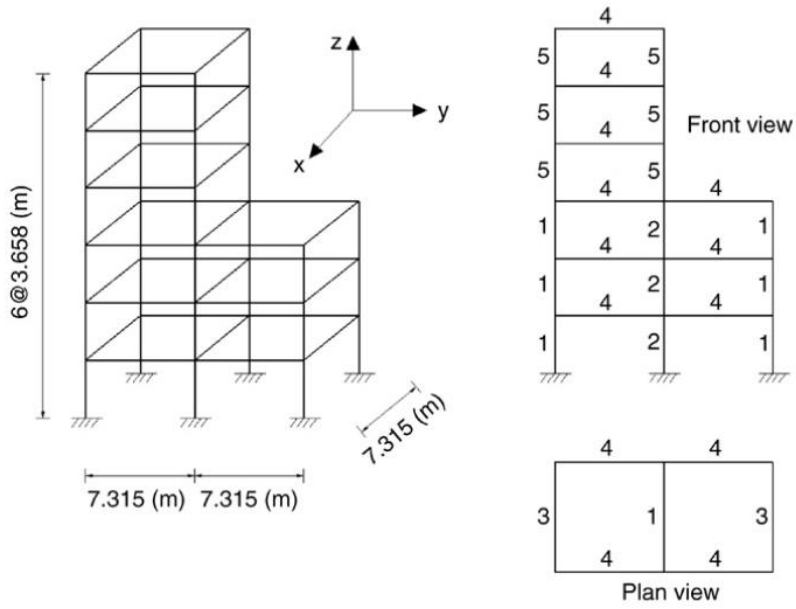

Figure 12. Six-storey space frame configuration [108]

Hejazi et al. [109] developed an optimization procedure for the energy dissipation system that consists of viscous dampers. The goal was to find the optimum damping coefficients for the viscous dampers installed in 5-storey RC frame. This study developed a multi-objective optimization computation procedure based on the GA to enhance the performance of earthquake energy dissipation systems and to minimize the seismic response of structures in terms of damage to structural members and simultaneous displacements of all story levels. Nonlinear time history analysis has been performed within the GA and it resulted in 83 hours for optimization procedure to finish.

Several attempts to use GA and other evolutionary algorithms for structural optimization have been concentrated on structures equipped with MYDs, mainly BRBs. Both single and multi-criteria optimization have been performed. Structural cost [110] and BRB area [111], [112] were the most common single objectives. Structural cost and damage [113], installation cost and seismic repair cost [114], structural weight and dissipated energy [115], story drift and acceleration [116] were multiple criteria used within the optimization problem. No studies that included environmental criteria were found. Moreover, as with conventional buildings, NLTH analyses took a lot of time within the search for the most optimal solution since a lot of options needed to be evaluated. Approximated calculations as well as parallel computing were used to decrease the optimization time, but it still required hundreds of NLTH analyses to finish the optimization task.

Gholizadeh [117] proposed a novel approach that consists of a combination of meta-heuristic algorithm (evolutionary-based algorithm) and ANNs. Instead of performing structural analysis in FEM software as an intermediate stage of algorithm optimization as other mentioned researches, the author trained an ANN to predict the results of nonlinear pushover analysis and used it as a

structural constraint for the population generation. A Performance-based Design (PBD) procedure has been used to evaluate structural performance at different levels of earthquake intensity. Finally, three low-rise, mid-rise and high-rise planar steel moment-resisting frame structures have been successfully optimized for various performance levels. It was the only try to integrate ML-based surrogate models with the optimisation framework for buildings that require nonlinear seismic analysis. However, pushover analysis was used instead of NLTH and considered structures were not equipped with MYDs.

The abovementioned papers are summarised in Table 2. Even though a lot of layout optimisation problems were discussed in the literature for standard buildings and mentioned in the previous subchapter, for seismic resistant structure size optimisation problem is more prevalent. In particular, structural elements' cross-sections and dampers' parameters were the most common design variables to be optimised. Other studies concentrated on the best location of the damper, but none of them tried to optimise the entire building layout. Moreover, the choice of lateral load resisting system was fixed in all studies while it is a significant design variable in structural engineering design process. Structural safety was mainly used as an optimisation constraint to assure the generated solutions are feasible. Optimization criteria were restricted to structural performance and overall structural cost without considering sustainability aspects. Where optimisation time was reported, it usually took hours or even days for the process to finish. In 2 notable exceptions researchers used distributed computing and ML-based surrogate models to get a tremendous reduction in optimisation procedure running time. The application of EE in optimisation of seismic resistant structures was not found in the literature.

Study	Structure	Dissipative systems used	Design variables	Constraints	Optimisation criteria	Nonlinear seismic analysis used	Optimisation time
[105]	20-storey steel MRF	Viscous dampers	Dampers' location	Number of dampers	Structural damage (interstorey drifts, floor acceleration, etc.)	NLTH	-
[106]	5-storey steel MRF	-	Structural elements' cross-sections	-	Monetary cost, structural damage	Pushover	66,5 hours
[107]	10-storey steel MRF	-	Structural elements' cross sections	Code compliance	Initial and life-cycle monetary costs	Pushover	3,2 hours
[108]	6-storey 3D steel MRF with a setback	-	Structural elements' cross sections	Code compliance	Structural weight	NLTH	15-23 hours
[109]	5-storey RC frame	Viscous dampers	Damper's damping coefficient	Structural safety	Structural damage (displacements)	NLTH	83,3 hours
[110]	3-5 storeys RC frames	BRBs	BRBs' location	Structural safety	Monetary cost	Pushover	-
[111]	10-storey steel CBF	BRBs	BRB area	Storey ductility limit	Total area of all BRBs	NLTH	-
[112]	3, 9-storey steel MRF	BRBs	Thickness of BRB's steel core, thickness of welded plates attached to beams and columns	Structural safety	Total area of all BRBs	Pushover	-
[113]	8-storey steel CBF	BRBs	BRB area	Structural safety	Monetary cost, structural damage	NLTH	-
[114]	2D 9-storey steel CBF, 3D 3-storey RC building	BRBs	BRB area and location	Interstorey drift limit	BRB installation cost, post-earthquake damage cost	Pushover (2D) NLTH (3D)	0,1 – 5 hours (2D) 1 – 35 hours (3D)
[115]	3, 6-storey steel CBF	BRBs	BRB area, structural elements' cross sections	Structural safety	Structural weight, dissipated energy	NLTH	-
[116]	3, 6, 9-storey steel MRF	Curved dampers and BRBs	Dampers' characteristics	Yielding pattern	Interstorey drift and floor acceleration	NLTH	-
[117]	3, 6, 12-storey steel MRF	-	Structural elements' cross sections	Structural safety	Structural weight	Pushover with ML-based surrogate	0,3 hours

Table 2. Summary of structural optimisation studies

2.6 Added value of this research to the state of the art

The conclusions of the literature study and the added value of this research are subdivided into two subsections: one related to MYDs, and the other to data-driven structural design.

2.6.1 Added value of this research regarding MYDs

The following conclusions have been made based on this literature study:

- In currently developed hysteretic dissipative systems, environmental cost required for their manufacturing, repair and recycle has not been considered.
- Most of the considered studies quantify environmental or economic impact of seismic resistant structure without comparing different solutions (e.g., dampers vs non-dampers). The few studies that make this comparison concentrate either on LCA or on LCC but do not perform both comparisons at the same time. The study that quantifies both economic and environmental benefits of buildings equipped with MYDs has not been found in the literature.

To contribute to the existing state of the art and resolve the found limitations, the following has been done within this PhD project:

- The environmental cost of producing MYDs has been thoroughly evaluated in collaboration with a steel manufacturer and LCA experts. The findings were utilized to accurately estimate the environmental impact of buildings equipped with these systems.
- Comparative LCA and LCC analyses on buildings equipped with new types of MYDs and their conventional counterparts has been performed. The results showed that the introduction of MYDs could reduce both building's lifetime embodied carbon emissions and monetary cost.

2.6.2 Added value of this research regarding data-driven structural design

The following conclusions have been made based on this literature study:

- Attempts to reduce NLTH analysis running time based on physics failed to reach accurate and efficient procedure.
- Alternatively, ML-based surrogate models can be used to predict the results of NLTH analysis in accurate and fast manner. However, there is just one attempt to bring these models into the design practice.
- Genetic algorithm (GA) is the most common optimisation technique for structural engineering applications. It has been used in several studies for structural optimization purposes in seismic areas even for buildings equipped with MYDs. However, optimization criteria were restricted to structural performance and overall structural cost without considering sustainability aspects. In addition, the optimization procedure took a lot of time due to the need of performing NLTH analysis as an intermediate step of the algorithm. The attempts to reduce optimisation procedure time included using multiple computers at the same time and ML-based surrogate model to approximate the results of nonlinear seismic analysis.
- Alternatively, Exhaustive Enumeration (EE) can be used for structural optimisation. It is feasible only when the design space size is not huge.

To contribute to the existing state of the art and resolve the found limitations, the following has been done within this PhD project:

- ML-based surrogate models have been successfully trained to predict the results of NLTH analysis for structures equipped with MYDs and their conventional counterparts. Special

emphasis was placed on the practicality of these models within the structural engineering practice. To reach it, the wide range of input and output parameters has been considered in the trained models.

- An optimization tool for buildings in seismic areas has been developed, incorporating sustainability criteria in addition to monetary costs and structural safety. Both buildings equipped with MYDs, and their conventional counterparts are considered for the design space generation. The optimisation procedure takes less than a minute thanks to rapid NLTH analysis powered by ML-based surrogate models. The layout optimisation has been implemented to make an optimisation procedure more impactful compared to the literature studies where local cross-sectional optimisation has been used.

3 Methodology

The goal of this thesis is to improve sustainability of earthquake resistant structures using advanced digital technologies. Based on the literature study, buildings equipped with a new type of MYDs have been chosen as earthquake resistant structures as well as conventional buildings without any dampers. AI is used as an advanced digital technology, in particular ML is implemented for creating a surrogate model. Embodied carbon is used as a sustainability criteria. The detailed workflow of the research is presented in Figure 13. This workflow is applied to the particular new MYDs discussed in this thesis. However, it can also be generalised to any type of MYDs given that all the steps shown in Figure 13 are followed. The PhD project consists of 3 parts:

- Experimental, LCA and LCC data collection from physical tests and numerical calibrations.
- Creation of ML-based surrogate models.
- Development of the optimisation tool.

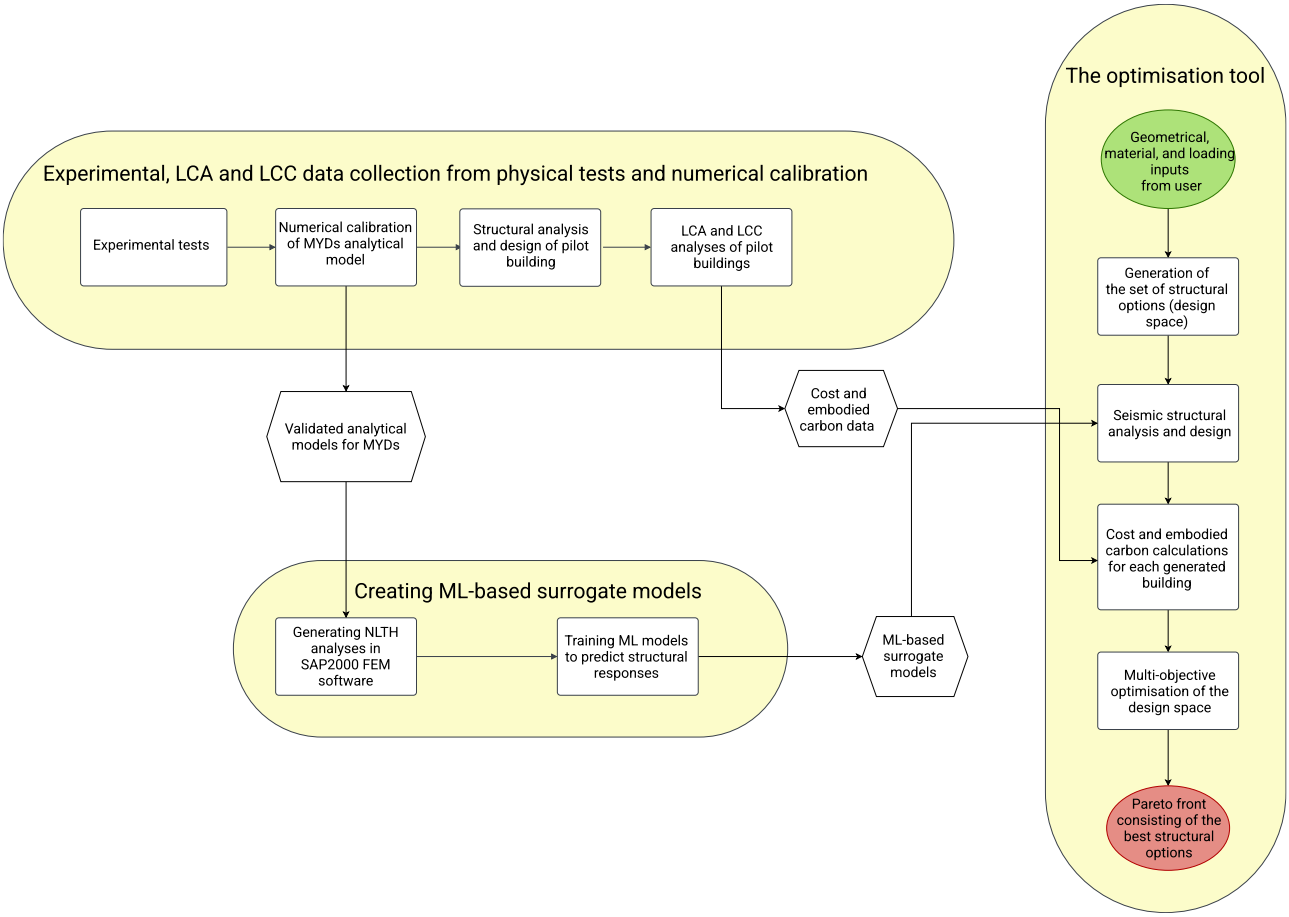

Figure 13. Research workflow

The experimental, LCA and LCC data is collected within DISSIPABLE research project [8]. New MYDs have been created during that project, while this PhD thesis will focus on two of them – one for moment resisting frame (MRF) configuration and another for the concentric braced frame (CBF) one. Half-scale 3D buildings equipped with these dampers have been tested on shaking table to calibrate the analytical models of the developed dissipative components. These validated analytical models are then used in FEM simulations to generate the data for ML models training.

Finally, with the involvement of steel producer and industrial experts comparative LCA and LCC has been performed to see if the integration of MYDs has any benefits in terms of cost and

embodied carbon. Two different levels have been considered: “Product level” and “Building level”. For the assessment at Product level, the results have been evaluated individually, with reference to 1 MYD considering as system boundaries the phases from raw material extraction and processing to product manufacturing (“cradle to gate”). In the modular approach defined within EN 15804 [118], such phases correspond to modules A1-A3 (Figure 14). Technical documents have been prepared for each of the components (DRBrC, DRBeS) in accordance with the calculation rules in the Product Category Rules “Construction Products and Construction Services” of The International Environmental Product Declaration (EPD) System. These documents are specifically tailored to DRCs and can serve as valuable resources for future EPD applications. The EPD, which is a type III environmental declaration based on ISO 14025 [119], provides a reliable and comprehensible means to communicate the environmental performance of products. It enables effective comparisons with alternative solutions, thereby facilitating market acceptance and adoption. Regarding the building level, two 6-storey pilot buildings have been designed for the life-cycle analyses – one equipped with new MYDs (DISSIPABLE building) and its conventional counterpart (Conventional building) without any integrated dampers. For the assessment at building level, the system boundaries apart from modules A1-A3 also include the building construction phase (A4-A5), the use stage (B1-B7) and the end of life (C1-C4). This “cradle to grave” assessment allows to include in the assessment also the repair phase (after a seismic event) and the decommissioning of the building (Figure 14), providing more details about the main differences between the DISSIPABLE and the Conventional buildings. The results of these analyses are then used in the calculations of optimisation criteria in the optimisation tool.

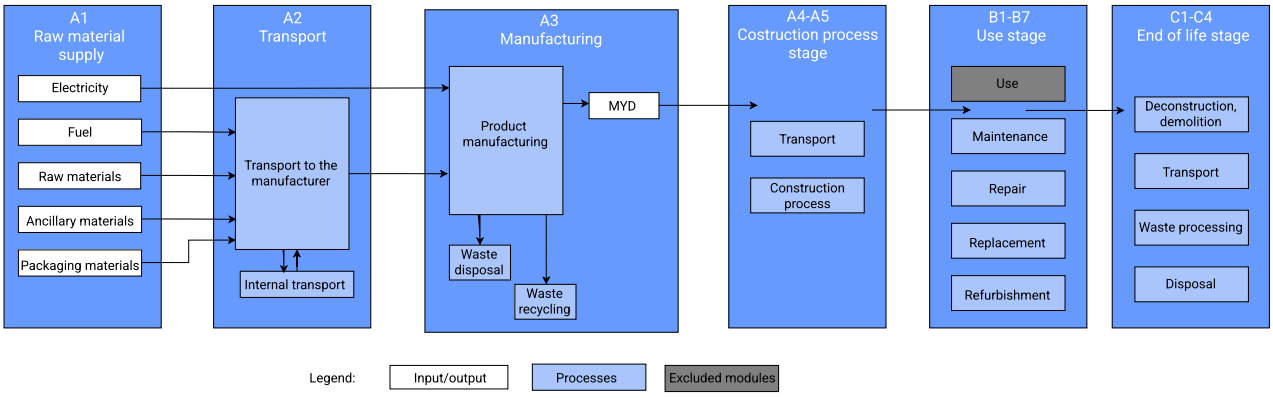

Figure 14. System boundary for the LCA assessment at building level

To quantify the environmental and economic impacts, all the information related to the life cycle phases has been translated into material and energy flows. These flows were then utilized to construct life cycle inventories. Subsequently, these inventories were converted into environmental and economic results. The environmental impacts were calculated using the LCA software GaBi [120] and the professional database ecoinvent 3.6 [121]. The calculation of environmental impacts followed the indicators and methods specified in the amended standard EN 15804 [118]. The result of the life cycle inventory for both case studies are shown in Appendix A. By employing these software tools and adhering to standardized methodologies, the study ensures a rigorous evaluation of the environmental implications associated with the analysed components and buildings throughout their life cycles.

In the context of Life Cycle Costing (LCC), the economic impacts are expressed in monetary units. Different stakeholders are involved at various stages of the supply chain, each with their own costs and gains. For this thesis, a single perspective has been adopted, assuming that the component producer corresponds to the building contractor. The assessment does not include the influence of capital expenditures (CAPEX) since the actual production volume is limited. It is

challenging to evaluate the direct impact of CAPEX on the final cost under such circumstances. However, as the production volume increases, the contribution of CAPEX is likely to become negligible. With reference to the building level, considering the contractor's point of view, equipment as such as cranes could be considered as CAPEX, but due to lack of the reliable information, they have been excluded from the study.

The ML-based surrogate modelling is an iterative process. In general, a huge amount of data is needed to train the ML algorithm. Since that kind of data is not widely available even for conventional structures and especially for the buildings equipped with new MYDs, it must be generated synthetically via FEM simulations. Then, for each of the generated structural configurations, NLTH analysis is performed to get the structural seismic response. SAP2000 [122] FEM software has been chosen for this purpose due to its wide seismic analysis capabilities and convenient Application Programming Interface (API). The data is generated for 4 building frame types which are then considered in the optimisation tool:

- MRF.
- MRF equipped with new MYDs.
- CBF.
- CBF equipped with new MYDs.

Due to the time-consuming nature of NLTH analysis and regular plan configurations of the buildings in the optimisation tool, 2D FEM analyses were executed instead of 3D. The 2D models have been validated with studies found in literature [123], [124] to ensure that the results of FEM analysis are reliable. After the data is generated, ML model training starts according to the workflow explained in Figure 7. The trained model is validated by checking its error and comparing it to the predefined threshold. In this study, the error metric is Mean Absolute Percentage Error (MAPE) and the threshold is 10% on average between all types of structural response. If the error is above the threshold, the sample space gets updated which in the context of this thesis means more data is being generated. Otherwise, the procedure stops, and the obtained ML model is treated as a final one. The whole procedure is explained in detail in chapter 5.

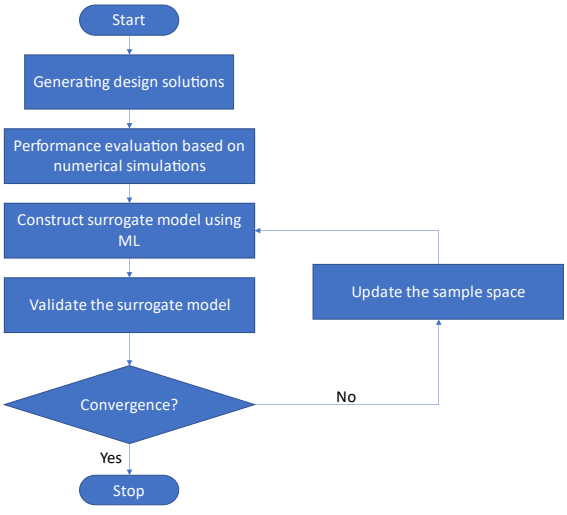

Algorithm: ML-based surrogate modeling

Input: Initial number of design solutions N, convergence rule O

1. Generate an array of design solutions $P_t = \{X_1, \dots, X_N\}$, where each design solution $X = \{x_1, \dots, x_n\}$, set $t = 0$
2. Evaluate the performance of each design solution $f = \{f(X_1), \dots, f(X_N)\}$
3. Construct the surrogate model $\hat{f}$ using ML
4. Evaluate the performance of the surrogate model $O(\hat{f})$
5. **If** $O(\hat{f})$ unsatisfies O
6. Update the design sampling
7. Repeat Step 2 to Step 4
8. $t = t + 1$
9. **Else**
10. **return** $\hat{f}(X)$
11. **End If**

Output: Surrogate model $\hat{f}(X)$

Figure 15. The flowchart of the ML based surrogate modelling process and corresponding algorithm

These surrogate models are then used within the optimisation tool to perform structural design of generated buildings and ensure that they can sustain the given seismic action. It must be noted that surrogate models can accurately predict the response of the structures withing defined geometric and earthquake loading ranges (indicated in chapter 5). Therefore, the design space for the optimisation procedure is restricted according to these ranges.

The final deliverable of this PhD project is a web-based optimization tool SUSTEZ (Sustainable Structures in Earthquake Zones) that synthesizes all preceding research phases and presents the thesis's results in an interactive way. It has a user interface that allows the user to insert the necessary inputs such as building geometry, material grades, gravity and seismic loading parameters, unit cost of materials, etc. Then, a huge set of all possible structural configurations is generated, i.e., the design space is created. All the structures in the design space have optimised cross-sections. As it was stated in the previous paragraph, the geometry of generated buildings is restricted by the surrogate model's limitations. The generated buildings are analysed and designed with the use of ML-based surrogate models, after which life-cycle cost and embodied carbon are calculated to launch multi-objective optimisation search through the entire design space. The aim of this search is to create a pareto front of the most optimised design solutions for the engineer to choose from. The resulted structures are ranked according to non-dominated sorting procedure and solutions with the highest ranks are shown to the user. It involves the partitioning of the population into subpopulations based on their dominance ranks. The procedure begins by assigning a rank of 1 to the non-dominated set of solutions, followed by iteratively assigning subsequent ranks to the remaining solutions based on their non-dominated status until all solutions are ranked (Figure 16)

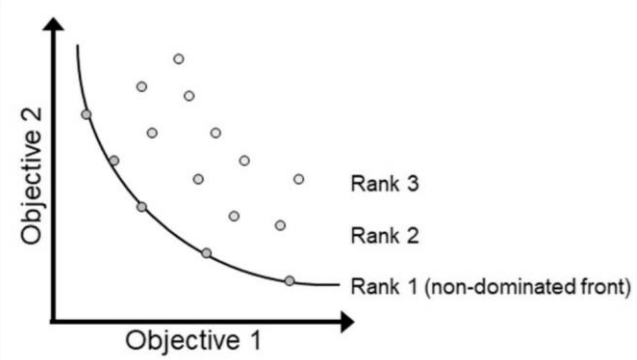

Figure 16. Non-dominated fronts [125]

Eventually, the engineer (final user) is able to compare the cost and embodied carbon of different lateral load resisting systems and quantify the impact of inserting new MYDs into them ensuring a truly data-driven design. Therefore, SUSTEZ performs both local (cross-sectional) and global (layout) structural optimisations. The details of the optimisation tool creation and capabilities are given in chapter 6.

4 Experimental, LCA and LCC data collection from physical tests and numerical calibration

This PhD thesis is based on experimental results, and Life Cycle Analysis (LCA) performed on buildings equipped with MYDs within EU-funded DISSIPABLE project [8]. The following MYDs have been analysed:

- Dissipative Repairable Beam Splice (Figure 17. a, c).
- Dissipative Repairable Bracing Component (Figure 17. b, d).

Dissipative Repairable Beam Splice (DRBeS) was introduced during the FUSEIS [126] project and resembles "replaceable plastic hinges" for moment-resisting frames. Depending on the type of connection this damper is divided into two systems: bolted or welded beam splices. In this research the focus is given to the bolted beam splice. It consists in a cross-sectional weakening located at the beam ends at a certain distance from the beam-to-column connections (Figure 17. a, c), avoiding in this way potential brittle failures at the welds. It acts as dissipative seismic fuse, forcing the plastic hinge to develop at the fuse through concentration of inelastic behaviour, preventing the spreading of damage into the beams and columns. DRBeS achieves seismic resistance performance by introducing a discontinuity on the composite beams of a moment resisting frame and assembling the two parts of the beam through steel plates bolted to the web and flange of the beam. The connections between the steel plates and the beams are obtained by means of high strength friction grip (HSFG) bolts. The part of the beam near the connection is reinforced with additional steel plates welded to both web and flange of the beam.

Dissipative Repairable Bracing Component (DRBrC) is the optimized version of the pin device from INERD [127] project. DRBrC corresponds to a pin component mounted in the bracing system within a box connecting a bracing element with a column, as shown in Figure 17. b. The concept of this connection is a pin that is subjected to four-point bending which behaves in a relatively simple and predictable way (that can be related to a beam), dissipating earthquake energy through its yielding and failing due to low cycle fatigue, by an accumulation of permanent plastic deformations.

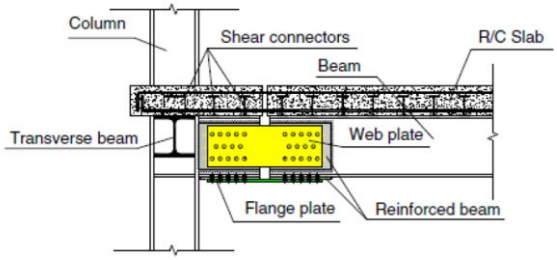

a. DRBeS

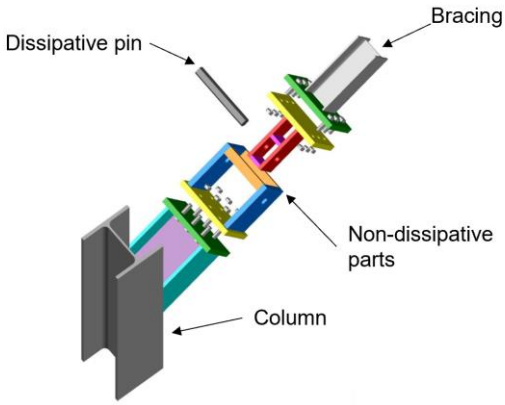

b. DRBrC

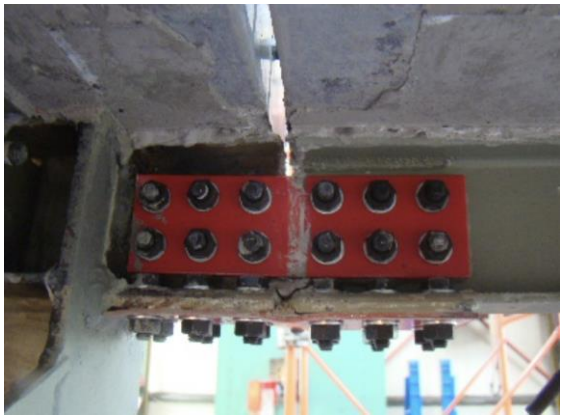

c. Deformed DRBeS

d. Deformed DRBrC

Figure 17. MYDs

4.1 Experimental campaign and calibration

The numerical models for these MYDs have been calibrated by use of experimental campaign. The purpose of this task was to experimentally investigate the dynamic behaviour of the pilot buildings with DRBeS and DRBrC subjected to biaxial lateral earthquake ground motions. Then numerical models have been developed and calibrated according to these test results. 2D hybrid tests were performed by University of Trento (UNITN), while within this PhD thesis a couple of 3D shaking table tests were designed and calibrated. In particular:

- 3D shaking table tests of 2-storey half-scale building (Figure 18. a);
- 3D shaking table tests of 2-storey half-scale building with 5% of mass eccentricity in both principal structural directions (Figure 18. b);

a. Test specimen without mass eccentricity

b. Test specimen with 5% mass eccentricity

Figure 18. 3D shaking table specimens

Both tests were performed at the Laboratory for Earthquake Engineering (LEE) of the National University of Athens (NTUA). The experimental investigation of the seismic response has been performed on 1:2 scale, two-storey 3D steel concrete composite specimens with MYDs, subjected to biaxial lateral earthquake ground motions. The examined structure was a moment resisting frame equipped by DRBeS in one direction and braced frame with DRBrC in orthogonal direction. For similitude purposes, as the specimen was designed in 1:2 scale, additional masses were placed on each storey. A series of shaking table tests at limit states Damage Limitation (DL), Significant Damage (SD) and Near Collapse (NC) were carried out to examine the response of the building at each limit state.

These structures were numerically modelled in FEM software SAP2000 [122] with the goal to calibrate experimental results with the numerical model and achieve as accurate numerical formulation of MYDs as possible. Furthermore, numerical and experimental structures were subjected to the same accelerograms. The 3D view of the structure in SAP2000 [122] software is presented in Figure 19.

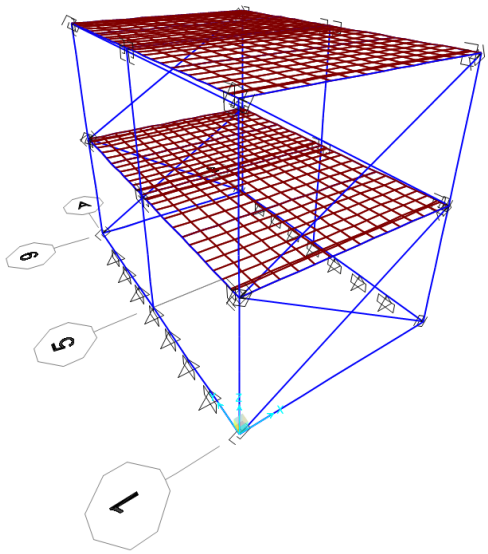

Figure 19. SAP2000 model of shaking table test

The particular attention is given to the slab stiffness, that was taken:

- Full for Damage Limitation (DL) limit state since no cracks were expected.
- 0.5 of full for Structural Damage (SD) limit state. To take into account the effects of cracks as it is proposed in EN 1998-1 [2].
- 0.1 of full for Near Collapse (NC) limit state for the same reason.

The comparison between the test and FE model results for the building without mass eccentricity are presented in two principal directions of the structure (X - MRF equipped with DRBeS, Y – braced frame equipped with DRBrC) in terms of structural periods (Table 3) and base shear – displacement relationship (Table 4 and Table 5).

Limit state	Period X (s)	Period Y (s)
Experimental - DL	0.63	0.42
Numerical - DL	0.59	0.18
Experimental – SD	0.65	0.45
Numerical - SD	0.62	0.18

Table 3. Structural periods comparison

Limit state	MAX displ. (mm)		MIN displ. (mm)		MAX base shear (kN)		MIN base shear (kN)	
	Exp.	Num.	Exp.	Num.	Exp.	Num.	Exp.	Num.
DL	36.55	30.96	-32.99	-29.94	47.26	42.05	-40.51	-40.28
SD	73.56	71.94	-77.30	-57.74	63.90	73.69	-76.11	-71.82

Table 4. Maximum and minimum base shears and displacements in X direction

Limit state	MAX displ. (mm)		MIN displ. (mm)		MAX base shear (kN)		MIN base shear (kN)	
	Exp.	Num.	Exp.	Num.	Exp.	Num.	Exp.	Num.
DL	11.49	2.48	-8.10	-2.76	39.21	36.78	-33.63	-40.02
SD	25.66	5.69	-13.37	-5.70	66.50	59.50	-47.82	-58.05

Table 5. Maximum and minimum base shears and displacements in Y direction

The good correlation is reached in X (MRF) direction of the structure. Therefore, it can be concluded that the stiffness of the structure that is modelled in SAP2000 [122] software and the structural behaviour are close to the tested specimen in X direction. However, in Y (bracing) direction the results are very close in terms of forces and deviate in terms of displacements. FE model is stiffer than the test specimen in this direction. The reason for this difference is the gap between the pin and plates (internal and external) in DRBrC. This gap induces displacement in the component with very low amount of force applied (lower than 1kN). Based on test calibration reports produced by the author and other DISSIPABLE project participants it was decided by all partners of the project to modify an original formulation of DRBrC and include the influence of gap between the pin and the plates by adding a particular value (depending on the size of the gap and geometry of braced frame, Table 6) to global structural displacements per storey for displacement-based checks (interstorey drift, p-delta effects). The values reported in Table 6 were achieved within experimental and numerical investigation during INNOSEIS project. This decision is based on the fact that according to the experience of project's participants, braced systems do not usually have problems with deformability. Therefore, even when global structural displacements are calculated in an approximate way, it will not cause problems with structural safety. The final conclusion of the experimental campaign is that the building with 5% mass eccentricity behaves in a very similar way to the building without any mass eccentricity (Figure 20).

		Diagonal inclination [degrees]						
		30	35	40	45	50	55	60
Additional displacement per floor [mm]	Gap = 0.5 mm	0.82	0.86	0.92	1.00	1.10	1.23	1.41
	Gap = 1 mm	1.63	1.73	1.85	2.00	2.20	2.47	2.83

Table 6. Additional displacement [mm]

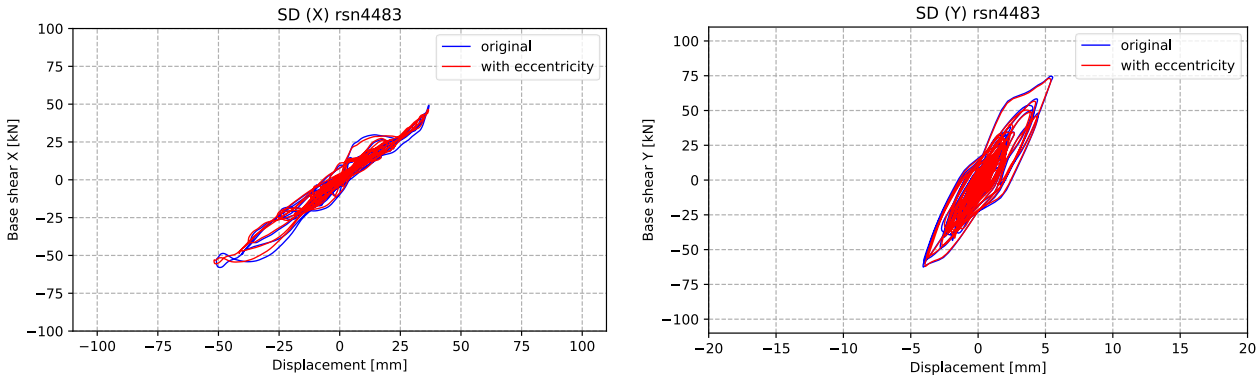

a. Global structural behaviour in X direction

b. Global structural behaviour in Y direction

Figure 20. Influence of mass eccentricity on the global structural behaviour

4.2 Numerical simulations

Based on the test results I calibrated the numerical model of the MYDs and in collaboration with other academical partners of DISSIPABLE project [8] defined the updated design rules and guidelines for them. Then, I performed a parametric study, where I simulated 4 buildings with and without dissipative systems and compare their structural performance during the seismic excitation. Additionally, I performed the Life Cycle Assessment (LCA) and Life Cycle Costing (LCC) of one of the numerically tested structures and compared it with the conventional building's environmental performance in collaboration with (RINA Consulting S.p.A.)

This chapter refers to the seismic design of new six-story composite steel-concrete office building. It aims to demonstrate the implementation of DRBeS and DRBrC components that were tested and calibrated by me within DISSIPABLE project. The elaborated case study comprises the conceptual design, modelling and analysis by nonlinear time history design method (NLTH), design of main dissipative and non-dissipative structural members, and structural detailing of bolted DRBeS and DRBrC components. Moreover, the conventional structure without any DISSIPABLE components is also designed for comparative purposes and called further in the text as "State of the art (Conventional) building".

The steel-concrete composite 6-storey building is regular in plan and elevation. The number of bays in both directions is 3 with a span length of 6.6 m in the X direction and a span length of 5m in the Y direction. The height of each story is equal to 4 m (Figure 21). The gravity frames are composed of composite steel-concrete beams and steel columns, located at each structural axis. Lateral forces in the Y direction are resisted by the moment resisting frames (MRFs) only for Conventional building and MRFs with DRBeS components for DISSIPABLE building. In the X direction lateral loads are resisted by concentrically braced frames (CBF) only for Conventional building and by CBF with DRBrC components for DISSIPABLE building. In this respect, beam-to-column joints and column bases are assumed as fully fixed in the Y direction and nominally pinned in the X direction. The concrete slab with a thickness of 130mm made from C25/30 concrete with B500

reinforcement is used. The structural geometry and slab's thickness were adopted from 3D shaking table tests to obtain the consistency between experimental campaign and numerical simulations.

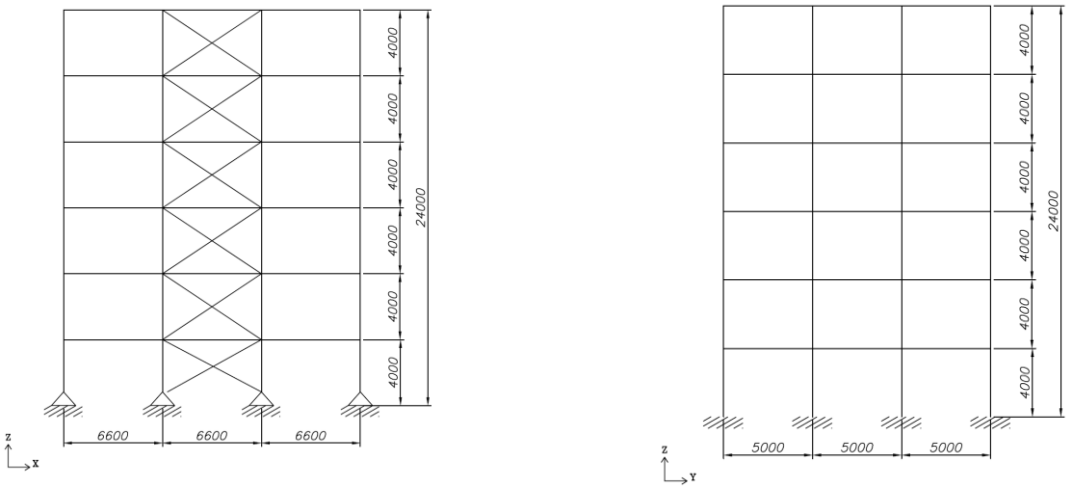

a. CBF in the X direction

b. MRF in the Y direction

Figure 21. Structural geometry in both directions

Both DISSIPABLE and Conventional are subjected to the same set of 7 accelerograms for 3 limit states (DL, SD and NC) to perform the NLTH analysis. The selection of seismic records considered as far as possible the regional tectonic environment, earthquake magnitude, source-to-site distance, and local conditions of the recording site, relevant for the return period of the seismic actions of interest. The criteria for the search of accelerograms used in this study are presented in Appendix B. Due to scarcity of appropriate records on soil category A, the database search was broadened to include soils with site category B. The spectral accelerations of the selected accelerograms is compatible with the elastic response spectrum (Appendix C) in the period range from $0.2T_1$ to $1.5T_1$, where T1 is the fundamental period of the structure in the direction where the base motion is applied. All the recorded accelerograms were selected from the NGA-West2 PEER database [128] and the ESM database [129] and scaled by National Technical University of Athens (NTUA). Moreover, the gravity loads acting on both structures are the same. The used accelerograms can be found in Appendix D.

Both buildings are modelled with frame and shell type elements, using the SAP2000 [122] software. Diaphragm constraint is applied on each floor. The slab behaviour is simulated by means of thin shell element. The reduction of concrete stiffness by half is applied according to EN 1998-1 [1] to simulate the possible cracks in the slabs during the earthquake. The composite beams are modelled by means of the section designer command offered by SAP2000 [122] with the effective width of the composite section corresponding to EN 1998-1 [1]. Plastic hinges are placed in main beams', bracings', and columns' ends to check if they stay elastic during the analysis. P-delta effects was considered explicitly during the structural analysis by SAP2000 [122] software. DRBeS are simulated by plastic links with pivot hysteresis. DRBrC are simulated by plastic links with kinematic hysteresis Both structures were designed in a way to respect capacity design rules of EN 1998-1 [1] and DISSIPABLE design guidelines for the dissipative composite steel-concrete buildings developed within my PhD. Overall, in the DL limit state no damage was observed in both buildings while in the SD limit state main beams and braces yielded in the Conventional building (Figure 22 a, c), and only DRBrC and DRBeS components yielded in the DISSIPABLE building (Figure 22 b, d) which makes this structure highly and easily repairable after the major seismic event. The interstorey drifts diagrams can be found in Appendix E. The legend for Figure 22 is explained in Appendix K.

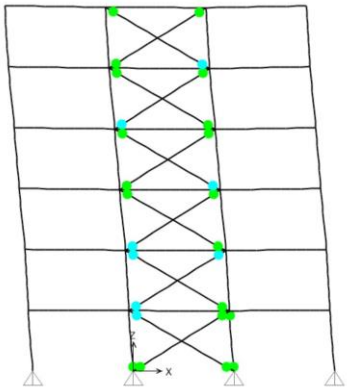

a. Maximum deformation (envelope) and yielded elements in X direction in the SD limit state for the Conventional building

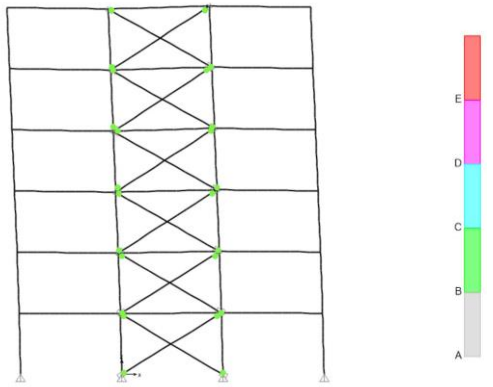

b. Maximum deformation (envelope) and yielded elements in X direction in the SD limit state for the DISSIPABLE building

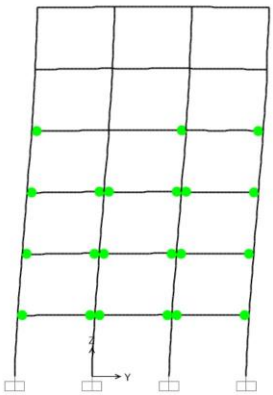

c. Maximum deformation (envelope) and yielded elements in Y direction in the SD limit state for the Conventional building

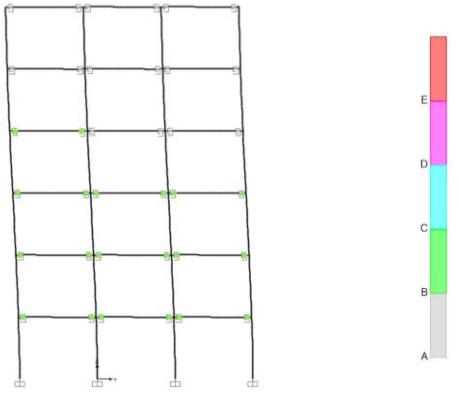

d. Maximum deformation (envelope) and yielded elements in Y direction in the SD limit state for the DISSIPABLE building

Figure 22. Deformed shape envelopes and yielded elements for the SD limit state for both buildings

4.3 LCA and LCC analyses results

The data regarding MYDs' manufacturing, results of 3D shaking table tests, and numerical structural analysis have been sent to RINA Consulting S.p.A for LCA and LCC analyses. In particular, the manufacturing data has been collected from SOFMAN and integrated into life cycle inventory (Appendix A). While the time required for repairability has been measured during experimental campaign. The repairing and reassembling procedures were included into experimental campaign (Figure 23) and the outcomes of these experiments are incorporated into life cycle inventory used for LCA and LCC analyses. Moreover, the guidelines of how to repair these dampers have been developed [8].

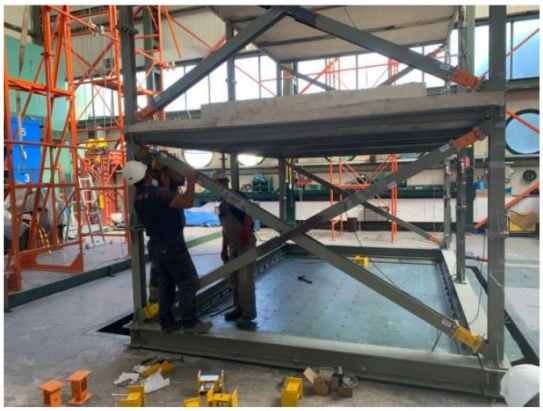

a. Replacement of DRBrCs

b. Replacement of DRBeS

Figure 23. Replacement of MYDs

The purpose was to create a comparative analysis between Conventional and DISSIPABLE buildings to understand the difference in environmental and economic metrics. The following assumptions of the study are considered:

- Although the foundation types of Conventional and DISSIPABLE buildings could be slightly different, only the unburied parts of the building are considered, and the foundations are not included in this study. In addition, only the structural parts of the buildings are considered, and the not/structural ones are considered out of scope.
- No difference is considered during the use phase (in terms of energy consumption of the buildings). Consequently, this phase is excluded from the assessment.
- For the assessment at building level, the average lifespan (RSP) of the building has been assumed at 50 years.
- It has been assumed that 1 seismic event could occur during the 50 years. Consequently, the Life cycle phases of building have been modelling according to the following time scale (Figure 24):
    - Year 0: Both Buildings, Conventional and DISSIPABLE are manufactured; the lifespan of buildings should be 50 years.
    - Every 5 years: maintenance operations on steel structures.
    - Year 30: Seismic event occurs.
    - Conventional building is demolished and reconstructed. The lifetime of new building is 50 years.
    - DISSIPABLE building is repaired accounting the replacement of seismic devices. It is considered that the performance of the repaired structure is equal to the to the previous one (Pre-earthquake): the lifetime of building is extended at 50 years.
    - Year 80: Both structures should be demolished considered the end of the lifetime.

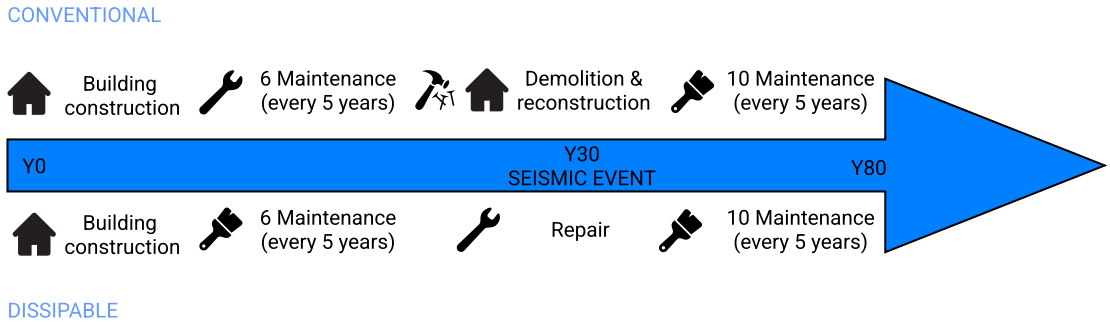

Figure 24. Scenarios for the LCA and LCC analyses

In general, the data use to model the scenarios have been collected in the following ways:

- Directly measured:
  - Consumption for the MYDs production (from steel manufacturer).
  - Consumption for the MYDs repair (from laboratory tests).
- Calculated:
  - Amount of material for the building construction.
- Estimated, based on the experience of the technicians:
  - Consumption for the maintenance of the building (from the contractor of the test specimens).
  - Costs for materials, energy, waste management for both dissipative components and building (using the data from the contractor's practice for the year 2022).

The LCA and LCC analyses has been performed according to the current standard and norms [118], [130], [131]. Figure 25 shows that the environmental impact (embodied CO_2) and cost related to the construction of the DISSIPABLE buildings are higher due to the higher amount of necessary steel (for the structural frame). However, the impacts associated to the repair/ substitution of the device after the seismic event are quite limited: for this reason, when comparing the necessity to demolish and re-construct the Conventional building after a seismic event, the overall life cycle impacts are lower for the DISSIPABLE buildings.

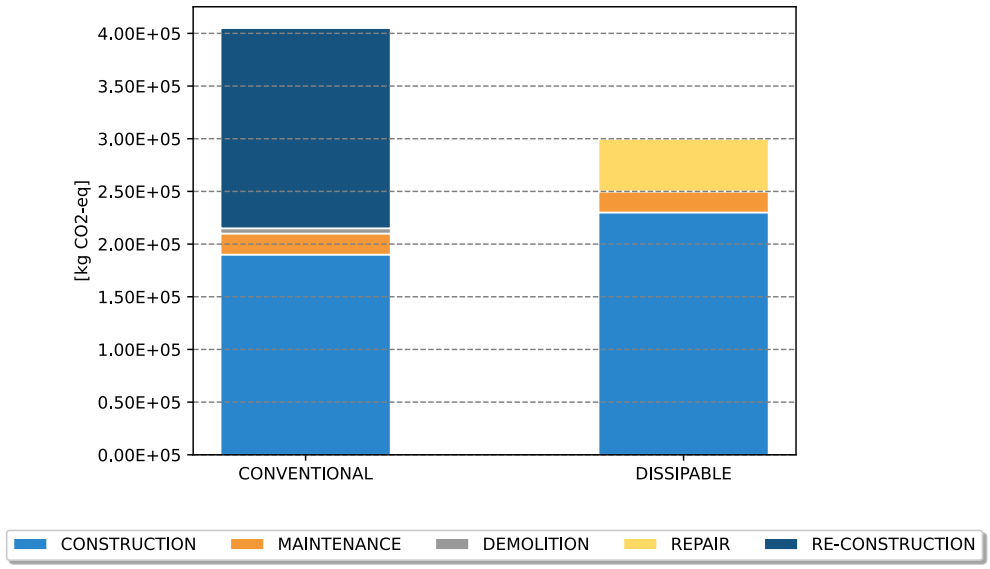

a. Comparison in terms of embodied CO_2

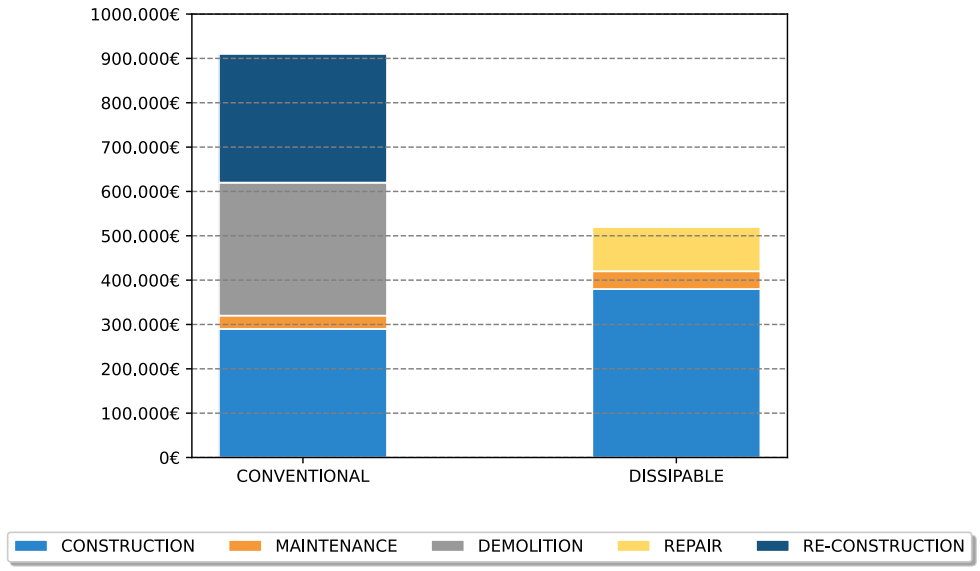

b. Comparison in terms of cost

Figure 25. LCA and LCC analyses results

4.4 Discussion about experimental campaign and comparative LCA and LCC analyses

The following conclusions can be reached based on the results presented in this chapter:

- The empirical formulations of MYDs have been approved by shaking table tests. Therefore, it can be concluded that the resulted FEM models are on agreement with an experimental campaign.
- Including repairability in the analysis allowed for a more accurate assessment LCC and LCA impacts of structures. MYDs can be replaced or repaired after a seismic event without necessitating extensive demolition or reconstruction of the entire structure. The experimental campaign allowed to accurately assess the monetary and environmental impacts of repairability.
- The case study showed that thanks to the MYDs' repairability DISSIPABLE buildings are cheaper than conventional buildings (by 45%) and emit less embodied carbon (by 25%). However, these results are applicable for the whole life-cycle of the building considering one

seismic event happening within its life. Due to the relatively low cost and environmental impact of MYDs' repair DISSIPABLE buildings can be considered beneficial to their conventional counterparts where the reconstruction of the whole building is needed.

5 Training and deployment of ML-based surrogate models

In this chapter the process of creating ML-based surrogate models to predict the results of NLTH analysis is presented. It starts with a detailed explanation of synthetic data generation in FEM software where also the boundaries of the model's application are discussed. It continues with the details about ML model training and its accuracy. Finally, the information about model's deployment is given. The key success criteria considered in developing these models include:

- Accuracy: Ensuring the surrogate models can accurately predict the nonlinear seismic response by training them on a comprehensive dataset generated from detailed FEM analyses (10% mean error percentage threshold was established).
- Speed: The models are designed to deliver quick predictions, reducing the time needed for nonlinear seismic analysis from hours to minutes.
- Generalizability: The models are trained using a wide range of input parameters (e.g., structural geometry, material properties, seismic loading conditions) to ensure they can generalize well to different structural configurations.

5.1 Synthetic data generation

The data for training of ML-based surrogate models have been generated synthetically via API of SAP2000 software [122]. Figure 26 shows the general flowchart of this process applied to one frame.

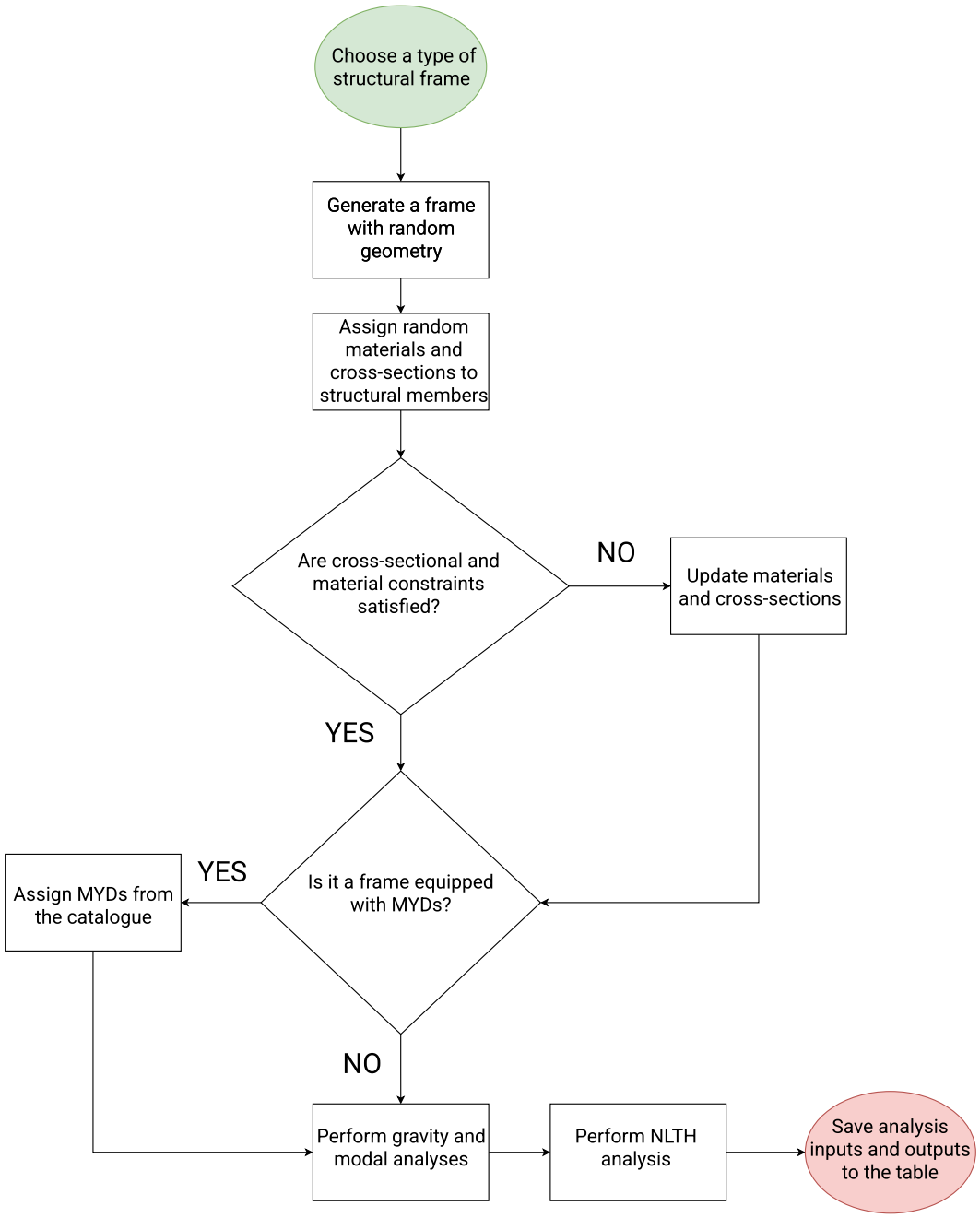

Figure 26. Data generation flowchart

First, the type of frame is chosen from the following options:

- Typical MRF
- MRF equipped with DRBeS
- Typical CBF
- CBF equipped with DRBrC

Secondly, the frame with a random geometry is generated. Each parameter and its boundaries are shown in Table 7. These boundaries were chosen to be big enough to allow a large set of realistic structures during the design space generation while also not being too big to violate the accuracy of ML models. To generate the frame, the random value was sampled from each of the geometric variables.

Geometric variable	Minimum value	Maximum value	Step
Number of spans	1.0	6.0	1.0
Span width [m]	3.0	8.0	1.0
Number of floors	1.0	6.0	1.0
Floor height [m]	3.0	4.0	0.5

Table 7. Geometric boundaries

Then, the random materials and cross-sections from all the possible options (Table 8) are assigned to each generated frame element. The decision to generate random structures instead of using a set of pre-designed ones is made to give ML model an opportunity to better learn structural behaviour dealing with under and over designed buildings as well. In the engineering practice, it is common to start with not optimal solution and then iteratively find the best one. Therefore, ML model must correctly also predict the initial guesses that can be far from the optimal designs. Nevertheless, to ensure that generated structures are at least realistic, the choice of cross-sections is guided by constraints. First of all, they were grouped by floors and assigned to elements according to the height distribution indicated in Table 8. Additionally, lower and upper boundary constrains are applied to columns and beams cross-sections. Regarding lower boundary constraint, it is ensured that columns and beams can withstand the acting gravity loads. The preliminary bending moment (for beams) and axial forces (for columns) calculations are performed using simplified engineering formulas and the obtained actions are compared with the resistance of a randomly assigned cross-section. If the check is not passed, the cross-section is increased until its resistance is bigger than acting force. For the upper boundary, the arbitrary value is chosen to avoid having too large cross-sections for small frames. Regarding the material, the constraint is implemented to verify that neither beam's nor bracing's steel grade exceeds the one of a column. It is implemented to satisfy the dissipative behaviour of a frame according to Eurocode 8. The typical S235, S275, and S355 material grades are available for the random choice.

Structural element	The smallest cross-section	The biggest cross-section	Distribution along the height	Upper boundary
Column	HEA100	HEM1000	Each 3 floors decrease the cross-section size	Max. HEA550 if the frame has 3 floors or less
Beam	IPE80	HEA700	The same along the height	Max. IPE600 if the frame has 3 floors or less
Bracing	CHS 76.1 / 3.2	CHS 711 / 8.0	Each 2 floors decrease the cross-section size	Max. CHS 168.3 / 4.0 if the frame has 2 floors or less. Max. CHS 457 / 8.0 if the frame has 4 floors or less

Table 8. Cross-sectional boundaries

The next step is to assign MYDs if the frame should be equipped with them according to the initial choice. DRBeS is assigned in the vicinity of beam ends while DRBrC is inserted between the bracing and the column. Both dampers are modelled as link elements with the nonlinear behaviour obtained and validated via experimental campaign and reported in previous chapter briefly and the DISSIPABLE guidelines in detail [132]. According to these guidelines, their initial dimensions depend on the connected structural member (beam or bracing). Therefore, the catalogue has been created where for each available beam and bracing cross-section there is a predefined MYD. The example of one randomly generated structure with elements' cross-sections for each type of frame is shown in Figure 27.

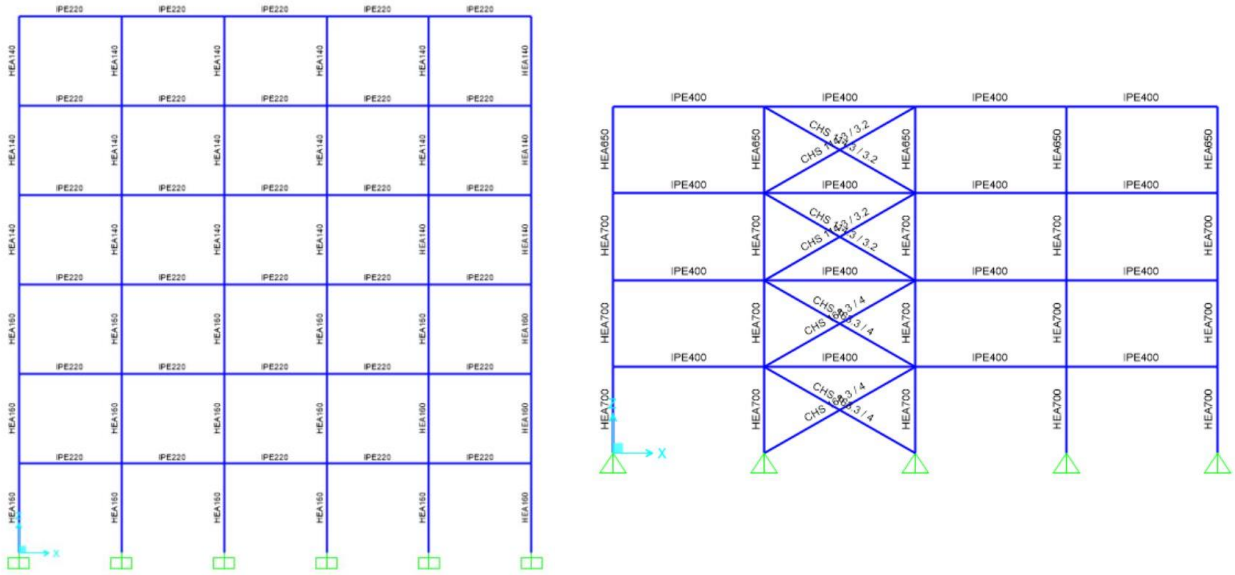

a. MRF b. CBF

Figure 27. Example of randomly generated structures

Live, self-weight, superimposed dead, and facade loads are considered as gravity loads acting on the frame. The range for the load quantity is shown in Table 9. These loads are applied as distributed loads acting on beams except for the case of self-weight dead load that is automatically applied by the FEM software. The value of the gravity loads is randomly taken from Table 9 and for superimposed dead and live loads multiplied by the tributary width for the gravity loads from Figure 28. The span width out of plane for tributary width calculation is randomly taken from the

range indicated in Table 7. Then, the modal analysis is performed considering maximum 12 structural modes.

Gravity load type	Minimum value	Maximum value
Superimposed dead [kN/m^2]	1.0	6.0
Live [kN/m^2]	1.0	5.0
Facade [kN/m]	0.0	4.0

Table 9. Gravity loads boundaries.

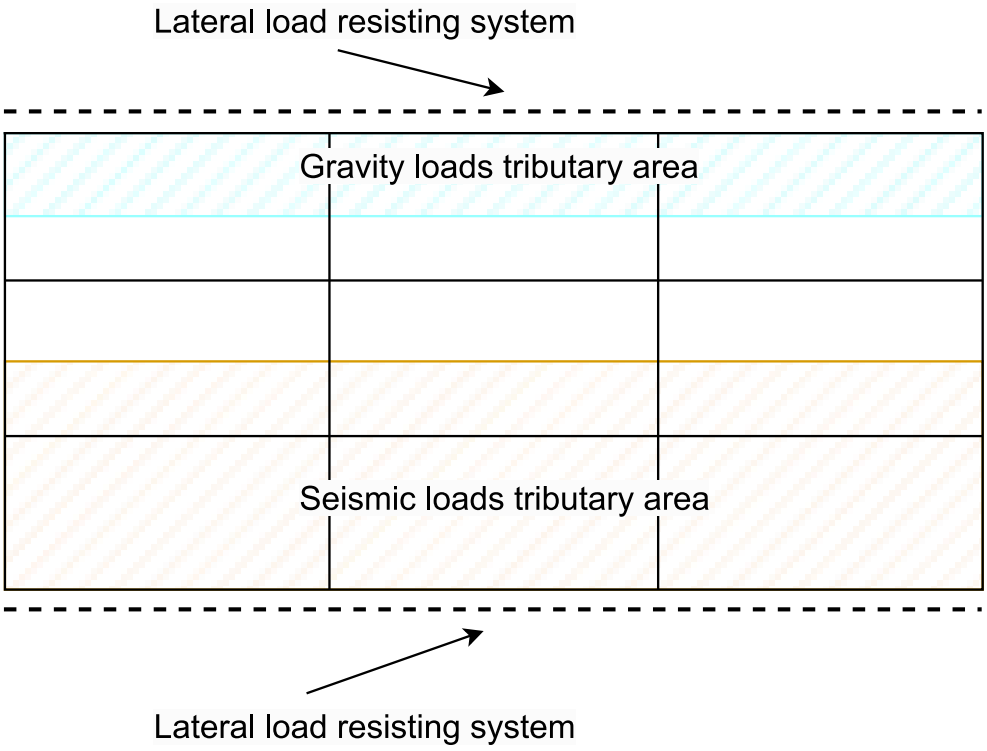

Figure 28. Building plan. Tributary areas for gravity and seismic loads for 2D frames extracted from 3D building.

After the gravity and modal analyses are finished, NLTH analysis starts. It uses deformed shape and stiffness matrix from gravity analysis to realistically replicate the initial building conditions when the earthquake arrives. Nonlinear behaviour of structural elements is simulated via plastic hinges assigned to columns, beams, and braces. The exact formulation of plastic behaviour is automatically taken from American design codes [3] by SAP2000 software [122]. P-delta effects are included during NLTH analysis while 5% damping is assigned to the structure. Rayleigh damping is used while mass and stiffness coefficients are calculated based on first 2 structural periods of the frame calculated during the modal analysis. In order to achieve an accurate approximation of a 3D building seismic structural behavior using 2D frames, the floor mass is calculated according to the seismic tributary area (Figure 28). This mass is assigned to the 2D frame using nodal masses in the structural joints in each floor. To calculate the floor mass, out of plane number of spans and their width is randomly sampled from Table 7. The out of span width is taken the same as for the gravity loads calculations for the consistency purposes. The ground motions used for NLTH analysis are taken from Peer [128], and ESM [129] databases and reported in Table 10. The ground motions are not scaled to any design spectrum since in that case the application would be limited to a particular

location. Instead, accelerograms with a vast variety of ground shaking intensity have been chosen to have a better generalization of an ML model.

Ground motion name	Magnitude	Peak Ground Acceleration [g]	Distance to fault [km]	Shear wave velocity [m/s]
Corinth_ Greece	6.60	0.300	10.27	361.40
Griva_ Greece	6.10	0.100	32.84	551.30
Viktoria, Mexico	6.33	0.150	18.96	242.05
Northridge-01	6.69	0.110	35.66	549.75
Spitak_ Armenia	6.77	0.200	23.99	343.53
Christchurch_New Zealand	6.20	0.150	13.91	649.67
Friuli Italy-01	6.50	0.354	15.82	505.23
Parkfield	6.19	0.123	12.90	256.82
Umbria Marche_ Italy	6.00	0.171	17.28	293.00
Taiwan SMART1(5)	5.90	0.140	25.50	309.41
Landers	7.28	0.283	19.74	352.98

Table 10. Ground motions

Overall, for each frame type 1819 randomly generated structures were subjected to 11 ground motions each which results to 20009 NLTH analyses per frame and 80036 overall. The number of generated structures was obtained by trial-and-error procedure where different number of datapoints for ML training has been generated until the acceptable accuracy of the prediction has been achieved (following the algorithm from Figure 8). The resulting number of structures represents just a tiny bit of the entire space of possible options. Through the application of elementary permutation methodologies, encompassing exhaustive examination of geometric configurations, material properties, cross-sectional profiles, and gravity loads, within the specified ranges indicated in the aforementioned tables, the total combinatorial abundance of structural arrangements amounts to approximately 4.7 billion distinct possibilities. Notably, the utilization of ML techniques proves exceptionally beneficial in this context, as merely a modest subset of the exhaustive permutations, comprising fewer than 2000 generated structures, suffices to achieve an acceptable accuracy in terms of response predictions. Consequently, the ML model's aptitude extends beyond the analysed subset, thereby permitting the approximate determination of response characteristics for all other potential configurations. Overall, it took around 800 hours to generate all the data on a personal computer (36 seconds per one analysis) with 2,8 GHz Quad-Core Intel Core i7 processor and 16 GB 2133 MHz memory. The overall inputs and outputs for each type of frame is shown in Table 11. Since ML models work only with numerical type of values, the elements' cross-sections are encoded as their mechanical properties – moment of inertia and area respectively. Indicated in Table 11 parameters are be used as features (inputs) and labels (outputs) of ML-based surrogate model. Therefore, the range of all the features is reported to get an understanding of its boundaries and applicability. The following outputs are obtained from NLTH analysis:

- Interstorey displacement. The maximum value of an interstorey displacement among all floors of the frame during the seismic excitation. This output can be used to calculate maximum interstorey drift used in global serviceability building checks.
- Axial force in a column. The maximum axial force during the seismic excitation among all 1st storey columns.

- Bending moment in a column (MRF only). The maximum bending moment during the seismic excitation on the most axially stressed column. This and the previous outputs can be used to perform columns seismic design.
- Bending moment in a beam (MRF only). The maximum bending moment during the seismic excitation among all beams. This output can be used to perform beams seismic design.
- Axial force in a bottom bracing (CBF only). The maximum axial force during the seismic excitation among all 1st storey bracings. This output can be used to perform bracings seismic design.

Incorporating a wide range of input and output parameters in machine learning-based surrogate models is crucial for comprehensive modeling, generalizability, and practicality in structural engineering applications, including the development of an accurate and practical optimization tool. A broad set of input parameters ensures accurate capture of complex interactions and behaviors of different structural configurations under seismic loading, leading to more reliable predictions of structural responses. By considering various input scenarios, the models can generalize better to new, unseen configurations, enhancing their applicability to a wider range of buildings. Furthermore, engineers can leverage these models to explore multiple design options quickly, thanks to the comprehensive set of outputs, which helps ensure adequate design of all main frame components, such as columns, beams, and bracings, resulting in practical and efficient solutions. This set of input and output parameters is vital for making an optimization tool like SUSTEZ accurate and practical, enabling efficient exploration and optimization of structural designs for seismic performance.

Inputs					
Feature name	MRF	MRF with DRBeS	CBF	CBF with DRBrC	Range (min-max)
Column Fy [Mpa]	✓	✓	✓	✓	235-355
Beam Fy [Mpa]	✓	✓	✓	✓	235-355
Bracing Fy [Mpa]	×	×	✓	✓	235-355
Columns 1-3 I [mm^4*10^6]	✓	✓	✓	✓	3.49-6447
Columns 4-6 I [mm^4*10^6]	✓	✓	✓	✓	0-5538
Beam I [mm^4*10^6]	✓	✓	✓	✓	1.71-1752
Bracing 12 A [mm^2]	×	×	✓	✓	733-15130
Bracing 34 A [mm^2]	×	×	✓	✓	0-2377.07
Bracing 56 A [mm^2]	×	×	✓	✓	0-1341.76
Number of spans	✓	✓	✓	✓	1-6
Span width [m]	✓	✓	✓	✓	3-8
Number of floors	✓	✓	✓	✓	1-6
Floor height [m]	✓	✓	✓	✓	3-4
MYD's stiffness	×	✓	×	✓	318.55-135357.77 [kNm/rad] for DRBeS 1.37E+05-1.36E+06 [kN/m] for DRBrC
MYD's Yielding limit	×	✓	×	✓	6.24-536.57 [kNm] for DRBeS 43.99-1113.71 [kN] for DRBrC
MYD's Ultimate limit	×	✓	×	✓	3.30-283.36 [kNm] for DRBeS 134.77-3412.20 [kN] for DRBrC
MYD's flange area [mm^2]	×	✓	×	×	210-4000
Number of braced spans	×	×	✓	✓	1-2
Floor mass [kg]	✓	✓	✓	✓	568.99-884936.45
Facade load [kN/m]	✓	✓	✓	✓	0-4
Distributed super-imposed dead load [kN/m]	✓	✓	✓	✓	3-48
Distributed live load [kN/m]	✓	✓	✓	✓	3-40

Peak Ground Acceleration [g]	✓	✓	✓	✓	0.10-0.354
Magnitude	✓	✓	✓	✓	5.90-7.28
Distance to fault [km]	✓	✓	✓	✓	10.27-35.66
Shear wave velocity [m/s]	✓	✓	✓	✓	242.05-649.67
Fundamental period [s]	✓	✓	✓	✓	0.05-10.48 for MRF 0.06-13.08 for MRF with DRBeS 0.04-4.02 for CBF 0.04-5.11 for CBF with DRBrC
Outputs					
Insterstorey displacement [mm]	✓	✓	✓	✓	0.12-287.75 for MRF 0.26-299.33 for MRF with DRBeS 0.10-122.18 for CBF 0.10-232.67 for CBF with DRBrC
Axial force in a column [kN]	✓	✓	✓	✓	6.15-3278.18 for MRF 11.77-2818.89 for MRF with DRBeS 8.96-9468.09 for CBF 13.03-6326.29 for CBF with DRBrC
Bending moment in a column [kNm]	✓	✓	×	×	1.95-3291.59 for MRF 0.76-6484.13 for MRF with DRBeS
Bending moment in a beam [kNm]	✓	✓	×	×	1.82-1455.36 for MRF 9.56-1672.16 for MRF with DRBeS
Axial force in a bottom bracing [kN]	×	×	✓	✓	2.59-3846.45 for CBF 2.96-2559.72 for CBF with DRBrC
Bending moment in DRBeS [kNm]	×	✓	×	×	1.06-532.30
Axial force in a bottom DRBrC [kN]	×	×	×	✓	2.98-2502.57

Table 11. ML model inputs and outputs

5.2 ML models training

The training of ML models follows the general workflow shown in Figure 7. The synthetic data generated by SAP2000 software [122] was used to train ML models to predict the analysis

outputs based on their inputs. To evaluate the accuracy of the trained algorithm, Mean Average Percentage Error (MAPE) is used:

$$MAPE = \frac{1}{n}\sum_{i=1}^{n}\frac{|A_i - P_i|}{A_i}$$

Where:

- n is a total number of observations.
- Ai is an actual value.
- Fi is a predicted value.

This error metric is chosen since it can be easily interpreted by a reader as well as a final user of the tool. In fact, it can be interpreted as "how many percents the prediction deviates from the reality on average". The use of percentages as a unit of measure also eliminates the need to know the mean value of the predicted label to interpret the scale of the error which is present when other error metrics are used, such as Mean Absolute Error (MAE) or Root Mean Squared Error (RMSE). Since there is no way to know which ML algorithm will be the best for the given data in advance, all algorithms proven powerful in the literature have been used and compared (Table 12). Python programming language [133] was used for the models training. The data has been split for training and testing with 95% (19000 datapoints) related to training and 5% (1000 datapoints) to testing data. Stratified by magnitude data splitting was used to verify that in both training and testing data ground motions acting on frames are equally represented. Both training and testing errors are reported to verify the reliability of the training process (testing error is expected to be higher than training one) and check algorithms for a potential overfitting. To increase the accuracy of ML models, instead of training one model to predict all the outputs at the same time, separate models were used for each output. It resulted to 4 ML-surrogates for MRF, 5 ML-surrogates for MRF with DBBeS, 3 ML-surrogates for CBF, and4 ML-surrogates for CBF with DRBrC respectively. Table 12 shows MAPE for all the algorithms with their default parameters. Linear Regression (LR), K-Nearest Neighbors (KNN), Decision Trees (DT), Random Forests (RF), XG Boost (XGB) and Light Gradient Boosting Machine (LGBM) algorithms have been implemented.

Predicted output	Dataset	LR	KNN	DT	RF	XGB	LGBM
MRF							
Interstorey Displacement	Train	121.29	71.53	0.00	4.41	12.73	19.00
	Test	133.28	124.75	10.75	8.06	17.67	18.92
Axial force in a column	Train	54.65	27.82	0.00	5.64	10.0	11.26
	Test	58.76	41.89	22.88	14.85	14.80	13.16
Bending moment in a column	Train	146.98	73.45	0.00	8.64	18.55	23.21
	Test	164.98	114.02	30.59	23.47	28.61	26.17
Bending moment in a beam	Train	81.71	43.7	0.00	7.32	13.57	16.23
	Test	87.95	62.94	28.11	20.60	18.94	18.52
MRF with DRBeS							
Interstorey Displacement	Train	97.04	50.44	0.00	5.94	13.13	19.93
	Test	94.80	69.88	23.58	16.30	20.48	22.36
Axial force in a column	Train	40.65	22.16	0.00	4.18	7.38	8.28
	Test	38.15	31.52	16.11	10.87	10.07	9.14
Bending moment in a column	Train	132.03	73.55	0.00	11.35	22.04	30.76
	Test	126.88	107.12	37.46	30.40	36.73	29.70
Bending moment in a beam	Train	60.19	28.69	0.00	6.34	10.58	13.76
	Test	58.93	38.82	24.04	16.26	13.85	14.76
Bending moment in DRBeS	Train	63.82	29.03	0.00	4.46	8.90	11.68
	Test	63.96	40.47	16.16	11.81	11.16	13.11
CBF							
Interstorey Displacement	Train	107.41	62.42	0.00	3.92	12.19	17.48
	Test	104.94	99.69	13.27	10.03	15.60	17.99
Axial force in a column	Train	96.67	38.74	0.00	5.96	11.39	15.69
	Test	92.90	57.54	22.91	15.41	15.89	16.70
Axial force in a bottom brace	Train	82.12	44.34	0.00	5.79	13.71	18.46
	Test	80.70	65.62	22.03	15.55	17.90	20.11
CBF with DRBrC							
Interstorey Displacement	Train	112.47	55.50	0.00	4.92	14.31	21.52
	Test	110.78	90.84	16.35	11.07	19.32	21.41
Axial force in a column	Train	68.49	30.61	0.00	5.67	9.34	13.06
	Test	59.38	44.09	23.02	15.41	12.93	13.91
Axial force in a bottom brace	Train	57.80	31.69	0.00	4.65	9.15	13.00
	Test	56.03	47.56	18.85	13.00	13.04	14.21
Axial force in a bottom DRBrC	Train	57.21	31.14	0.00	4.50	8.71	13.02
	Test	55.52	46.81	17.56	12.68	12.24	14.49

Table 12. MAPE for training and testing data of various ML models

Following observations can be made from the obtained results:

- RF, XGB, and LGBM algorithms are the most accurate ones for a given problem.
- DT overfitted (fit training data too well failing to generalise on a testing dataset) for all the case studies. It was expected since overfitting is one of main drawbacks of this algorithm.
- LR model failed at this task since this algorithm expects linear dependence between inputs and outputs that is clearly not the case in NLTH analysis.
- KNN also turned out to be too simple for this problem.
- Interstorey displacement predictions have the best accuracy while columns bending moments were the hardest to predict.

Based on the obtained preliminary results, RF, XGB, and LGBM algorithms have been chosen for hyperparameter tuning. It consists of testing different parameters of the algorithm on a given data to find the ones that give the best accuracy. For that reason, a range of parameters is chosen for

each algorithm. For hyperparameter tuning the original training data is used which is further divided for training and validation datasets, where the ML model is fit on training data and tested on validation one. Then, the obtained final algorithm is tested on testing data and results of the testing error are shown in Table 13. Additionally, the Voting Ensemble (VE) algorithm which combines the best 2 ML models for each predicted output is tested. Based on these results the highlighted algorithm is chosen for each ML-based surrogate model and then deployed on the web and into the final optimisation tool.

		MRF		
Predicted output	RF	XGB	LGBM	VE
Interstorey Displacement	8.02	11.25	10.92	**8.14**
Axial force in a column	14.76	9.15	8.05	**7.84**
Bending moment in a column	23.31	15.17	**11.57**	11.65
Bending moment in a beam	20.35	11.66	10.27	**9.95**
		MRF with DRBeS		
Interstorey Displacement	16.14	15.94	14.77	**11.40**
Axial force in a column	10.71	7.03	5.87	**5.76**
Bending moment in a column	31.64	23.53	**11.01**	16.96
Bending moment in a beam	16.04	9.92	8.80	**8.53**
Bending moment in DRBeS	11.77	8.85	7.69	**7.45**
		CBF		
Interstorey Displacement	9.84	13.21	10.89	**9.40**
Axial force in a column	15.38	9.93	9.23	**8.88**
Axial force in a bottom brace	15.45	11.80	11.55	**11.05**
		CBF with DRBrC		
Interstorey Displacement	11.14	15.56	12.21	**10.65**
Axial force in a column	15.34	9.05	8.46	**8.20**
Axial force in a bottom brace	11.45	9.30	8.79	**8.50**
Axial force in a bottom DRBrC	12.59	9.61	8.61	**8.45**

Table 13. MAPE for the best ML algorithms with hyperparameter tuning

The hyperparameter tuning did not give a significant improvement for RF algorithm while it made both XBG and LGBM algorithms much more accurate. VE is the most accurate algorithm in most cases which is expected since it combines the best 2 ML models and uses statistical techniques to get the best out of both at the same time. In frames equipped with MYDs, displacement predictions yielded lower accuracy compared to their conventional counterparts. It can be attributed to their higher range which was shown in Table 11. However, for all other predicted parameters frames with MYDs have higher accuracy compared to conventional ones. The reason for this lies in a high predictability of features associated with MYD (such as stiffness and yielding limit) and discussed in detail in the next subchapter.

Finally, since the data is generated synthetically its amount can be controlled. Therefore, the sensitivity analysis of the amount of data and the resulting MAPE is performed. 5000, 10000, 15000, and 20000 datapoints are used. For the consistency purposes, for each dataset 90% of data is used for training ML algorithms while 10% for the testing. This choice was made since 5% of testing data (used previously) results in too few testing samples to adequately evaluate the performance of algorithms applied on data with 5000 and 10000 datapoints. The resulting testing MAPE for the best ML model for each predicted output is shown in Table 14.

MRF				
Predicted output	5000 datapoints	10000 datapoints	15000 datapoints	20000 datapoints
Interstorey Displacement	13.17	9.75	8.90	7.83
Axial force in a column	11.39	8.73	7.96	7.87
Bending moment in a column	19.55	14.51	13.13	11.85
Bending moment in a beam	15.36	12.46	11.13	10.18
MRF with DRBeS				
Interstorey Displacement	19.38	15.24	14.54	11.94
Axial force in a column	8.08	7.11	6.19	5.73
Bending moment in a column	17.19	14.46	12.32	11.34
Bending moment in a beam	13.01	11.31	10.31	9.37
Bending moment in DRBeS	11.24	8.84	8.26	7.65
CBF				
Interstorey Displacement	15.67	11.61	10.75	9.90
Axial force in a column	12.75	10.32	9.55	8.86
Axial force in a bottom brace	16.74	14.16	12.12	10.95
CBF with DRBrC				
Interstorey Displacement	15.38	14.10	12.09	10.68
Axial force in a column	10.19	9.69	8.50	7.81
Axial force in a bottom brace	11.45	10.26	8.79	8.35
Axial force in a bottom DRBrC	11.12	9.89	8.75	8.24

Table 14. The dependence of MAPE on the amount of data

The increase of the amount of data improves the accuracy of ML models for all the outputs. However, when MAPE becomes small (lower than 10%), the increase of the size of the data does not substantially reduce the error anymore.

5.3 ML models interpretation

Even though LGBM and VE models are the most accurate for the NLTH analysis prediction, they are hard to interpret. They are based on the simple concept of decision trees, but due to the complex math applied to proceed from basic decision trees to these advance algorithms it can be extremely difficult to understand why model gives a particular prediction given a particular set of inputs and which inputs affect the outputs more than others. To solve this issue and improve the explainability of ML models, SHAP (SHapley Additive exPlanations) values are used [134]. It is a method of explaining the predictions of ML models by decomposing the prediction into the contribution of each feature or input variable [135]. The SHAP value for a feature represents the difference between the expected model output and the actual model output when the feature is included in the prediction, compared to when it is excluded.

SHAP values are based on the Shapley value, a concept from cooperative game theory that assigns a value to each player in a coalition based on their marginal contribution to the coalition's total value [136]. In the context of ML, the players are the features, and the coalition is the set of features used in the prediction. SHAP values have several advantages over other methods of interpreting ML models. They are model-agnostic, meaning they can be applied to any black-box model, and they provide local explanations that are specific to individual instances rather than global explanations that apply to the entire dataset. Additionally, SHAP values are consistent, meaning that they satisfy a set of desirable properties for feature attribution methods.

Figure 29, Figure 30, Figure 31, Figure 32 show a global and local SHAP values for each of the ML-based surrogate model for MRF. Results of global analysis are shown via summary plots where the most important features for the prediction of each output are located from top to bottom. Additionally, the colourmap indicates how the increase or decrease of feature value affects the prediction. For the local analysis waterfall plots are used. They show the importance of each feature on the chosen datapoint. In particular, they indicate how starting from expected value (mean value of all predictions for the entire dataset – E[f(x)]) the model arrives to its final prediction – f(x) and how the value of each feature impacts this prediction. For instance, Figure 29, b shows how starting from expected value of interstorey displacement equal to 19.96 mm each important feature contributed to the final prediction of 14.12 mm which is very close to the original value of 14.10 mm. The original value is indicated on the top of each local analysis plot to show the accuracy of the chosen prediction. Regarding global analysis, Figure 29, a is an example of structural period being the most predictive features of all for interstorey displacement prediction. The x axis consists of dots where each dot corresponds to SHAP value (numbers indicated inside the bars for each feature in Figure 29, b).

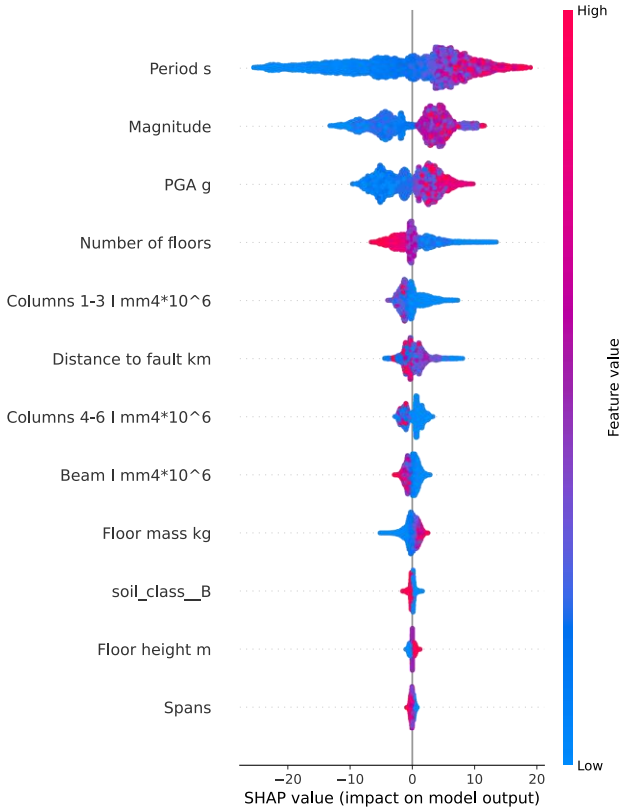

a. Interstorey displacements global analysis

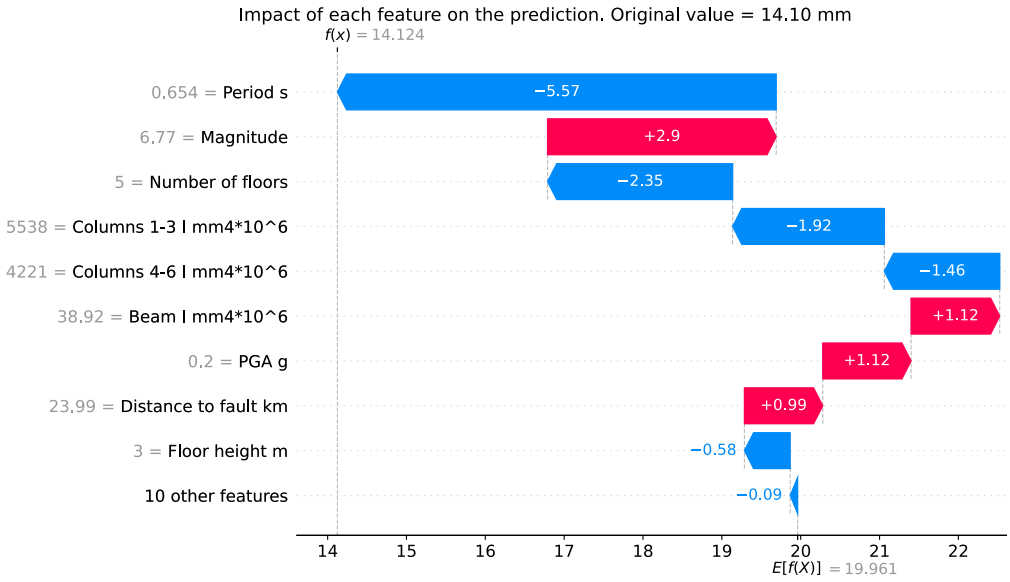

b. Interstorey displacements local analysis

Figure 29. SHAP analysis for ML model used for MRF interstorey displacement prediction

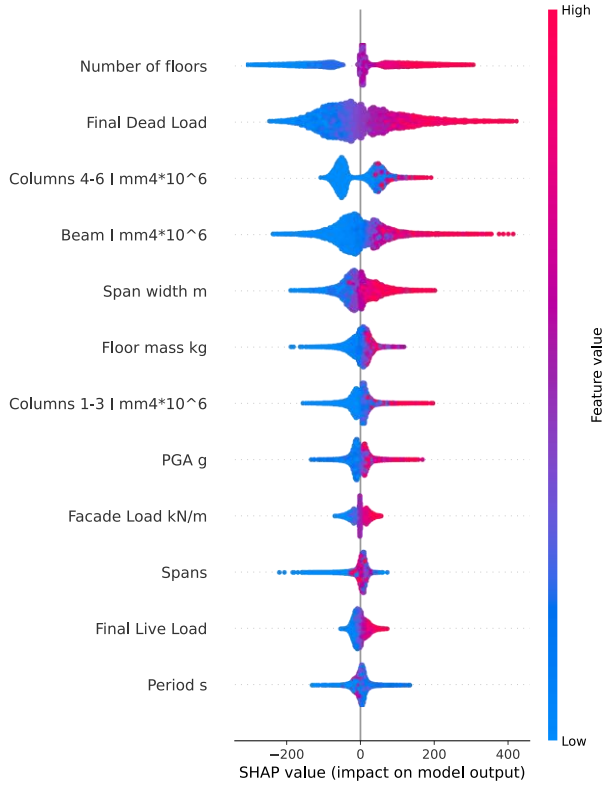

a. Column axial force global analysis

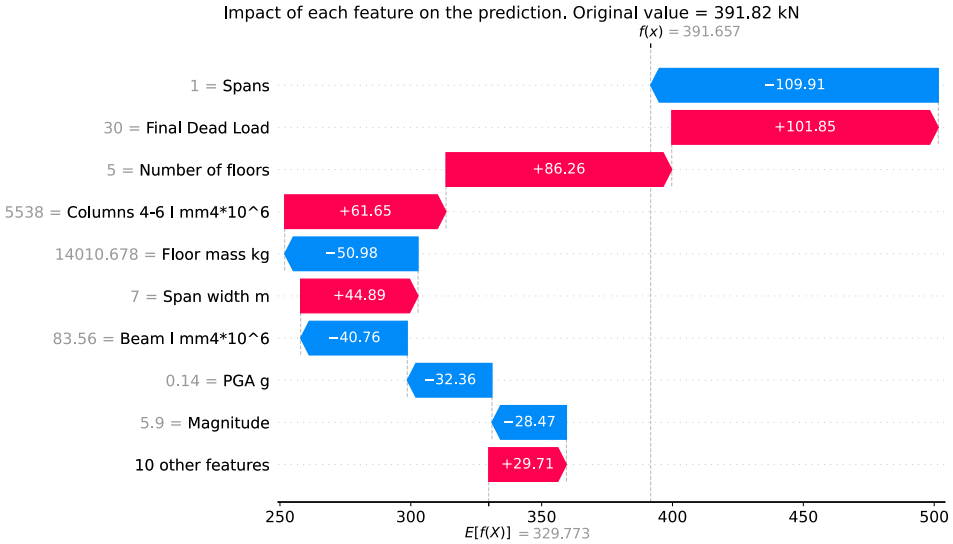

b. Column axial force local analysis

Figure 30. SHAP analysis for ML model used for MRF column axial force prediction

a. Column bending moment global analysis

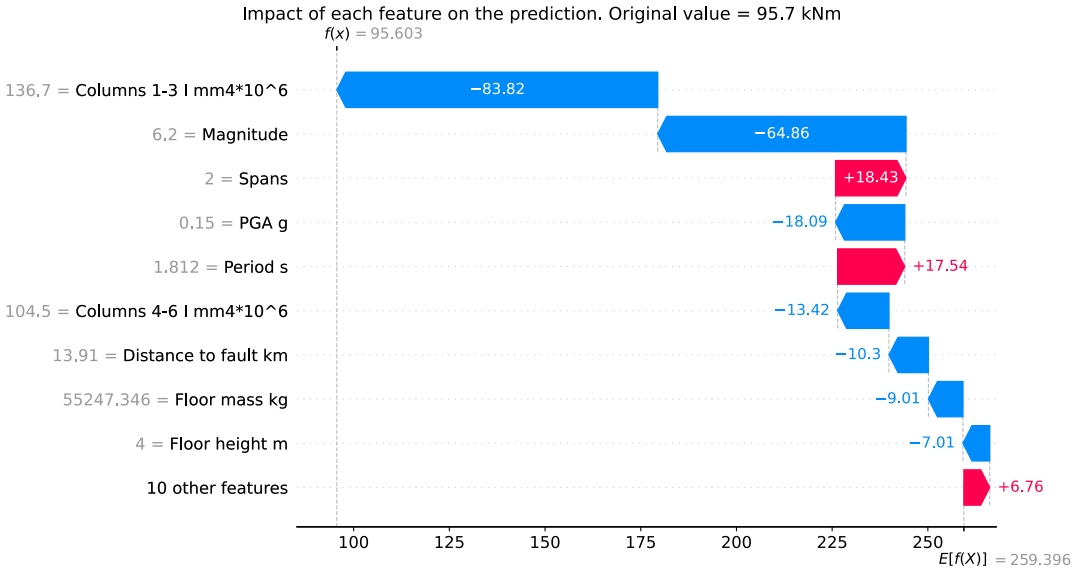

b. Column bending moment local analysis

Figure 31. SHAP analysis for ML model used for MRF column bending moment prediction

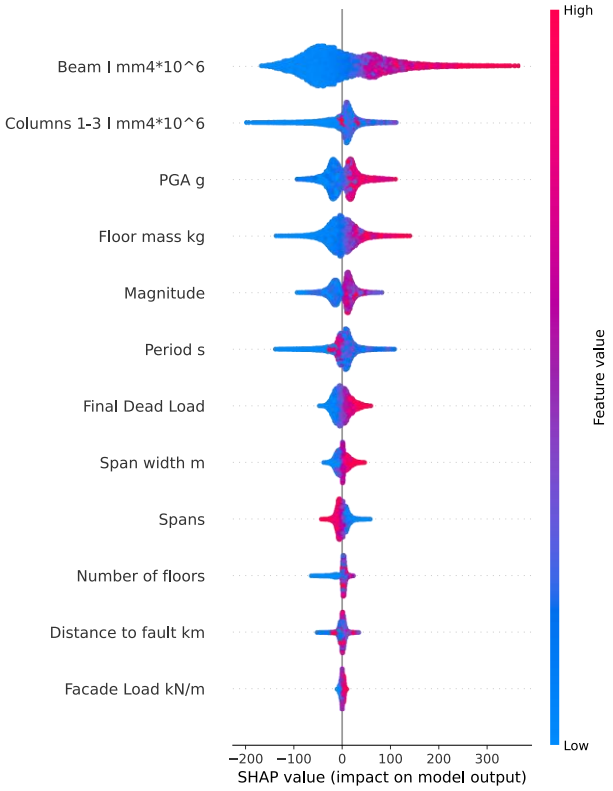

a. Beam bending moment global analysis

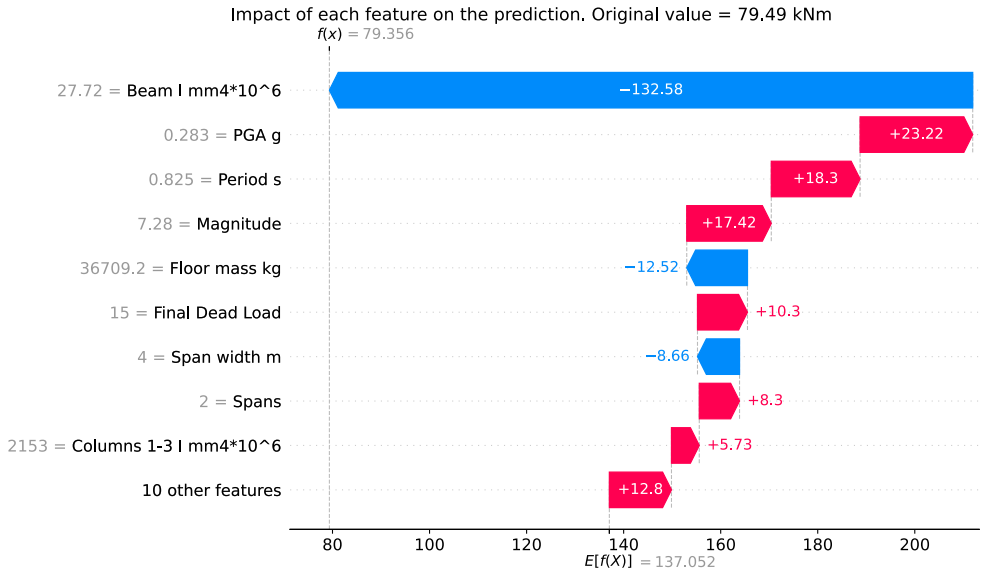

b. Beam bending moment global analysis

Figure 32. SHAP analysis for ML model used for MRF beam bending moment prediction

Following conclusions can be made:

- Period and seismic parameters (PGA, magnitude) are the most impactful features for the interstorey displacement prediction. Moreover, higher period and PGA correspond to higher displacements which shows that the ML model correctly learned the fundamentals of underlying physics behind NLTH analysis. Moreover, columns' stiffness has a significant impact on the predictions.

- For column's axial force, the number of floors and acting gravity loads have a big impact on the predictions results, as well as their stiffness, which is also aligned with physics-based analysis since columns' stiffness and acting vertical loads affect the acting axial force in a column during the seismic excitation.
- Regarding the bending moment in columns, their stiffness, acting floor mass and seismic parameters have the biggest impact on the predictions.
- For beams' bending moment, their stiffness is the most impactful feature as it could be expected. As stiffer the beams as higher forces they attract during the seismic excitation.

Similar analysis is performed for MRF equipped with DRBeS. The results are reported in Figure 33, Figure 34, Figure 35, Figure 36, and Figure 37.

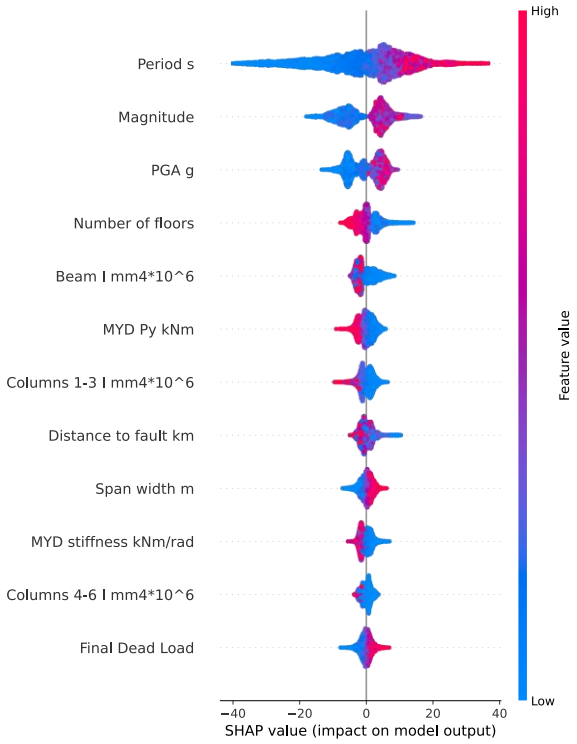

a. Interstorey displacements global analysis

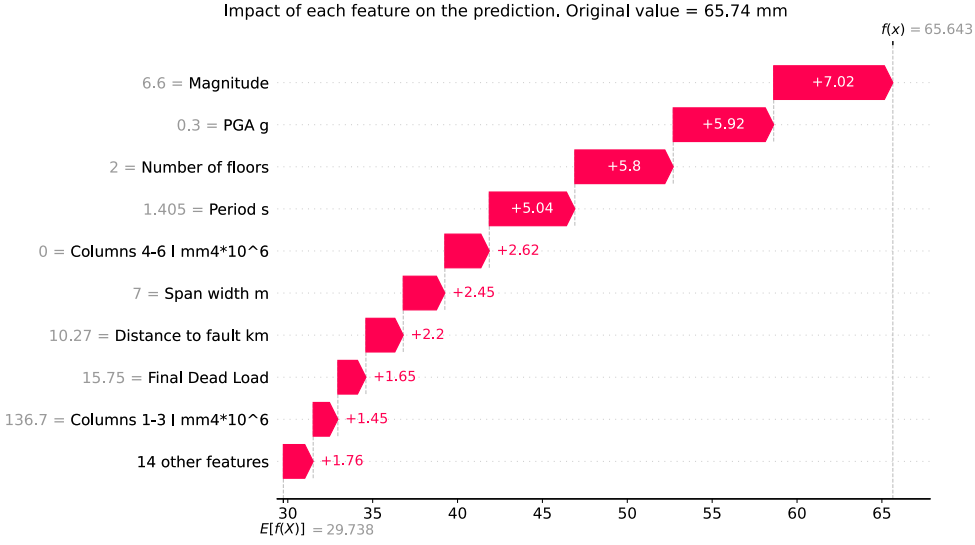

b. Interstorey displacements local analysis

Figure 33. SHAP analysis for ML models used for MRF equipped with DRBeS interstorey displacement prediction

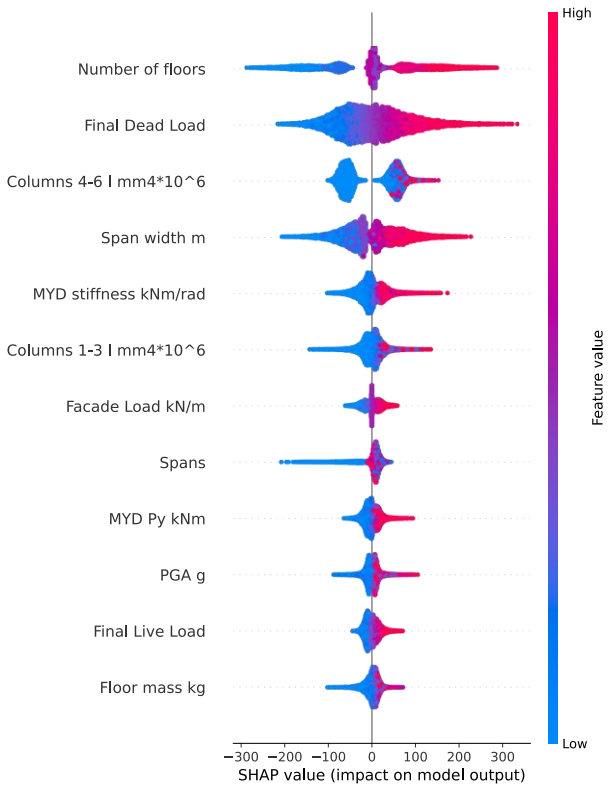

a. Column axial force global analysis

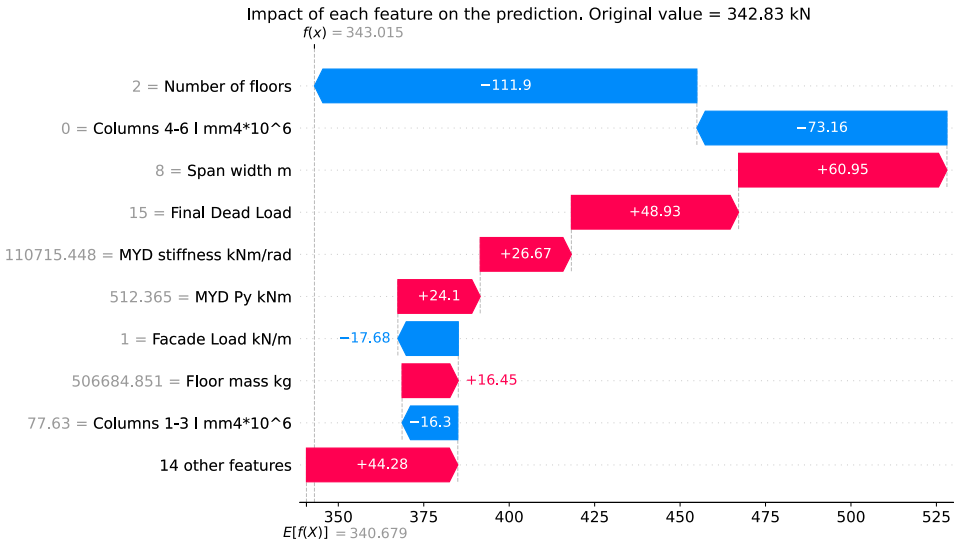

b. Column axial force local analysis

Figure 34. SHAP analysis for ML models used for MRF equipped with DRBeS column axial force prediction

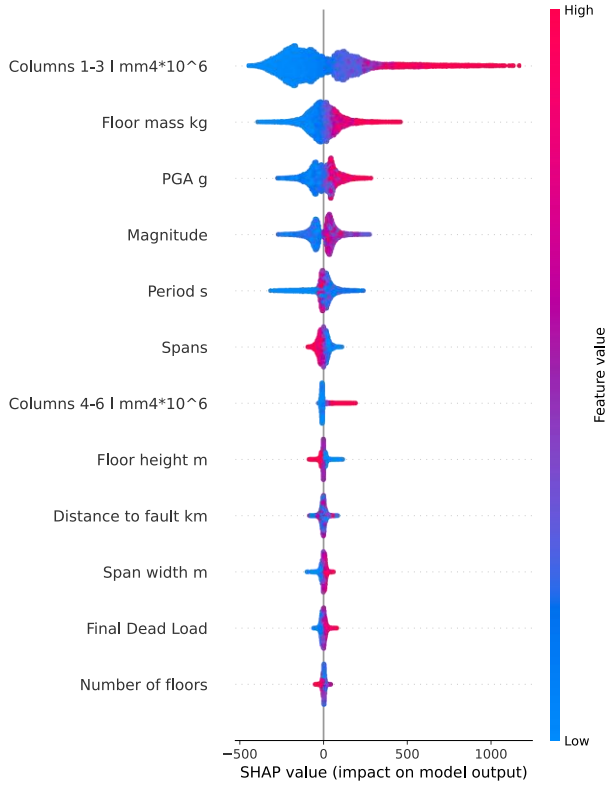

a. Column bending moment global analysis

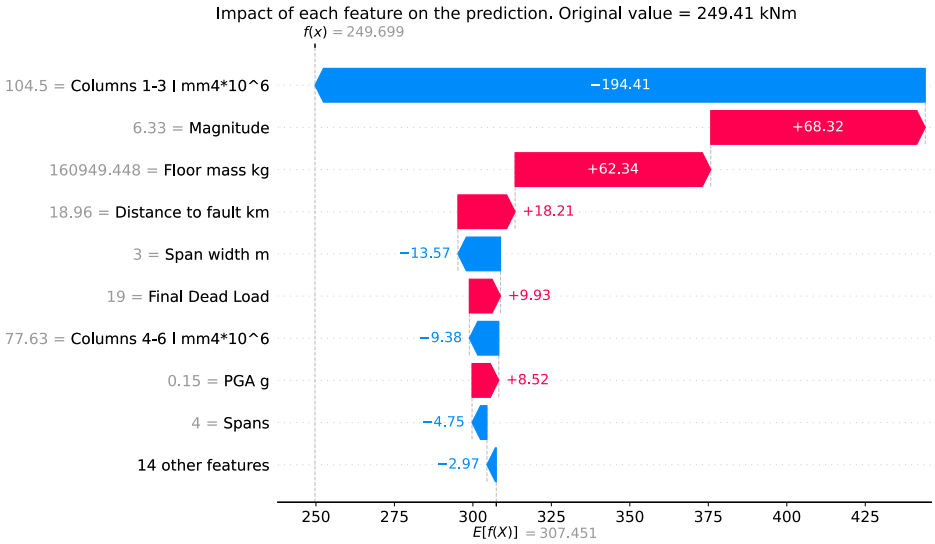

b. Column bending moment local analysis

Figure 35. SHAP analysis for ML models used for MRF equipped with DRBeS column bending moment prediction

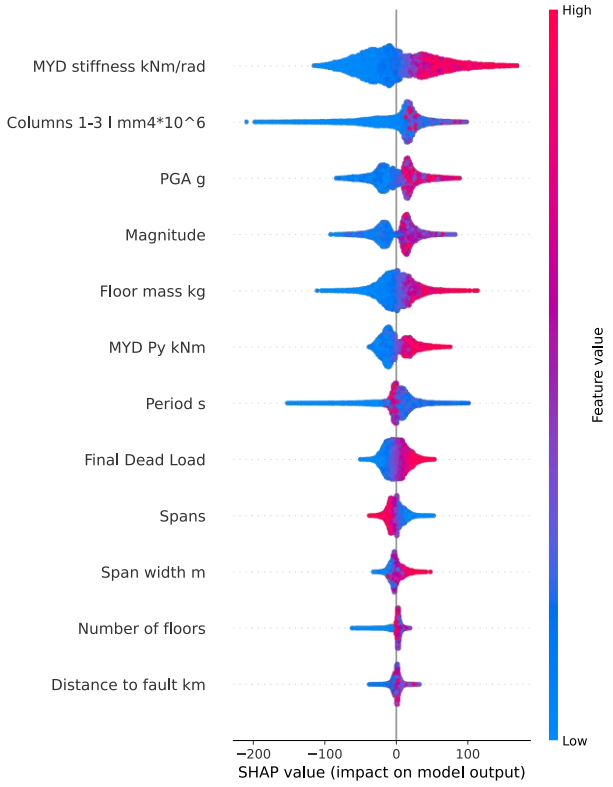

a. Beam bending moment global analysis

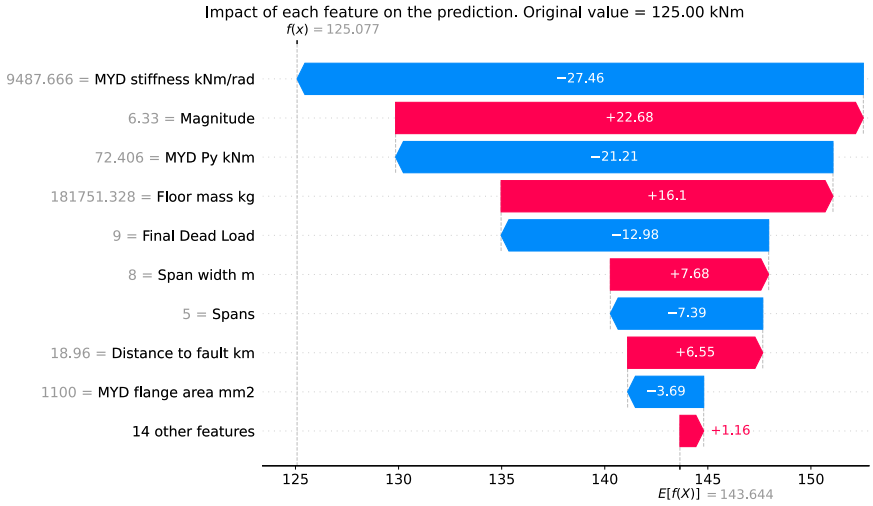

b. Beam bending moment local analysis

Figure 36. SHAP analysis for ML models used for MRF equipped with DRBeS beam bending moment prediction

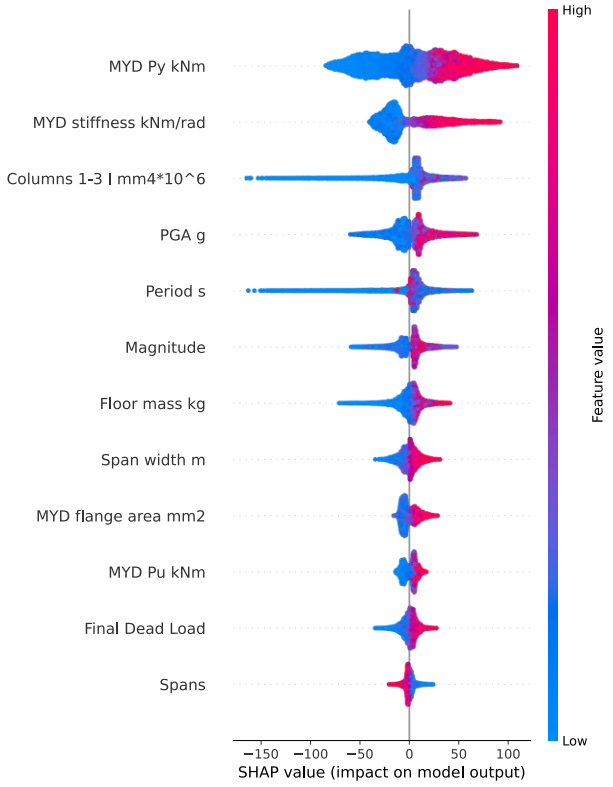

a. DRBeS bending moment global analysis

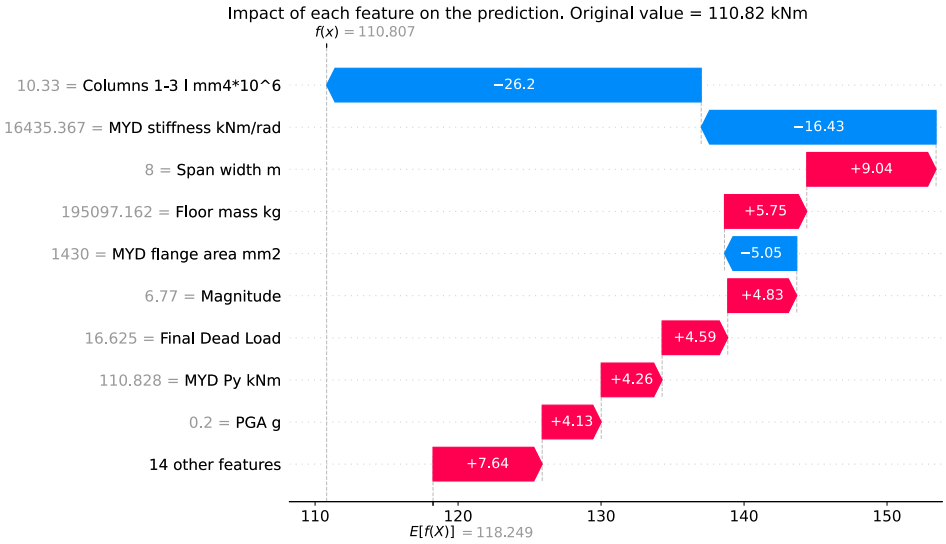

b. DRBeS bending moment global analysis

Figure 37. SHAP analysis for ML models used for MRF equipped with DRBeS MYD bending moment prediction

Following conclusions can be made:

- Period and seismic parameters (PGA, magnitude) are the most impactful features for the interstorey displacement prediction as well as in case of conventional MRF.
- For column's axial force, the number of floors and acting gravity loads have a big impact on the predictions results, as well as their stiffness, which is also like simple MRF case.
- Regarding the bending moment in columns, their stiffness, acting floor mass and seismic parameters have the biggest impact on the predictions.

- For beams' bending moment, MYD stiffness is the most impactful feature (compared to beam's stiffness in conventional MRF case). It shows the impact of DRBeS on beam's bending moment which is expected since seismic behaviour of the beam is highly affected by the introduction of this MYD. As stiffer the DRBeS as higher forces they attract to the beam during the seismic excitation.
- DRBeS yielding limit and stiffness are the most impactful features to MYD's bending moment. The correlation is similar as in case of beams – as stiffer and stringer DRBeS as more seismic forces it attracts.

Analogously, Appendix G shows a global and local SHAP values for each of the ML-based surrogate model for CBF. Following conclusions can be made:

- Period and PGA are the most impactful features for the interstorey displacement prediction. Moreover, higher period and PGA correspond to higher displacements which shows that the ML model correctly learned the fundamentals of underlying physics behind NLTH analysis.
- For columns, their cross-sections have a big impact on the predictions results, as well as acting gravity loads, which is also aligned with physics-based analysis since columns' stiffness and acting vertical loads affect the acting axial force in a column during the seismic excitation.
- Regarding axial forces in bracings, their areas are playing more important role than in the prediction of other outputs. Moreover, as bigger the bracings as higher forces they attract which represents a solid engineering knowledge learned by ML model. The same can be mentioned about the number of braces spans, since the more spans are braced, the lower force will be acting in each brace.

Similar analysis is performed for CBF equipped with DRBrC. The results are reported in Following conclusions can be made:

- As for conventional CBF, period and PGA are the most impactful features for the interstorey displacement prediction.
- Bracing areas are the most impactful features for column axial forces prediction.
- For bottom bracing and DRBrC axial forces, bracing areas, floor mass and PGA have the most impact while MYD's stiffness does not have a high SHAP value.

5.4 Error analysis for the trained ML models

MAPE metric gives a good indication for the average error among training and testing data. However, more sophisticated error analysis can be done to better investigate how the predicted by ML-surrogate models values relate to the reality. Figure 38, Figure 39, Figure 40, and Figure 41 show an error distribution of the testing datapoints. Most predictions have an error below 10% MAPE that was taken as a threshold. However, in few examples the prediction error is rather large, exceeding 40% and even 60%. Moreover, the waterfall plot with local SHAP analysis is shown for the datapoint that has the highest error.

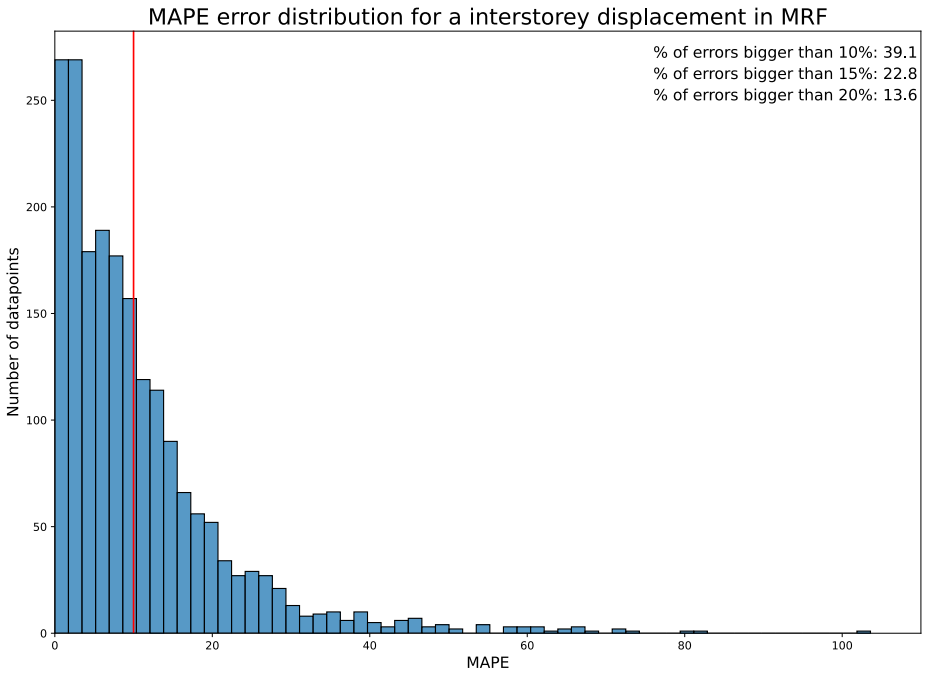

a. Interstorey displacements error distribution

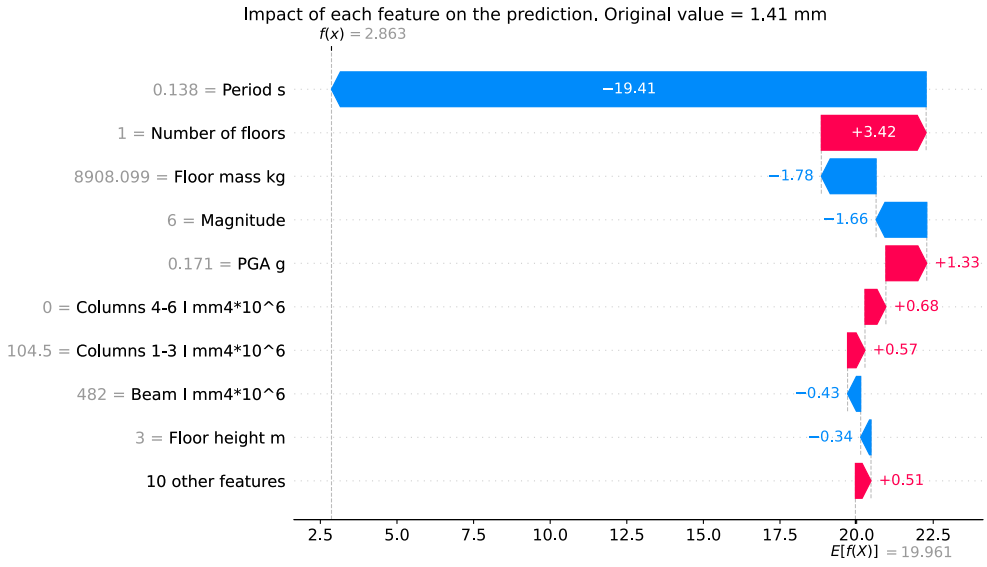

b. Interstorey displacements biggest error analysis

Figure 38. Error analysis for ML models used for MRF interstorey displacement prediction

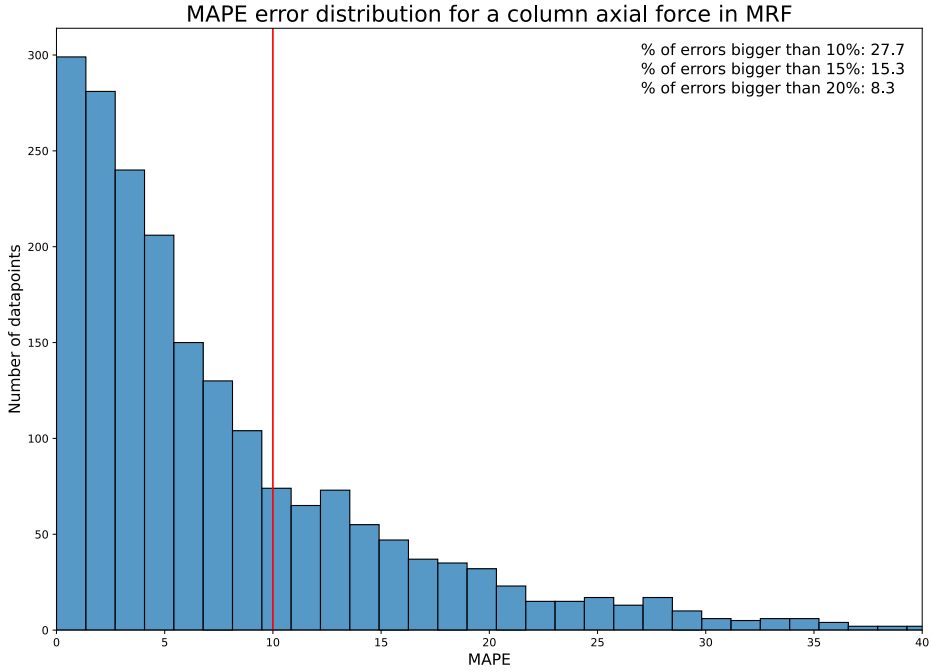

a. Column axial force error distribution

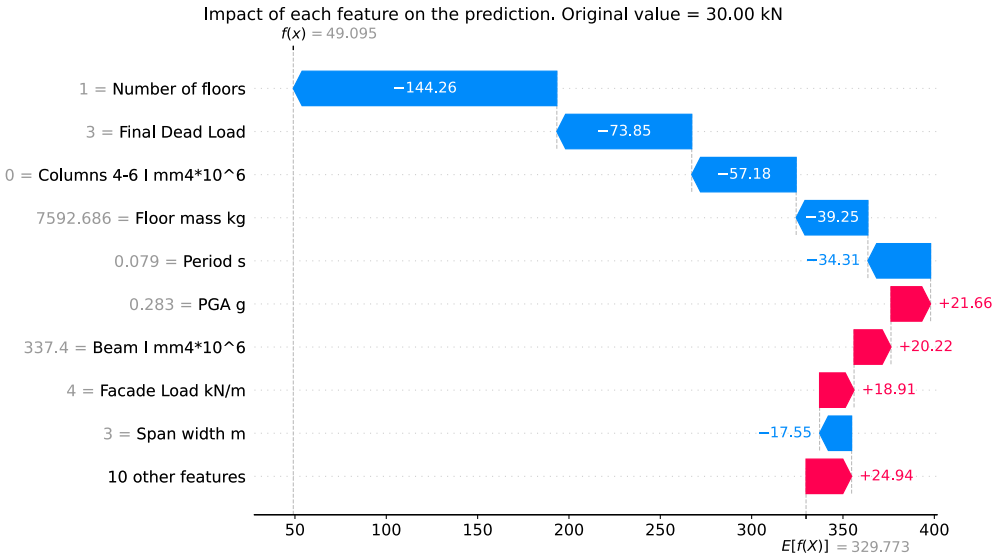

b. Column axial force biggest error analysis

Figure 39. Error analysis for ML models used for MRF column axial force prediction

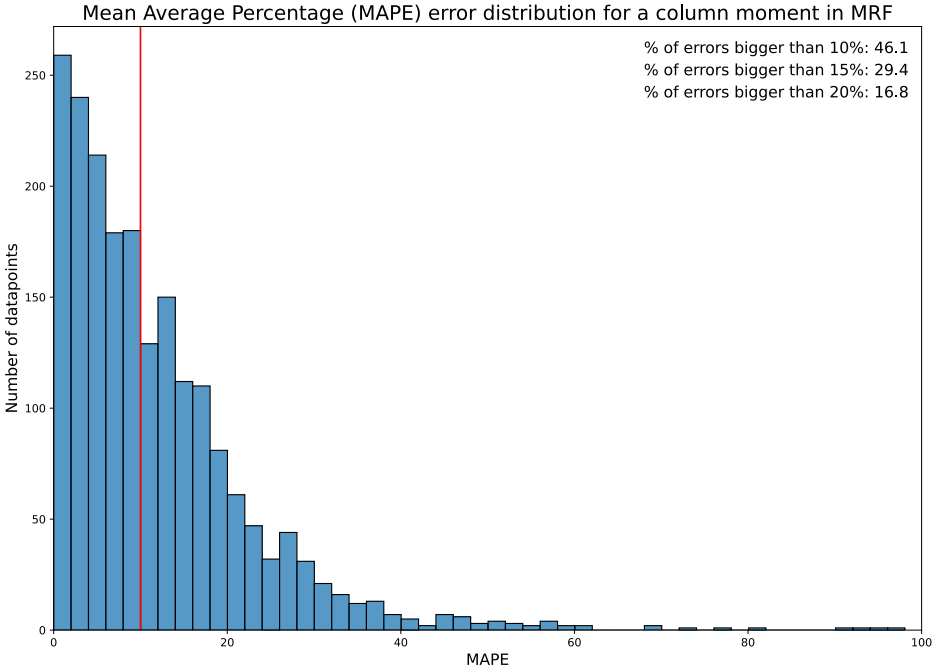

a. Column bending moment error distribution

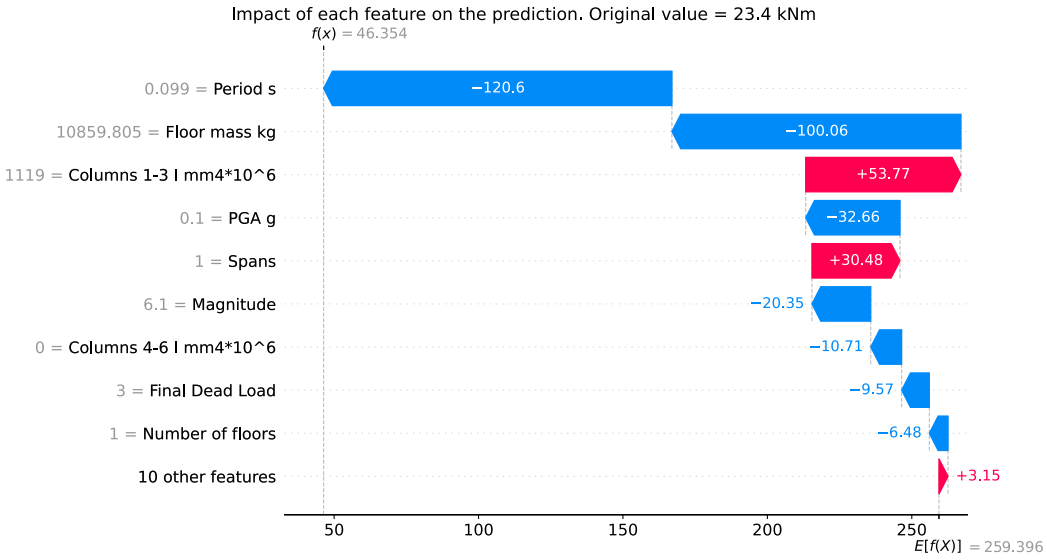

b. Column bending moment biggest error analysis

Figure 40. Error analysis for ML models used for MRF column bending moment prediction

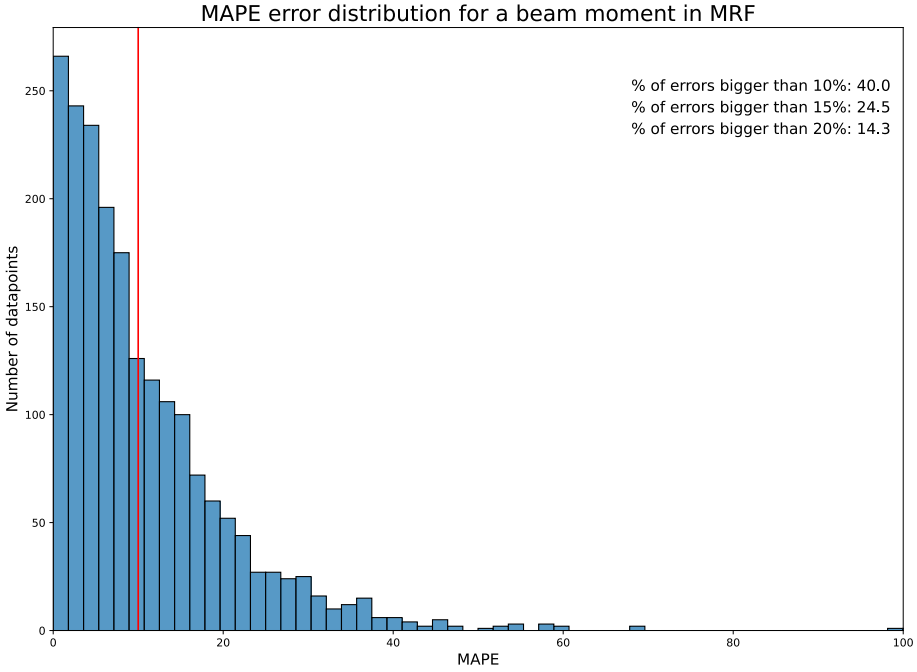

a. Beam bending moment error distribution

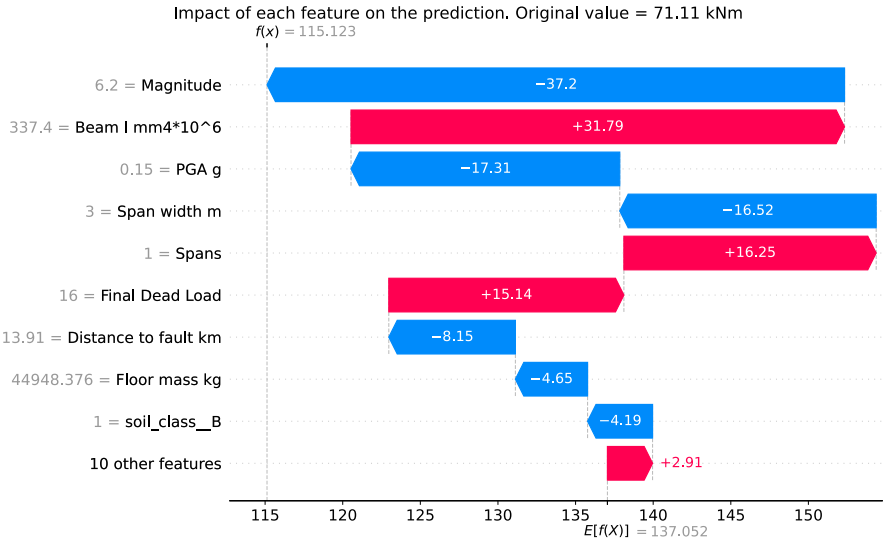

b. Beam bending moment biggest error analysis

Figure 41. Error analysis for ML models used for MRF beam bending moment prediction

Following conclusions can be made:

- The biggest MAPE for interstorey displacement is quite low in absolute values (1.4 mm). The relatively small period contributes significantly to reducing the prediction value comparing to the mean one.
- For axial forces in columns, the biggest error is observed for small 1 storey structure with 1 span which can be considered as an outlier.
- Regarding bending moments in columns, the biggest error is observed in one span, one storey structure with high columns' cross-section (HEA550). It is an overdesigned structure, which can be considered unrealistic but still permitted to be generated to give ML models better understanding of structural engineering principles.

- Also, for bending moments in beams, the biggest error is observed with a structure which has extremely large columns.

Similar analysis is performed for MRF equipped with DRBeS. The results are reported in Figure 42, Figure 43, Figure 44, Figure 45, Figure 46.

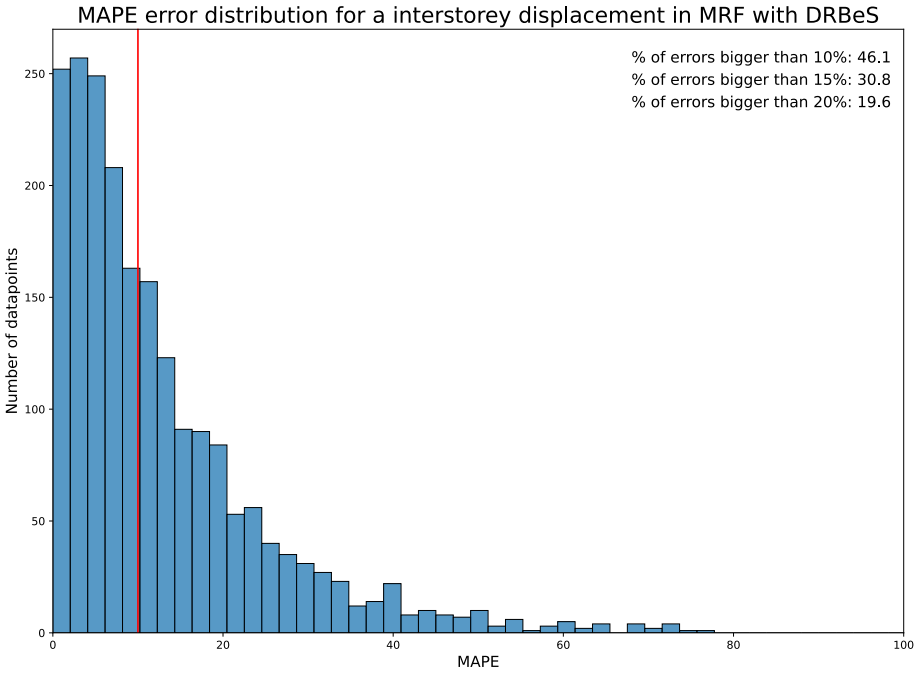

a. Interstorey displacements error distribution

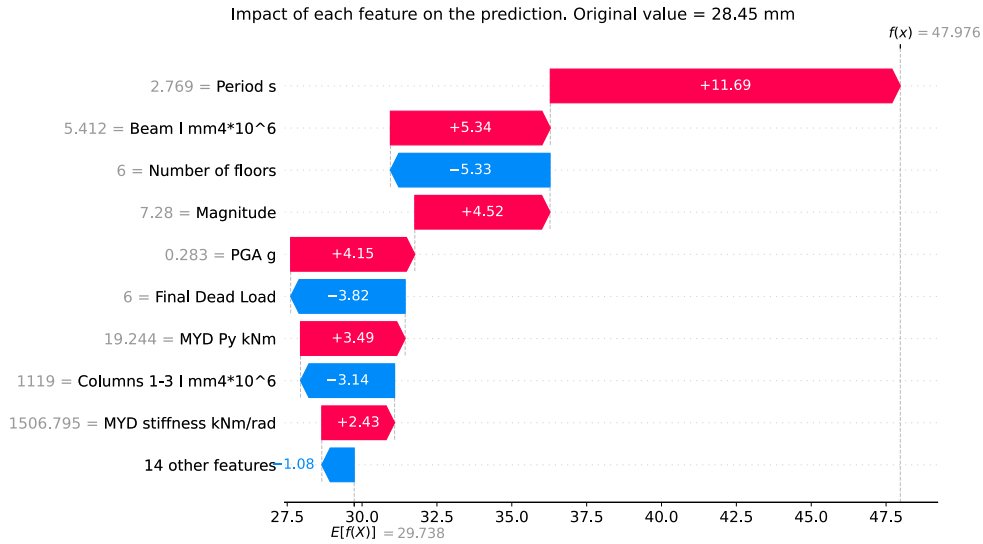

b. Interstorey displacements biggest error analysis

Figure 42. Error analysis for ML models used for MRF equipped with DRBeS interstorey displacement prediction

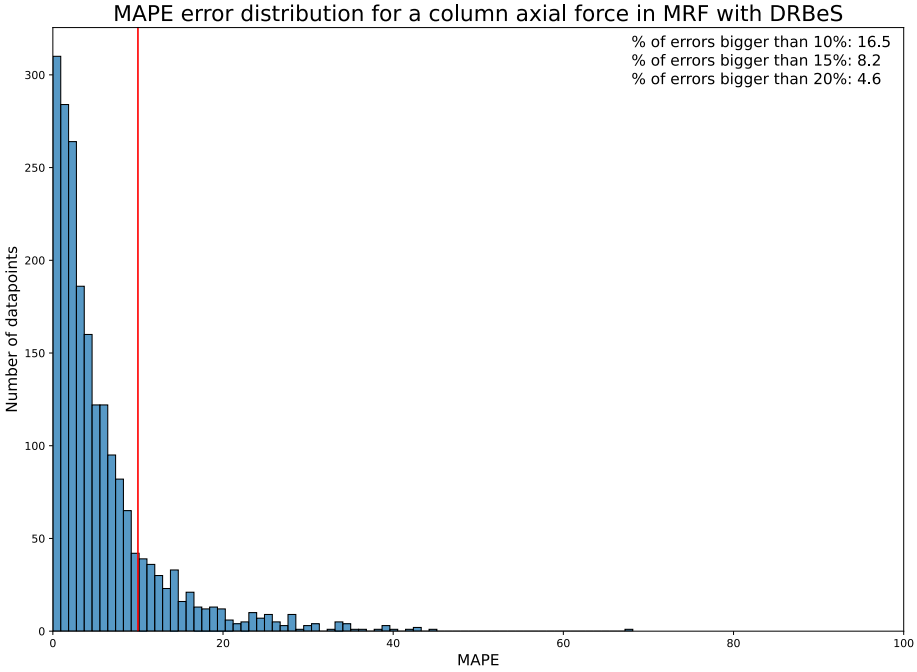

a. Column axial force error distribution

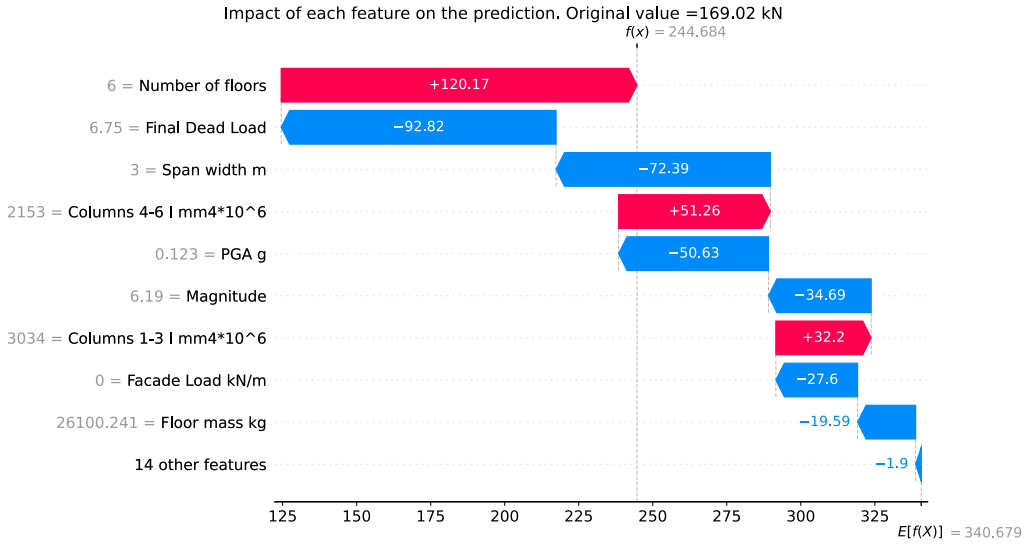

b. Column axial force biggest error analysis

Figure 43. Error analysis for ML models used for MRF equipped with DRBeS column axial force prediction

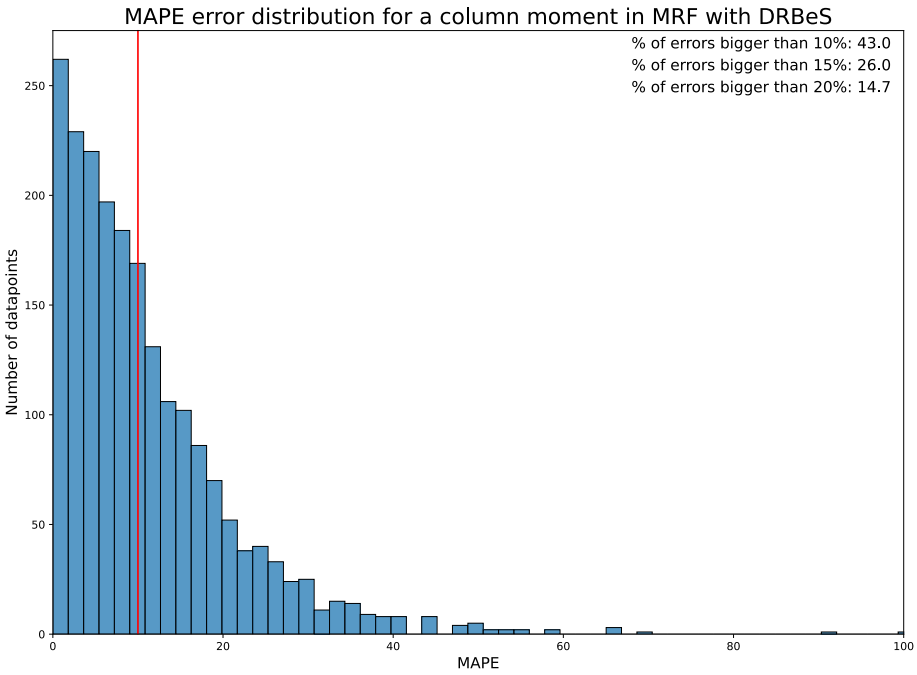

a. Column bending moment error distribution

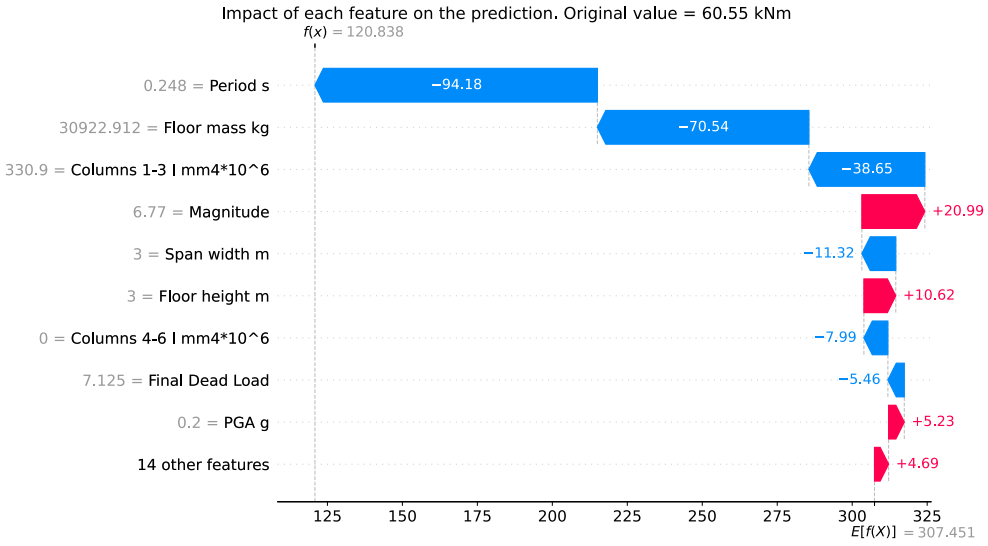

b. Column bending moment biggest error analysis

Figure 44. Error analysis for ML models used for MRF equipped with DRBeS column bending moment prediction

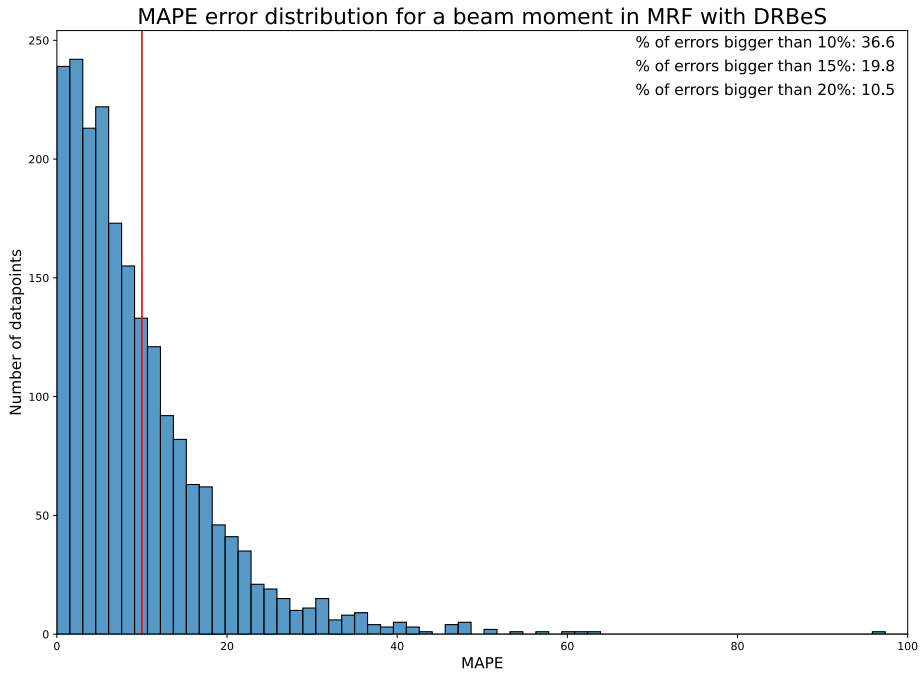

a. Beam bending moment error distribution

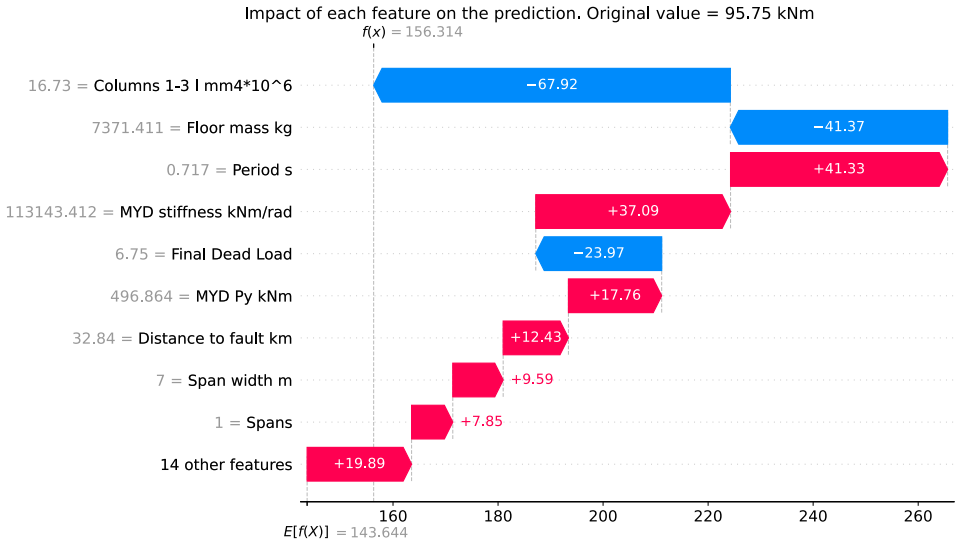

b. Beam bending moment biggest error analysis

Figure 45. Error analysis for ML models used for MRF equipped with DRBeS beam bending moment prediction

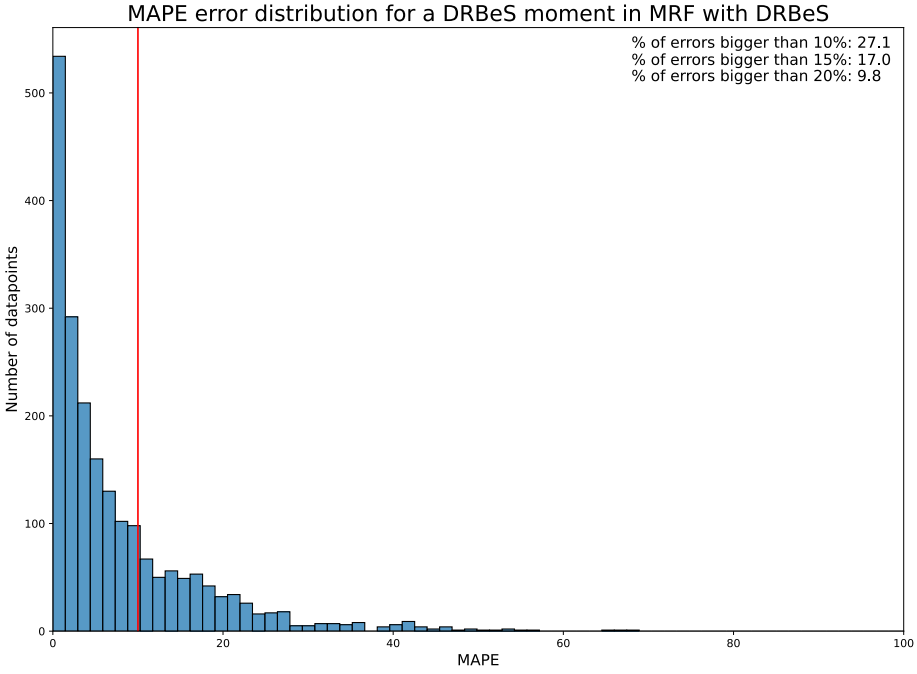

a. DRBeS bending moment error distribution

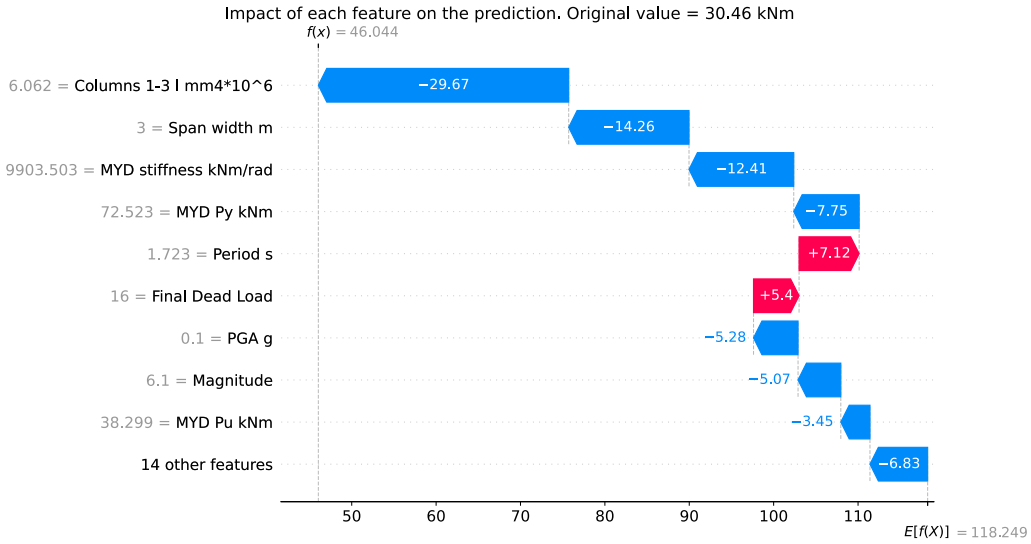

b. DRBeS bending moment biggest error analysis

Figure 46. Error analysis for ML models used for MRF equipped with DRBeS MYD bending moment prediction

Following conclusions can be made:

- The biggest MAPE for interstorey displacement is quite low in absolute values (19 mm). The relatively high period contributes significantly to reducing the prediction value comparing to the mean one.
- For axial forces in columns, the biggest error is observed for a structure with columns on 4-6 storey having HEA700 cross-section. It is an overdesigned structure, which can be considered unrealistic but still permitted to be generated to give ML models better understanding of structural engineering principles.

- Regarding bending moments in columns, the biggest error is observed for small 1 storey structure with 1 span which can be considered as an outlier. Similar situation is observed for the biggest error of beam and DRBeS bending moment predictions.

Analogously, Appendix I shows the error distribution and local SHAP analysis for the biggest error for all ML-based surrogate models for CBF. Following conclusions can be made:

- The biggest MAPE for interstorey displacement is quite low in absolute values (0.4 mm). The relatively small period contributes significantly to reducing the prediction value comparing to the mean one.
- For axial forces in columns the biggest MAPE is achieved for the 1 storey structure with the lowest columns' cross-sections possible.
- Regarding the bottom bracings, the biggest error is reached in a structure with very big columns' cross-sections (HEA 900) which is pushing the prediction further from the ground truth. It is an overdesigned structure, which can be considered unrealistic but still permitted to be generated to give ML models better understanding of structural engineering principles.

Similar analysis is performed for CBF equipped with DRBrC. The results are reported in Appendix J. Following conclusions can be made:

- The biggest MAPE for interstorey displacement is quite low in absolute values (7 mm). It is associated to untypically small cross-sections of both bottom and upper columns of 5 storey building equal to HEA100. This datapoint can be considered as an outlier. The same happens for the worst prediction of axial force in a bottom bracing.
- For axial forces in columns the worst prediction represents unrealistic structure that has enormous columns' cross-sections (HEA 1000) which is pushing the prediction further from the ground truth.
- Regarding the worse prediction of the axial force of the DRBrC, extremely high bracing section pushing prediction far from a real value. Cross-section of that size is not characteristic for a 4 storey structure with a low level of seismic action (0.15g PGA in this case).

5.5 Surrogate models validation

In this chapter several case studies are performed to verify the abilities of ML-surrogate models to successfully interpolate within defined in Table 11 inputs ranges. Moreover, the extrapolation capabilities of trained algorithms are discovered testing them on the data outside of training range of the features. Since prediction errors for the same response types among different frames are similar (Table 13) only 1 frame type is considered in each case study and the obtained conclusions could be applicable for all other frame types as well.

5.5.1 Interpolation capabilities of trained ML models

To discover interpolation capabilities of trained ML models, 2 case studies are performed:

- Interpolation within geometry and cross-section input ranges.
- Interpolation within ground motion input ranges.

For the first check an MRF structure with properties indicated in Table 15 is tested (Figure 47). The truthfulness of the interpolation check lies in a fact that this particular structure could not have been included in neither training not testing data of any trained ML algorithm. In the original structure generation procedure only HEA cross-sections were used in columns, while gravity loads, and span width could have only integer values. In this case study HEB cross-sections are implemented for

columns while span width and gravity loads have float values. However, since it is an interpolation check, all the inputs lie within the original ranges of ML models training.

Input	Value	ML training range (min-max)
Column Fy [Mpa]	355	235-355
Beam Fy [Mpa]	235	235-355
Columns 1-3 I [mm^4*10^6]	*576.80 (HEB 400)*	3.49-6447
Columns 4-6 I [mm^4*10^6]	*431.90 (HEB 360)*	0-5538
Beam I [mm^4*10^6]	57.90 (IPE 270)	1.71-1752
Number of spans	5	1-6
Span width [m]	*5.30*	3-8
Number of floors	4	1-6
Floor height [m]	3	3-4
Floor mass [kg]	228759.49	568.99-884936.45
Facade load [kN/m]	*2.70*	0-4
Distributed superimposed dead load [kN/m]	6.88	3-48
Distributed live load [kN/m]	6.40	3-40
Peak Ground Acceleration [g]	0.30	0.10-0.354
Magnitude	6.60	5.90-7.28
Distance to fault [km]	10.27	10.27-35.66
Shear wave velocity [m/s]	361.40	242.05-649.67
Fundamental period [s]	1.68	0.05-10.48

Table 15. Input values for geometry, gravity loads and cross-sections interpolation case study

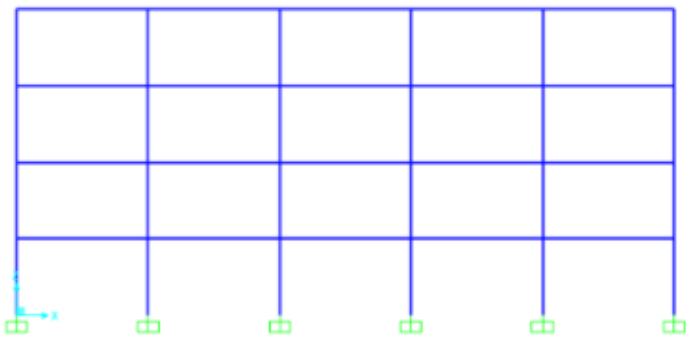

Figure 47. MRF structure for geometry, gravity loads and cross-sections interpolation case study

Percentage error for all the predicted responses (FEM simulation in SAP 2000 vs ML model prediction) is shown in Table 16 along with original testing MAPE errors for the best ML algorithm from the previous chapter for the comparison purposes. The errors for this case study are lower than average ones which shows the ability of the trained ML models to successfully interpolate within the given cross-sections, geometry, and vertical loads ranges.

Predicted output	FEM results	ML model prediction	% error	Original MAPE
Interstorey Displacement [mm]	31.1	32.2	3.23	8.14
Axial force in a column [kN]	290.72	294.83	1.41	7.84
Bending moment in a column [kNm]	802.00	719.28	10.31	11.57
Bending moment in a beam [kNm]	113.69	128.48	3.90	9.95

Table 16. Error analysis for geometry, gravity loads and cross-sections interpolation case study

In a second case study, CBF structure with properties indicated in Table 17 is tested. In this case the interpolation accuracy is evaluated in a context of ground motions parameters. The accelerogram which has not been used for model training is applied (El Centro from PEER database). Its PGA and magnitude lie within the original ranges of accelerograms used for ML models training, while distance to fault and shear wave velocity do not. However, since the impact of these two features on the surrogate models' prediction is very low (as discussed in a previous chapter), this ground motion was considered suitable for interpolation case study.

Input	Value	ML training range (min-max)
Column Fy [Mpa]	355	235-355
Beam Fy [Mpa]	355	235-355
Bracing Fy [Mpa]	355	235-355
Columns 1-3 I [mm^4*10^6]	450.70 (HEA 400)	3.49-6447
Columns 4-6 I [mm^4*10^6]	330.90 (HEA 360)	0-5538
Beam I [mm^4*10^6]	19.43 (IPE 200)	1.71-1752
Bracing 12 A [mm^2]	989 (CHS 101.6 / 3.2)	733-15130
Bracing 34 A [mm^2]	862 (CHS 88.9 / 3.2)	0-2377.07
Bracing 56 A [mm^2]	733 (CHS 76.1 / 3.2)	0-1341.76
Number of spans	3	1-6
Span width [m]	6	3-8
Number of floors	5	1-6
Floor height [m]	3.50	3-4
Number of braced spans	1	1-2
Floor mass [kg]	106019.11	568.99-884936.45
Facade load [kN/m]	3	0-4
Distributed superimposed dead load [kN/m]	10	3-48
Distributed live load [kN/m]	9	3-40
Peak Ground Acceleration [g]	*0.28*	0.10-0.354
Magnitude	*6.95*	5.90-7.28
Distance to fault [km]	*6.09*	10.27-35.66
Shear wave velocity [m/s]	*213.44*	242.05-649.67
Fundamental period [s]	1.20	0.04-4.02

Table 17. Input values for ground motion interpolation case study

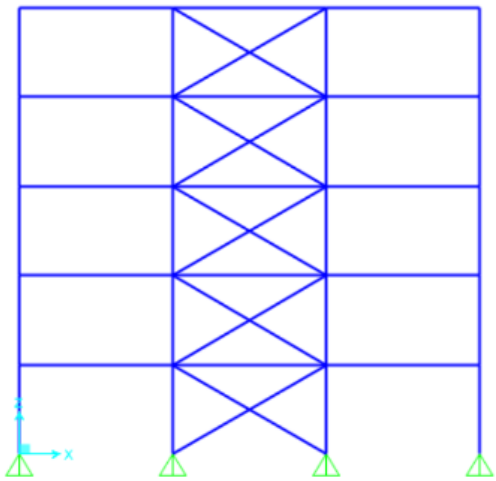

Figure 48. CBF structure for ground motion interpolation case study

Percentage error for all the predicted responses (FEM simulation in SAP 2000 vs ML model prediction) is shown in Table 18 along with original testing MAPE errors for the best ML algorithm from the previous chapter for the comparison purposes. The errors for this case study are lower than average ones for axial forces in a column and bottom brace while higher for interstorey displacement. The higher error in displacement prediction can be attributed to spectral characteristics of the considered earthquake. As it was already mentioned, the ground motions used for training were not scaled to any response spectrum for the generalisation purposes and structural displacements are particularly sensible to ground motion characteristics. However, the obtained error for interstorey displacements is still below 15% and quite low in absolute values (2 mm) for the unseen accelerogram. Considering lower that original MAPE errors for column and bracing axial forces, it can be concluded that trained ML models are capable for the accurate interpolation also in terms of ground motions.

Predicted output	FEM results	ML model prediction	% error	Original MAPE
Interstorey Displacement [mm]	13.50	15.50	14.81	9.40
Axial force in a column [kN]	1388.29	1331.51	4.09	8.88
Axial force in a bottom brace [kN]	393.62	399.32	1.45	11.05

Table 18. Error analysis for ground motion interpolation case study

5.5.2 Extrapolation capabilities of trained ML models

In a similar manner, for the extrapolation 2 case studies have been considered:

- Extrapolation outside of geometry input ranges.
- Extrapolation outside of ground motion input ranges.

Unlike of interpolation, the ability of ML models to extrapolate highly depends on the field of application. Therefore, just 1 example is not enough to adequately estimate it, so for each case study 100 structures are generated to obtain statistically reliable conclusions.
For a first case study, CBFs with geometric ranges outside of the original ones (Table 19) have been generated. The number of spans and span width has also been increased for the tributary width calculation for seismic loads. Consequently, the maximum potential values of floor mass have

increased. All abovementioned changes affected the range of structural period, where maximum value has increased almost 2 times. The range for all other inputs stayed the same, therefore they are not reported in the table. One of the 100 of generated structures is shown in Figure 49.

Input	Case study range	ML training range (min-max)
Number of spans	7-10	1-6
Span width [m]	3-10	3-8
Number of floors	7-8	1-6
Floor mass [kg]	100236.5-2883712	568.99-884936.45
Fundamental period [s]	0.81-9.21	0.04-4.02

Table 19. Input values for geometry extrapolation case study

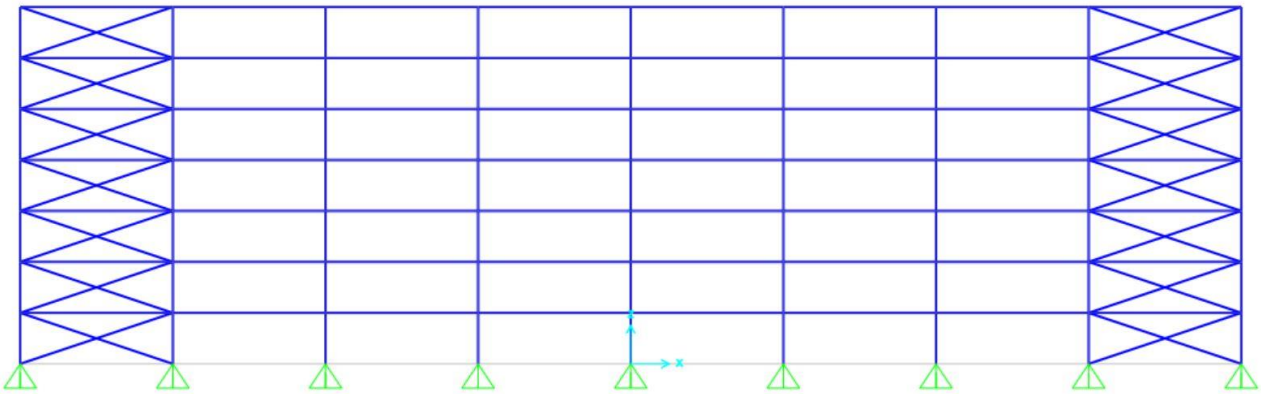

Figure 49. Example of CBF for geometry extrapolation case study

MAPE for all the predicted responses (100 FEM simulations in SAP 2000 vs 100 ML model predictions) is shown in Table 20 along with original testing MAPE errors for the best ML algorithm from the previous chapter for the comparison purposes. For all the responses MAPE is much higher compared to the original one. It is especially evident for the displacement prediction. However, the errors do not exceed 100% (2 times difference) which shows that ML models learned a physics behind NLTH analysis well enough to extrapolate outside of their training range without giving extremely wrong predictions.

Predicted output	MAPE for this case study	Original MAPE
Interstorey Displacement [mm]	86.23	9.40
Axial force in a column [kN]	30.18	8.88
Axial force in a bottom brace [kN]	46.12	11.05

Table 20. Error analysis for geometry extrapolation case study

For the second extrapolation case study, 100 MRF structures were subjected to ground motions with parameters outside of training range. Kobe and Chi Chi ground motions were extracted prom PEER database. Since the purpose of this case study was to investigate the sensitivity of ML models to extrapolate seismic loading input, all other features (geometry, cross-sections, gravity loads, etc.) are kept within their training range.

Input	Case study range	ML training range (min-max)
Peak Ground Acceleration [g]	0.48-0.52	0.10-0.354
Magnitude	6.90-7.62	5.90-7.28
Distance to fault [km]	7.08-13.46	10.27-35.66

Table 21. Input values for ground motions extrapolation case study

MAPE for all the predicted responses (100 FEM simulations in SAP 2000 vs 100 ML model predictions) is shown in Table 22 along with original testing MAPE errors for the best ML algorithm from the previous chapter for the comparison purposes. For all the responses MAPE is higher compared to the original one. It is especially evident for the displacement prediction which is highly dependent on PGA and magnitude. However, the errors do not exceed 50% (2 times difference) and are much lower than in geometry extrapolation case. For column axial force the error is even below 20%. It shows that ML models learned a physics behind NLTH analysis well enough to extrapolate also for ground motions outside of their training range without giving extremely wrong predictions.

Predicted output	MAPE for this case study	Original MAPE
Interstorey Displacement [mm]	44.2	8.14
Axial force in a column [kN]	17.59	7.84
Bending moment in a column [kNm]	35.19	11.57
Bending moment in a beam [kNm]	25.57	9.95

Table 22. Error analysis for ground motions extrapolation case study

5.5.3 Validation with an experimental test

The last check of ML-based surrogate model performance is the validation with an experimental test. Since 3D shaking table tests performed within this thesis concerned half-scale 2-storey buildings which properties lie outside of ML models training range, 2D hybrid full-scale tests explained in detail in [137] and [138] are used for the comparison. The tests were performed on 6-storey 2D frames where only part of the frame was subjected to a physical test while the rest of the structure was modelled numerically. Two structures have been considered (Figure 50):

- 6-storey MRF equipped with DRBeS. Where 1.5 storeys are physical, and 4.5 storeys are numerical.
- 6-storey CBF equipped with DRBrC. Where 1 storey is physical, and 5 storeys are numerical.

Structural details that are also inputs to ML model are shown in Table 23.

a. MRF with DRBeS

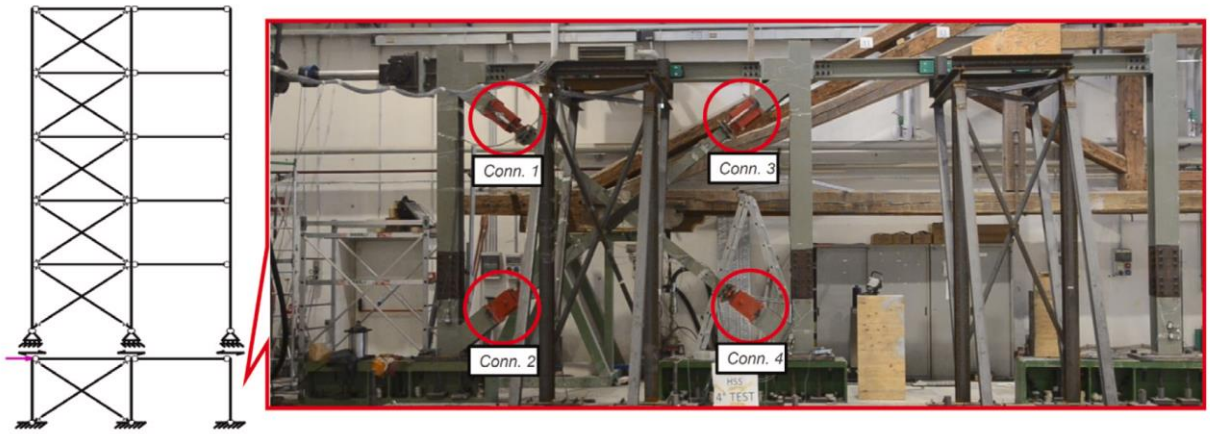

b. CBF with DRBrC

Figure 50. Physical and numerical subdomains of a hybrid tests [137], [138]

Input	MRF with DRBeS	CBF with DRBrC
Column Fy [Mpa]	355	355
Beam Fy [Mpa]	355	355
Bracing Fy [Mpa]	-	355
Columns 1-3 I [mm^4*10^6]	149.20 (HEB 260)	149.20 (HEB 260)
Columns 4-6 I [mm^4*10^6]	112.60 (HEB 240)	112.60 (HEB 240)
Beam I [mm^4*10^6]	57.90 (IPE 270)	83.56 (IPE 300)
Bracing 12 A [mm^2]	-	3142 (HEA140)
Bracing 34 A [mm^2]	-	2534 (HEA120)
Bracing 56 A [mm^2]	-	2124 (HEA100)
Number of spans	2	2
Span width [m]	4.275	4.275
Number of floors	6	6
Floor height [m]	3.50	3.50
MYD's stiffness	15814 [kNm/rad]	73832 [kN/m]
MYD's Yielding limit	150 [kNm]	123 [kN]
MYD's Ultimate limit	224 [kNm]	338 [kN]
MYD's flange area [mm^2]	1200	-
Number of braced spans	-	1
Floor mass [kg]	17809	35150
Facade load [kN/m]	4	4
Distributed superimposed dead load [kN/m]	2.36	9.48

Distributed live load [kN/m]	2.03	8.12
Peak Ground Acceleration [g]	0.42	0.42
Magnitude	6.93	6.93
Distance to fault [km]	9.96	9.96
Shear wave velocity [m/s]	729.65	729.65
Fundamental period [s]	1.35	0.99

Table 23. Input values for experimental test validation case study

The comparison between experimental results and ML model prediction are shown in Table 24. Only column moment and internal forces in MYDs are presented since these are the only values reported in the test report [137], [138]. The MAPE for all the outputs is lower 30% while column moment prediction has the highest error of all as it was in original algorithm training. The error for DRBrC axial force is even lower than 5%. The results show the validity of trained ML algorithm and the fair correlation between training data generated in FEM and experimental results, which also proves the accuracy of FEM modelling used for this thesis.

Predicted output	Experimental results	ML model prediction	% error	Original MAPE
Bending moment in a column [kNm]	280.0	202.40	27.71	11.01
Bending moment in DRBeS [kNm]	102.0	117.10	14.80	7.45
Axial force in DRBrC [kN]	165.0	158.12	4.17	8.45

Table 24. Error analysis for experimental test validation case study

5.6 ML model deployment

To expose the ML model to engineering community, get a professionals' feedback and share the results of this thesis, trained surrogate models for conventional MRF and CBF have been deployed to the web. The resulting prototype can be accessed here. The user can provide its inputs that lie within ML model range and get an immediate output of NLTH analysis for a given frame (Figure 51).

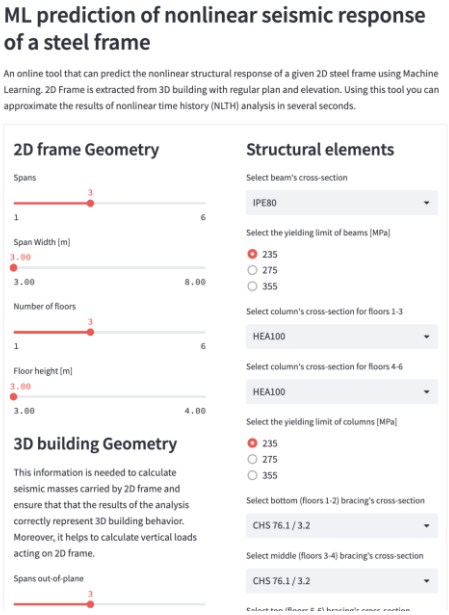

a. Input menu

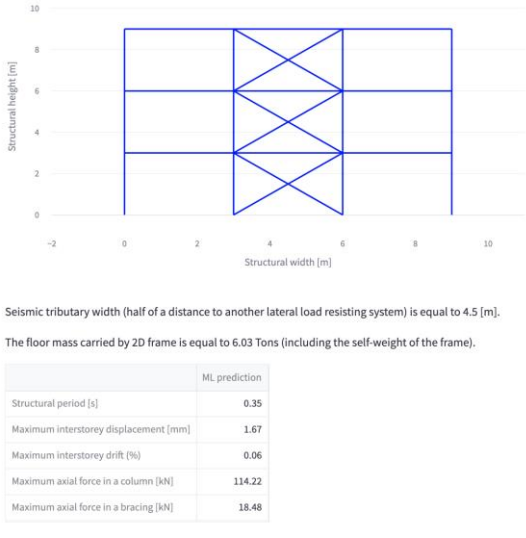

b. 2D frame under consideration and ML output

Figure 51. The interface of a web tool

Another activity related to the sharing of the research results is the creation of the competition on the Kaggle platform [139]. A chunk of data with MRF interstorey displacements has been published and around 30 teams around the world participated in the competition trying to predict the structural response using the most accurate algorithm. The goal of the competition was to encourage a data sharing culture in structural engineering industry and invoke the interest in ML for young engineers. More information about the competition is given in Appendix L.

5.7 Discussion about the training and validation of ML-based surrogate models

In this chapter the procedure for data generation and training of ML-based surrogate models has been presented. Based on the obtained results, following conclusions can be made:

- Even though some structural responses have higher prediction accuracy than others, MAPE for all of them lie around 10%. It shows that given that ML model has reached a particular accuracy for a given response, it is most likely that similar accuracy will be achieved also for other structural responses given the same source and features' ranges of training data.
- Since the data for training the models was generated synthetically, its amount can be controlled. More data gives better accuracy. However, since the difference in accuracy between 15 and 20 thousands of datapoints was small, in order to reach a significant improvement further, most likely a big data (more than 100 thousands points) is needed. It was also the case in [80] where to reach very high accuracy millions of datapoints were used.
- Trained ML models were able to catch some physics behind NLTH analysis. It is proven by the fact that the most predictive features for the response prediction were well expected given the reader's knowledge of basic structural and seismic engineering concepts.
- Trained ML models have better abilities to interpolate rather than extrapolate, which was expected from the literature. However, the trained algorithms were able to predict some structural responses for ground motion outside of the training range with a fair accuracy. It highlights a generalisation capability of the trained surrogate models.

The Table 25 compares two approaches for structural analysis: the FEM and ML-based surrogate modeling. In terms of accuracy, FEM is considered the closest to the ground truth, with an average error of 9.17%, while the accuracy of surrogate modeling depends on the quality of the training data and the model itself. Regarding speed, surrogate modeling offers a significant advantage, taking only 0.03 seconds for a single analysis, compared to 432 seconds for FEM. This speed advantage makes surrogate modeling highly practical for exploring a vast design space quickly. However, FEM has the advantage of being able to analyze all possible geometries and dimensions, while surrogate modeling is limited to the range of training data, typically rectangular plans in this case. In terms of scalability, FEM becomes increasingly time-consuming and impractical for analyzing large numbers of structures, while surrogate modeling excels in this regard, allowing for the rapid generation and analysis of a huge design space.

	FEM	Surrogate modelling
Accuracy	The closest to the groung truth	9.17% of average error from the ground truth
Speed (for 1 analysis)	432 seconds	0.03 seconds
Practicality	All the possible geometries and dimensions	Only rectangular plan, the dimensions within the range of the training data
Scalability	Limited.Very time-consuming and unatractive for large amount of structures.	High. Allows for the quick generation of a huge design space.

Table 25. FEM vs Surrogate modelling comparison

Overall, while FEM provides highly accurate results and can handle any geometry, its computational expense and limited scalability make it less attractive for large-scale design exploration and optimization tasks. In contrast, surrogate modeling, although limited by its training data, offers significant advantages in speed, and scalability, making it a valuable tool for efficient design space exploration and optimization in structural engineering applications.

6 The optimisation tool (SUSTEZ)

The final tool is called SUSTEZ – Sustainable Structures in Earthquake Zones. It incorporates all the parts of the thesis in user-friendly web-based software. The main goal of this tool is to help structural engineers to make efficient and fast choices for structures located in seismic areas. Eventually, the most sustainable and cost-efficient structural configurations can be found from the vast design space. Moreover, the final development allows the user to quantify the benefits of buildings equipped with MYDs compared to conventional ones. This chapter presents the information about the parametric creation of structural configuration, structural design of the generated solutions, and the graphical user interface (GUI) of the tool. Moreover, several case studies showcase the capability of the developed software to help the user to make a data-driven decision and consequently optimise the structural configuration.

6.1 Structural generation

Following the general methodology shown in Figure 13, the user inputs are followed by the generation of structural solution, i.e., creating a design space. The tool must allow layout optimisation on a global level to cause a higher impact on the cost and embodied carbon compared to local cross-sectional optimisation. Therefore, oppositely to the studies considered in the state of the art chapter where dampers' properties and location were used as the design variables [110] - [116] in this study the following parameters are being optimised:

- Columns' spans in both orthogonal directions.
- The type of lateral load resisting system (LLRS).

The columns' spans are taken as an optimisation variable since they can have a tremendous impact on the building's embodied carbon [140] while LLRS is being optimized to explore the impact of MYDs on the cost and embodied carbon of structures during the design space exploration process. The location of MYDs is predetermined. For DRBeS these are ends of each beam when MRF is chosen as LLRS while for DRBrC these are ends of a bracing member. Another fixed parameter that cannot be chosen by the user is the material of the structure – steel is considered for all beams, columns, and bracings, while the slab is made of concrete. The floor configuration is fixed as composite steel-concrete. The last two parameters are fixed since the ML-based surrogate model is trained on composite steel-concrete frames. To potentially consider other structural materials and floor types, the surrogate model must be significantly extended, otherwise the accuracy of the predictions could be low. The same applies for the material grade of the concrete used. Another fixed parameter is the shape of the plan, which is rectangular. Other shapes have not been considered due to the potential plan eccentricities and consequent additional stresses not included in the surrogate model. Moreover, since the model has been trained on 2D frames approximating 3D frames behaviour, the plan must be regular to establish the validity of this approximation. Cross-sections of all structural elements and the dimensions of MYDs come from the result of the structural design procedure which is explained in detail in the next subchapters. Table 26 provides a summary of which structural parameters are being optimised, can be chosen by the user, and are fixed. Other parameters are allowed to be modified by the user.

Structural parameter	Status
Structural material	Fixed (steel for the frame, concrete for the slab)
Material grade for steel	User's choice
Material grade for concrete	Fixed (C30/37)
Slab type	Fixed (composite steel-concrete)
Slab's thickness	User's choice
Columns' span	To be optimised
LLRS	To be optimised
Building's dimensions in plan	User's choice
Shape of the plan	Fixed (rectangular)
Interstorey height	User's choice
Number of storeys	User's choice
Location of MYDs	Fixed (beam ends for DRBeS, bracing ends for DRBrC)
Frame elements' cross-sections	Taken from the structural design
MYD's dimensions	Taken from the structural design
Acting gravity loads	User's choice
Acting seismic loads	User's choice

Table 26. Structural parameters and their status in a tool

Consequently, the optimisation question can be formulated in a following way:

"Given the dimensions of the building and the acting loads, which span of columns and type of lateral load-resisting system would provide the most sustainable and cost-efficient structural solution?"

The range of potential columns' span and its number is consistent with one used for ML models training (Table 27). It is done to assure that trained surrogate models are applicable and accurate for each generated structure. Consequently, the largest possible structure that can be evaluated by the tool has 6 storeys and is 48 x 48 meters in plan. The building generation is parametric. It starts with creating a columns' layout given the overall building dimensions provided by the user. The columns are spaced equally in each orthogonal direction, which sometimes cause the last of them to be out of the defined plan. In this case, the building plan dimensions are adjusted to include this column. For example, if the building's dimension is equal to 20m in X direction and column's spacing in the same direction is 7m, the former one is augmented up to 21m (to fit 4 columns located at points with X coordinate 0, 7, 14, and 21). Then, beams connect all columns in both orthogonal directions, creating a typical structural grid. Slabs are put on top of the beams covering the whole building in plan. The example of a generated structure is shown in Figure 52.

Parameter	Range	Total possible options
Columns' span in X direction	3-8 m (with a step of 0.5)	11
Columns' span in Y direction	3-8 m (with a step of 0.5)	11

Table 27. Range of columns' spans used for structural generation

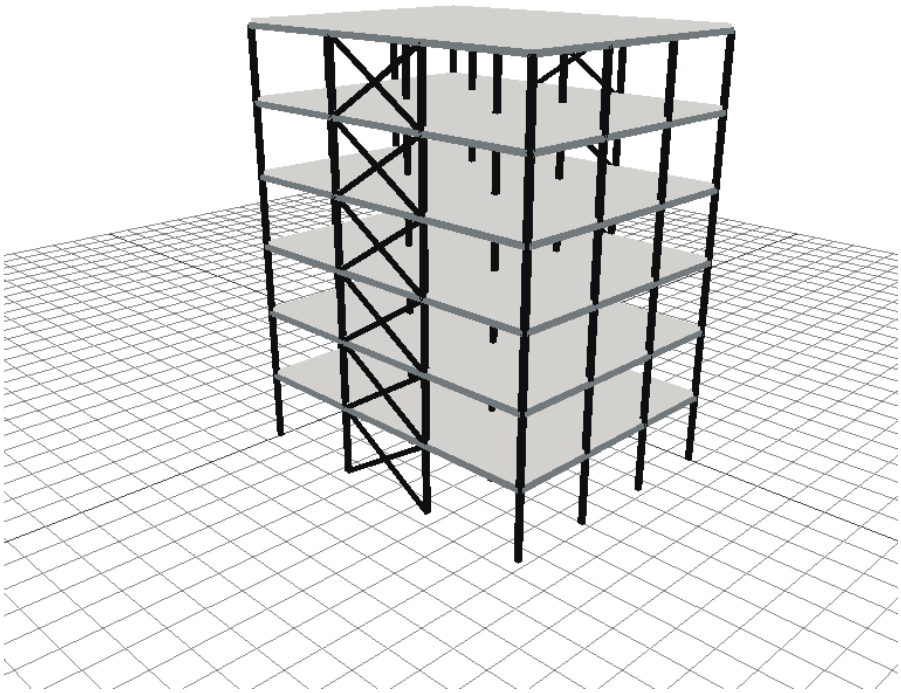

Figure 52. The example of a generated structure

Considering LLRSs, conventional ones as well as frames equipped with MYDs are used. Moreover, since there are 2 orthogonal directions, the combination of the two types is also implemented (i.e., conventional frames in one direction and frames equipped with MYDs in another one). Table 28 shows all possible configurations of LLRS considered by the tool. Regarding the location of the bracing tower, when only one is needed, it is placed on a central bay, while when two of them are required, they are located on the edge bays. Figure 52 shows a structure where CBF is used in one structural direction while MRF in an orthogonal one.

LLRS in X direction	LLRS in Y direction
MRF	MRF
MRF	CBF
MRF	MRF with DRBeS
MRF	CBF with DRBrC
CBF	CBF
CBF	MRF
CBF	CBF with DRBrC
CBF	MRF with DRBeS
MRF with DRBeS	MRF
MRF with DRBeS	MRF with DRBeS
MRF with DRBeS	CBF
MRF with DRBeS	CBF with DRBrC
CBF with DRBrC	CBF
CBF with DRBrC	CBF with DRBrC
CBF with DRBrC	MRF
CBF with DRBrC	MRF with DRBeS

Table 28. All the possible LLRS combinations

The total number of all possible structural configurations is equal to:

$$Total = Columns' spans in X direction \cdot Columns' spans in Y direction \cdot LLRSs$$
$$= 11 \cdot 11 \cdot 16 = 1936 \; structures$$

Due to the strict discretisation of the geometrical parameters, the resulting value of all possible solutions is not as high as in seen in the literature where GA was commonly used (Table 29). The high number of generated buildings in other studies is related to either the use of continuous values such as area of the dampers' cross-section (which makes the iteration through all possible solutions impossible) or an extreme size of the total design space (due to a lot of parameters being optimised simultaneously). Consequently, given the relatively small solutions space, there is no need to use complex evolutionary solvers such as GA and simple exhaustive enumeration (EE) algorithm is suitable for solving the optimisation problem in this study.

Study	Algorithm	Number generated solutions needed for algorithm to converge
This thesis	EE	1 936
[92]	GA	38 104
[108]	GA	10 000
[116]	GA	14 000

Table 29. Comparison of the generated solutions between this study and the literature

6.2 Structural design

After all the structures are generated, the structural design stage initiates. The building is firstly designed for a gravity loads and then the resulted configuration is being subjected to seismic loads. Following the current seismic design standards and recommendations for columns' optimisation in plan [141], only columns located on the edges of the building are designed to resist seismic loads, while ones located inside are designed only for gravity loads (Figure 53). Following the same intention, MRFs are allowed to be located only on the edges of the building and not on every bay as it was frequently done in the past.

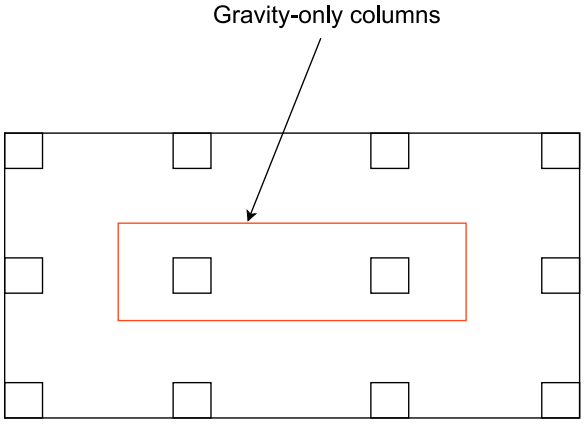

Figure 53. Location of gravity-only column in a generic plan

The design for gravity loading starts from collecting loads acting on each group of beams and columns based on their tributary area (Figure 54). In case of beams, the load from the slab is assumed to be distributed along the longer span. The Ultimate Limit State (ULS) load combination from Eurocode 1 [142] is used to get a final value of the acting gravity load:

$$q = \gamma_g \cdot G + \gamma_q \cdot Q$$

Where:

- γ_g is a multiplier for a gravity load equal to 1.35
- G is a nominal value of an acting dead load [kN/m]

- γ_q is a multiplier for a gravity load equal to 1.5
- G is a nominal value of an acting live load [kN/m]

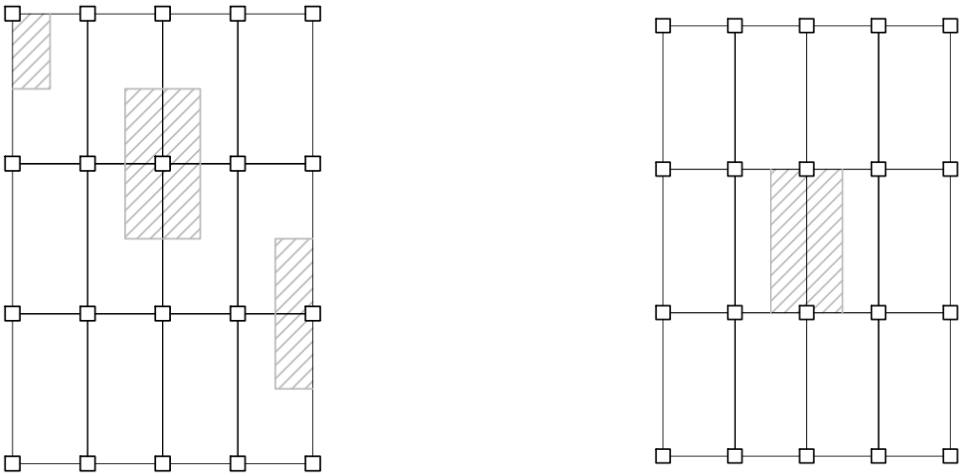

a. Tributary load area for internal and external columns b. Tributary area for beams

Figure 54. Tributary areas for beams and columns [92]

Then, the acting bending moments and axial loads are calculated using simple engineering formulas. In particular, axial force acting on columns is calculated using the following formula:

$$N = q \cdot L_x \cdot L_y \cdot NS$$

Where:

- q is a final value of the acting gravity load in ULS combination [kN/m].
- L_x is the tributary width in x direction [m].
- L_y is the tributary width in y direction [m].
- NS is the number of stories above the column.

Beams can be classified depending on their connection type (pinned or rigid) and the role in the gravity load path (primary and secondary). Only beams located in MRFs on the edge of the structure are assumed to have a rigid connection while all others are pinned. Secondary beams receive the load from the slab and transfer it to the primary beam which receives this load and the weight of the secondary beam itself. The final gravity load acting on a secondary beam equal to:

$$q_{sec} = q \cdot L_{sec}$$

Where:

- q is a final value of the acting gravity load in ULS combination [kN/m]
- L_{sec} is the tributary width of a secondary beam [m]

While the final gravity load acting on a primary beam is calculated in a following manner:

$$q_{pr} = (q + \gamma_g \cdot W_{sec}) \cdot L_{pr}$$

Where:

- q is a final value of the acting gravity load in ULS combination [kN/m]
- γ_g is a multiplier for a gravity load equal to 1.35
- W_{sec} is a distributed self-weight of a secondary beam [kN/m]
- L_{pr} is the tributary width of a primary beam [m]

Finally, the bending moment acting on a beam is calculated in the following manner:

$$M = \frac{q_{beam} L^2}{K}$$

Where:

- q is a final value of the acting gravity load on a beam [kN/m]
- L is a span of a beam
- K is a coefficient related to a constraint. It is equal to 8 for pinned beams and to 12 for rigidly connected ones.

Columns that have a rigid connection with beams (in MRF frames) are assumed to have the same bending moment coming from the gravity loads as beams (since beams transfer their moment entirely to columns in MRFs). To achieve the local optimisation, the following elements' groups are defined based on the acting vertical loads and restraints:

- Internal (gravity-only) columns for floors 1-3.
- Internal columns for floors 4-6.
- Edge columns for floors 1-3.
- Edge columns for floors 4-6.
- Internal beams
- External MRF beams
- External CBF beams

The distinction between columns is made since columns on upper floors support lower number of stories compared to columns on the bottom floors. Consequently, their acting axial loads are lower, and the dimension of cross-section can be smaller than for bottom columns. The same logic is followed regarding internal and external columns where the former ones have higher tributary area and must resist larger axial loads as a consequence. The distinction for internal and external beams follows the same logic while the difference between CBF and MRF beams lies in acting bending moment and reflected in a formula above. Figure 55 presents the workflow for an automated gravity loads design implemented in the tool. After getting acting internal loads, the check on column and beam is performed according to Eurocode 3 [143]. Then, the cross-sections of structural elements are increased until the check is satisfied. Since bracing members do not have any gravity loads acting on them, their cross-sections are taking as the smallest ones from the catalogue (Table 8). The distribution along heigh is similar as in ML training – different cross-sections in each 2 stories, having the largest in the bottom floors and the smallest in the upper ones (Table 8). For example, if the building has 6 storeys, the smallest cross-sections from catalogue will be assigned on the upper two stories, then for stories 3-4 the second smallest cross-sections will be used, and finally first two stories will receive the third smallest cross-section. Figure 55 summarises the workflow for structural design for the gravity loads.

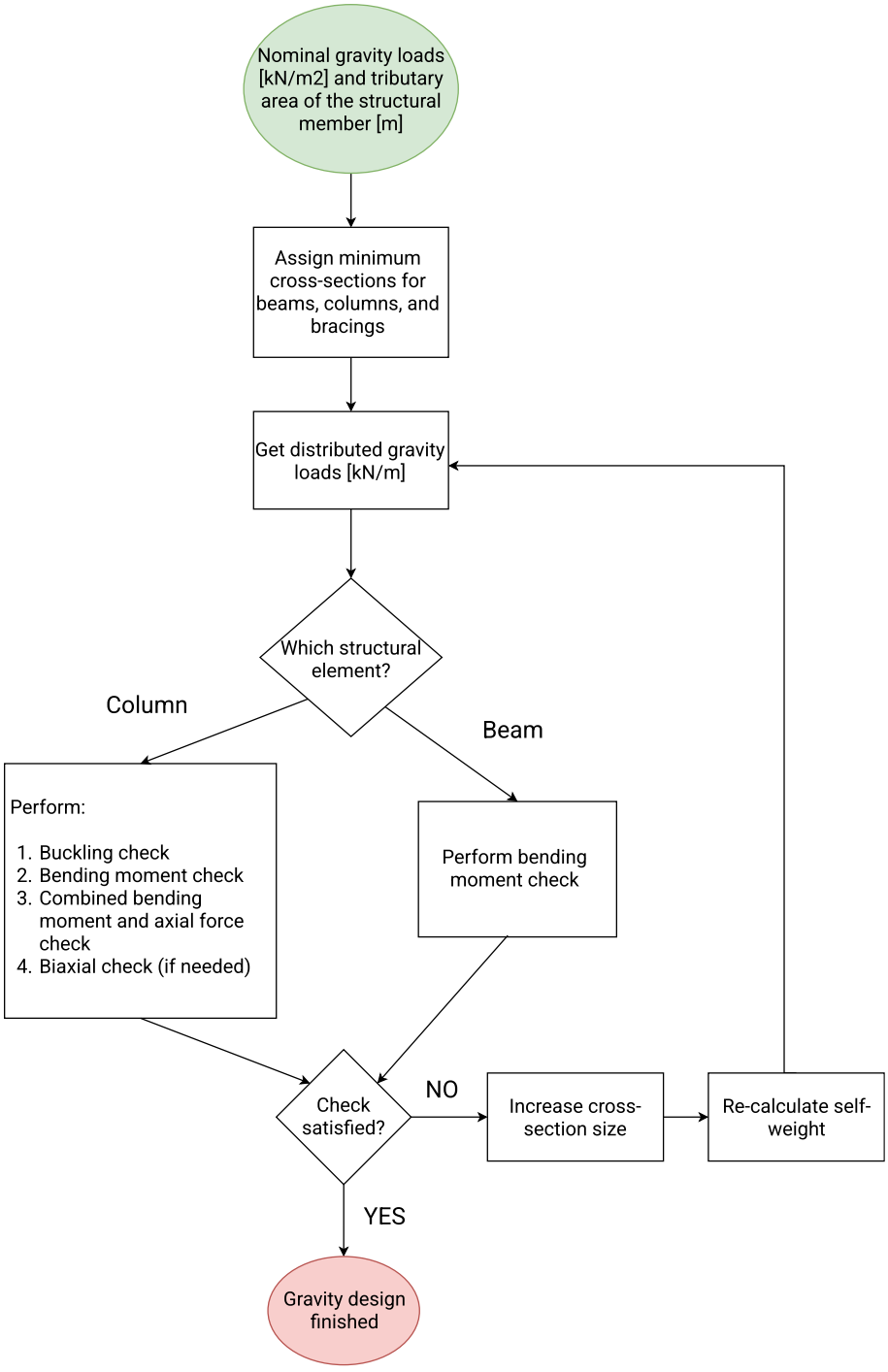

Figure 55. Diagram for the structural design for the gravity loads

After the structure is designed for a gravity loads, and all cross-sections are optimised a seismic design starts. First of all, seismic requirements such as strong-column-weak-beam and bracing slenderness limits imposed by Eurocode 8 are verified. For the seismic loads two, already mentioned, limit states are considered: DL and SD. In DL limit state the serviceability criterion is checked. In this study, as it is commonly used for structural seismic design, this criterion is an interstorey drift that must be lower than 1% of the interstorey height in accordance with Eurocode 8. Moreover, no yielding of any structural element is allowed in this limit state. SD limit state reflects ultimate limit state design where only building components' and MYDs resistance is checked. Following the code and DISSIPABLE guidelines [132] suggestions, in the conventional structures yielding of beam (in

MRF) and bracings (in CBF) is allowed in this limit state given that columns are not damaged. In the meantime, for buildings equipped with MYDs, only dampers are allowed to yield while all other structural elements must stay elastic. The type and number of structural checks for beams and columns in seismic scenario are the same as for the gravity loads case and shown in Figure 55. While for bracings both yielding and buckling checks are performed. Only beams and columns comprising LLRS (i.e., located on the edge of the building) are subjected to seismic loads and being updated during the seismic design step, while gravity-only columns and beams are left unchanged after the end of the gravity analysis. Figure 56 summarises the steps performed in seismic design in a form of a diagram. The result of this step is the structure designed to resist both gravity and seismic loads. However, since some structural elements are allowed to yield, their repair status is recorded to accurately estimate the cost and embodied carbon of each generated and designed configuration.

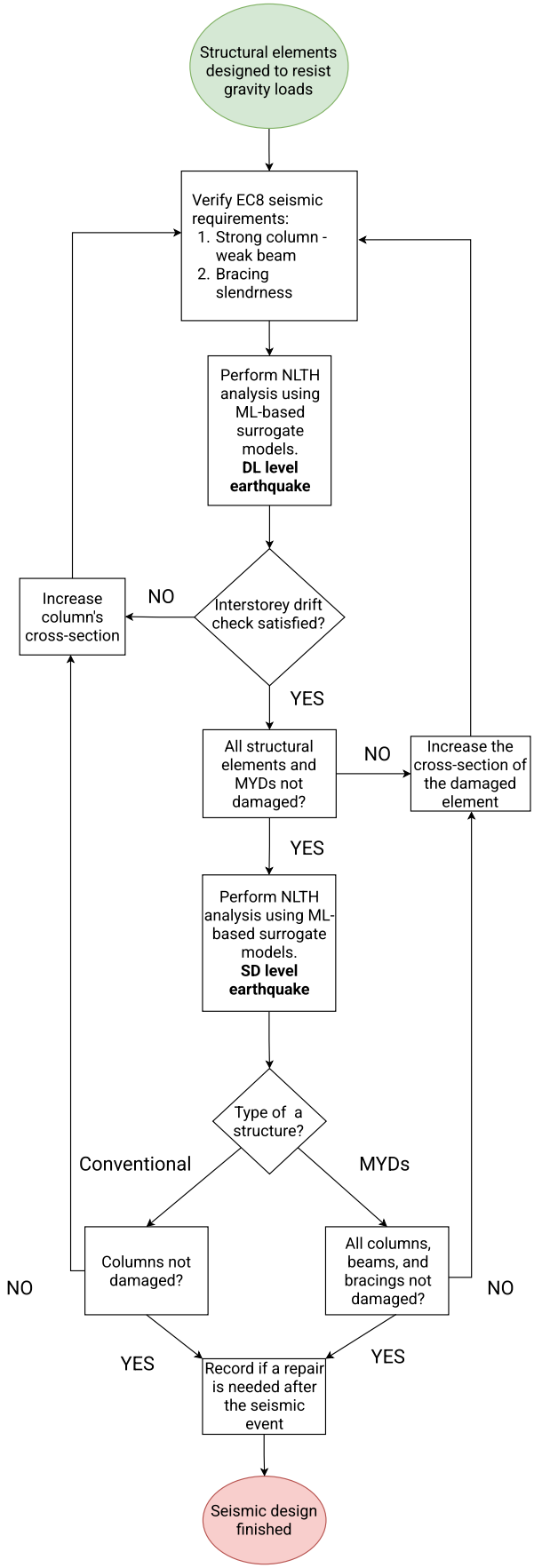

Figure 56. Diagram for the structural design for the seismic loads

6.3 Cost and embodied carbon calculation

After each structure is designed, its cost and embodied carbon are calculated. Structural weight is calculated first since both parameters are the function of it. The weight is calculated separately for structural elements (steel) and floor slab (reinforced concrete). The monetary cost accounts for both the material cost and the workmanship cost. They have been considered directly proportional to the material quantity and can be calculated as follows:

$$C_{\text{elements}} = W \cdot (uc_{\text{m}} + uc_{\text{l}})$$

Where:

- W is the total weight of the material under consideration
- uc_m – unitary cost of the material
- uc_l – unitary cost of the labour

The values for unitary costs are specified in Table 30 for the different material types. The price generator of Cype website has been used as a reference to extract the unitary costs of materials and labour [144]. The price highly depends on the market factors and can be a bit higher or lower depending on the time of the read. However, since the same unit price is applied to all structures, the exact amount of it does not matter in terms of the results of the optimisation procedure (which tries to identify which columns' spans and LLRS lead to the cheapest structures). Even though the exact price of the cheapest structures can be different in reality compared to this thesis, the conclusion regarding of which optimisation parameters lead to the price decrease will be still valid. The quantity of reinforcement in the concrete is estimated approximately according to [145]. The values for MYDs are taken from comprehensive LCC study which is explained in detail in [146].

	Steel S275	Steel S355	MYDs	Reinforcing steel
Unitary material cost (uc_m)	0.86 €/kg	0.96 €/kg	393 € (DRBrC)	0.81 €/kg
Unitary labor cost (uc_l)	0.42 €/kg		48 € (DRBeS)	-

Table 30. Unitary costs of steel and concrete materials and labor

The cost of the floor system can be easily calculated with the floor surface and the unitary floor cost per quadratic meter.

$$C_{\text{floor}} = A_{\text{f}} \cdot \text{NS} \cdot (uc_{\text{m}} + uc_{\text{l}})$$

Where:

- Af is the floor area of one storey [m^2]
- NS total number of storeys
- uc_m – unitary cost of the material for steel-concrete composite slab, taken as 41.85 €/m^2
- uc_l – unitary cost of the labour for steel-concrete composite slab, taken as 28.70 €/m^2

Finally, the total monetary cost is calculated as a sum of structural elements and floor costs.

Regarding the embodied carbon, the approach officially adopted by the current standards and recommendations [131], [147] is implemented in this study. In particular:

$$E = W \cdot \sum Coef$$

Where:

- W is the total weight of the material under consideration [kg]
- $\sum Coef$ is a sum of carbon coefficient [kgco2 / kg]

Carbon coefficients are reported in Table 31 separately for steel and concrete materials. They are taken from the ICE database [148] which is commonly used in the engineering practice [142]. In this case, a cradle-to-gate approach has been chosen for the embodied carbon calculation and thus the embodied carbon factors A1-A3, and C have been considered. The factors referring to the construction stage (A4-A5) are not included since they are highly dependent on the project location and factors related to the use stage (B1-B7) are also not included since their contribution in embodied carbon for structural elements is relatively very low [149]. The values for MYDs are taken from comprehensive LCA study which is explained in detail in [146].

Product	A1-A3	C1-C4	Total
Hot rolled plate and structural sections [kg co2e / kg of product]	2.50	0.0135	2.51
Concrete RC30 [kg co2e / kg of product]	0.20	0.0135	0.21
Reinforcing steel [kg co2e / kg of product]	1.96	0.0135	1.97
MYDs [damper]		296 (DRBrC) 43.5 (DRBeS)	

Table 31. Embodied carbon coefficients

Finally, the impact of the structural damage and consequent repair status on cost and embodied carbon is considered (Table 32). In the absence of damage both parameters are expectedly not affected. While the damage in beam or bracing leads to full building repair and reconstruction, following the assumptions in LCA analysis described in chapter 4 of this thesis. The repair of MYDs leads to 20% increase in cost and embodied carbon according to the results of the LCA analysis (Figure 25).

Damage	Repair status	Impact on cost and embodied carbon
No damaged	No repair	-
Beam/bracing yielded or buckled	Full building repair	2x increase in both
MYDs yielded	MYDs repair	0.1x increase in both

Table 32. Impacts of repair status on cost and embodied carbon

6.4 Graphical User Interface (GUI)

GUI allows the user to communicate with a software and extract a value out of it. The resulting tool was developed using Javascript programming language [150]. The starting screen presents a generic 3D structure and several menu buttons (Figure 57):

- “Inputs” where the user can provide the geometrical, loading, price and carbon inputs for the design space generation and evaluation.
- “Pareto front” where the exploration of the best design options and cost-embodied carbon trade-off happens.
- “Details” where each of the chosen from pareto front solutions can be explored in detail.
- “Info” providing the general information of the toll and its capabilities.

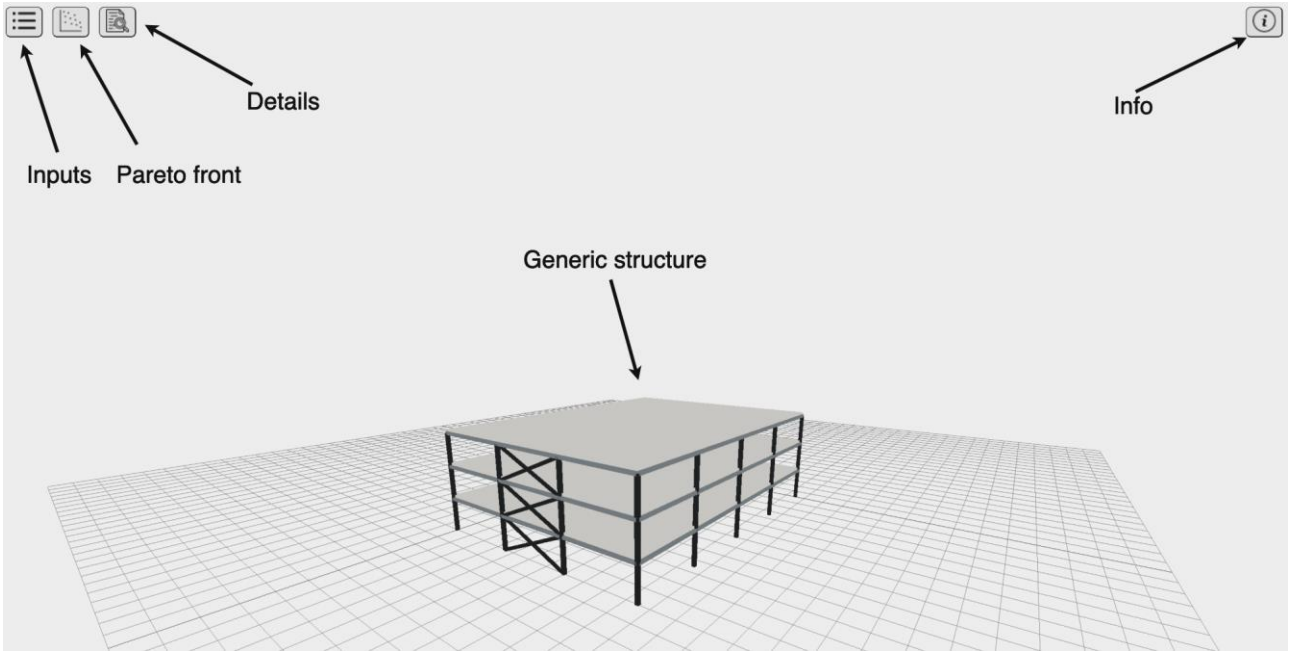

Figure 57. Starting screen of the tool

After “inputs” button is pressed, three tabs appear: building parameters, cost parameters, and CO2 parameters (Figure 58). Structural geometry such as overall building dimensions in X and Y directions, number of floors and floor height are inserted first. The column span and LLRS are the parameters to be optimised as it was mentioned in the previous subchapters. Therefore, they are not presented in the building parameters tab. Material grades and acting gravity loads are other essential inputs that must be chosen before the launch of the analysis. Unitary cost and CO2 coefficients can vary significantly by location and materials’ producers. Therefore, the user can modify these parameters while the default inputs were explained in the previous subchapter. After all the inputs are set the “submit” button must be pushed to launch the design space generation.

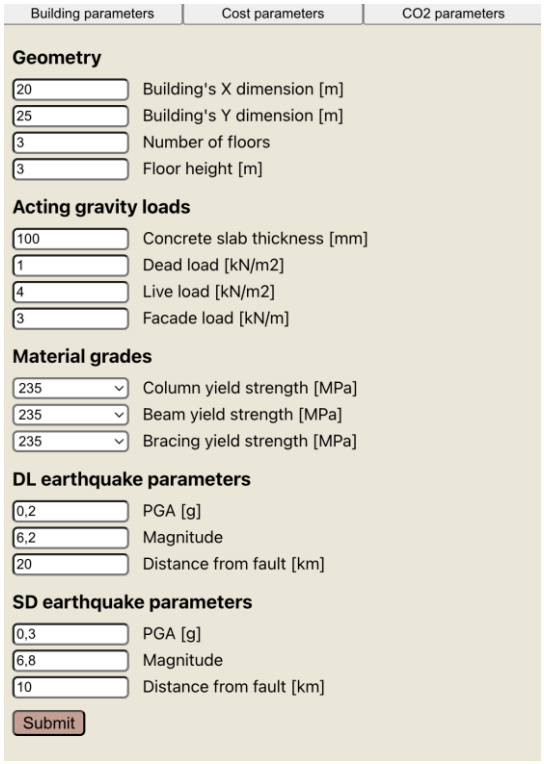

a. Building parameters

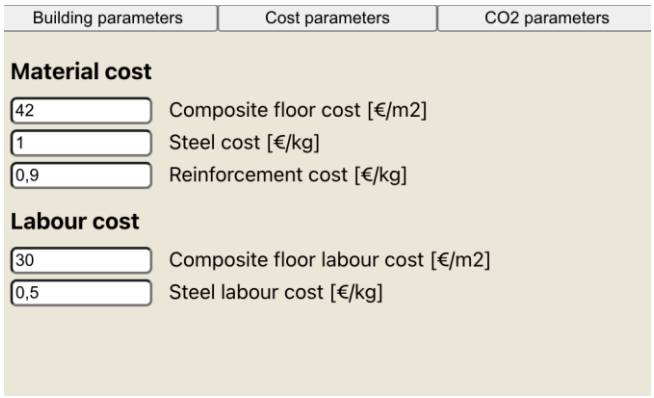

b. Cost parameters

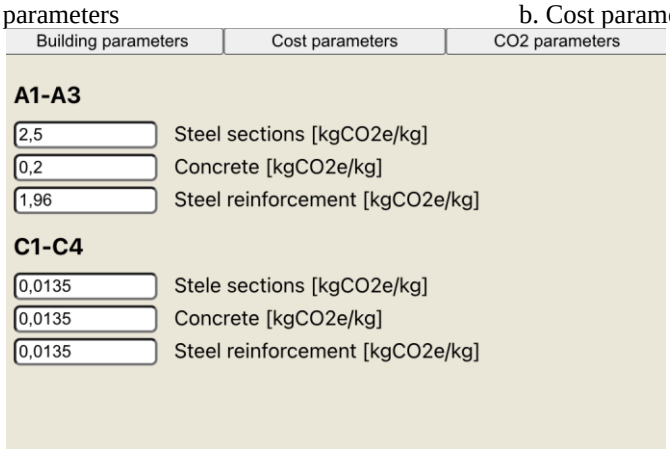

c. CO2 parameters

Figure 58. Inputs menu

After the design space is generated, it can be interactively explored pressing “pareto front” button (Figure 59). First of all, the number of the best designs to show must be chosen. “Best” designs are chosen according to non-dominant multi criteria search, where the rank is assigned for all the possible structural configurations and the whole design space is sorted according to this rank in the ascending order (meaning solutions with rank 1 are the best ones). Then, optimisation criteria must be chosen. By default, they are cost and embodied carbon, but only one of them could be selected as well. Finally, there is an option to not include designs with MYDs if the user is not familiar with them and wants to explore only traditional frames. As an output, the pareto front graph is shown where each structure is placed as a dot with y coordinate corresponding to its total cost and x coordinate corresponding to its embodied carbon emissions normalised per gross internal area (GIA). The latter one has been chosen instead of the total emissions, since it is normalised, and a more accepted and clear way to report embodied CO2 in structural engineering practice [147].

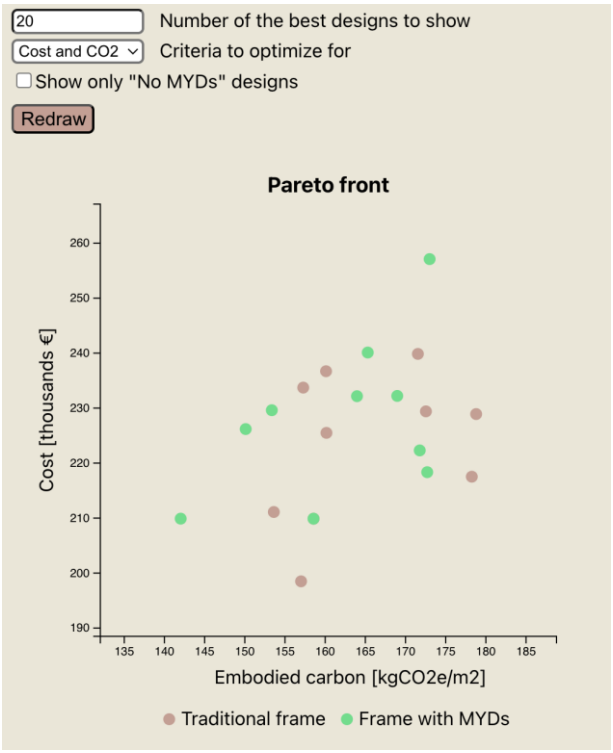

a. Default pareto front

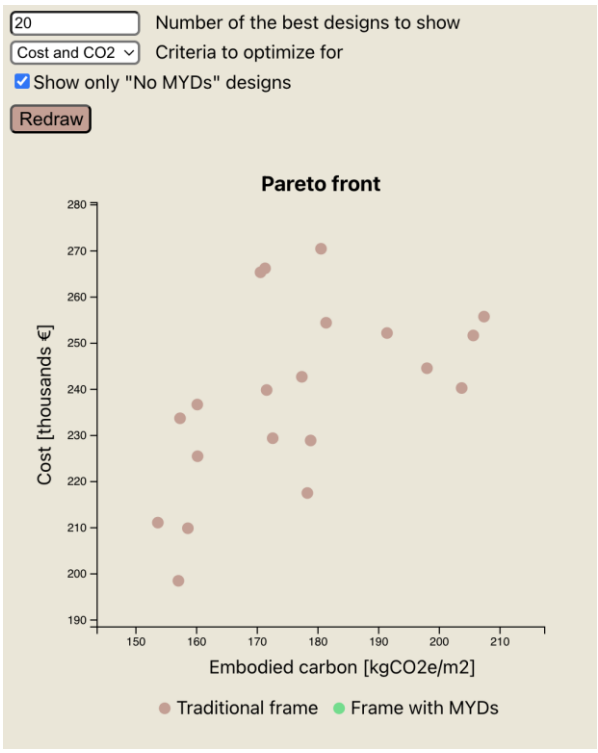

b. Pareto front with only traditional frames

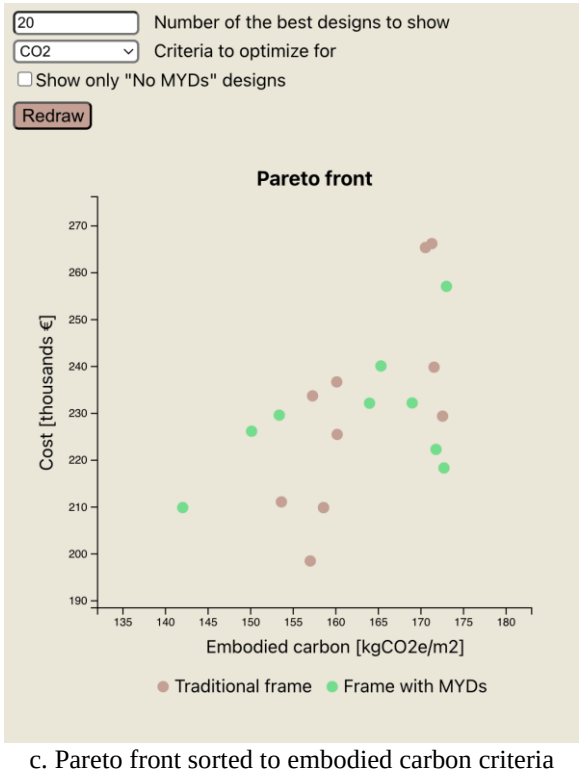

c. Pareto front sorted to embodied carbon criteria

Figure 59. Pareto front

The user can click on each of the dots in pareto front graph to see the corresponding structural solution visualised in 3D in the main screen. Moreover, clicking the “details” button, structural details for this solution such as LLRS, elements’ cross-sections, MYDs dimensions, structural periods, interstorey drifts and elements’ damage status can be explored (Figure 60). Eventually, following a back-and-forth process between pareto front visualisation and structural details exploration, the user

can choose the best solution for his/her particular case and justify the decision by the data taken from this tool. This workflow ensures that local (cross-sectional) optimisation is handled automatically by the tool, while global (layout) optimisation must be finalised by the engineer given the design requirements and constraint.

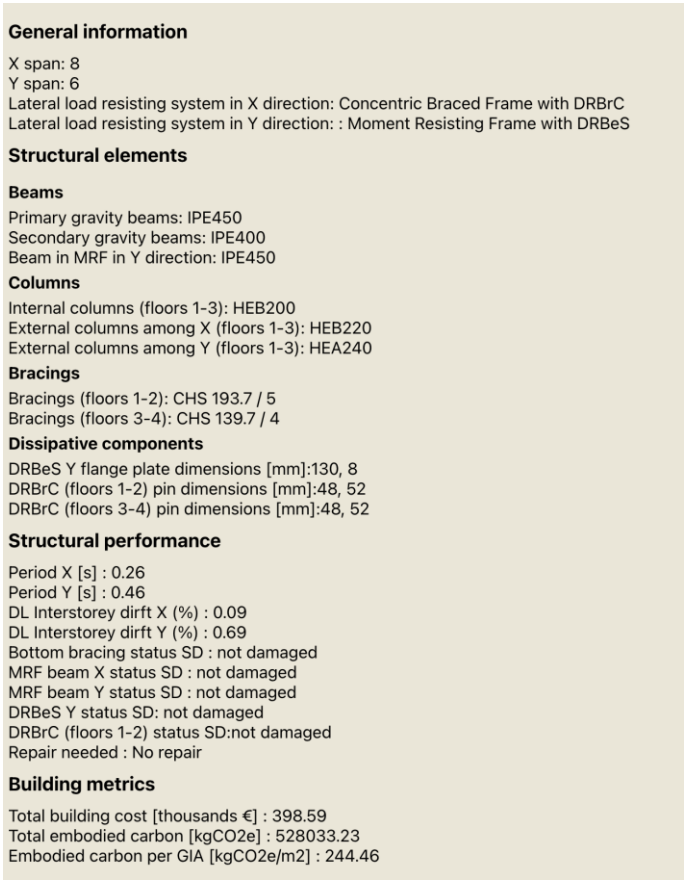

Figure 60. Solution details

6.5 Case studies

To show the validity and the impact of the tool in structural engineering practice, 3 case studies are analysed:

- 4-storey generic building
- 5-storey building taken from the literature [151]
- 3-storey building taken from DISSIPABLE project

6.5.1 4-storey generic building

In this case study, 4-storey building with generic plan dimensions and acting loadings is considered. The purpose of this example is to showcase the potential application of the developed tool in the engineering practice and quantify the potential impacts of its use. The building input parameters are shown in Figure 61. The seismic action is assumed to have the same magnitude and distance to fault with just PGA increasing from DL to SD limit state. This is done to reflect a common practice of NLTH analysis where the same ground motion is scaled up in terms of PGA to reflect different limit states. Cost and CO2 parameters are kept as default.

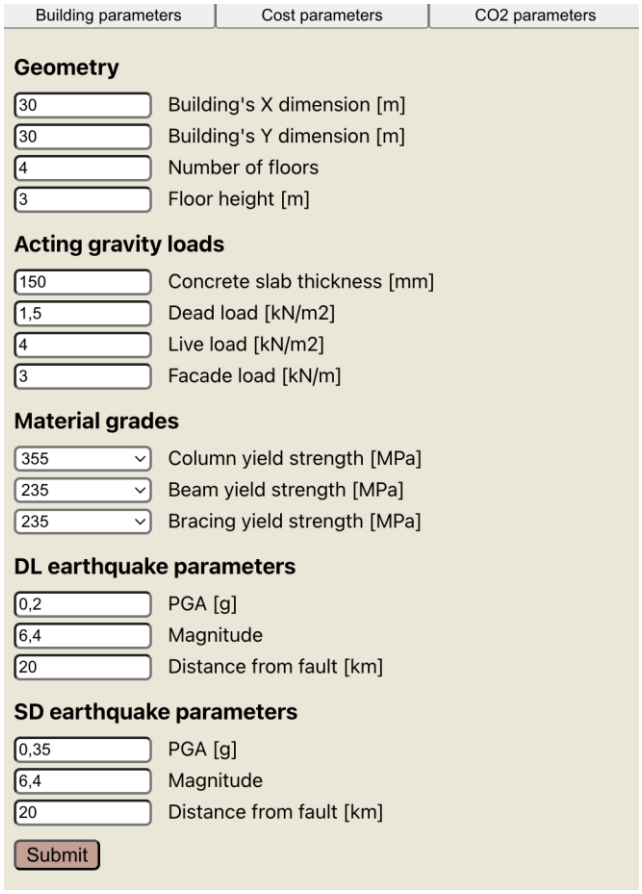

Figure 61. Input parameters for 4-storey generic building case study

After pressing the submit button, the design space generation procedure started. It took just 500 seconds (around 8 minutes) for the web version of SUSTEZ to generate and design 1936 structures. That speed was possible thanks to the use of ML-based surrogate models which rapidly predicted the results of NLTH analyses for each structure. Moreover, this speed was reduced by the limited computer power available on the cloud server where ML model is deployed. On the local computer of the author of the thesis. The generation took just 50 seconds. If for each case, the NLTH analysis would be performed in FEM software instead, it would take on average 36 seconds for each 2D frame (which was measured and reported during data generation procedure for ML training). Considering that 3D building consists of two 2D frames, each of which is subjected to 2 ground motions (DL and SD) and averagely 3 design iterations (invoked by "No" in Figure 56), the average time of FEM analysis of 1 structure will be 432 seconds. Consequently, for 1936 buildings, it will take 836352 seconds or approximately 232 hours which results in almost 10 full days. However, this increase of the speed comes at the cost of the error related to the FEM analysis results. Table 33 shows the comparison between surrogate models and conventional FEM for the design space generation in terms of time (the generation time in a local computer is reported for the fairness of the comparison) and analysis error. The error for surrogate models is taken as an average of the best models for each response presented in Table 13.

Method	Time of design space creation (s)	Error (%)
ML-based surrogate models	50	9.17
Conventional FEM	836 352 (10 days)	0.00

Table 33. Comparison of design space generation using surrogate models and conventional FEM

The resulting pareto front for this case study is shown in Figure 62. The best 30 solutions (Figure 62, a) are shown along with the whole design space (Figure 62, b). On the whole design space

visualisation, the correlation between cost and embodied carbon is clear. It is expected since both of the criteria depend on the weight and the unit cost and carbon coefficients are taken the same for all solutions.

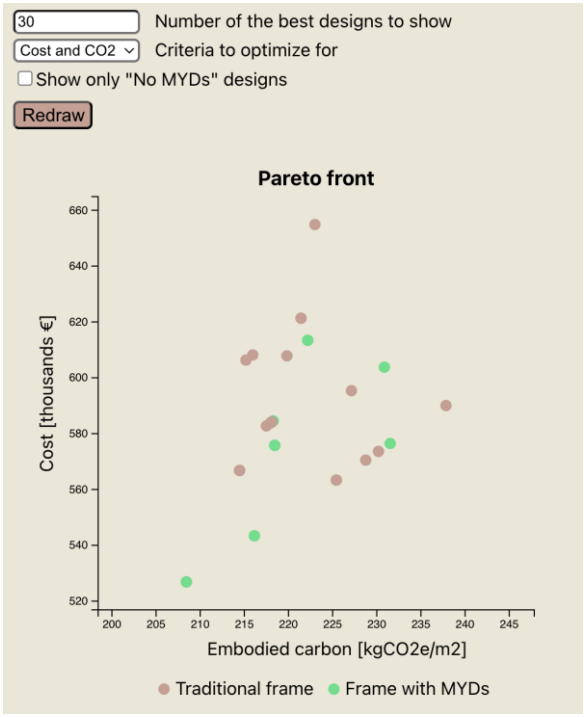

a. Pareto front for the best 30 solutions

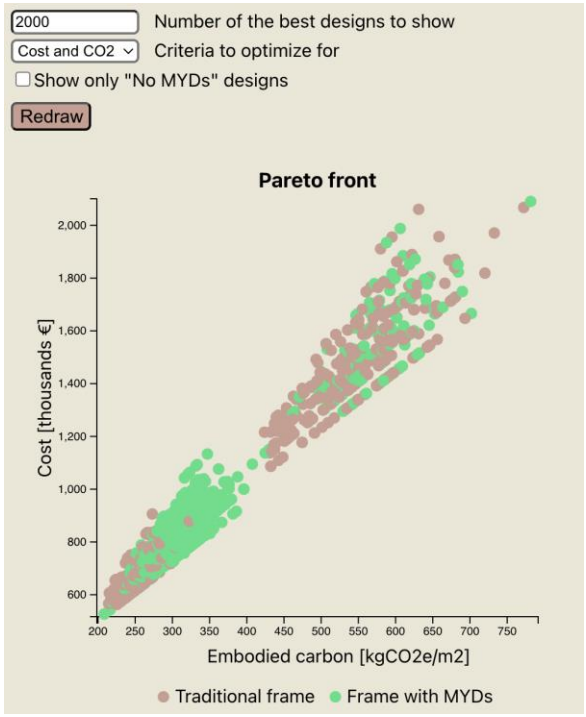

b. Pareto front for the entire design space

Figure 62. Pareto fronts for 4-storey generic building case study

The details for one of the generated solutions are shown in Figure 63. The structural span is equal to 5.5 meters in X direction and 5 meters in Y direction, while LLRS is a mix of traditional MRF and CBF equipped with DRBrC.

General information

X span: 5.5
Y span: 5
Lateral load resisting system in X direction: Concentric Braced Frame with DRBrC
Lateral load resisting system in Y direction: : Moment Resisting Frame

Structural elements

Beams

Primary gravity beams: IPE360
Secondary gravity beams: IPE300
Beam in MRF in Y direction: IPE360

Columns

Internal columns (floors 1-3): HEB280
External columns among X (floors 1-3): HEB280
External columns among Y (floors 1-3): HEB280
Internal columns (floors 4-6): HEA100
External columns among X (floors 4-6): HEB160
External columns among Y (floors 4-6): HEB160

Bracings

Bracings (floors 1-2): CHS 168.3 / 4
Bracings (floors 3-4): CHS 101.6 / 3.2

Dissipative components

DRBrC (floors 1-2) pin dimensions [mm]:36, 42
DRBrC (floors 3-4) pin dimensions [mm]:36, 42

Structural performance

Period X [s] : 0.30
Period Y [s] : 0.76
DL Interstorey dirft X (%) : 0.10
DL Interstorey dirft Y (%) : 0.81
Bottom bracing status SD : not damaged
MRF beam X status SD : not damaged
MRF beam Y status SD : not damaged
DRBrC (floors 1-2) status SD:not damaged
Repair needed : No repair

Building metrics

Total building cost [thousands €] : 770.3
Total embodied carbon [kgCO2e] : 1145017.77
Embodied carbon per GIA [kgCO2e/m2] : 289.15

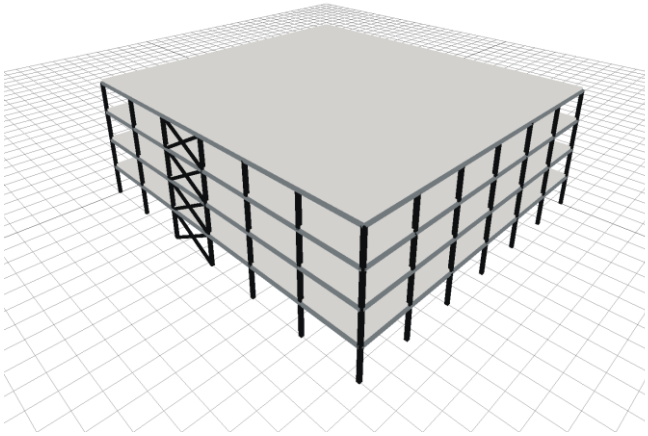

a. Building's information b. Building's visualisation

Figure 63. Details of the solution for 4-storey generic building case study

Finally, to evaluate the potential impact of the tool. The best (the dot in the bottom left corner of Figure 62, a) and worst (the dot in the upper right corner of Figure 62, b) structural solutions are compared in terms of cost and embodied carbon. It is done to evaluate the range of both criteria in a structural configuration for a fixed building volume. Table 34 shows the drastic difference (around 3 times) between the best and worst solutions for each criteria. It shows that even for a constrained volume, just the change of structural span and LLRS can create structural solutions that are 3 times more sustainable than others. The developed tool allows a seamless design space exploration to discover these differences and come up with the best decision according to the project's requirements.

	Total cost [thousands €]	Total embodied carbon [tons CO2e]	Embodied carbon per GIA [tons CO2e/m2]
The best solution	543	778	216
The worst solution	2091	3202	782
Absolute difference	1543	2424	566
% difference	285	312	262

Table 34. The comparison of the worst and the best solutions for 4-storey generic building case study

6.5.2 5-storey building taken from the literature

The reference structure for the next case study is taken from Eurocode 8: Seismic Design of Buildings
Worked examples [151]. It is a design manual commonly used as a reference by structural engineers in Europe. 6-storey structure having CBF as LLRS in both directions is taken as an example from there. The goal of this case study is to find the reference structure inside the generated design space, explore the design differences between the tool's automated design procedure and the manual one performed by the authors of [151], and propose the alternative design solutions found by the

tool. The input for the case study is shown in Figure 64. Since the reference structure has been analysed by means of response spectrum analysis, to make the comparison fair, the San Fernando accelerogram from PEER database was scaled to match this response spectrum. The visual comparison between the spectrum and the scaled accelerogram can be found in Appendix F. PGA for SD earthquake was taken from the scaled accelerogram while for DL earthquake this PGA was divided by 1.5 following Eurocode 8 assumption DL to SD ratio. All other input parameters were taken according to the reference structure in [151].

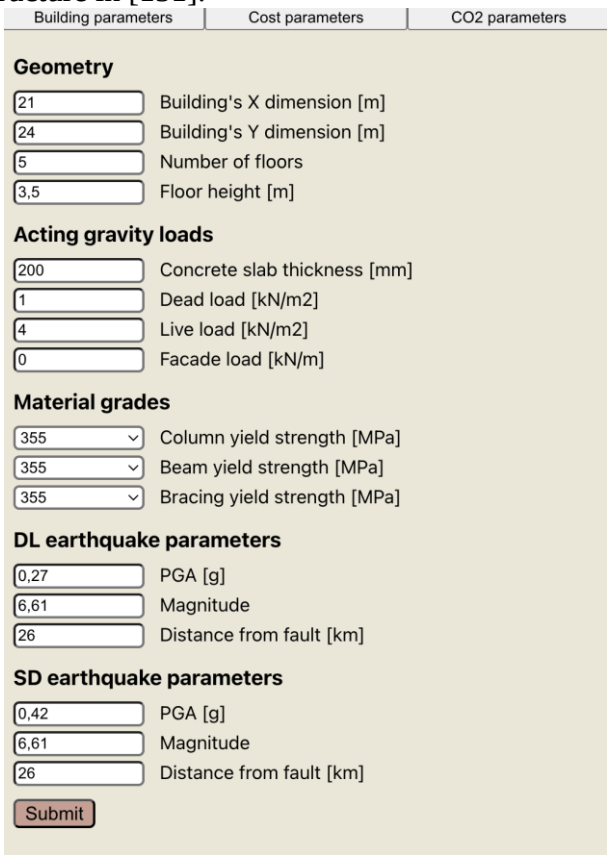

Figure 64. Input parameters for 5-storey building taken from the literature case study

First of all, the validation between the tool and the reference structure is performed. It consists of comparing the results of structural design in terms of found elements' cross-section. Table 35 shows this comparison in detail. Columns' cross-sections are a bit lower in the tool compared to the reference. It can be attributed to different column alignment along the height (uniform in the reference and smaller columns in the last 2 floors in the tool). Beams' cross-sections are harder to compare since in the reference composite steel-concrete beam is used. It is expected then to see larger beams designed by the tool since the interaction between steel and concrete is not considered for beams in there. Finally, bracings areas are very similar which shows a good convergence between the tool and the reference structure. Apart from above mentioned reasons for the discrepancy in the structural design, it was expected to get slightly different results between these 2 cases since linear analysis was used in one and nonlinear in another. Even though the accelerogram was scaled to match the response spectrum, the different nature of analyses inevitably could cause some difference in the results.

General information

X span: 7
Y span: 6
Lateral load resisting system in X direction: Concentric Braced Frame
Lateral load resisting system in Y direction: : Concentric Braced Frame

Structural elements

Beams

Primary gravity beams: IPE400
Secondary gravity beams: IPE330

Columns

Internal columns (floors 1-3): HEB240
External columns among X (floors 1-3): HEB240
External columns among Y (floors 1-3): HEB240
Internal columns (floors 4-6): HEB160
External columns among X (floors 4-6): HEB200
External columns among Y (floors 4-6): HEB200

Bracings

Bracings (floors 1-2): CHS 177.8 / 5
Bracings (floors 3-4): CHS 168.3 / 4
Bracings (floors 5-6): CHS 168.3 / 4

Structural performance

Period X [s] : 0.27
Period Y [s] : 0.29
DL Interstorey dirft X (%) : 0.19
DL Interstorey dirft Y (%) : 0.17
Bottom bracing status SD : not damaged
MRF beam X status SD : not damaged
MRF beam Y status SD : not damaged
Repair needed : No repair

Building metrics

Total building cost [thousands €] : 499.58
Total embodied carbon [kgCO2e] : 814804.43
Embodied carbon per GIA [kgCO2e/m2] : 323.34

a. Building's information

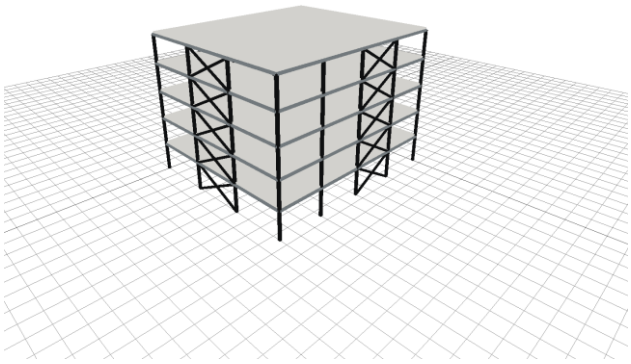

b. Building's visualisation

Figure 65. Details of the found solution for validation with a literature

	Columns	Beams	Bracing area [mm^2]
The tool	HEB 240 (upper) HEB 200 (bottom)	IPE 330 (secondary) IPE 400 (primary)	2714
Reference structure	HEB 260	IPE 270 (composite)	2510

Table 35. Comparison between the tool and the reference structure

After the validation is completed, the reference structure can be considered in the context of the whole design space. Figure 66 shows that the chosen by the authors of [151] solution is far from the worst possible, but there are also a lot of structural configurations that result to lower cost and embodied carbon emissions. Table 36 presents the comparison between the best traditional frame solution found by the tool in comparison to the reference structure. It shows that the developed tool allows the discovery of the structural configuration that is cheaper by 122 thousand € and emits around 200 tons less in embodied carbon compared to the solution found by the engineering professionals.

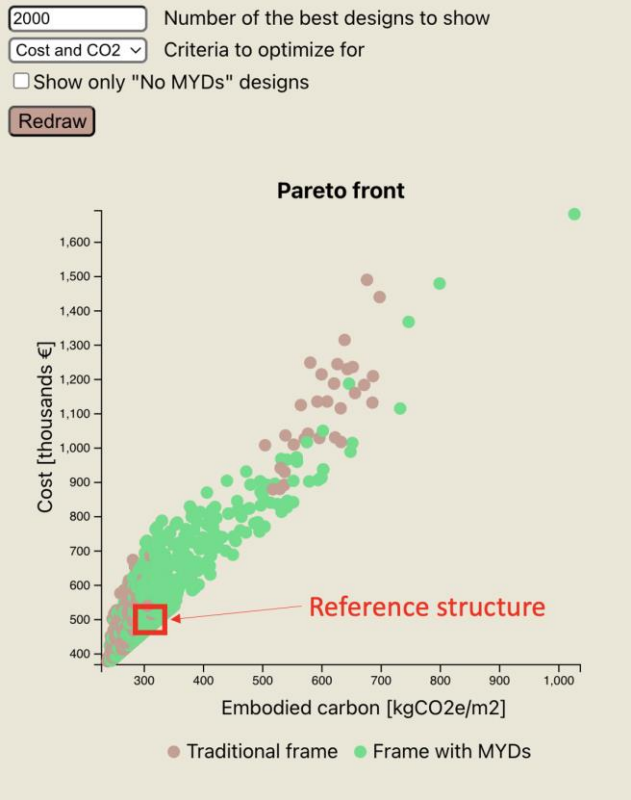

Figure 66. Pareto front for 5-storey building taken from the literature case study

	Total cost [thousands €]	Total embodied carbon [tons CO2e]	Embodied carbon per GIA [tons CO2e/m2]
The best solution	378	612	238
Reference structure	500	815	323
Absolute difference	122	203	85
% difference	24	25	26

Table 36. The comparison of the reference and the best solutions for 5-storey building taken from the literature case study

6.5.3 3-storey building taken from DISSIPABLE project

The final case study considers a structural configuration considered in DISSIPABLE project. The goal is to validate the structure (like it was done in the previous case study for the traditional frame) and then explore the reference solution in the context of the whole design space. The building under consideration is a 3-storey building from a case study reported in [132]. The input building parameters for the tool validation are shown in Figure 67. Since 7 accelerograms were used for the design of the reference structure, their mean PGA and magnitude for DL and SD limit states are taken as the input for the tool.

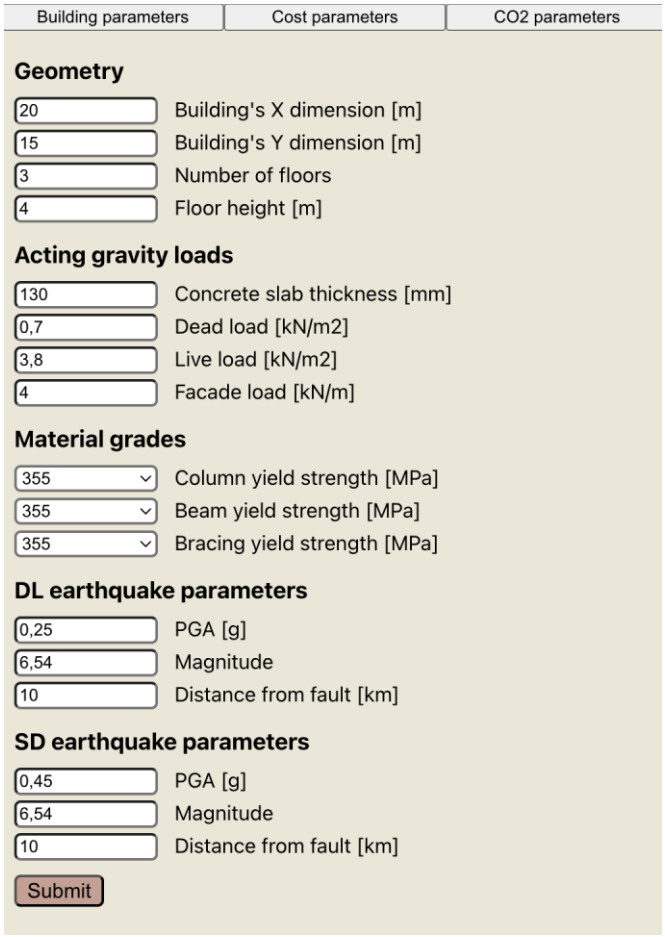

Figure 67. Input parameters for 3-storey building taken from DISSIPABLE case study

Figure 68 shows a found solution in the tool corresponding to the reference structure while in Table 37 the detailed comparison between the structural configuration found in the tool and the reference one is reported. The found cross-sections are relatively close to each other even though some differences are found. In terms of beams, they can be attributed to the use of composite beams in the reference structure and pure steel beams in the tool. Other differences (with columns, bracings and MYDs) are attributed to the inevitable error in the approximation of 7 ground motions by only one with the average parameters and ML-based surrogate models' errors.

General information

X span: 6.5
Y span: 5
Lateral load resisting system in X direction: Concentric Braced Frame with DRBrC
Lateral load resisting system in Y direction: : Moment Resisting Frame with DRBeS

Structural elements

Beams

Primary gravity beams: IPE330
Secondary gravity beams: IPE270
Beam in MRF in Y direction: IPE330

Columns

Internal columns (floors 1-3): HEB400
External columns among X (floors 1-3): HEB400
External columns among Y (floors 1-3): HEB400

Bracings

Bracings (floors 1-2): CHS 244.5 / 5
Bracings (floors 3-4): CHS 168.3 / 4

Dissipative components

DRBeS Y flange plate dimensions [mm]:90, 9
DRBrC (floors 1-2) pin dimensions [mm]:62, 68
DRBrC (floors 3-4) pin dimensions [mm]:62, 68

Structural performance

Period X [s] : 0.20
Period Y [s] : 0.64
DL Interstorey dirft X (%) : 0.03
DL Interstorey dirft Y (%) : 0.95
Bottom bracing status SD : not damaged
MRF beam X status SD : not damaged
MRF beam Y status SD : not damaged
DRBeS Y status SD: yielded
DRBrC (floors 1-2) status SD:not damaged
Repair needed : DRD repair

Building metrics

Total building cost [thousands €] : 181.16
Total embodied carbon [kgCO2e] : 257247.42
Embodied carbon per GIA [kgCO2e/m2] : 293.16

a. Building's information

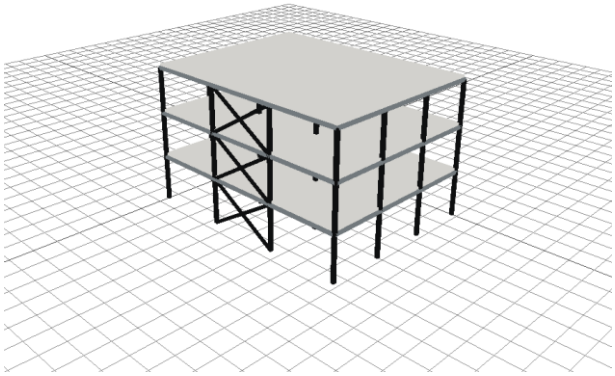

b. Building's visualisation

Figure 68. Details of the found solution for validation with DISSIPABLE

	Columns	Beams	Bracing area [mm^2]	DRBeS dimensions	DRBrC dimensions
The tool	HEB 400	IPE 330 (primary) IPE 270 (secondary)	7524	90x9	68x62
Reference structure	HEB 340	IPE 270 (composite, primary) IPE 200 (composite, secondary)	8113	150x14	80x70

Table 37. Comparison between the tool and the reference DISSIPABLE structure

After the validation is completed, the reference structure can be considered in the context of the whole design space. Figure 69 shows that the chosen by the authors of [132] solution is far from the worst possible, but there are also a lot of structural configurations that result to lower cost and embodied carbon emissions. Table 38 presents the comparison between the best traditional frame solution found by the tool in comparison to the reference structure. It shows that the developed tool allows the discovery of the structural configuration that is cheaper by 45 thousand € and emits around 76 tons less in embodied carbon compared to the solution found during DISSIPABLE research project by academics.

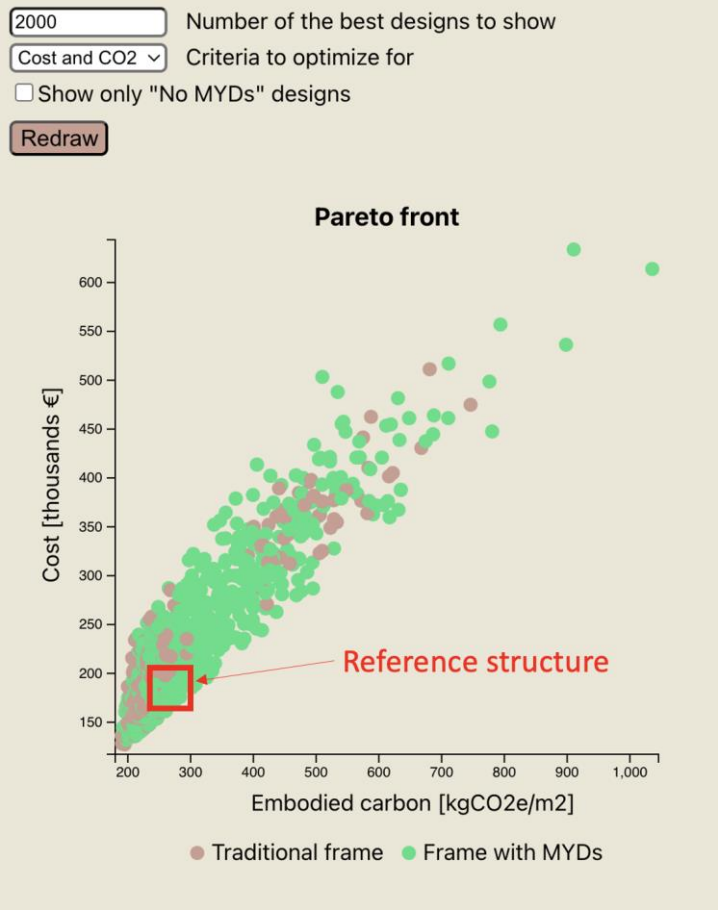

Figure 69. Pareto front for 3-storey building taken from DISSIPABLE case study

	Total cost [thousands €]	Total embodied carbon [tons CO2e]	Embodied carbon per GIA [tons CO2e/m2]
The best solution	136	182	192
Reference structure	181	258	293
Absolute difference	45	76	101
% difference	25	30	34

Table 38. The comparison of the reference and the best solutions for 3-storey building taken from DISSIPABLE case study

6.6 Discussion about SUZTEZ's functionality and the results of case studies

As the result of the presented tool functionality and investigated case studies, the following conclusions can be made:

- The use of ML-based surrogate models significantly accelerates the design space exploration compared to conventional FEM method (from 10 days to 50 seconds). However, the price for it is the accuracy of the analysis. Particularly, in the developed tool the average error of ML predictions is around 10%. Additionally, the design space is restricted by the limitations of the trained surrogate model (the range of its inputs) to ensure that this error is not exceeded.
- Just the change of span and LLRS can lead to drastically different economic and environmental performance of structural configuration for a given building plan and elevation. The best solutions can be around 3 times cheaper and environmentally friendly.
- The developed tool was validated by both engineering design guidelines and EU research project's approved technical report. It proves the reliability of the generated structural solutions and the research findings.
- There is a correlation between the cost and embodied carbon since both of them are related to material weight and the type of material as well as the type of the slab were fixed in this study.
- The cheapest and lowest in embodied carbon solutions have small spans. It can be attributed to the lower cross-sections needed for columns and beams since they carry less gravity and seismic load compared to the configurations with larger spans.
- In terms of LLRS no such correlation was found. The best solutions have all the potential configurations without strong inclination to any of them.

7 Conclusions

This thesis presents a data-driven method for the design of sustainable buildings equipped with innovative dampers. The methodology involves the use of advanced digital technologies, in particular machine learning, to develop surrogate models for predicting the response characteristics of composite steel-concrete buildings equipped with hysteric MYDs. The trained surrogate models are incorporated into the web tool to offer a computationally fast design space exploration and help engineers with finding the best structural configuration according to their needs. This final chapter summarizes the novel intellectual work of the dissertation and offers concluding remarks.

Regarding LCA and LCC studies for buildings equipped with MYDs:
The DISSIPABLE project has led to the development of new types of MYDs. Experimental data from shaking table tests have been gathered to ensure accurate modelling of structures equipped with these dampers, and to estimate the amount of time and resources required for repairability of the dampers. Additionally, production data for the MYDs was sourced from a steel manufacturer. This data was used to conduct the first (according to the author knowledge) comparative Life Cycle Assessment (LCA) and Life Cycle Cost (LCC) analyses on buildings equipped with MYDs (referred to as DISSIPABLE buildings) and their conventional counterparts. The study made several key assumptions: only the above-ground parts of the buildings were considered, foundations were excluded from the analysis, and the focus was solely on structural components. A 50-year average building lifespan was assumed, with one seismic event occurring during that time.
The LCA and LCC analyses, conducted in accordance with established standards, revealed that DISSIPABLE buildings have higher initial environmental impacts and construction costs due to increased steel usage in their structural frames. However, these buildings showed a significant advantage in overall life cycle impacts - a 45% reduction in monetary cost and a 25% reduction in embodied CO2. This is attributed to the high reconstruction cost and environmental impact for conventional buildings, while the MYDs in DISSIPABLE buildings can be easily repaired after a seismic event.
The study underscores the critical role of high repairability in enhancing the sustainability of seismic-resistant structures. Moreover, it emphasizes the importance of comparative LCA and LCC to justify the use of buildings equipped with MYDs instead of conventional frames. Overall, integrating repairability, LCA, and LCC analyses into the design and implementation of structures with MYDs significantly enhances the accuracy of sustainability and economic assessments.

Regarding ML-based surrogate models:
The intricate world of ML-based surrogate models, promising tools for structural analysis, was explored. One of the main goals of this thesis was to focus on the practicality of these models for structural engineering practice. Therefore, multiple ML models have been trained for each type of lateral load resisting frame to predict the most important outputs needed for structural design A Mean Absolute Percentage Error (MAPE) of 10% was achieved with 20,000 data points. Generating this data synthetically took almost a month in FEM software, which highlights the unique challenge in the field of structural engineering where, unlike other industries, existing data is scarce. To help address this issue, a portion of the generated data was published on the web, and a Machine Learning competition was created. This not only contributes to the pool of available data but also encourages further development and innovation in the field.
It was found that a particular level of accuracy for one response can anticipate similar accuracy for others within the same source and feature range of training data. It was also discovered that the volume of synthetic training data played a crucial role in improving model accuracy. While increasing data volume led to only marginal improvements after 15,000 datapoints, further significant gains may require datasets exceeding 100,000 points.

The exploration also uncovered that ML models were not merely statistical black boxes but effectively captured the underlying physics of NLTH analysis. This was evident as the most predictive features for ML models were aligned with fundamental principles of structural and seismic engineering. These models excelled at interpolation, as anticipated from previous research about ML models behaviour, yet still demonstrated fair accuracy when venturing into uncharted territory outside the training data range, especially in terms of unseen ground motions. This underlined the generalization capabilities of the trained surrogate models. Finally, the trained models have succeeded in predicting the results of a 2D hybrid test.

Regarding the optimisation tool:
The optimisation tool has been designed to aid structural engineers in making efficient and fast choices for structures located in seismic areas. While in the existing literature, the focus is given to the monetary cost and structural performance, in this thesis also environmental impact (in a form of embodied carbon) is considered as an optimisation criteria. The tool allows to find the most sustainable and cost-efficient structural configurations from a vast design space. It allows users to quantify the benefits of buildings equipped with MYDs compared to conventional ones.
The tool follows a general methodology where user inputs lead to the generation of structural solutions, creating a vast design space consisting of 1936 structural configurations. Unlike the literature where local optimisation was employed (considering structural elements' and MYDs' cross-sections), this study is concentrated on a global optimisation since it has bigger impact on monetary cost and embodied carbon. Consequently, the tool optimizes global structural variables such as columns' spans in both orthogonal directions and the type of lateral load resisting system (LLRS). The optimization problem can be formulated as: "Given building's dimensions and acting loads, which columns' span and lateral load resisting system will provide the most sustainable and cost-efficient structural solution". The largest possible structure that can be evaluated by the tool has 6 storeys and is 48 x 48 meters in plan.
To design the structures the nonlinear seismic structural analysis was required since the yielding of the damper must be considered in the structural analysis for the buildings equipped with MYDs. Cross-sections of all structural elements and the dimensions of MYDs come from the result of the structural design procedure performed using ML-based surrogate models. They significantly accelerated design space exploration, reducing analysis time from 10 days (if it would be done in FEM software) to 50 seconds. However, this comes at the cost of an average 10% error in predictions, and the building's dimension constraints coming from the input range of surrogate models. Given the relatively small solutions space, there was no need to use complex evolutionary solvers such as GA and a simple exhaustive enumeration (EE) algorithm was suitable for solving the optimisation problem in this study.
The case studies revealed that changes in span and LLRS can substantially impact the economic and environmental performance of structural configurations, potentially making solutions up to three times cheaper and more sustainable. A correlation exists between cost and embodied carbon, both linked to material weight and type. Small spans tend to yield the cheapest and lowest in terms of embodied carbon solutions. However, the open plan space can be limited in this case which highlights the challenges in considering multiple design goals in structural engineering practice and the need for the tool that outputs multiple design configuration and not just the one most optimised from the mathematical perspective. The developed tool has been validated by engineering design guidelines and an EU research project's technical report, affirming the reliability of generated structural solutions and research findings. Thanks to this development, more sustainable (up to 30%) and cost-efficient (up to 25%) structures could be found compared to the manual approach of engineering professionals and academics.

Regarding the broad implications of this research to the Architecture Engineering and Construction (AEC) industry:
Benefits brought by the introduction of MYDs from the structural engineering standpoint include enhanced energy dissipation during earthquakes, as the yielding of steel material in MYDs helps dissipate seismic energy, protecting primary structural components from damage. Additionally, MYDs offer improved repairability, as they can be more easily repaired or replaced after a seismic event, reducing downtime and enabling quicker recovery of the building's functionality. Furthermore, MYDs increase safety by localizing inelastic deformations, maintaining the overall structural integrity and reducing the risk of collapse, thereby enhancing occupant safety during earthquakes.
From the design process standpoint, the research findings have significant implications for modernizing design workflows in the AEC industry:

- Increased Efficiency: By integrating ML-based surrogate models, the design process becomes much faster, allowing for quick iterations and evaluations of numerous design scenarios. This accelerates the overall workflow and reduces the time required for seismic analysis and optimization. More importantly, this speed could be a differentiating factor of considering the use of MYDs in the buildings.
- Enhanced Sustainability: The research demonstrates the potential for significant reductions in embodied carbon emissions (up to 25%) for buildings equipped with MYDs. This aligns with the industry's growing emphasis on sustainability and environmental responsibility.
- Data-Driven Design: The adoption of data-driven methodologies, supported by AI and ML technologies, facilitates more informed decision-making, enabling engineers to optimize structures for both performance and sustainability criteria effectively.
- Broader Impact: The research highlights the importance of considering repairability and life cycle assessments in structural design, promoting the development of resilient and sustainable buildings that can better withstand and recover from seismic events.

Overall, these findings support the transition towards more sustainable and efficient design practices in the AEC industry, addressing critical challenges related to the digitalisation, embodied carbon emissions and long-term environmental impacts.

7.1 Future work

The following extensions to the presented developments can be done in the future:

- Considering other materials and MYD types. This thesis is concentrated on steel-concrete composite structures with a particular MYDs developed within DISSIPABLE project. In the future, the same methodology can be applied to other structural materials as well as other damper types.
- Extending the range of ML-based surrogate models. The biggest possible structure that can be considered in this thesis has 6 floors and 48x48 meters plan dimensions. In the future, more data can be generated to extend this range (without losing the accuracy of the model) and increase the applicability of the tool.
- Using supercomputers for the synthetic data generation. One of the most common paths to improve the accuracy of ML models is to get more data. The use of supercomputers can allow

to generate millions of datapoints and consequently lead to surrogate models with a wide application and very high accuracy.

- Incorporating other design variables for the optimisation. This thesis showed that column span and LLRS are impactful variables for the global structural optimisation problem. However, other components such as slab type, material type, etc. can be considered in the future.
- Creating additional optimisation criteria. Monetary cost and embodied carbon have been considered as optimisation criteria in this study. Other significant aspects of the structure such as ease of constructability, construction time, the size of free space, etc. can be considered in the future.
- Extending the geometrical boundaries of the plan and columns' placement. In this study only rectangular plans with equidistant column placement are considered. Since it is not always the case in the reality, more complex plan forms as well not equidistant column spacing can be considered in the future. However, it will lead to further complications for surrogate models development since its training data must contain some of these potential complex scenarios.
- Extending the number of applied ground motions during the structural analysis. The current version of the tool applies only 1 ground motion for each limit state to pre-design a structure. In the future, their amount can be increased to 3 or even 7 to align better with the code requirements.

References

[1] The European Committee for Standardization, “EN1998-1 Eurocode 8: Design of structures for earthquake resistance,” 2004. doi: 10.1680/cien.2001.144.6.55.

[2] “Seismic Provisions for Structural Steel Buildings, ANSI/AISC 341-10,” *American Institute of Steel Construction*, 2016, doi: 10.1201/b11248-8.

[3] International Institute of Earthquake Engineering and Seismology, “17 January Earthquakes.” Accessed: Mar. 08, 2023. [Online]. Available: http://www.iiees.ac.ir/en/16466/

[4] Global Alliance for Buildings and Construction, “2020 Global Status Report for Buildings and Construction_ Towards a Zero-emissions, Efficient and Resilient Buildings and Construction Sector - Executive Summary,” 2020. Accessed: Mar. 08, 2023. [Online]. Available: https://wedocs.unep.org/handle/20.500.11822/34572

[5] P. Castaldo, *Passive energy dissipation devices*, no. November 2014. 2018. doi: 10.1007/978-3-319-02615-2.

[6] M. Saravanan, R. Goswami, and G. S. Palani, “Replaceable Fuses in Earthquake Resistant Steel Structures: A Review,” *International Journal of Steel Structures*, vol. 18, no. 3, pp. 868–879, Sep. 2018, doi: 10.1007/s13296-018-0035-9.

[7] A. Kanyilmaz *et al.*, “EU-RFCS DISSIPABLE project.,” 2022. [Online]. Available: www.dissipable.ntua.gr

[8] H. Salehi and R. Burgueño, “Emerging arti fi cial intelligence methods in structural engineering,” *Eng Struct*, vol. 171, no. November 2017, pp. 170–189, 2018, doi: 10.1016/j.engstruct.2018.05.084.

[9] R. Falcone, C. Lima, and E. Martinelli, “Soft computing techniques in structural and earthquake engineering : a literature review,” *Eng Struct*, vol. 207, no. June 2019, p. 110269, 2020, doi: 10.1016/j.engstruct.2020.110269.

[10] Y. Xie, M. Ebad Sichani, J. E. Padgett, and R. DesRoches, “The promise of implementing machine learning in earthquake engineering: A state-of-the-art review,” *Earthquake Spectra*, vol. 36, no. 4, pp. 1769–1801, Nov. 2020, doi: 10.1177/8755293020919419.

[11] M. D. Symans *et al.*, “Energy Dissipation Systems for Seismic Applications: Current Practice and Recent Developments,” *Journal of Structural Engineering*, vol. 134, no. 1, pp. 3–21, 2008.

[12] and L. J. A. A. S.Whittaker, V. V. Bertero, C. L.Thompson, “Seismic testing of steel plate energy dissipation devices,” *Earthquake Spectra*, vol. 7, no. 4, pp. 563–604, 1991.

[13] S. M. S. Alehashem, A. Keyhani, and H. Pourmohammad, “Behavior and performance of structures equipped with ADAS & TADAS dampers (a comparison with conventional structures),” *The 14th World Conference on Earthquake Engineering*, no. January, p. 8, 2008.

[14] J. C. De la Llera, C. Esguerra, and J. L. Almazán, “Earthquake behavior of structures with copper energy dissipators,” *Earthq Eng Struct Dyn*, vol. 33, no. 3, pp. 329–358, 2004, doi: 10.1002/eqe.354.

[15] T. Kobori, Y. Miura, and E. Fukuzawa, “Development and application of hysteresis steel dampers,” *Earthquake Enginnering, Tenth World Conference*. pp. 2341–2346, 1992.

[16] R. W. K. Chan and F. Albermani, “Experimental study of steel slit damper for passive energy dissipation,” *Eng Struct*, vol. 30, no. 4, pp. 1058–1066, 2008, doi: 10.1016/j.engstruct.2007.07.005.

[17] M. Nakashima, T. Akazawa, and B. Tsuji, “Strain-Hardening Behavior of Shear Panels Made of Low-Yield Steel. II: Model,” *Journal of Structural Engineering*, vol. 121, no. 12, pp. 1750–1757, 1995, doi: 10.1061/(asce)0733-9445(1995)121:12(1750).

[18] M. Iwata, “Applications-design of buckling restrained braces in Japan,” *13th World Conference on Earthquake Engineering*, no. 3208, 2004, [Online]. Available: http://www.iitk.ac.in/nicee/wcee/article/13_3208.pdf
[19] Y. Koetaka *et al.*, “Mechanical property of beam-to-column moment connection with hysteretic dampers for column weak axis,” *Eng Struct*, vol. 27, no. 1, pp. 109–117, 2005, doi: 10.1016/j.engstruct.2004.09.002.
[20] F. Morelli and W. Salvatore, “Seismic protection of structures through an innovative steel-based self-centering hysteretic device : numerical analysis and tests .,” 2011.
[21] A. Ioan, A. Stratan, and D. Dubina, “Numerical simulation of bolted links removal in eccentrically braced frames,” *Pollack Periodica*, vol. 8, no. 1, pp. 15–26, 2013, doi: 10.1556/Pollack.8.2013.1.2.
[22] A. Benavent-Climent, “A brace-type seismic damper based on yielding the walls of hollow structural sections,” *Eng Struct*, vol. 32, no. 4, pp. 1113–1122, 2010, doi: 10.1016/j.engstruct.2009.12.037.
[23] B. Palazzo, P. Castaldo, and I. Marino, “The dissipative column: A new hysteretic damper,” *Buildings*, vol. 5, no. 1, pp. 163–178, 2015, doi: 10.3390/buildings5010163.
[24] SIMPSON Strong-Tie, “Yield-Link® Moment Connection Design Guide (F-L-YLMCDG20),” 2020.
[25] AISC, “ANSI/AISC 358-16. Prequalified Connections for Special and Intermediate Steel Moment Frames for Seismic Applications, including Supplement No. 1,” 2016.
[26] AISC, “AISC 358 CHAPTER 15 DuraFuse Frames Connection,” 2022.
[27] E. C. Communication, “The European Grean Deal,” 2019.
[28] C. Menna, D. Asprone, F. Jalayer, A. Prota, and G. Manfredi, “Assessment of ecological sustainability of a building subjected to potential seismic events during its lifetime,” *International Journal of Life Cycle Assessment*, vol. 18, no. 2, pp. 504–515, Feb. 2013, doi: 10.1007/s11367-012-0477-9.
[29] J. P. S. Chhabra, V. Hasik, M. M. Bilec, and G. P. Warn, “Probabilistic Assessment of the Life-Cycle Environmental Performance and Functional Life of Buildings due to Seismic Events,” *Journal of Architectural Engineering*, vol. 24, no. 1, Mar. 2018, doi: 10.1061/(asce)ae.1943-5568.0000284.
[30] C. Feese, Y. Li, and W. M. Bulleit, “Assessment of Seismic Damage of Buildings and Related Environmental Impacts,” *Journal of Performance of Constructed Facilities*, vol. 29, no. 4, Aug. 2015, doi: 10.1061/(asce)cf.1943-5509.0000584.
[31] E. Asadi, A. M. Salman, and Y. Li, “Multi-criteria decision-making for seismic resilience and sustainability assessment of diagrid buildings,” *Eng Struct*, vol. 191, pp. 229–246, Jul. 2019, doi: 10.1016/j.engstruct.2019.04.049.
[32] K. A. Hossain, B. Gencturk, and A. M. Asce, “Life-Cycle Environmental Impact Assessment of Reinforced Concrete Buildings Subjected to Natural Hazards,” 2014, doi: 10.1061/(ASCE).
[33] D. Dubina, A. Stratan, C. Vulcu, and A. Ciutina, *High strength steel in seismic resistant building frames*, vol. 7, no. 3. 2014. doi: 10.1002/stco.201410028.
[34] S. J. Welsh-Huggins, A. B. Liel, and S. M. Cook, “Reduce, Reuse, Resilient? Life-Cycle Seismic and Environmental Performance of Buildings with Alternative Concretes,” *Journal of Infrastructure Systems*, vol. 26, no. 1, Mar. 2020, doi: 10.1061/(asce)is.1943-555x.0000510.
[35] R. A. Salgado, D. Apul, and S. Guner, “Life cycle assessment of seismic retrofit alternatives for reinforced concrete frame buildings,” *Journal of Building Engineering*, vol. 28, Mar. 2020, doi: 10.1016/j.jobe.2019.101064.

[36] C. Raposo, F. Rodrigues, and H. Rodrigues, “BIM-based LCA assessment of seismic strengthening solutions for reinforced concrete precast industrial buildings,” *Innovative Infrastructure Solutions*, vol. 4, no. 1, Dec. 2019, doi: 10.1007/s41062-019-0239-7.
[37] Y. Ribakov, I. Halperin, and S. Pushkar, “Seismic Resistance and Sustainable Performance of Retrofitted Buildings by Adding Stiff Diaphragms or Seismic Isolation,” *Journal of Architectural Engineering*, vol. 24, no. 1, Mar. 2018, doi: 10.1061/(asce)ae.1943-5568.0000280.
[38] M. (Max) Liu and B. Mi, “Life cycle cost analysis of energy-efficient buildings subjected to earthquakes,” *Energy Build*, vol. 154, pp. 581–589, 2017, doi: 10.1016/j.enbuild.2017.08.056.
[39] Z. Shen, H. Zhou, and S. Shrestha, “LCC-based framework for building envelope and structure co-design considering energy efficiency and natural hazard performance,” *Journal of Building Engineering*, vol. 35, Mar. 2021, doi: 10.1016/j.jobe.2020.102061.
[40] E. Matta, “Lifecycle cost optimization of tuned mass dampers for the seismic improvement of inelastic structures,” *Earthq Eng Struct Dyn*, vol. 47, no. 3, pp. 714–737, Mar. 2018, doi: 10.1002/eqe.2987.
[41] S. Hu, W. Wang, M. Shahria Alam, and K. Ke, “Life-cycle benefits estimation of self-centering building structures,” *Eng Struct*, vol. 284, Jun. 2023, doi: 10.1016/j.engstruct.2023.115982.
[42] Y. Zheng, Y. Dong, and Y. Li, “Resilience and life-cycle performance of smart bridges with shape memory alloy (SMA)-cable-based bearings,” *Constr Build Mater*, vol. 158, pp. 389–400, Jan. 2018, doi: 10.1016/j.conbuildmat.2017.10.031.
[43] M. Aghajani and P. Asadi, “Life-cycle cost analysis of steel frames with shape-memory alloy based dampers,” *Structures*, vol. 52, pp. 794–812, Jun. 2023, doi: 10.1016/j.istruc.2023.04.022.
[44] M. Lamperti Tornaghi, A. Loli, and P. Negro, “Balanced evaluation of structural and environmental performances in building design,” *Buildings*, vol. 8, no. 4, 2018, doi: 10.3390/buildings8040052.
[45] J. L. Domingues Costa, R. Bento, V. Levtchitch, and M. P. Nielsen, “Simplified non-linear time-history analysis based on the theory of plasticity,” *WIT Transactions on the Built Environment*, vol. 81, pp. 375–385, 2005.
[46] J. C. Reyes, E. Kalkan, and A. Sierra, “FAST NONLINEAR RESPONSE HISTORY ANALYSIS,” vol. 1673, no. Abstract ID, 2017.
[47] A. Faroughi and M. Hosseini, “Incremental dynamic analysis of sdof by using nonlinear earthquake accelerograms based on modified inverse Fourier transform,” *Journal of Vibroengineering*, vol. 19, no. 8, pp. 6170–6182, 2017, doi: 10.21595/jve.2017.18322.
[48] T. Mehmood, P. Warnitchai, and P. Suwansaya, “Seismic Evaluation of Tall Buildings Using a Simplified but Accurate Analysis Procedure,” *Journal of Earthquake Engineering*, vol. 22, no. 3, pp. 356–381, 2018, doi: 10.1080/13632469.2016.1224742.
[49] N. Zhao, G. Huang, Q. Yang, X. Zhou, and A. Kareem, “Fast Convolution Integration–Based Nonstationary Response Analysis of Linear and Nonlinear Structures with Nonproportional Damping,” *J Eng Mech*, vol. 145, no. 8, p. 04019053, 2019, doi: 10.1061/(asce)em.1943-7889.0001633.
[50] L. A. Zadeh, “Fuzzy sets as a basis for a theory of possibility,” *Fuzzy Sets Syst*, vol. 1, no. 1, pp. 3–28, 1977, doi: https://doi.org/10.1016/S0165-0114(99)80004-9.
[51] P. Werbos and N. S. Foundation, “Beyond regression : new tools for prediction and analysis in the behavioral sciences,” 1974.
[52] R. W. David Rumelhart, Geoffrey Hinton, “Lerning representations by back-propagating errors,” *Nature*, vol. 323, pp. 533–536, 1986.

[53] L. B. Yann LeCun, Patrick Haffner and Y. Bengio, *Object recognition with Gradien-based learning*. 1999.
[54] R. A. Brooks, "Intelligence without representation," *Artif Intell*, vol. 47, no. 1–3, pp. 139–159, Jan. 1991, doi: 10.1016/0004-3702(91)90053-M.
[55] P. Khan *et al.*, "Machine Learning and Deep Learning Approaches for Brain Disease Diagnosis: Principles and Recent Advances," *IEEE Access*, vol. 9, pp. 37622–37655, 2021, doi: 10.1109/ACCESS.2021.3062484.
[56] Telefonica Tech, "Semi-Supervised Learning… the great unknown." Accessed: Mar. 04, 2024. [Online]. Available: https://telefonicatech.com/en/blog/semi-supervised-learning-the-great-unknown
[57] S. Ray, "A Quick Review of Machine Learning Algorithms," *Proceedings of the International Conference on Machine Learning, Big Data, Cloud and Parallel Computing: Trends, Prespectives and Prospects, COMITCon 2019*, pp. 35–39, Feb. 2019, doi: 10.1109/COMITCON.2019.8862451.
[58] L. Breiman, "Random forests," *Mach Learn*, vol. 45, no. 1, pp. 5–32, Oct. 2001, doi: 10.1023/A:1010933404324.
[59] H. Gong, Y. Sun, X. Shu, and B. Huang, "Use of random forests regression for predicting IRI of asphalt pavements," *Constr Build Mater*, vol. 189, pp. 890–897, Nov. 2018, doi: 10.1016/J.CONBUILDMAT.2018.09.017.
[60] C. Fan, Y. Sun, Y. Zhao, M. Song, and J. Wang, "Deep learning-based feature engineering methods for improved building energy prediction," *Appl Energy*, vol. 240, pp. 35–45, Apr. 2019, doi: 10.1016/j.apenergy.2019.02.052.
[61] A. Botchkarev, "A new typology design of performance metrics to measure errors in machine learning regression algorithms," *Interdisciplinary Journal of Information, Knowledge, and Management*, vol. 14, pp. 45–76, 2019, doi: 10.28945/4184.
[62] S. Razavi, B. A. Tolson, D. H. Burn, S. Razavi, B. A. Tolson, and D. H. Burn, "Review of surrogate modeling in water resources," *Water Resour Res*, vol. 48, p. 7401, 2012, doi: 10.1029/2011WR011527.
[63] C. T. Mueller and J. A. Ochsendorf, "Combining structural performance and designer preferences in evolutionary design space exploration," *Autom Constr*, vol. 52, pp. 70–82, 2015, doi: 10.1016/j.autcon.2015.02.011.
[64] P. (Institution of S. E. G. B. Debney, *Computational engineering*, 1.2. Institution of Structural Engineers (Great Britain), 2021.
[65] N. D. Lagaros and M. Papadrakakis, "Neural network based prediction schemes of the non-linear seismic response of 3D buildings," in *Advances in Engineering Software*, Elsevier Ltd, 2012, pp. 92–115. doi: 10.1016/j.advengsoft.2011.05.033.
[66] R. YOUSEFZADEH and X. CAO, "To what extent should we trust AI models when they extrapolate?," *IEEE International Conference on Program Comprehension*, vol. 2022-March, pp. 36–47, 2022, doi: 10.1145/nnnnnnn.nnnnnnn.
[67] G. L. Molas* A N D and F. Yamazaki', "NEURAL NETWORKS FOR QUICK EARTHQUAKE DAMAGE ESTIMATION," 1995.
[68] N. D. Lagaros and M. Fragiadakis, "Fragility assessment of steel frames using neural networks," *Earthquake Spectra*, vol. 23, no. 4, pp. 735–752, 2007, doi: 10.1193/1.2798241.
[69] O. R. de Lautour and P. Omenzetter, "Prediction of seismic-induced structural damage using artificial neural networks," *Eng Struct*, vol. 31, no. 2, pp. 600–606, Feb. 2009, doi: 10.1016/j.engstruct.2008.11.010.
[70] M. H. Arslan, "An evaluation of effective design parameters on earthquake performance of RC buildings using neural networks," *Eng Struct*, vol. 32, no. 7, pp. 1888–1898, Jul. 2010, doi: 10.1016/j.engstruct.2010.03.010.

[71] B. Doran, J. J. Shen, R. Wen, B. Akbas, and A. Bozer, “Neural network model for seismic response of braced buildings,” *Proceedings of the Institution of Civil Engineers: Structures and Buildings*, vol. 170, no. 3, pp. 159–167, Mar. 2016, doi: 10.1680/jstbu.16.00020.
[72] K. Morfidis and K. Kostinakis, “Seismic parameters’ combinations for the optimum prediction of the damage state of R/C buildings using neural networks,” *Advances in Engineering Software*, vol. 106, pp. 1–16, Apr. 2017, doi: 10.1016/j.advengsoft.2017.01.001.
[73] L. Stefanini, L. Badini, G. Mochi, G. Predari, and A. Ferrante, “Neural networks for the rapid seismic assessment of existing moment-frame RC buildings,” *International Journal of Disaster Risk Reduction*, vol. 67, Jan. 2022, doi: 10.1016/j.ijdrr.2021.102677.
[74] T. Kim, O. S. Kwon, and J. Song, “Response prediction of nonlinear hysteretic systems by deep neural networks,” *Neural Networks*, vol. 111, pp. 1–10, Mar. 2019, doi: 10.1016/j.neunet.2018.12.005.
[75] B. K. Oh, B. Glisic, S. W. Park, and H. S. Park, “Neural network-based seismic response prediction model for building structures using artificial earthquakes,” *J Sound Vib*, vol. 468, Mar. 2020, doi: 10.1016/j.jsv.2019.115109.
[76] A. Kia and S. Sensoy, “Classification of Earthquake-Induced Damage for R/C Slab Column Frames Using Multiclass SVM and Its Combination with MLP Neural Network,” *Math Probl Eng*, vol. 2014, 2014, doi: 10.1155/2014/734072.
[77] V. K. Gudipati and E. J. Cha, “Surrogate modeling for structural response prediction of a building class,” *Structural Safety*, vol. 89, Mar. 2021, doi: 10.1016/j.strusafe.2020.102041.
[78] H. D. Nguyen, N. D. Dao, and M. Shin, “Prediction of seismic drift responses of planar steel moment frames using artificial neural network and extreme gradient boosting,” *Eng Struct*, vol. 242, Sep. 2021, doi: 10.1016/j.engstruct.2021.112518.
[79] M. Zaker Esteghamati and M. M. Flint, “Developing data-driven surrogate models for holistic performance-based assessment of mid-rise RC frame buildings at early design,” *Eng Struct*, vol. 245, Oct. 2021, doi: 10.1016/j.engstruct.2021.112971.
[80] X. Guan, H. Burton, M. Shokrabadi, and Z. Yi, “Seismic Drift Demand Estimation for Steel Moment Frame Buildings: From Mechanics-Based to Data-Driven Models,” *Journal of Structural Engineering*, vol. 147, no. 6, p. 04021058, Jun. 2021, doi: 10.1061/(asce)st.1943-541x.0003004.
[81] D. Cook *et al.*, “A STRUCTURAL RESPONSE PREDICTION ENGINE TO SUPPORT ADVANCED SEISMIC RISK ASSESSMENT,” in *Eleventh U.S. National Conference on Earthquake Engineering*, 2018.
[82] Federal Emergency Management Agency, “FEMA P-58. Seismic Performance Assessment of Buildings Volume 1-Methodology. Second Edition,” 2018. [Online]. Available: www.ATCouncil.org
[83] M. J. Reddy and D. N. Kumar, “Elitist-Mutated Multi-Objective Particle Swarm Optimization for Engineering Design,” 2014, pp. 3534–3545. doi: 10.4018/978-1-4666-5888-2.ch346.
[84] Dieter Vermeulen, “Structural Dynam(o)ite: Optimized Design and Fabrication Workflows with Dynamo.” Accessed: Jul. 30, 2023. [Online]. Available: https://www.autodesk.com/autodesk-university/article/Structural-Dynamoite-Optimized-Design-and-Fabrication-Workflows-Dynamo-2019
[85] K. U. Bletzinger, M. Firl, J. Linhard, and R. Wüchner, “Optimal shapes of mechanically motivated surfaces,” *Comput Methods Appl Mech Eng*, vol. 199, no. 5–8, pp. 324–333, Jan. 2010, doi: 10.1016/j.cma.2008.09.009.
[86] Robert McNeel & Associates, “Grasshopper.” 2007.
[87] F. Flager, G. Soremekun, A. Adya, K. Shea, J. Haymaker, and M. Fischer, “Fully Constrained Design: A general and scalable method for discrete member sizing optimization of

steel truss structures," *Comput Struct*, vol. 140, pp. 55–65, Jul. 2014, doi: 10.1016/j.compstruc.2014.05.002.
[88] A. G. Weldeyesus, J. Gondzio, L. He, M. Gilbert, P. Shepherd, and A. Tyas, "Adaptive solution of truss layout optimization problems with global stability constraints," *Structural and Multidisciplinary Optimization*, vol. 60, no. 5, pp. 2093–2111, Nov. 2019, doi: 10.1007/s00158-019-02312-9.
[89] Mehdi Nourbakhsh, "GENERALIZABLE SURROGATE MODELS FOR THE IMPROVED EARLY-STAGE EXPLORATION OF STRUCTURAL DESIGN ALTERNATIVES IN BUILDING CONSTRUCTION," PhD Thesis, Georgia Institute of Technology, 2016.
[90] M. Turrin, P. Von Buelow, and R. Stouffs, "Design explorations of performance driven geometry in architectural design using parametric modeling and genetic algorithms," *Advanced Engineering Informatics*, vol. 25, no. 4, pp. 656–675, Oct. 2011, doi: 10.1016/j.aei.2011.07.009.
[91] B. Steiner, E. Mousavian, F. M. Saradj, M. Wimmer, and P. Musialski, "Integrated Structural–Architectural Design for Interactive Planning," *Computer Graphics Forum*, vol. 36, no. 8, pp. 80–94, Dec. 2017, doi: 10.1111/cgf.12996.
[92] T.-H. Kwon and H. Song, "Integrated Exploration of Building Shapes Based on Structural Performance," 2019, doi: 10.1061/(ASCE).
[93] A. Kanyilmaz, P. R. N. Tichell, and D. Loiacono, "A genetic algorithm tool for conceptual structural design with cost and embodied carbon optimization," *Eng Appl Artif Intell*, vol. 112, Jun. 2022, doi: 10.1016/j.engappai.2022.104711.
[94] J. M. Davila Delgado and H. Hofmeyer, "Automated generation of structural solutions based on spatial designs," *Autom Constr*, vol. 35, pp. 528–541, 2013, doi: 10.1016/j.autcon.2013.06.008.
[95] J. Reisinger, M. A. Zahlbruckner, I. Kovacic, P. Kán, X. Wang-Sukalia, and H. Kaufmann, "Integrated multi-objective evolutionary optimization of production layout scenarios for parametric structural design of flexible industrial buildings," *Journal of Building Engineering*, vol. 46, Apr. 2022, doi: 10.1016/j.jobe.2021.103766.
[96] N. C. Brown and C. T. Mueller, "Design for structural and energy performance of long span buildings using geometric multi-objective optimization," *Energy Build*, vol. 127, pp. 748–761, Sep. 2016, doi: 10.1016/j.enbuild.2016.05.090.
[97] W. Flager *et al.*, "Multidisciplinary process integration and design optimization of a classroom building," 2009. [Online]. Available: http://www.itcon.org/2009/38
[98] P. Sharafi, B. Samali, H. Ronagh, and M. Ghodrat, "Automated spatial design of multi-story modular buildings using a unified matrix method," *Autom Constr*, vol. 82, pp. 31–42, Oct. 2017, doi: 10.1016/j.autcon.2017.06.025.
[99] S. Boonstra, K. van der Blom, H. Hofmeyer, M. T. M. Emmerich, J. van Schijndel, and P. de Wilde, "Toolbox for super-structured and super-structure free multi-disciplinary building spatial design optimisation," *Advanced Engineering Informatics*, vol. 36, pp. 86–100, Apr. 2018, doi: 10.1016/j.aei.2018.01.003.
[100] Daniel Nagy, "Design optimization." Accessed: Mar. 14, 2023. [Online]. Available: https://medium.com/generative-design/design-optimization-2ec2ba3b40f7
[101] V. Machairas, A. Tsangrassoulis, and K. Axarli, "Algorithms for optimization of building design: A review," *Renewable and Sustainable Energy Reviews*, vol. 31. Elsevier Ltd, pp. 101–112, 2014. doi: 10.1016/j.rser.2013.11.036.
[102] B. Ekici, C. Cubukcuoglu, M. Turrin, and I. S. Sariyildiz, "Performative computational architecture using swarm and evolutionary optimisation: A review," *Building and Environment*, vol. 147. Elsevier Ltd, pp. 356–371, Jan. 01, 2019. doi: 10.1016/j.buildenv.2018.10.023.
[103] J.H. Holland, *Adaptation in natural and artificial systems*. 1975.

[104] J. Sedyono, H. Hadavinia, D. Venetsanos, and D. R. Marchant, “Enumeration search method for optimisation of stacking sequence of laminated composite plates subjected to buckling,” *Open Engineering*, vol. 5, no. 1, pp. 190–204, Jan. 2015, doi: 10.1515/eng-2015-0025.
[105] M. (Max) Liu, “Fast Procedure for Practical Member Sizing Optimization of Steel Moment Frames,” *Practice Periodical on Structural Design and Construction*, vol. 20, no. 4, Nov. 2015, doi: 10.1061/(asce)sc.1943-5576.0000240.
[106] N. Wongprasert and M. D. Symans, “Application of a Genetic Algorithm for Optimal Damper,” vol. 130, no. April, pp. 401–406, 2004, doi: 10.1061/(ASCE)0733-9399(2004)130.
[107] M. Liu, S. A. Burns, and Y. K. Wen, “Multiobjective optimization for performance-based seismic design of steel moment frame structures,” no. October 2003, pp. 289–306, 2005, doi: 10.1002/eqe.426.
[108] M. Fragiadakis, N. D. Lagaros, and M. Papadrakakis, “Performance-based multiobjective optimum design of steel structures considering life-cycle cost,” pp. 1–11, 2006, doi: 10.1007/s00158-006-0009-y.
[109] N. D. Lagaros, M. Fragiadakis, M. Papadrakakis, and Y. Tsompanakis, “Structural optimization : A tool for evaluating seismic design procedures,” vol. 28, pp. 1623–1633, 2006, doi: 10.1016/j.engstruct.2006.02.014.
[110] F. Hejazi, I. Toloue, and M. S. Jaafar, “Optimization of Earthquake Energy Dissipation System by Genetic Algorithm,” vol. 28, pp. 796–810, 2013, doi: 10.1111/mice.12047.
[111] G. Minafò and G. Camarda, “An open-source GA framework for optimizing the seismic upgrading design of RC frames through BRBs,” *Eng Struct*, vol. 251, Jan. 2022, doi: 10.1016/j.engstruct.2021.113508.
[112] E. W. Hoffman and P. W. Richards, “Efficiently Implementing Genetic Optimization with Nonlinear Response History Analysis of Taller Buildings,” *Journal of Structural Engineering*, vol. 140, no. 8, Aug. 2014, doi: 10.1061/(asce)st.1943-541x.0000943.
[113] R. K. Mohammadi, M. R. Garoosi, and I. Hajirasouliha, “Practical method for optimal rehabilitation of steel frame buildings using buckling restrained brace dampers,” *Soil Dynamics and Earthquake Engineering*, vol. 123, pp. 242–251, Aug. 2019, doi: 10.1016/j.soildyn.2019.04.025.
[114] F. Farhat, S. Nakamura, and K. Takahashi, “Application of genetic algorithm to optimization of buckling restrained braces for seismic upgrading of existing structures,” *Comput Struct*, vol. 87, no. 1–2, pp. 110–119, Jan. 2009, doi: 10.1016/j.compstruc.2008.08.002.
[115] K. Park, B. K. Oh, H. S. Park, and S. W. Choi, “GA-Based Multi-Objective Optimization for Retrofit Design on a Multi-Core PC Cluster,” *Computer-Aided Civil and Infrastructure Engineering*, vol. 30, no. 12, pp. 965–980, Dec. 2015, doi: 10.1111/mice.12176.
[116] H. Abedini, S. R. Hoseini Vaez, and A. Zarrineghbal, “Optimum design of buckling-restrained braced frames,” *Structures*, vol. 25, pp. 99–112, Jun. 2020, doi: 10.1016/j.istruc.2020.03.004.
[117] S. F. Fathizadeh *et al.*, “Trade-off Pareto optimum design of an innovative curved damper truss moment frame considering structural and non-structural objectives,” *Structures*, vol. 28, pp. 1338–1353, Dec. 2020, doi: 10.1016/j.istruc.2020.09.060.
[118] S. Gholizadeh, “Advances in Engineering Software Performance-based optimum seismic design of steel structures by a modified firefly algorithm and a new neural network,” *Advances in Engineering Software*, vol. 81, pp. 50–65, 2015, doi: 10.1016/j.advengsoft.2014.11.003.
[119] European Committee for Standardization, “EN 15804 : Sustainability of construction works. Environmental product declarations. Core rules for the product category of construction products,” pp. 1–44, 2012.

[120] ISO, “ISO14025: Environmental labels and declarations-Type III environmental declarations-Principles and procedures Marquages et déclarations environnementaux-Déclarations environnementales de Type III-Principes et modes opératoires,” 2006.
[121] University of Stuttgart, “Gabi software, version 8.” 2016. Accessed: May 08, 2023. [Online]. Available: http://www.gabi-software.com/i
[122] G. Wernet, C. Bauer, B. Steubing, J. Reinhard, E. Moreno-Ruiz, and B. Weidema, “The ecoinvent database version 3 (part I): overview and methodology,” *International Journal of Life Cycle Assessment*, vol. 21, no. 9, pp. 1218–1230, Sep. 2016, doi: 10.1007/s11367-016-1087-8.
[123] C. Computers and Structures Inc., Berkeley, “SAP2000. Integrated software for structural analysis and design, analysis reference manual.” 2021.
[124] X. Guan M.EERI, H. Burton M.EERI, and M. Shokrabadi, “A database of seismic designs, nonlinear models, and seismic responses for steel moment-resisting frame buildings,” *Earthquake Spectra*, vol. 37, no. 2, pp. 1199–1222, May 2021, doi: 10.1177/8755293020971209.
[125] A. Kanyilmaz, H. Degée, and C. A. Castiglioni, “An adjusted design approach for concentrically braced frames in low-to-moderate seismicity areas,” *Bulletin of Earthquake Engineering*, vol. 16, no. 9, pp. 4159–4189, Sep. 2018, doi: 10.1007/s10518-018-0402-0.
[126] Karim Chichakly, “Multiobjective Optimization.” Accessed: Jul. 30, 2023. [Online]. Available: https://blog.iseesystems.com/modeling-tips/multiobjective-optimization/
[127] I. Vayas *et al.*, *Dissipative devices for seismic-resistant steel frames (FUSEIS)*. 2014.
[128] A. Plumier, C. D. Catherine, C. Chevreuils, and B. Liege, *Two INnovations for Earthquake Resistant Design The INERD Project .*, no. July 2001. 2004.
[129] “PEER Ground Motion Database.” [Online]. Available: https://ngawest2.berkeley.edu/
[130] R. E. & O. W. Luzi L., Puglia R., “Engineering Strong Motion Database, version 1.0.,” Istituto Nazionale di Geofisica e Vulcanologia, Observatories & Research Facilities for European Seismology. [Online]. Available: https://esm.mi.ingv.it/
[131] ISO, “ISO 14040: Environmental Management - Life Cycle Assessment - Principles and Framework,” 2006. [Online]. Available: https://www.iso.org/standard/37456.html
[132] ISO, “ISO 14044: Environmental management — Life cycle assessment — Requirements and guidelines,” 2006. [Online]. Available: http://www.springerlink.com/index/10.1007/s11367-011-0297-3
[133] A. Kanyilmaz *et al.*, “Fully dissipative and easily repairable components for resilient buildings with composite steel-concrete structures (DISSIPABLE). Periodic technical report. Part B,” 2022.
[134] G. Van Rossum and F. L. Drake, “Python 3 Reference Manual.” CreateSpace, 2009.
[135] S. M. Lundberg, P. G. Allen, and S.-I. Lee, “A Unified Approach to Interpreting Model Predictions,” 2017. [Online]. Available: https://github.com/slundberg/shap
[136] C. Molnar, *Interpretable Machine Learning*, 2nd ed. 2023.
[137] S. Hart, “Shapley Value,” in *Game Theory*, London: The New Palgrave, 1989, pp. 210–216.
[138] R. Andreotti, G. Giuliani, and N. Tondini, “Experimental analysis of a full-scale steel frame with replaceable dissipative connections,” *J Constr Steel Res*, vol. 208, Sep. 2023, doi: 10.1016/j.jcsr.2023.108036.
[139] R. Andreotti, G. Giuliani, N. Tondini, and O. S. Bursi, “Hybrid simulation of a partial-strength steel–concrete composite moment-resisting frame endowed with hysteretic replaceable beam splices,” *Earthq Eng Struct Dyn*, vol. 52, no. 1, pp. 51–70, Jan. 2023, doi: 10.1002/eqe.3744.

[140] A. Kondratenko, “Predict the building safety under the earthquake,” Kaggle. Accessed: Aug. 31, 2023. [Online]. Available: https://www.kaggle.com/competitions/predict-the-building-safety-under-the-earthquake/leaderboard
[141] A. Kanyilmaz, V. Hoi Dang, and A. Kondratenko, “How does conceptual design impact the cost and carbon footprint of structures?,” *Structures*, vol. 58, Dec. 2023, doi: 10.1016/j.istruc.2023.105102.
[142] A. Charleson, *Seismic Design for Architects - Outwitting The Quake*. Routledge, 2008.
[143] “EN 1991-1-1: Eurocode 1: Actions on structures - Part 1-1: General actions - Densities, self-weight, imposed loads for buildings,” 1991.
[144] “EN 1993-1-1: Eurocode 3: Design of steel structures - Part 1-1: General rules and rules for buildings.”
[145] “Cype Price Index Generator.” Accessed: Sep. 01, 2023. [Online]. Available: https://www.indexfix.com/news/597/cype-index-price-generator
[146] One Click LCA, “Average quantities of reinforcement in concrete.” Accessed: Sep. 01, 2023. [Online]. Available: https://oneclicklca.zendesk.com/hc/en-us/articles/360020943800-Average-Quantities-of-Reinforcement-in-Concrete
[147] A. Kondratenko, A. Kanyilmaz, E. Rocco, and C. Vulcu, “Life-cycle performance of steel structures equipped with dissipative and repairable components,” *Structures (sent to publication)*, 2024.
[148] O. P. (Orlando P.) Gibbons and Institution of Structural Engineers (Great Britain), *How to calculate embodied carbon, version 2.0*, 2nd ed. 2022.
[149] “The ICE Database.” Accessed: Sep. 01, 2023. [Online]. Available: https://circularecology.com/embodied-carbon-footprint-database.html
[150] Arup & WBCSD, “Net-zero buildings Where do we stand?,” 2021.
[151] D. Flanagan, “JavaScript: the definitive guide.” O’Reilly Media, Inc., 2006.
[152] P. Bisch *et al.*, “Eurocode 8: Seismic Design of Buildings Worked examples Support to the implementation, harmonization and further development of the Eurocodes,” 2011. doi: 10.2788/91658.

Appendix A

In the figures below the LCI for DISSIPABLE and Conventional buildings are presented.

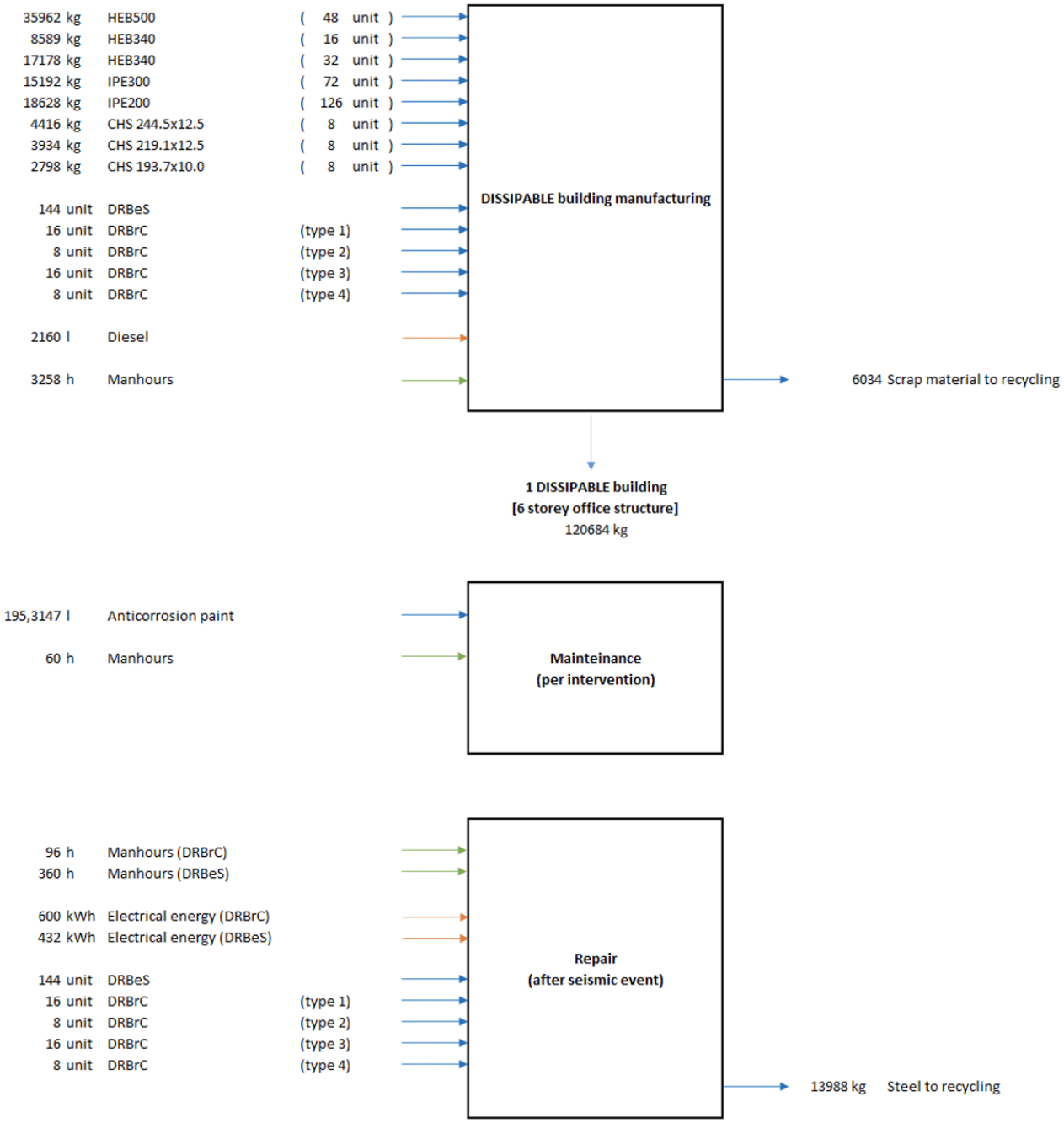

Figure 70. LCI for the DISSIPABLE building

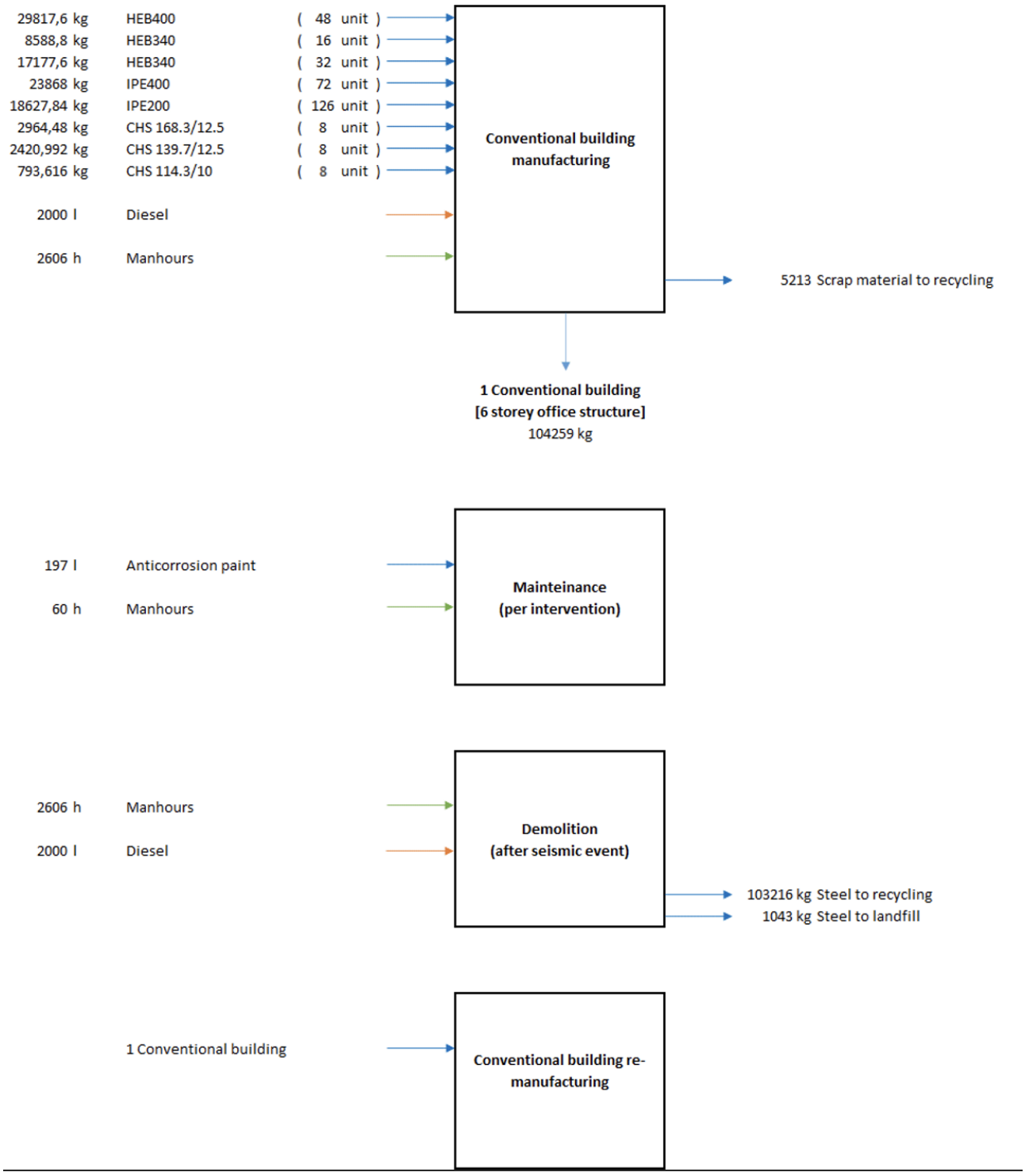

Figure 71. LCI for the Conventional building

Appendix B

Table 39 shows the criteria for the ground motion selection for all limit states.

Limit State	Consequence Class	EC8 Site Category	Return Period, T_R (years)	PGA (g)	R_{JB} = R_{RUP} (km)
DL – Damage Limitation	CC2	A	60	0.20	0-30
SD – Significant Damage			475	0.36	
NC – Near Collapse			1600	0.504	

Table 39. Parameters for the ground motions' selection

Appendix C

Table 40 shows the parameters of the elastic response spectrum to which accelerograms are scaled.

Importance factor (Class II)	γ_I=1.0
Peak ground acceleration	α_{gR}=0.20·g (DL) α_{gR}=0.36·g (SD) α_{gR}=0.504·g (NC)
Ground type	A
Smax	1.00
Tb	0.15 sec
Tc	0.40 sec
Td	2.00 sec
Lower bound factor	0.2

Table 40. Parameters of the elastic response spectrum for accelerograms' scaling

Appendix D

In this appendix all the accelerograms used in the NLTH analysis for 6-storey pilot buildings are present (unscaled version). Apart from the ground acceleration, also the ground velocity and displacement are shown for each record.

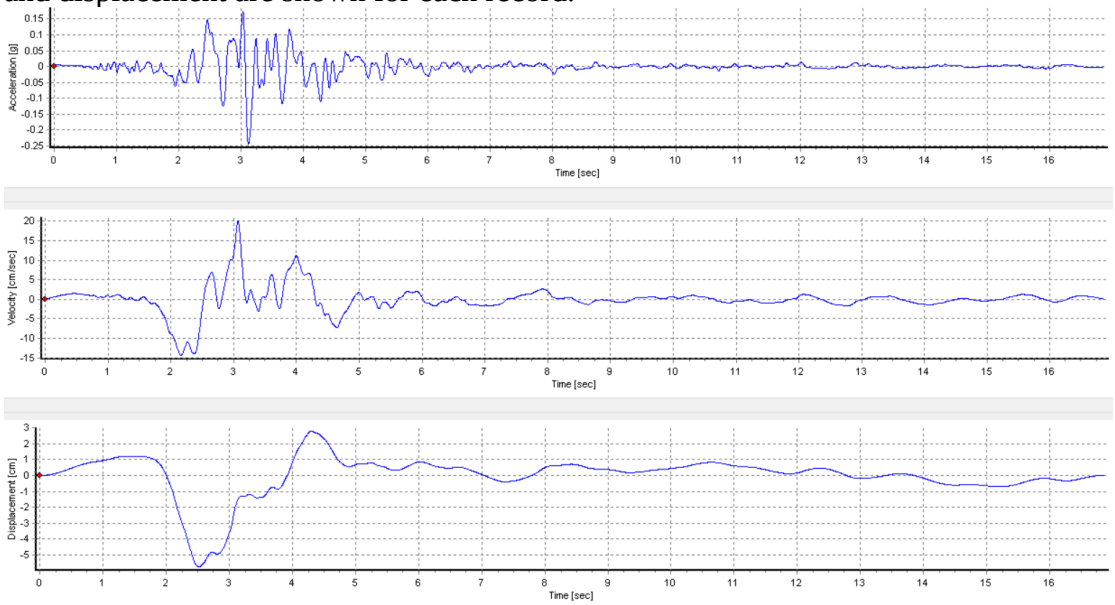

Figure 72. Acceleration, velocity and displacement for esrc0 record in Y structural direction

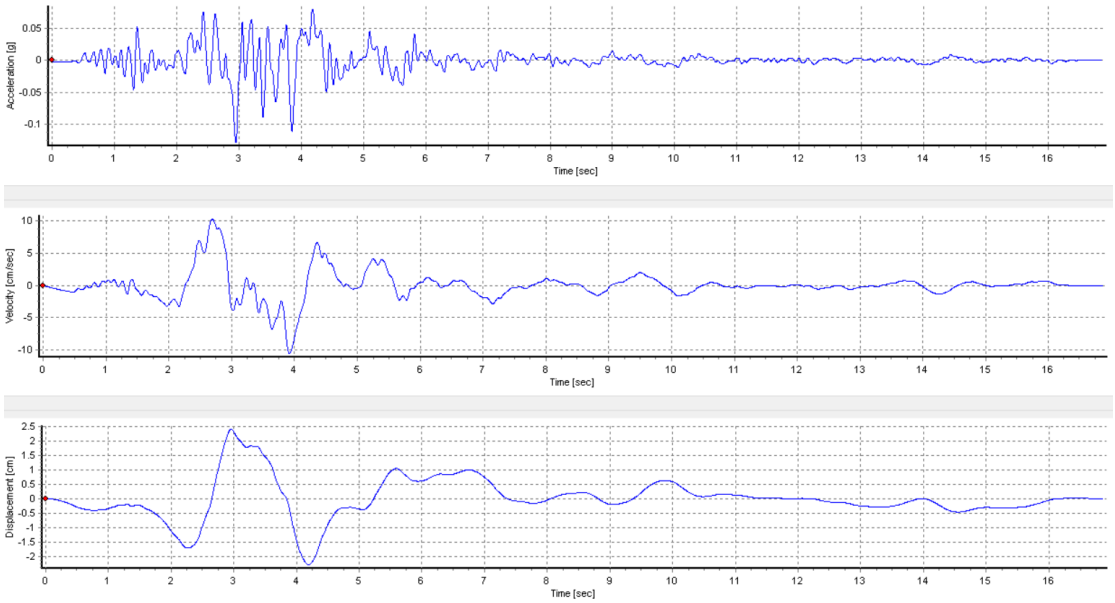

Figure 73. Acceleration, velocity and displacement for esrc0 record in X structural direction

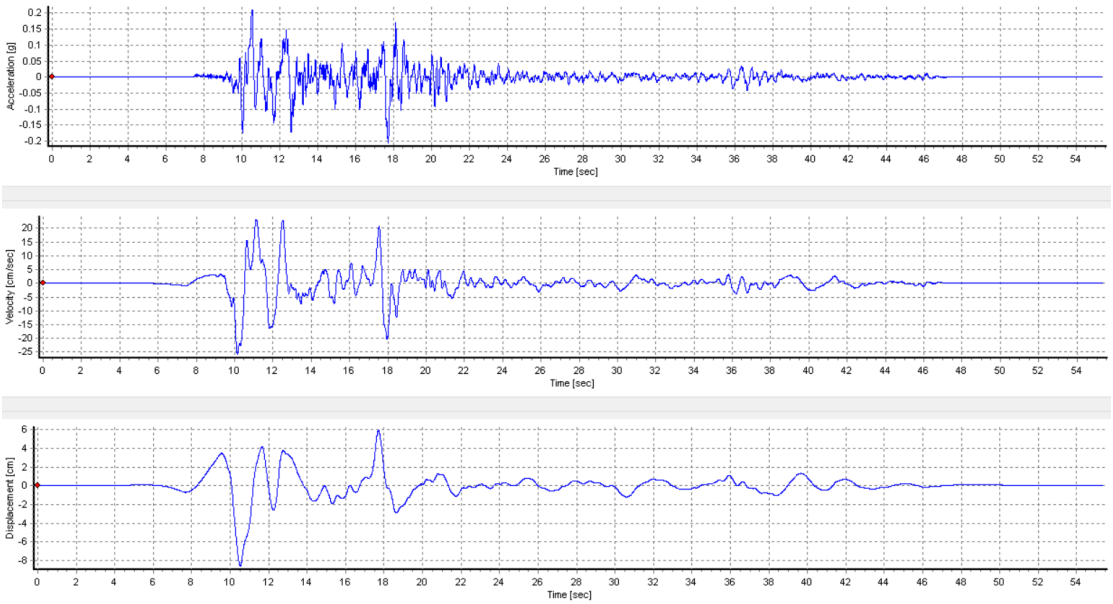

Figure 74. Acceleration, velocity and displacement for euula record in Y structural direction

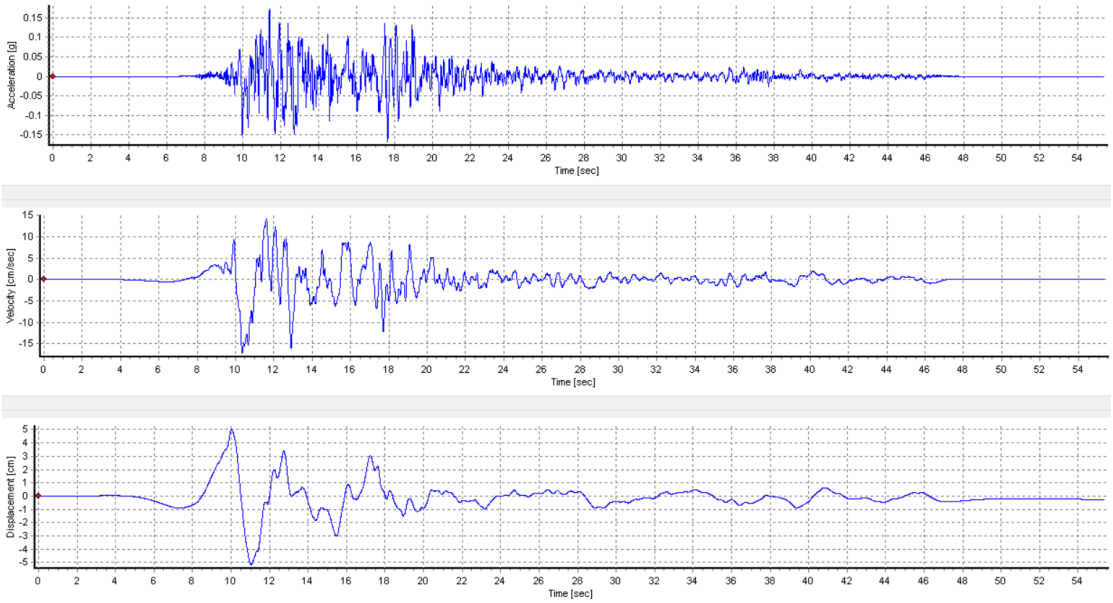

Figure 75. Acceleration, velocity and displacement for euula record in X structural direction

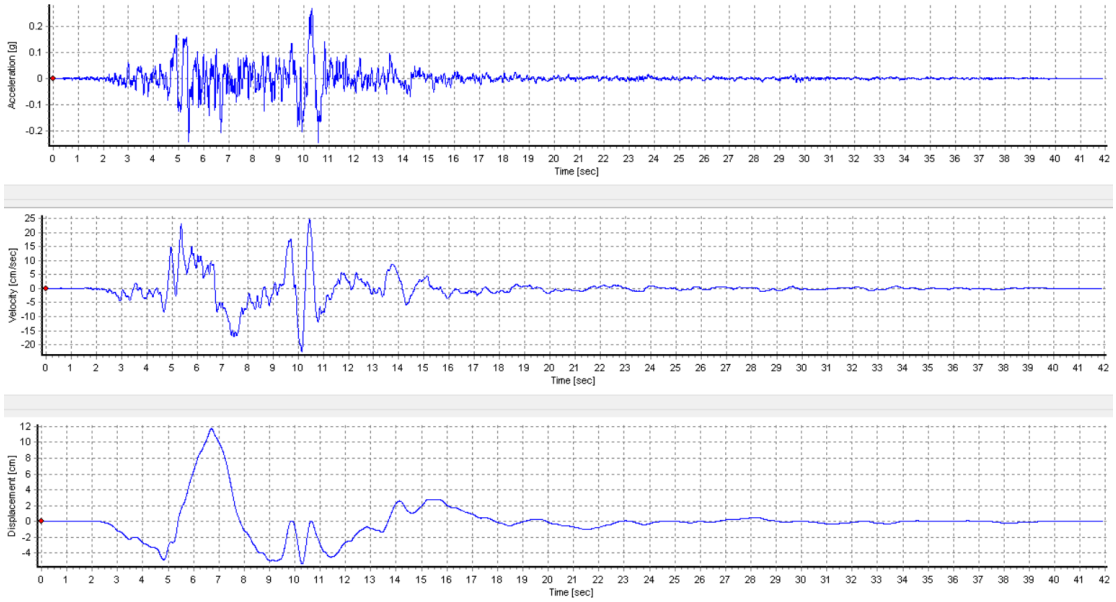

Figure 76. Acceleration, velocity and displacement for ivt1212 record in Y structural direction

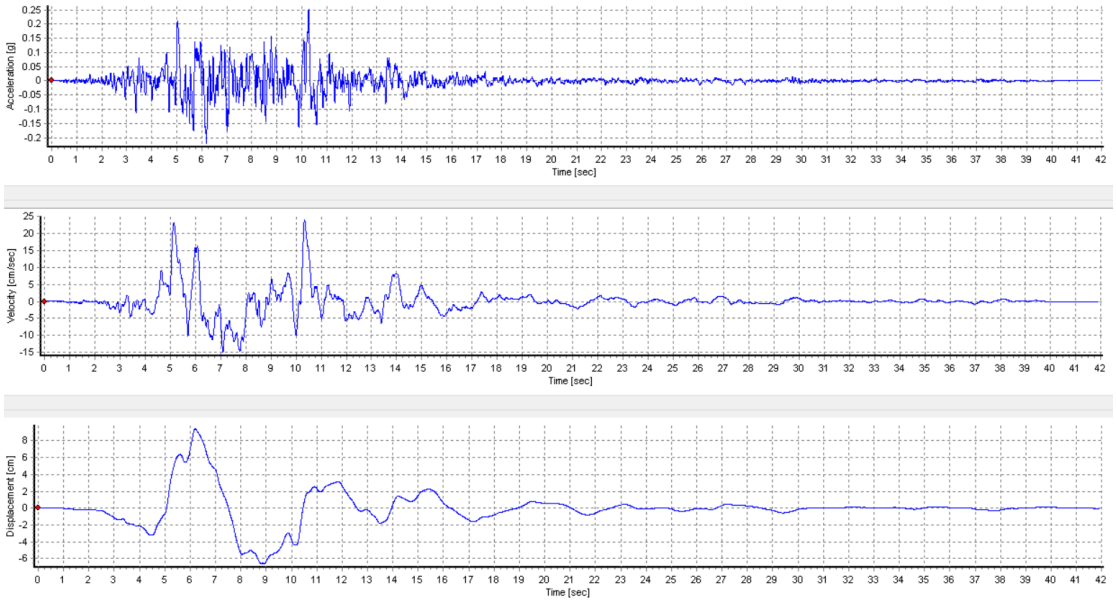

Figure 77. Acceleration, velocity and displacement for ivt1212 record in X structural direction

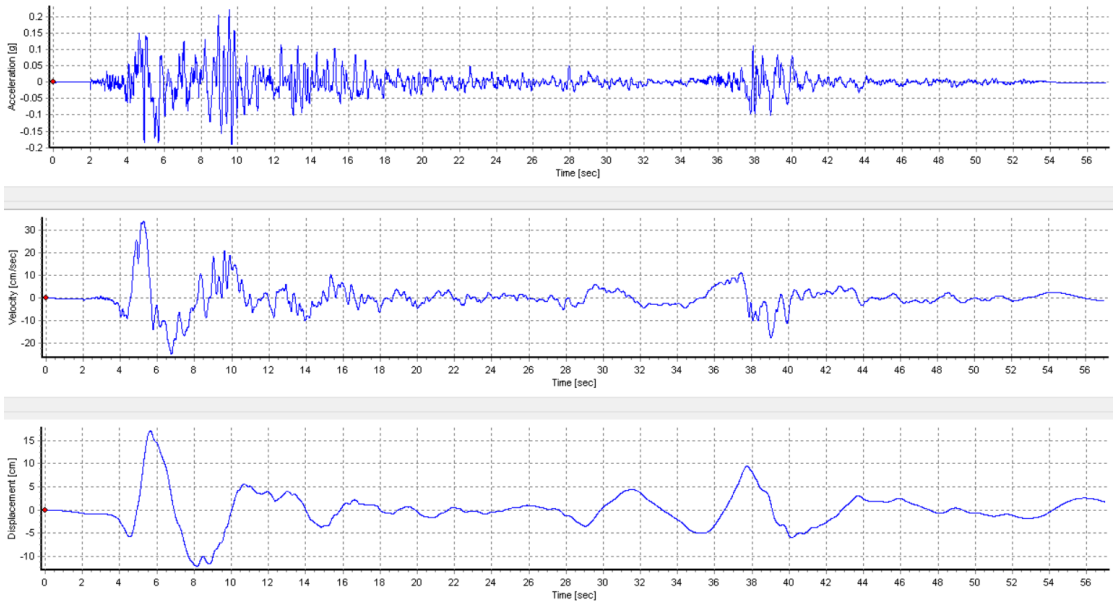

Figure 78. Acceleration, velocity and displacement for tk4101 record in Y structural direction

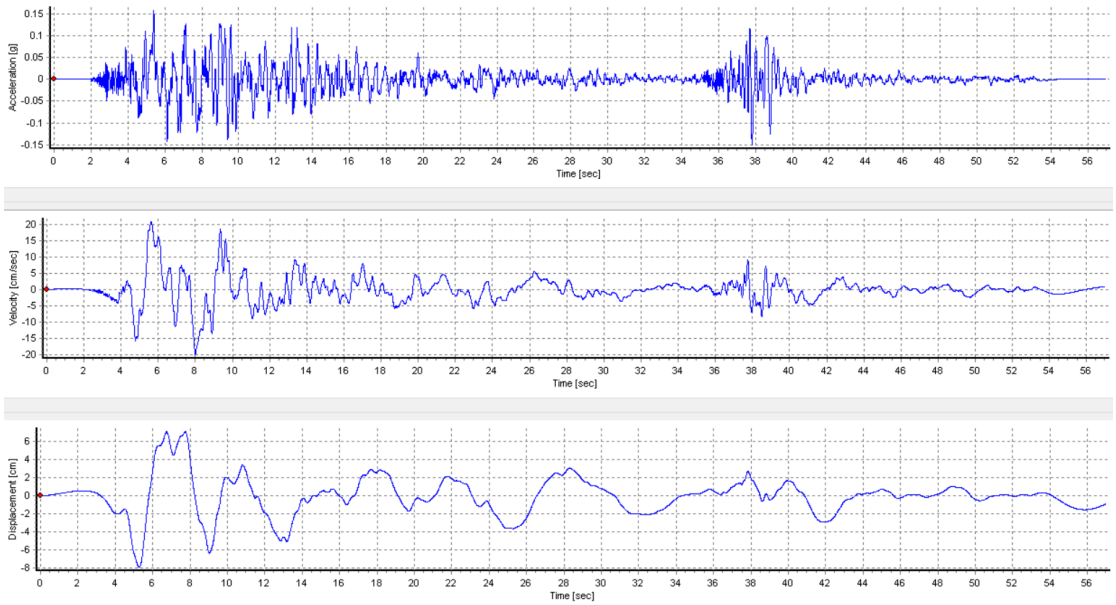

Figure 79. Acceleration, velocity and displacement for tk4101 record in X structural direction

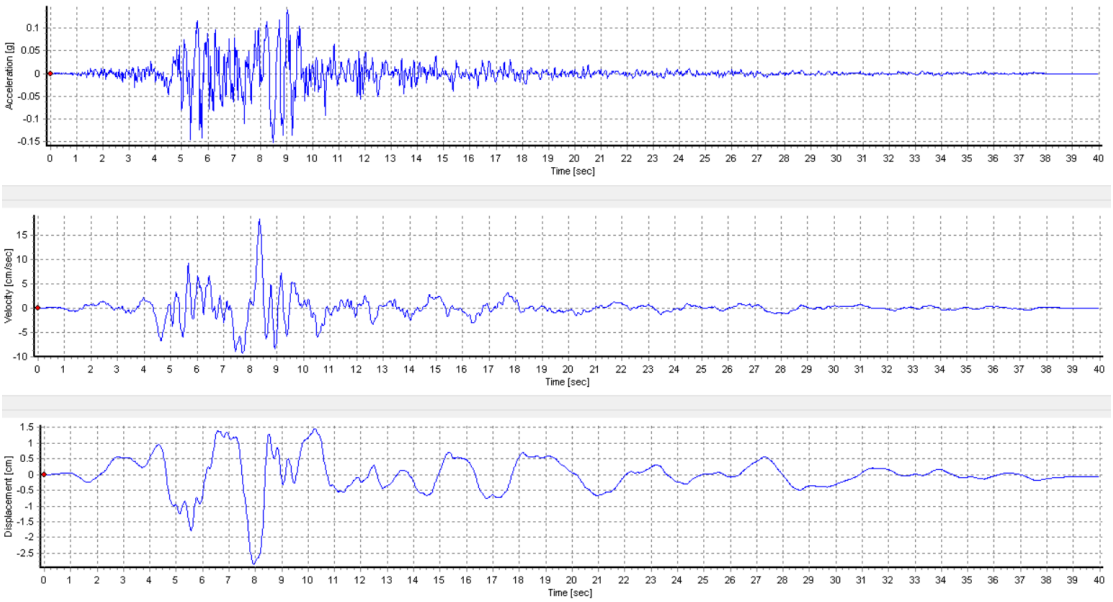

Figure 80. Acceleration, velocity and displacement for rsn1091 record in Y structural direction

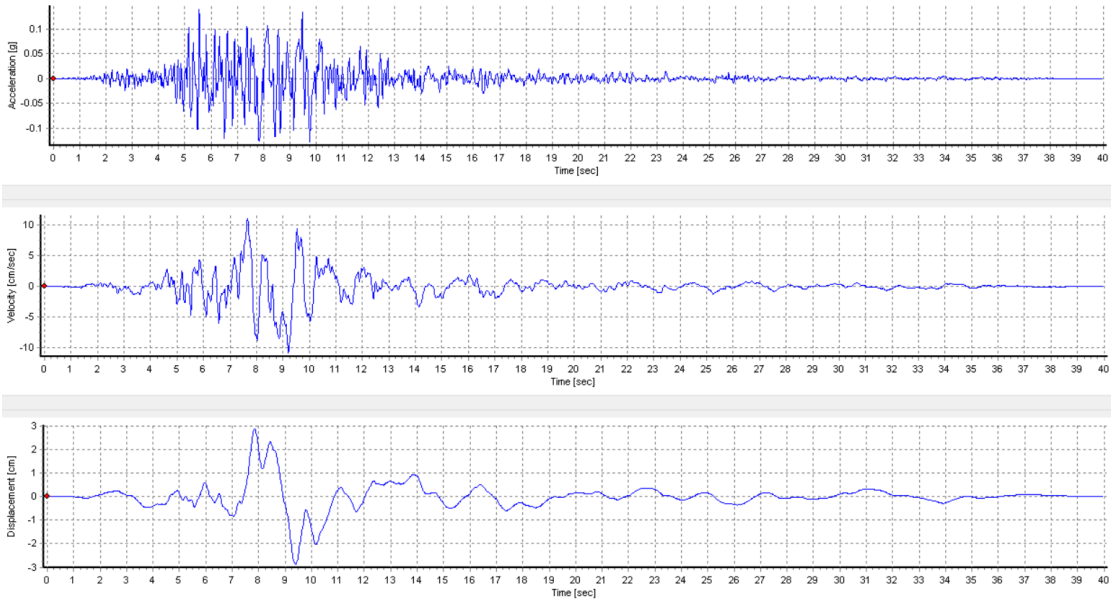

Figure 81. Acceleration, velocity and displacement for rsn1091 record in X structural direction

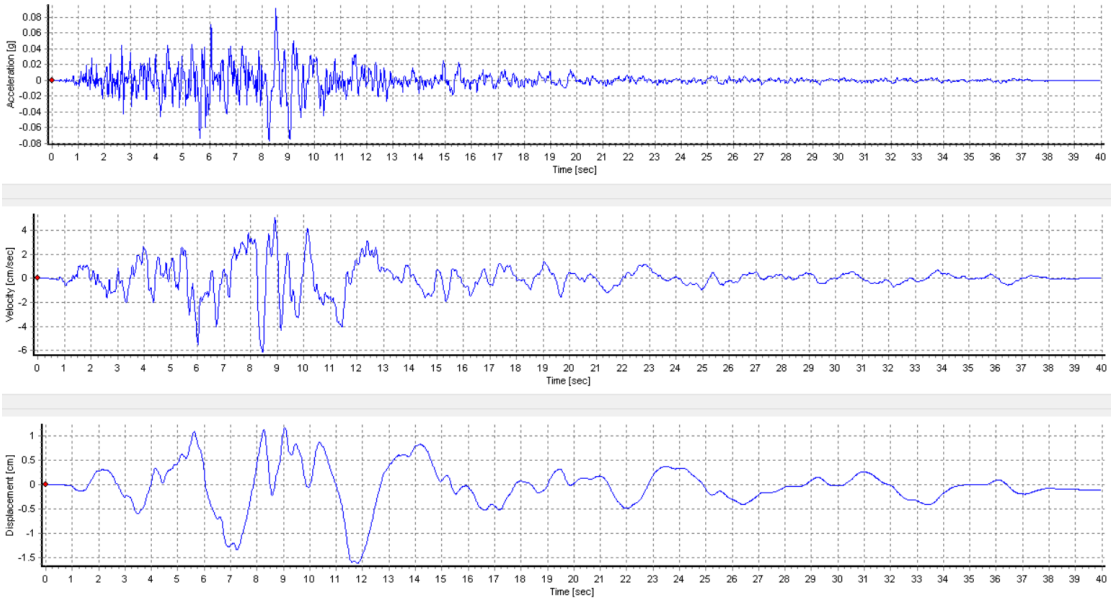

Figure 82. Acceleration, velocity and displacement for rsn4483 record in Y structural direction

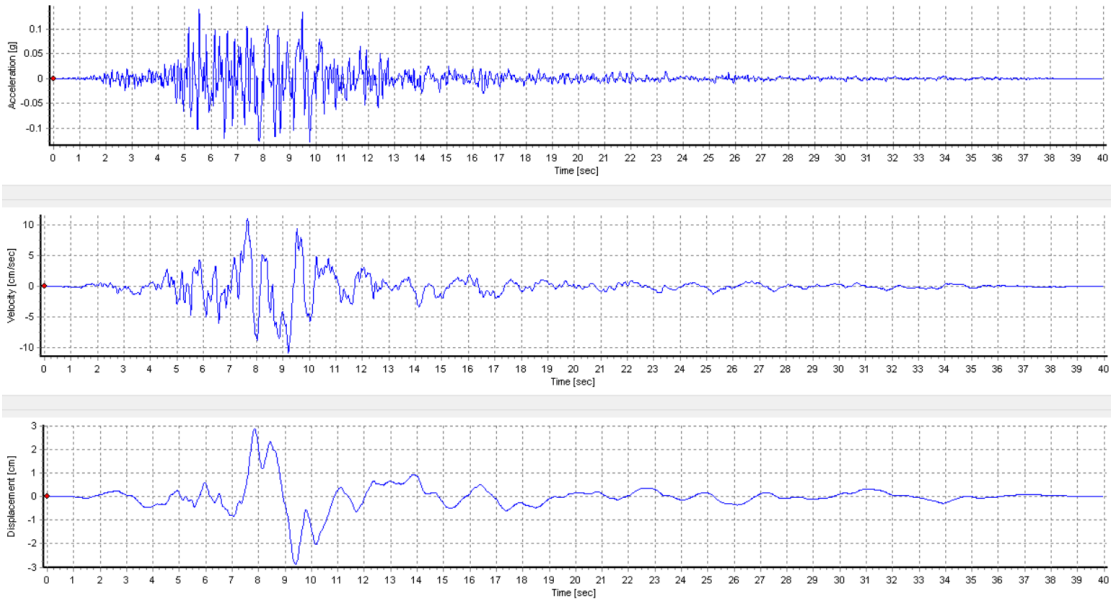

Figure 83. Acceleration, velocity and displacement for rsn4483 record in X structural direction

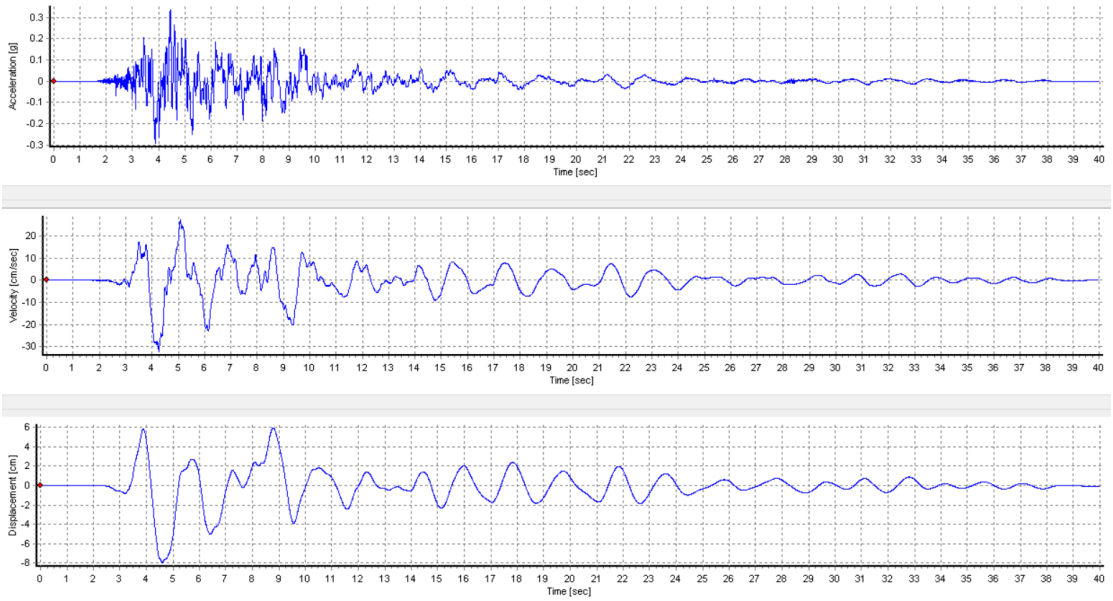

Figure 84. Acceleration, velocity and displacement for rsn5618 record in Y structural direction

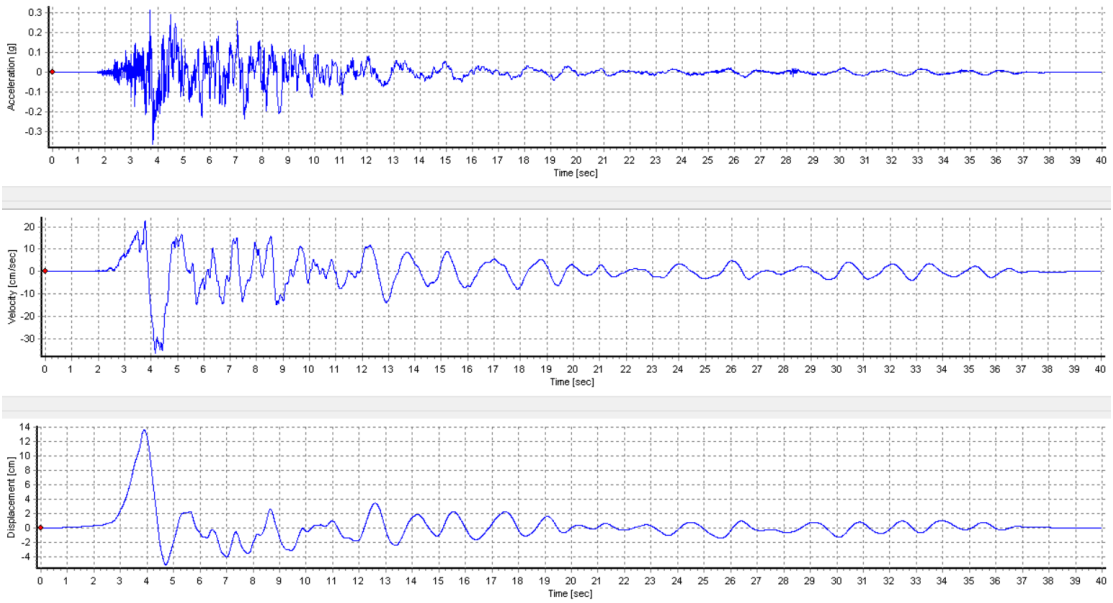

Figure 85. Acceleration, velocity and displacement for rsn5618 record in X structural direction

Appendix E

Interstorey drifts are shown in Figure 86 for Conventional building and Figure 87 for DISSIPABLE building only for DL limit state since this is the govern limit state for serviceability checks according to EN 1993-1 [1]. The average of maximum drifts among 7 accelerograms for each storey are reported in both positive and negative directions. It can be seen that average of maximum interstorey drifts among 7 accelerograms in both X and Y directions do not exceed 1% of height threshold that is required by EN 1993-1 [1].

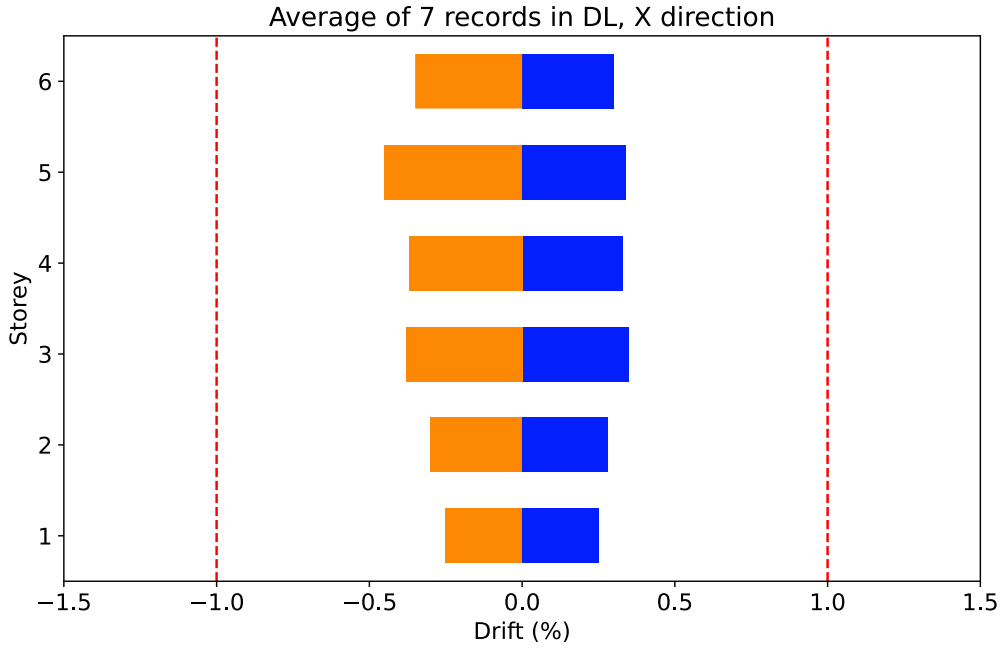

a. Average interstorey drift among 7 records in X direction

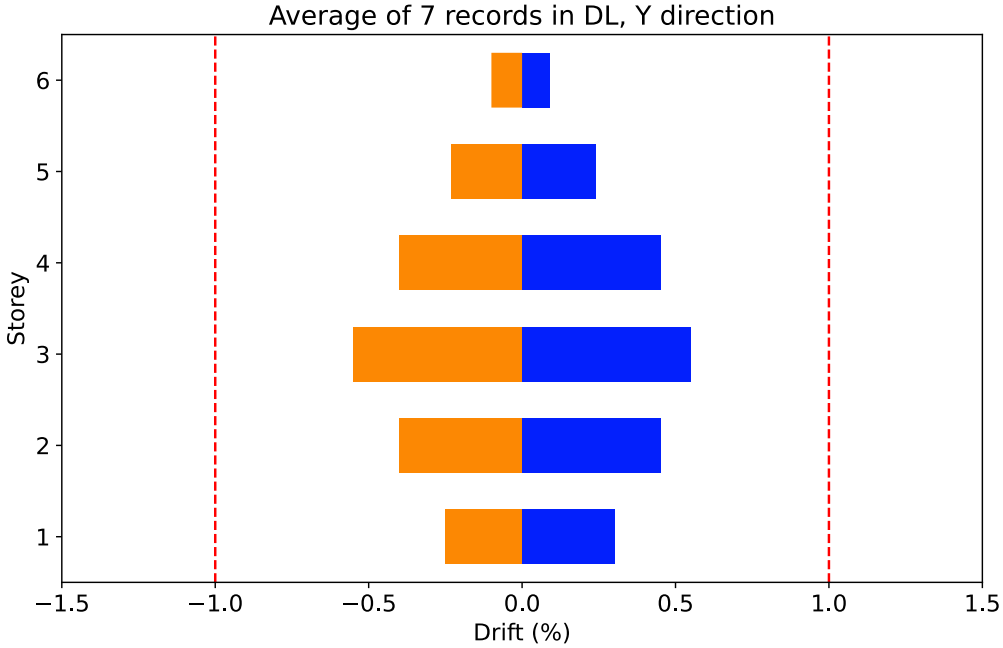

b. Average interstorey drift among 7 records in Y direction

Figure 86. Average intersotrey drift among 7 earthquakes for both X and Y directions for Conventional building

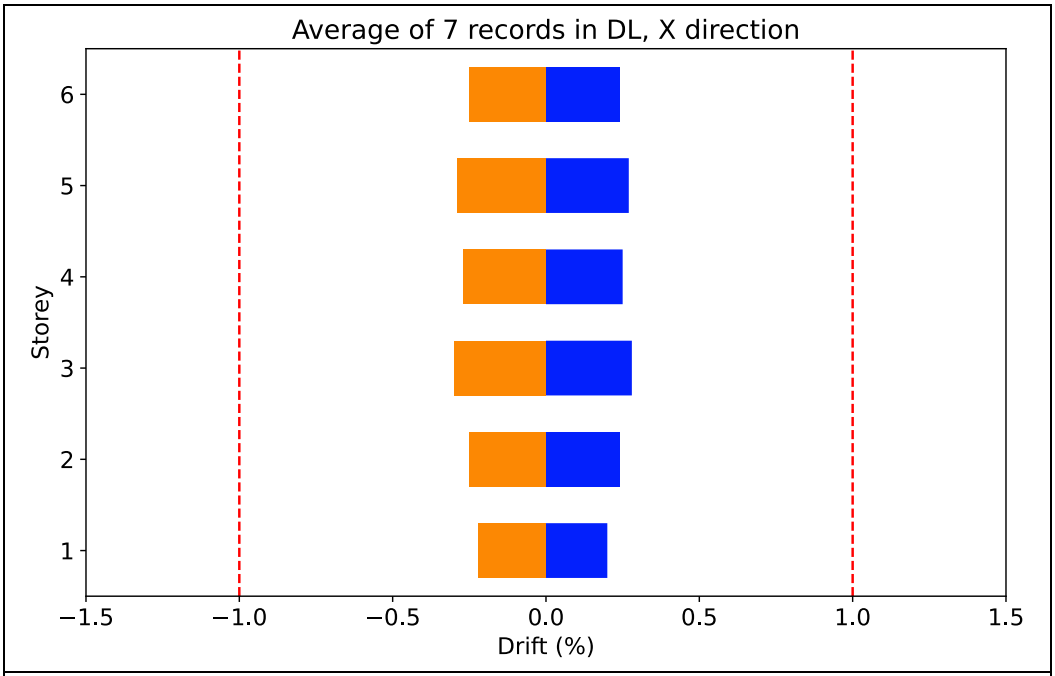

a. Average interstorey drift among 7 records in X direction

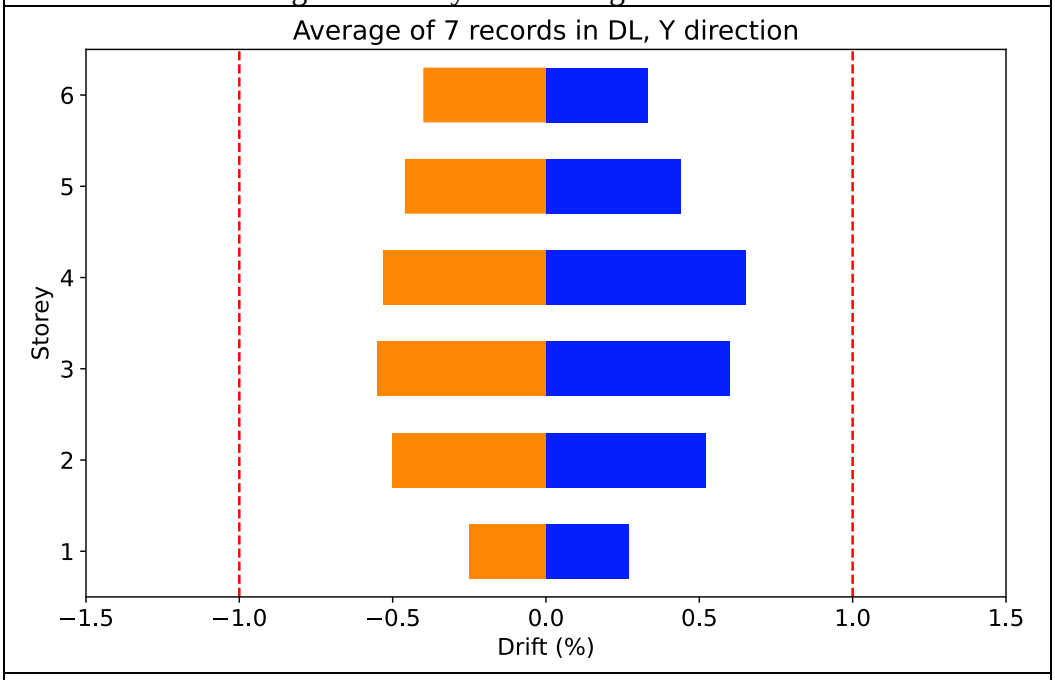

b. Average interstorey drift among 7 records in Y direction

Figure 87. Average intersotrey drift among 7 earthquakes for both X and Y directions for DISSIPABLE building

Appendix F

Figure 88 shows the comparison between target spectrum and the spectrum obtained from the scaled version of the San Fernando accelerogram.

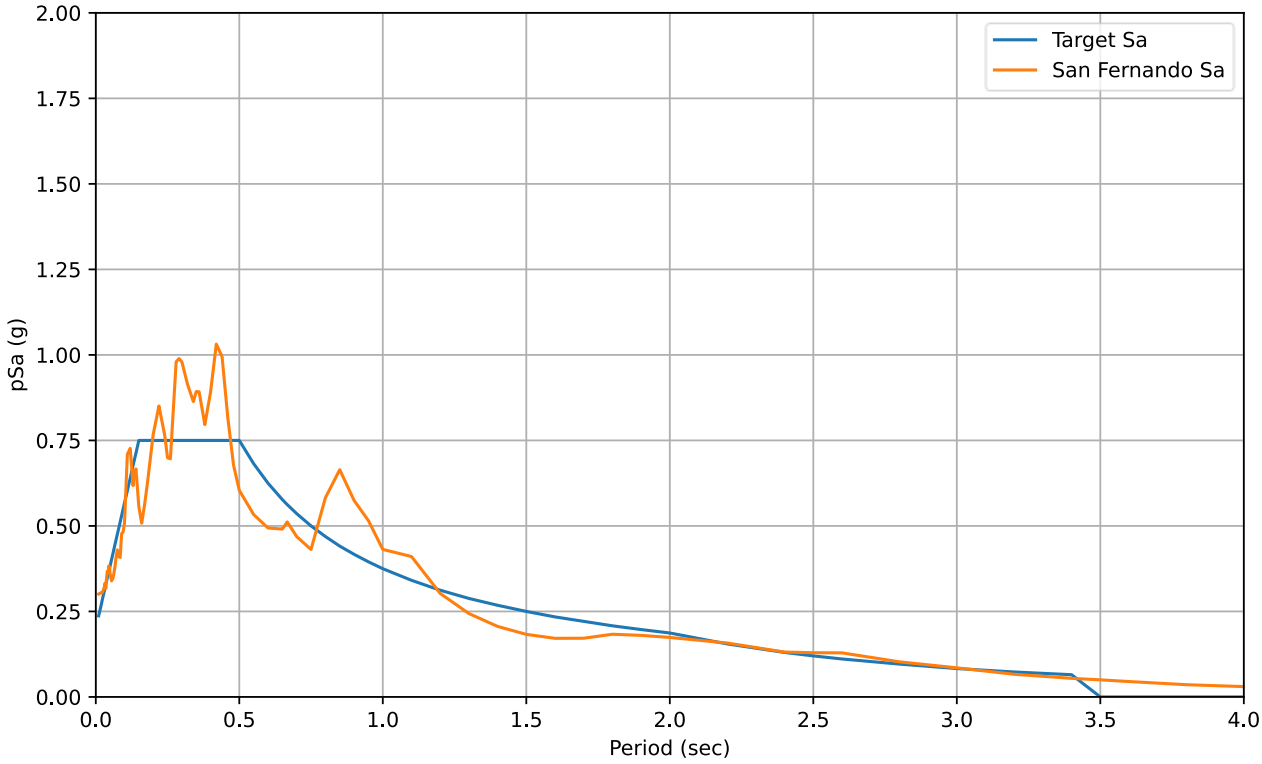

Figure 88. San Fernando accelerogram vs target response spectrum

Appendix G

Figures below show the results of the SHAP analysis for braced frames.

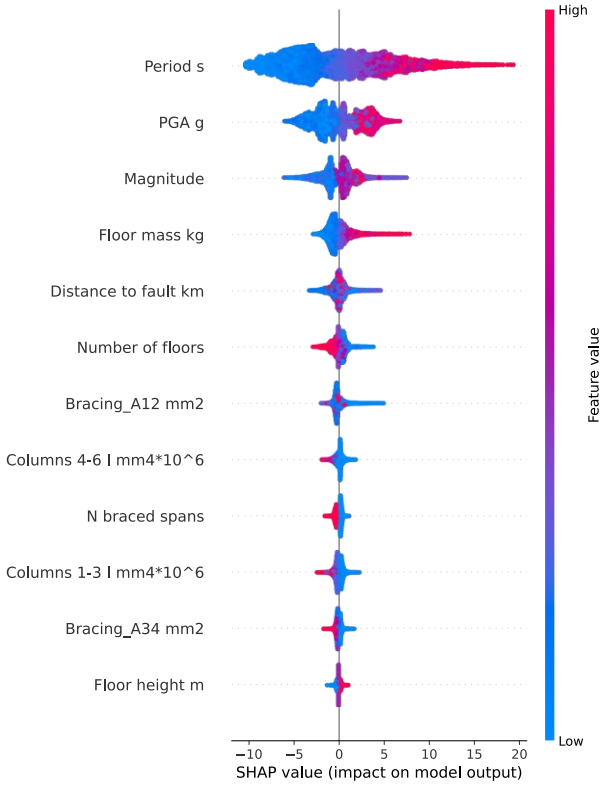

a. Interstorey displacements global analysis

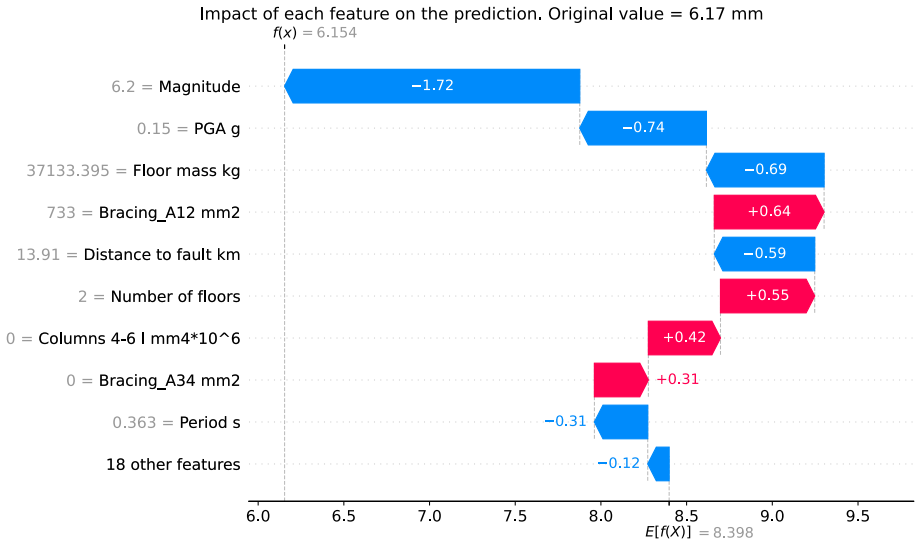

b. Interstorey displacements local analysis

Figure 89. SHAP analysis for ML models used for CBF interstorey displacement response prediction

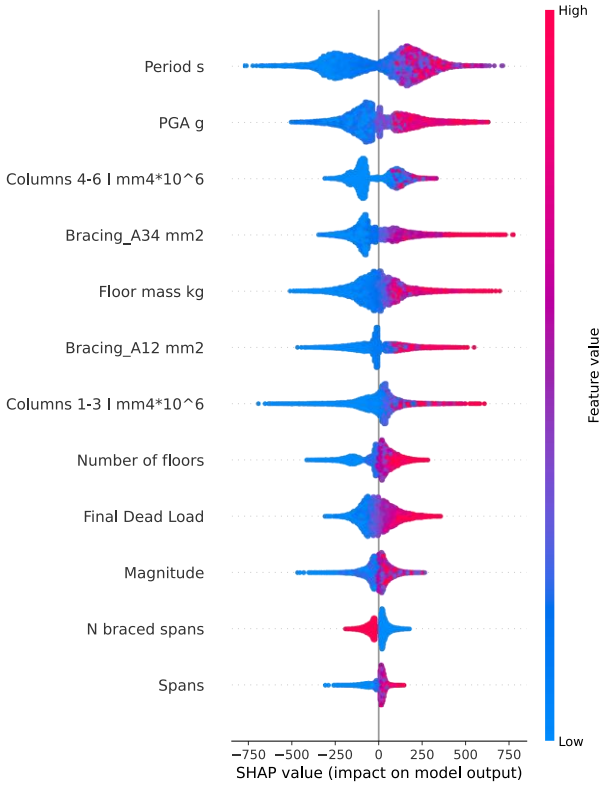

a. Column axial force global analysis

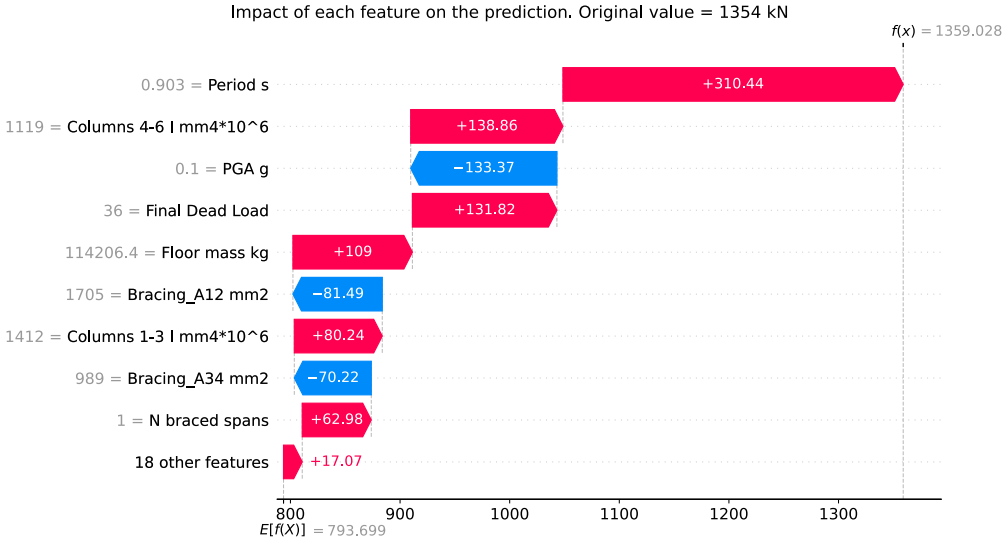

b. Column axial force local analysis

Figure 90. SHAP analysis for ML models used for CBF column axial force response prediction

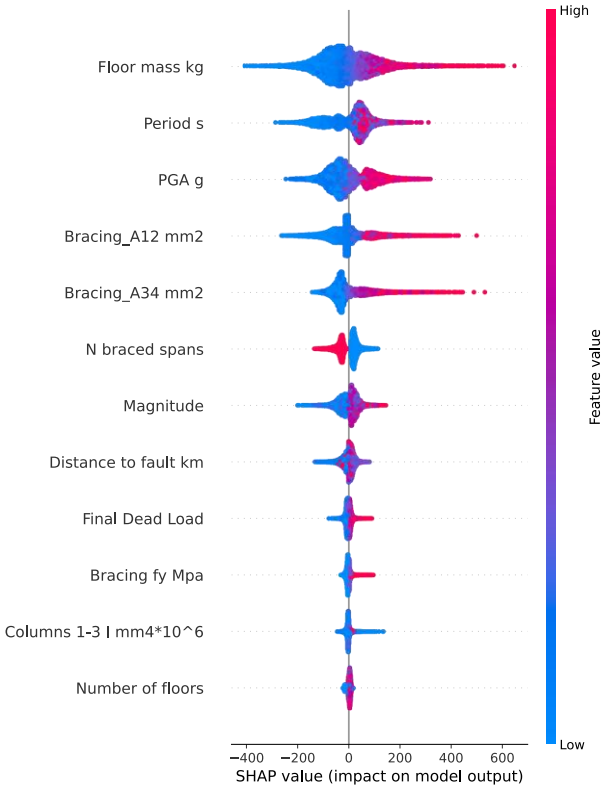

a. Bottom bracing axial force global analysis

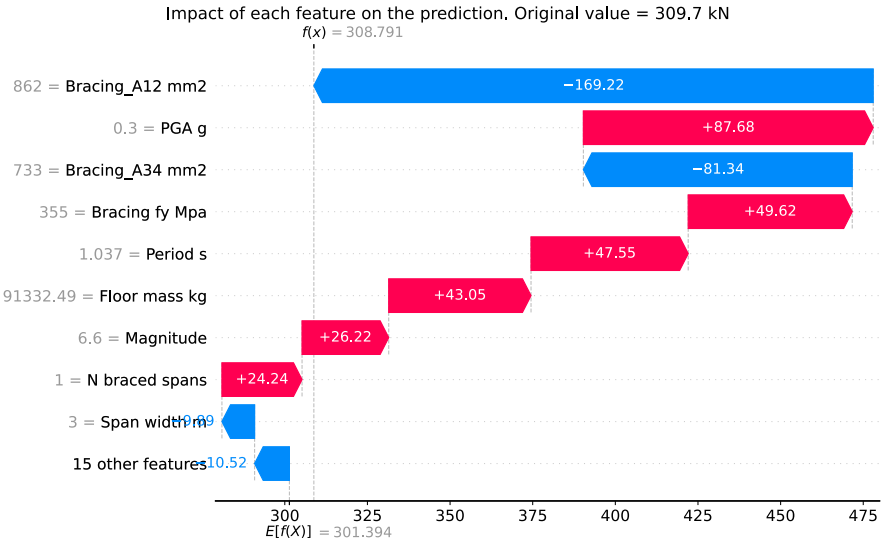

b. Bottom bracing axial force local analysis

Figure 91. SHAP analysis for ML models used for CBF bracing axial force response prediction

Appendix H

Figures below show the results of the SHAP analysis for braced frames equipped with DRBrCs.

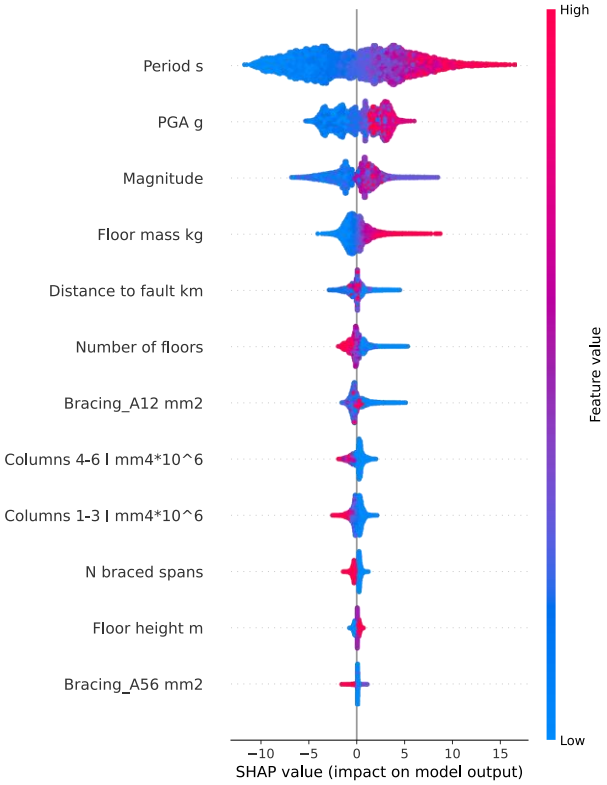

a. Interstorey displacements global analysis

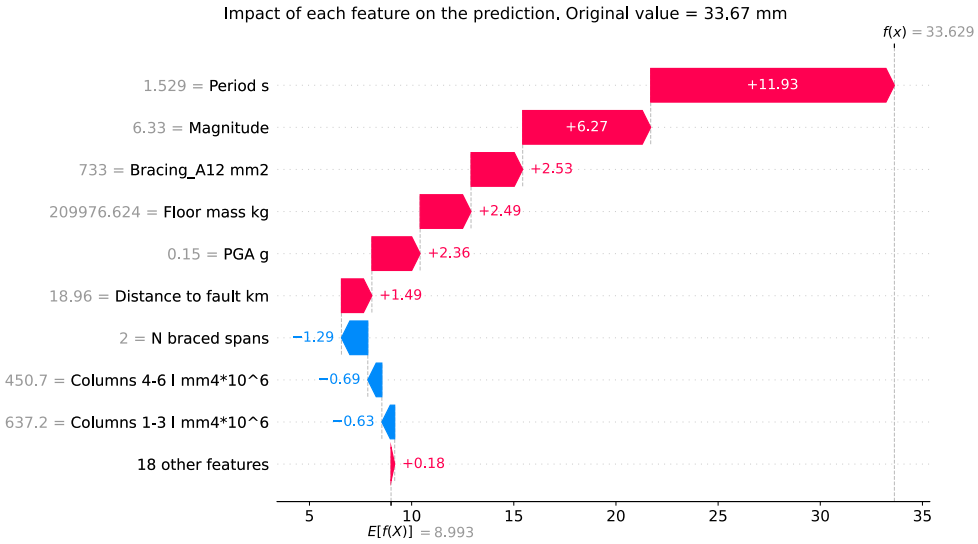

b. Interstorey displacements local analysis

Figure 92. SHAP analysis for ML models used for CBF equipped with DRBrC interstorey drift response prediction

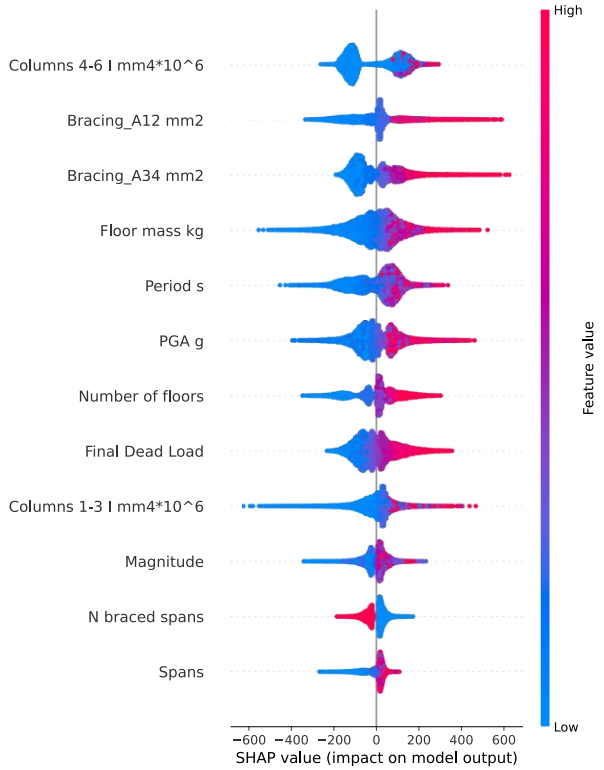

a. Column axial force global analysis

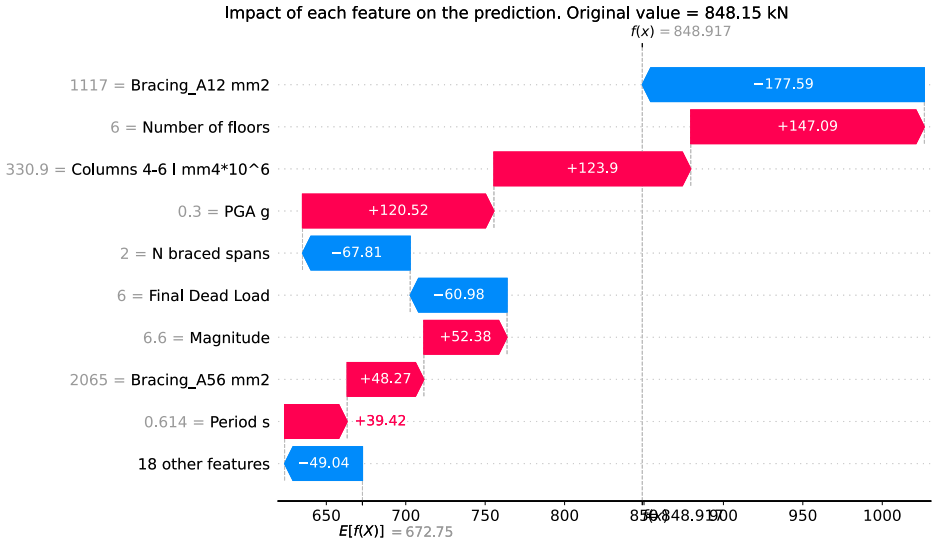

b. Column axial force local analysis

Figure 93. SHAP analysis for ML models used for CBF equipped with DRBrC column axial force response prediction

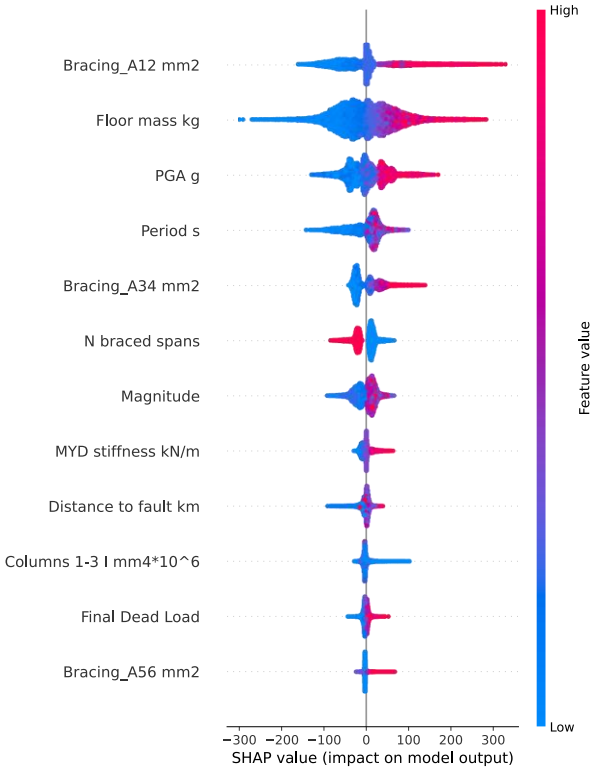

a. Bottom bracing axial force global analysis

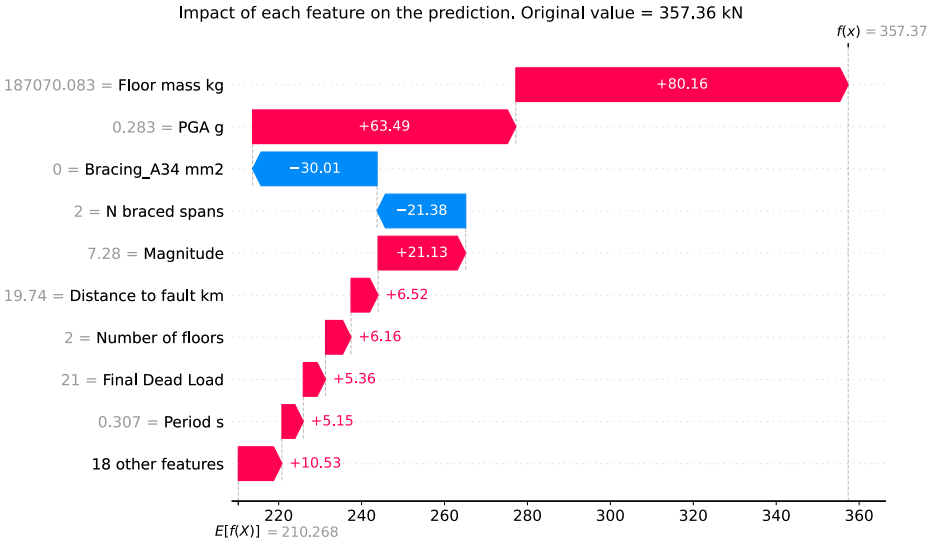

b. Bottom bracing axial force local analysis

Figure 94. SHAP analysis for ML models used for CBF equipped with DRBrC bracing axial force response prediction

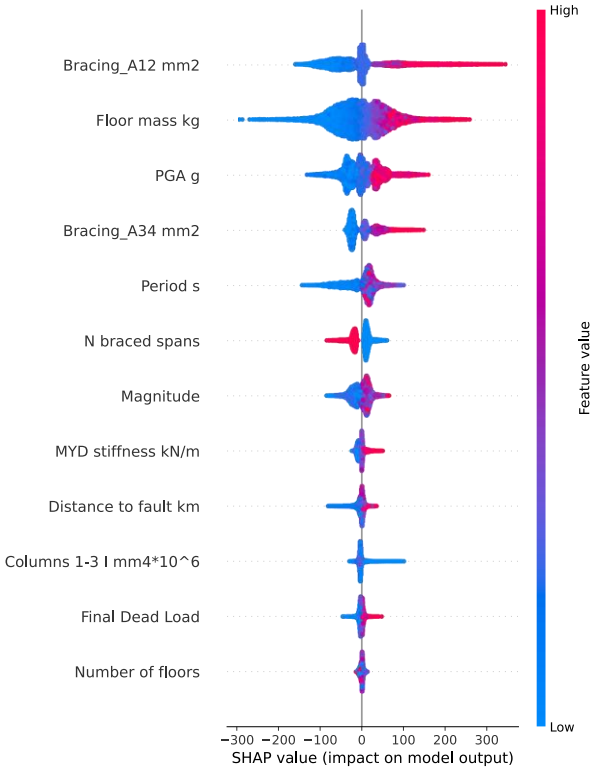

a. Bottom DRBrC axial force error distribution

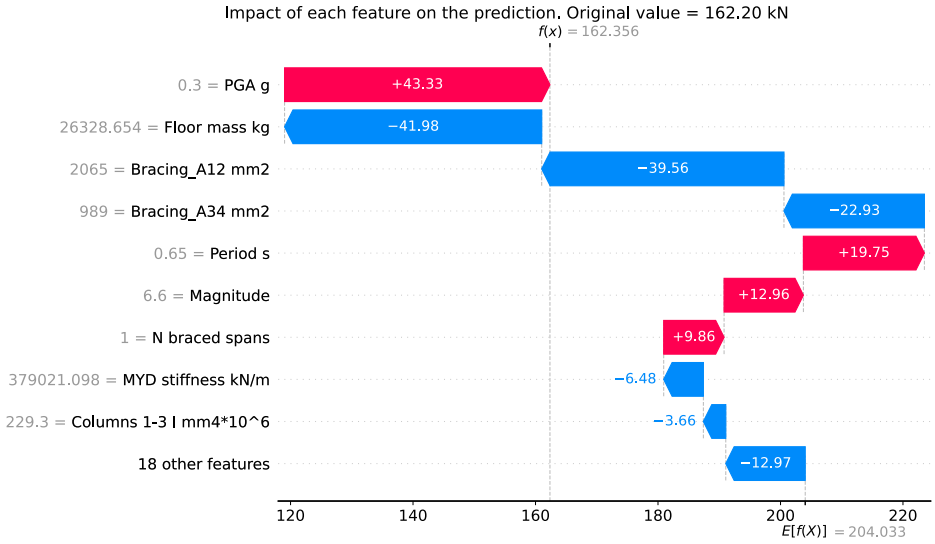

b. Bottom DRBrC axial force biggest error analysis

Figure 95. SHAP analysis for ML models used for CBF equipped with DRBrC MYD axial force response prediction

Appendix I

Figures below show the results of the error analysis for braced frames.

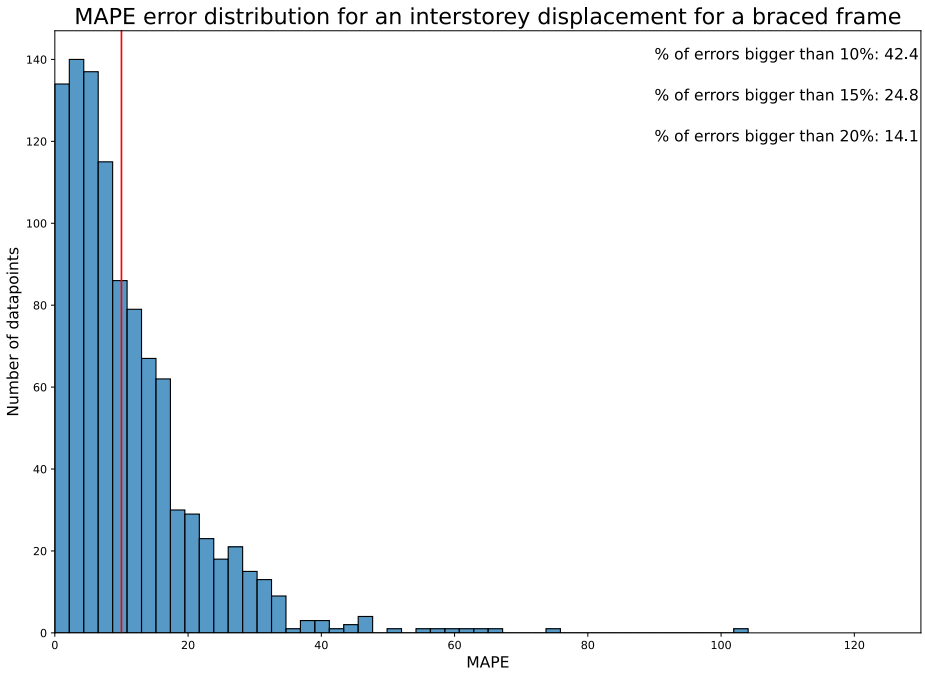

a. Interstorey displacements error distribution

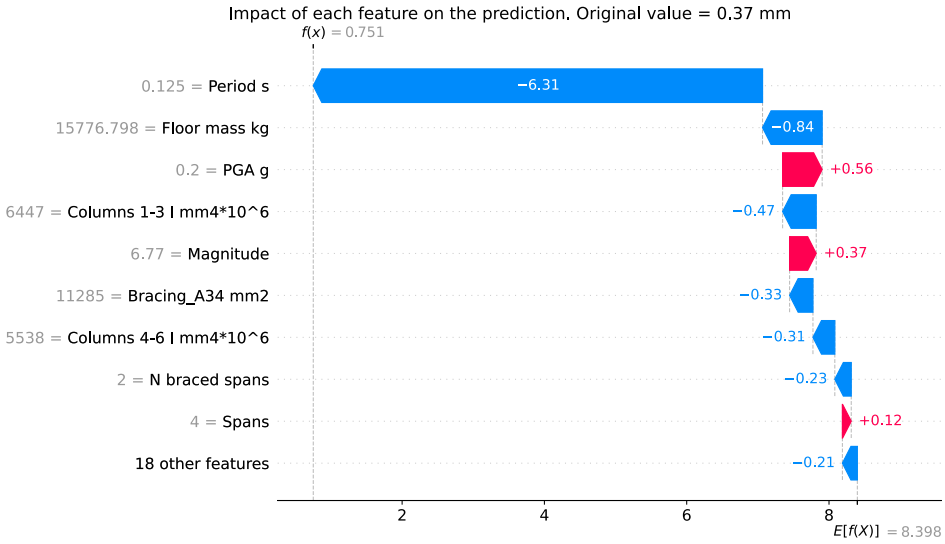

b. Interstorey displacements biggest error analysis

Figure 96. Error analysis for ML models used for CBF interstorey drift response prediction

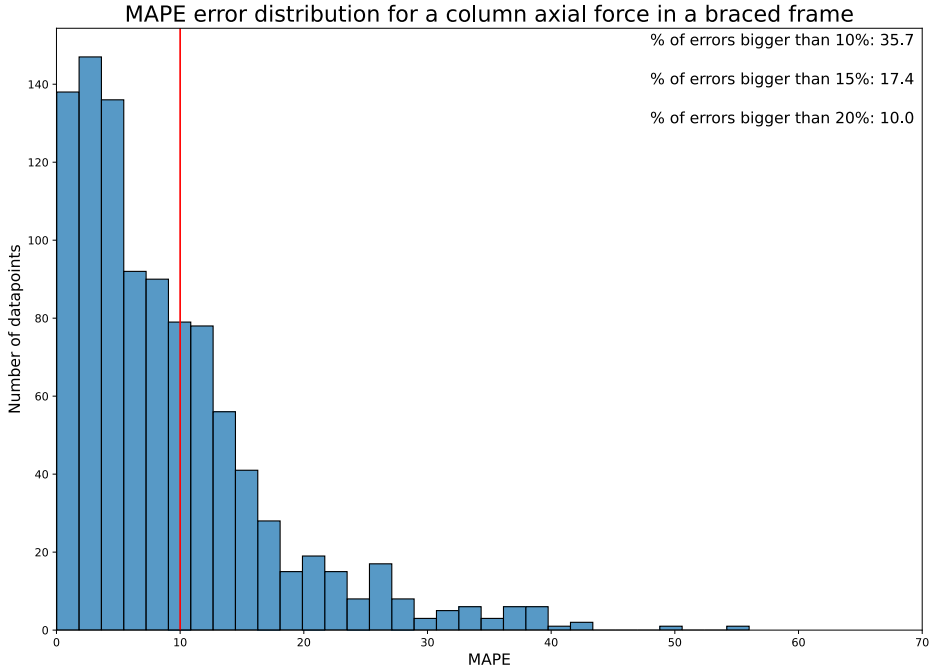

a. Column axial force error distribution

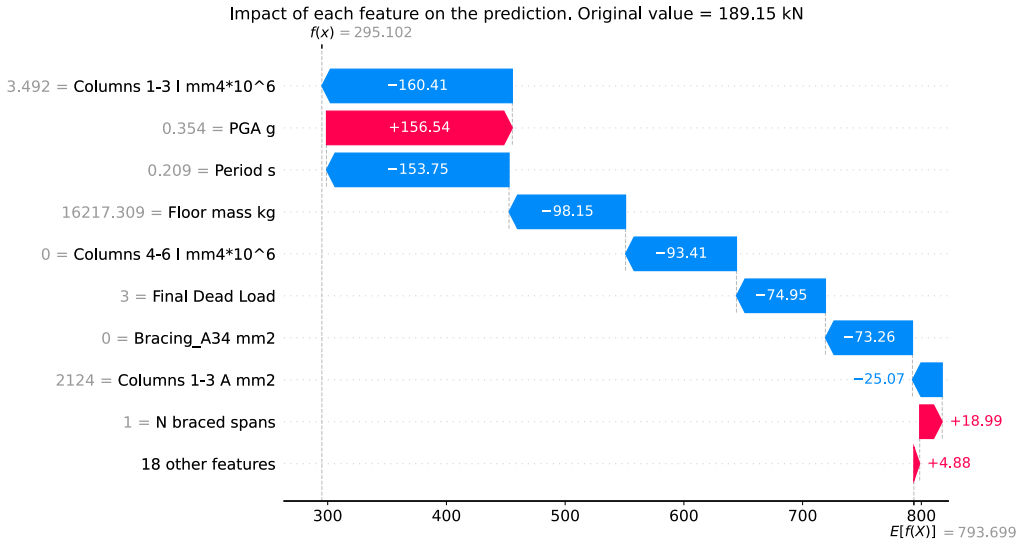

b. Column axial force biggest error analysis

Figure 97. Error analysis for ML models used for CBF column axial force response prediction

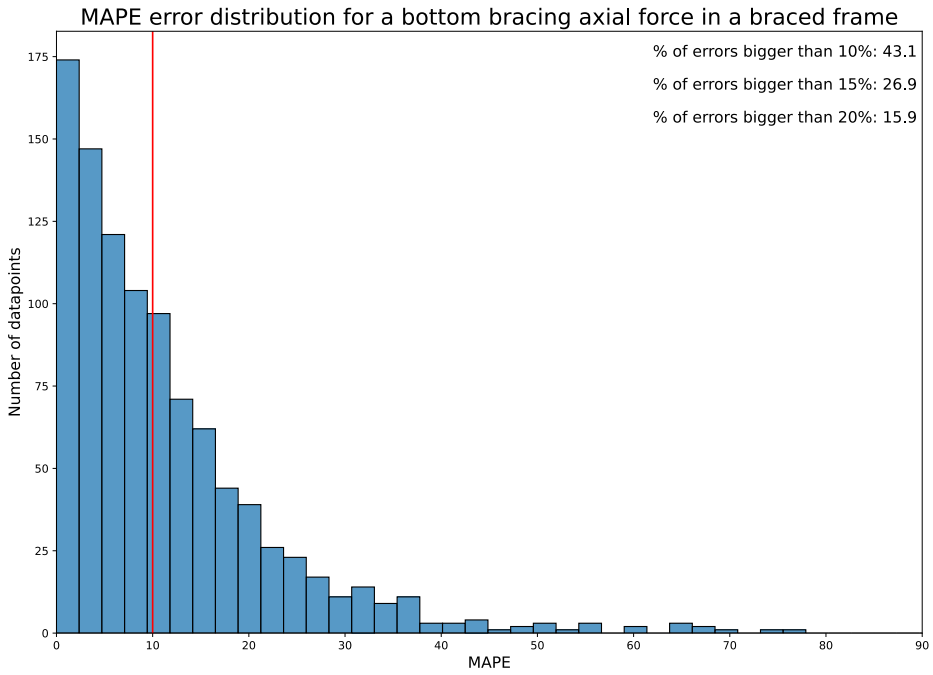

a. Bottom bracing axial force error distribution

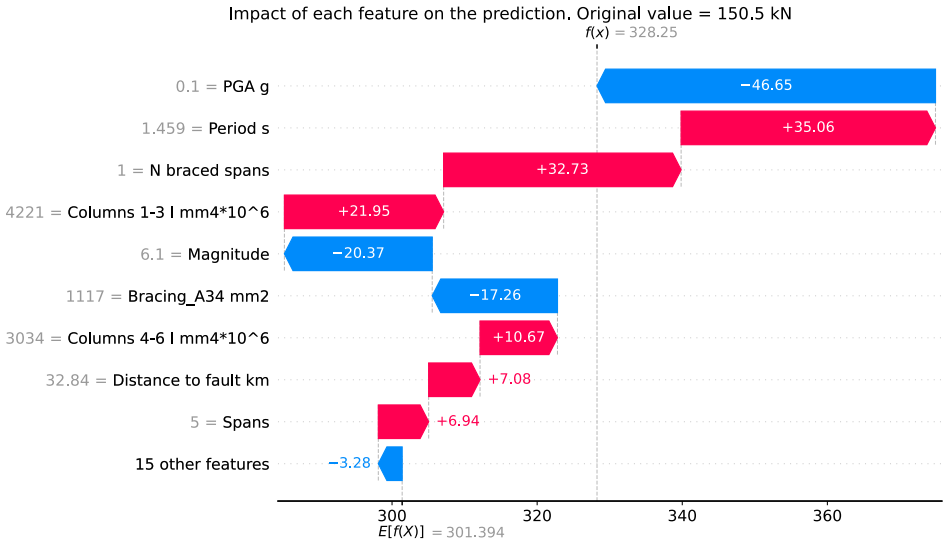

b. Bottom bracing axial force biggest error analysis

Figure 98. Error analysis for ML models used for CBF bracing axial force response prediction

Appendix J

Figures below show the results of the error analysis for braced frames equipped with DRBrCs.

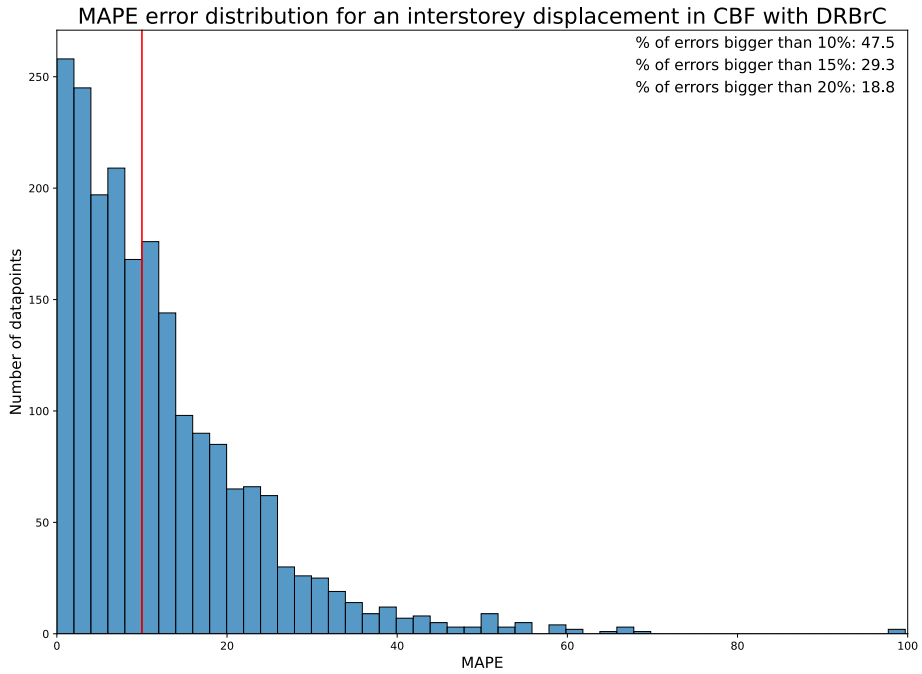

a. Interstorey displacements error distribution

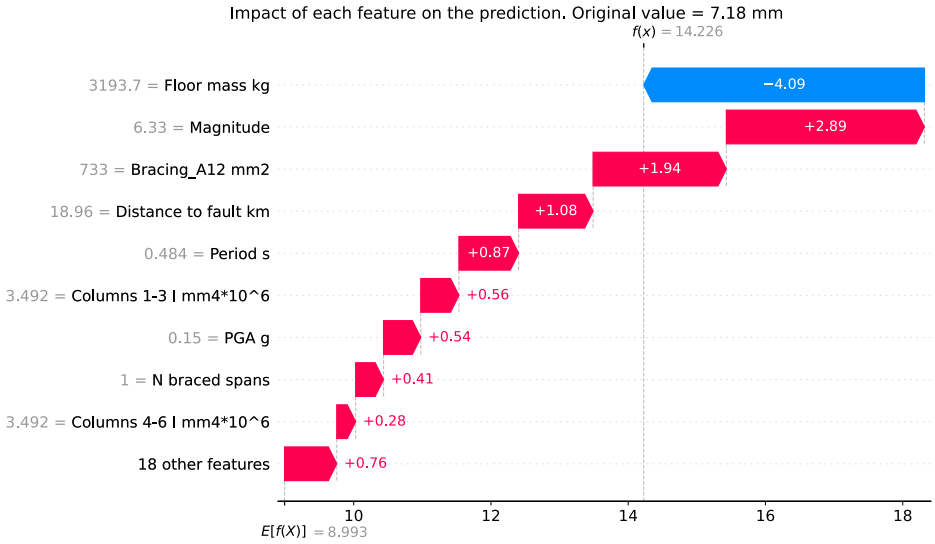

b. Interstorey displacements biggest error analysis

Figure 99. Error analysis for ML models used for CBF equipped with DRBrC interstorey displacement response prediction

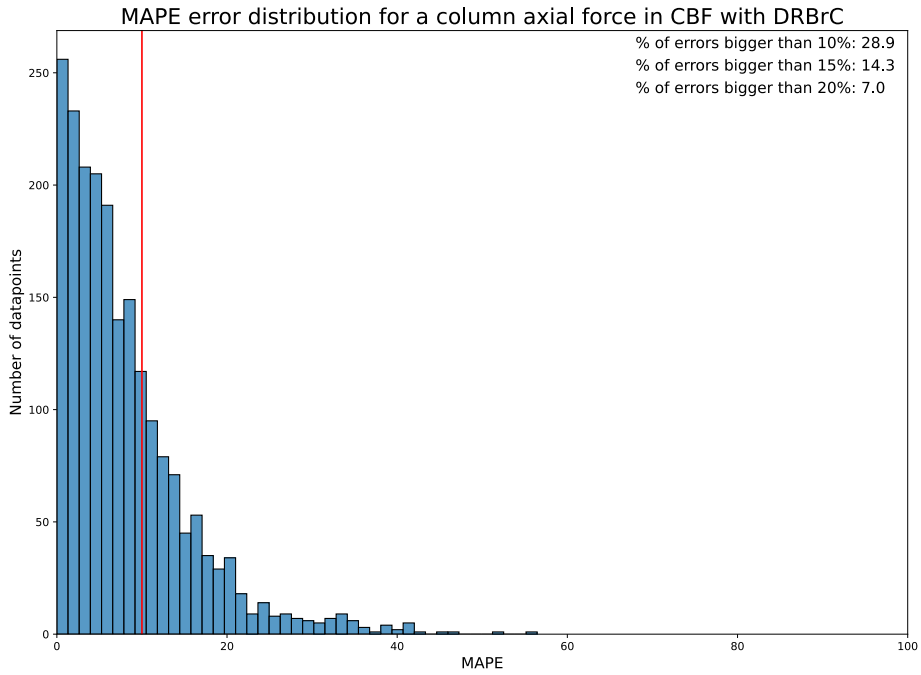

a. Column axial force error distribution

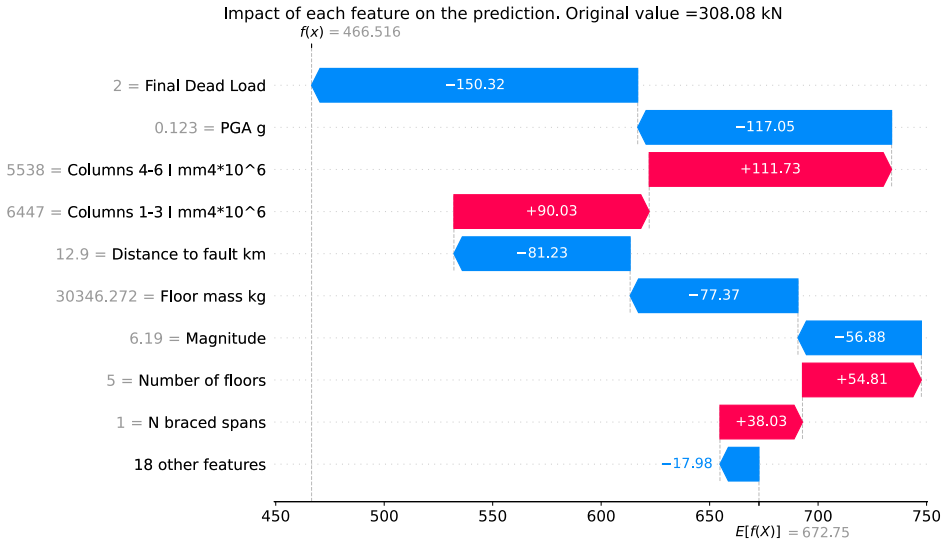

b. Column axial force biggest error analysis

Figure 100. Error analysis for ML models used for CBF equipped with DRBrC column axial force response prediction

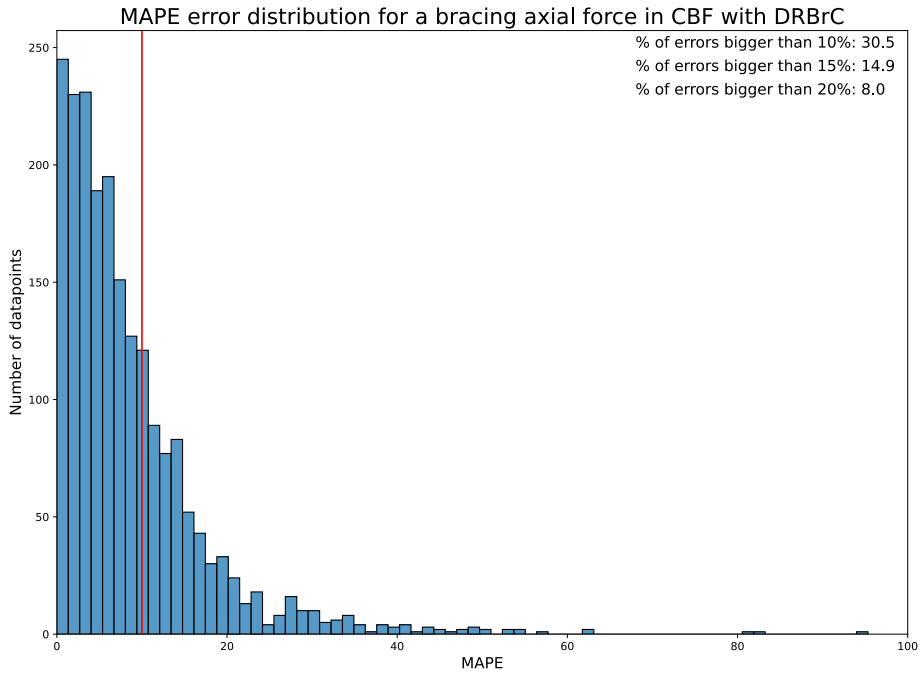

a. Bottom bracing axial force error distribution

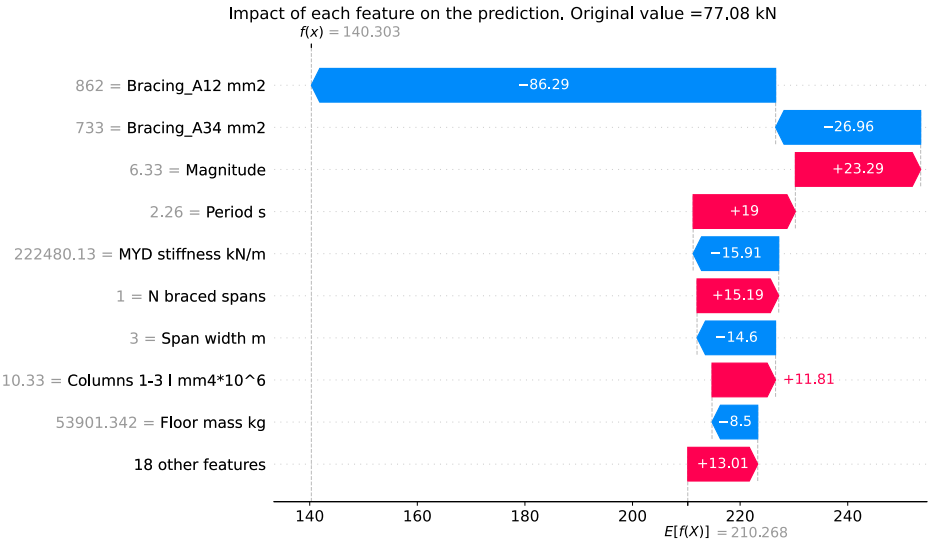

b. Bottom bracing axial force biggest error analysis

Figure 101. Error analysis for ML models used for CBF equipped with DRBrC bracing axial force response prediction

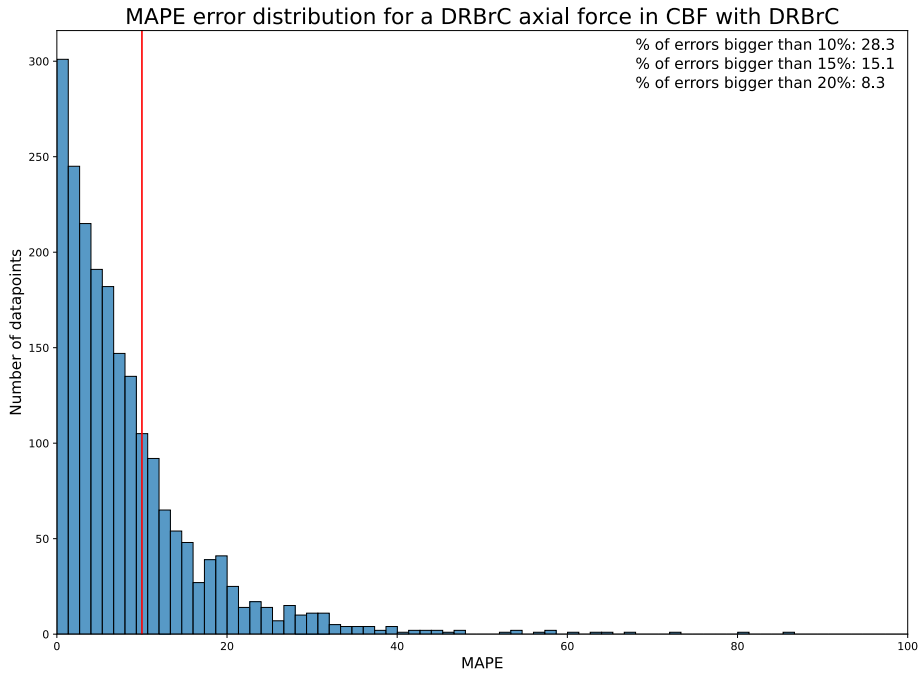

a. Bottom DRBrC axial force error distribution

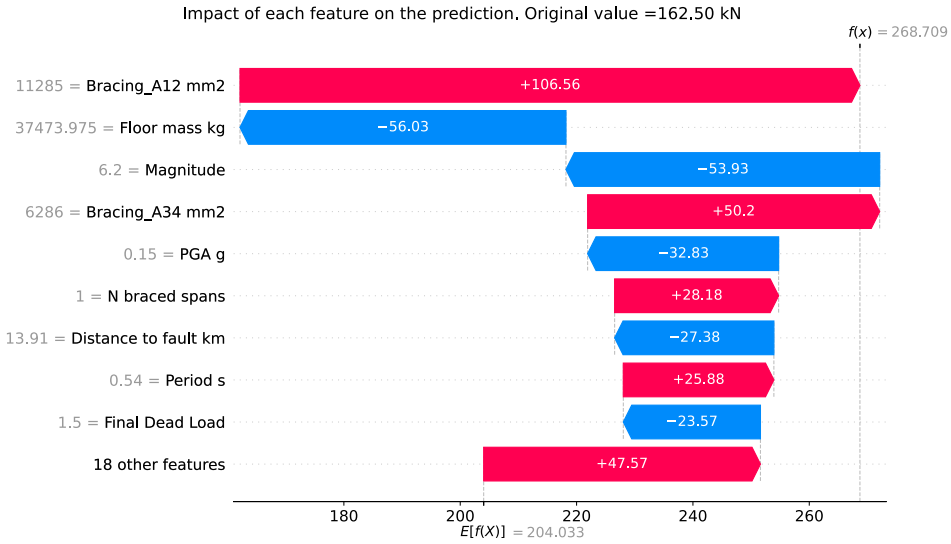

b. Bottom DRBrC axial force biggest error analysis

Figure 102. Error analysis for ML models used for CBF equipped with DRBrC MYD axial force response prediction

Appendix K

Figure 103 show the force-displacement relationship of the plastic hinge in SAP2000 software [122].

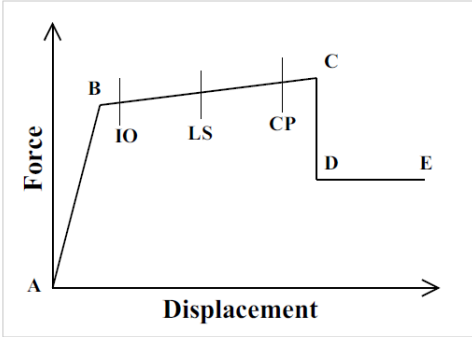

Figure 103. Legend explanation for plastic hinges in SAP2000

Appendix L

The Kaggle [139] competition lasted for 6 months from April 2023 to September 2023. The goal for the participants was to predict the interstorey displacements of the MRF frames given the same inputs as indicated in Chapter 5 of this thesis. Overall, 3000 datapoints were provided to the participants to train their models, and 300 datapoints were used for the evaluation of the predictions. 28 teams participated in the competition (Figure 104, a), and 10 solutions were voluntarily shared with the public by the participants (Figure 104, b). The findings from these solutions have been used in this thesis to improve the overall accuracy of the ML models.

#	Team	Members	Score	Entries	Last	Solution
1	Alex Dundore		8.76219	16	6mo	
2	Project Team		8.80597	14	9mo	
3	Alpay Abbaszade		10.14227	13	6mo	
4	mmtkc		11.56261	16	6mo	
5	gkitti		12.52949	1	9mo	
6	base_ml		12.53203	3	1y	
7	Esposte		13.69886	10	9mo	
8	Jay		13.95530	3	10mo	
9	ClapClapClap		13.98429	6	10mo	
10	midorigawa		14.07287	1	10mo	
11	GrootX		14.21311	3	10mo	

a. Leaderboard with the 11 best teams participarted in a competiton

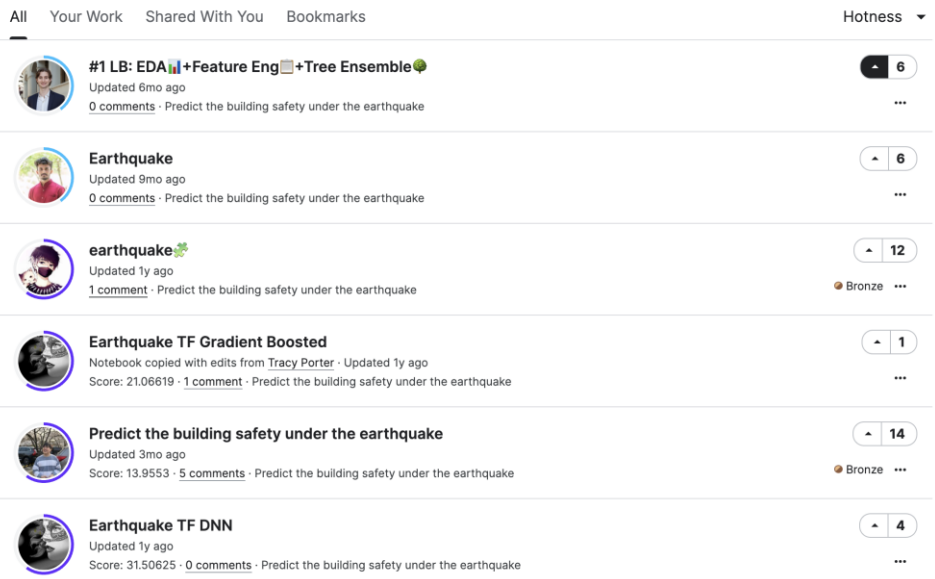

b. A sample of shared voluntarily solutions by the participants

Figure 104. The results of the Kaggle competition